DANMARKS OG GRØNLANDS GEOLOGISKE UNDERSØGELSE RAPPORT 2005/54

Linking the Faroese area and Greenland: an innovative, integrated provenance study

Final report prepared for SINDRI

Dirk Frei, Martina Frei & Christian Knudsen (eds)

GEOLOGICAL SURVEY OF DENMARK AND GREENLAND
MINISTRY OF THE ENVIRONMENT

GEUS

DANMARKS OG GRØNLANDS GEOLOGISKE UNDERSØGELSE RAPPORT 2005/54

Linking the Faroese area and Greenland: an innovative, integrated provenance study

Final report prepared for SINDRI

Dirk Frei, Martina Frei & Christian Knudsen (eds)

With contributions from Dirk Frei, Christian Knudsen, Andrew C. Morton, Martina Frei, Claire Hallsworth, Maiken Hansen Klünder, Michael Larsen, Thomas Rasmussen & Andrew G. Whitham

Released 16.09.2010

GEOLOGICAL SURVEY OF DENMARK AND GREENLAND
MINISTRY OF THE ENVIRONMENT

GEUS

Contents

Executive summary and recommendations for future hydrocarbon prospecting

This report presents the results of a detailed provenance study of Cretaceous to Eocene sedimentary successions exposed in the Kangerlussuaq area in East Greenland, and Paleocene to Eocene sedimentary successions from five wells in the UK sector of the Faroe-Shetland Basin, conducted during the SINDRI programme. The goals of the study were:

(1) to test, refine and evaluate computer controlled scanning electron microscopy (CCSEM) and laser ablation – inductively coupled plasma – mass spectrometry (LA-ICP-MS), two techniques novel for provenance analysis;

(2) to apply detailed major- and trace element geochemistry with a high stratigraphic resolution to provenance analysis;

(3) to integrate the results of these new techniques with conventional petrographic and mineral-chemical techniques in a multi-analyses approach; and

(4) to characterise the provenance specific signatures of the sedimentary successions in East Greenland and the UK sector of the Faroe-Shetland Basin.

The aim was to deepen our understanding of the link between the Faroese area and East Greenland and thereby contribute to the establishment of a framework for the identification of sands in the Faroe-Shetland Basin.

Conventional petrographic and mineral-chemical techniques

New heavy mineral provenance data for samples from the Kangerlussuaq area, the Orkney Islands, and wells in the UK sector of the Faroe-Shetland Basin derived by conventional petrographic and mineral-chemical techniques have been combined with published heavy mineral data and released but, as yet, unpublished data. Synthesis of this dataset identified influx from six distinct major sources to the Paleocene-Eocene successions in the UK sector of the Faroe-Shetland Basin. Five of these are interpreted as lying on the eastern (i.e. UK) margin whereas only one shares some characteristics with detritus in the Kangerlussuaq area. However, the detrital garnet compositions suggest that this source was also located on the UK margin. For the sedimentary successions exposed in the Kangerlussuaq Basin, the new heavy mineral provenance data indicate derivation from two distinct sources.

Comparison of CCSEM and EMPA

In a comparison study, the major element geochemistry of detrital garnet populations from 37 sandstones samples from all examined areas have been determined by CCSEM and electron microprobe analyser (EMPA). The results obtained by the two methods are in excellent agreement and validate CCSEM as a reliable, fast and inexpensive method for provenance studies based on garnet major element geochemistry. Furthermore, CCSEM yields data that were previously unattainable, such as the TiO_2-distribution of the Ti-mineral

fraction and modal abundances of individual heavy mineral species which are provenance sensitive characteristics of sediments.

Detrital garnet major element geochemistry

Application of CCSEM to detrital garnets from sandstones in the Kangerlussuaq Basin suggests derivation from two distinctive sources, in agreement with the findings from heavy mineral provenance data obtained by conventional petrographic and mineral-chemical techniques. The most striking finding is that the detrital garnets in the Kangerlussuaq Basin generally lack a high-Mg component that is characteristic for detrital garnets from wells in the UK sector of the Faroe-Shetland Basin.

TiO_2-distribution of detrital Ti-minerals

CCSEM analysis of the Ti-mineral fraction (i.e. rutile, ilmenite and leucoxene) demonstrates striking differences between stratigraphic groups of the Kangerlussuaq Basin. Samples from the Cretaceous are dominated by the presence of pseudorutile and leucoxene and the absence of primary ilmenite. This high degree of maturity points to derivation from a source that has been intensely chemically altered or intense alteration at the side of deposition. Lateral variations in maturity of the Early Paleocene Fairy Tale Valley Member reflect lithological differences (highly mature fluvial sandstones vs. immature marine shale dominated sediments), and hence variations in source and sediment history. High proportions of primary ilmenite in intra-basalt and post-basalt samples indicate influx from unaltered volcanic material.

Comparison of ^{207}Pb-^{206}Pb and U-Th zircon age dating techniques

The reliability of the results obtained by in-situ ^{207}Pb-^{206}Pb age dating of detrital zircons using quadrupole LA-ICP-MS was evaluated by comparison with high-precison U-Pb age dating techniques (SHRIMP and high resolution magnetic sectorfield LA-ICP-MS). The results conclusively demonstrate that ^{207}Pb-^{206}Pb dating is a reliable method for the determination of detrital zircon age distributions. However, the superior precision, high sample throughput, high degree of automatisation and hence comparatively low costs have established U-Pb dating by high resolution magnetic sectorfield LA-ICP-MS as the most suitable technique for future provenance studies based on detrital zircon age distributions.

Detrital zircon age distributions

Application of LA-ICP-MS made it possible to obtain age data during the present study for 4347 detrital zircons from 47 samples in the Kangerlussuaq Basin, wells in the UK sector of the Faroe-Shetland Basin and the Orkney Islands. This allowed the authors investigation of the age information recorded in detrital zircon populations in these successions with hiherto unprecedented resolution and detail. Observed detrital zircon age distributions in samples from the Kangerlussuaq Basin unequivocally demonstrate that the sedimentary successions are derived from two distinct sources, the first being Archaean basement situated to the south and southwest, and the second being younger, Proterozoic rocks situated to the north and northeast. Furthermore, the zircon age distributions allow tight constraints to be placed on the timing of changes in sediment supply, to validate the stratigraphic correlations drawn from litho- and sequence stratigraphy, and to exclude large-scale local reworking of sedimentary units in the Kangerlussuaq Basin. However, the most important feature of the zircon age distributions in sandstones from the Kangerlussuaq Basin is the

general presence of a characteristic Middle Archaean age component. This distinctive age component is almost completely absent from detrital zircon age distributions in samples from wells in the UK sector of the Faroe-Shetland Basin.

Bulk rock chemostratigraphy

During this project, 440 samples representing Cretaceous, Paleocene and Eocene clastic sediments from the sedimentary successions exposed in the Kangerlussuaq Basin (171 samples) and drilled in wells in the UK sector of the Faroe-Shetland Basin (269 samples) have been analysed for 10 major elements, 33 trace elements and loss on ignition. All elements have been analysed with high precision and accuracy at low detection levels using fusion X-ray fluoresence (XRF) combined with solution nebulisation – inductively coupled plasma - mass spectrometry (SN-ICP-MS). This novel approach allows the interpretation of new aspects of the geology in the potential reservoirs as well as in the mudstones. No evidence was found for a common source shared by the sediments from the Kangerlussuaq and the Faroe-Shetland areas, a finding that is in agreement with the conclusions drawn from heavy mineral provenance data, detrital garnet geochemistry, and detrital zircon age distributions. Furthermore, lateral variations in the Fairy Tale Valley Member are in accordance with the results from the Ti-minerals and zircon age dating studies. In the Faroe-Shetland area, strongly contrasting source areas are indicated.

Conclusions

In conclusion, the detailed provenance study conducted in this project revealed that the sedimentary successions from the Kangerlussuaq area and the eastern margin of the Faroe-Shetland Basin have differing signatures. These signatures allow distinction between a western, Greenlandic source and an eastern, predominantly UK margin source. The influence from a western source (Greenland) has not been proved in the examined stratigraphic intervals of wells from the UK sector of the Faroe-Shetland Basin. However, the structure of the Faroe-Shetland Basin suggests that the western, Greenlandic source might be much more important for the deeper, central parts of the basin towards the Faroes area.

Recommendations for future hydrocarbon prospecting

The results obtained during this project establish a robust framework for the identification of sands in the Faroe-Shetland Basin. The new techniques available for provenance studies and the distinctive signature of the greenlandic source characterised during this project provide a reliable way to distinguish the eastern and western provenance areas and should therefore be applied to wells in the Faroes area. Additional detrital zircon age data for samples from the UK margin could help to further refine the characterisation of the eastern sources and identify individual contributors.

This project demonstrates the potential of advanced, integrated provenance studies for modern hydrocarbon exploration. We conclude that the new techniques and methods have considerable potential for becoming standard tools in future hydrocarbon exploration.

Editorial and introduction

Dirk Frei, Martina Frei, Christian Knudsen

Geological Survey of Denmark and Greenland, Øster Voldgade 10, DK-1350 Copenhagen K, Denmark

A key issue for hydrocarbon exploration in the Faroes region is the understanding of sediment dispersal patterns and depositional systems in the Faroe-Shetland Basin prior to continental breakup in the Late Paleocene to Early Eocene. Identification of sediment provenance is crucial for this goal. Location of the source areas places important constraints on sediment transport pathways and intrabasinal sand body distribution. Furthermore, the nature of the sediment source has important implications for the porosity and permeability characteristics of the deposited sediments. Identified variations in source might also be used to establish correlation frameworks (at both local and regional scales) and can provide a basis for discrimination of individual sand bodies.

Sediment provenance studies on Cretaceous and Tertiary strata in the Greenland-Faroe-Shetland region addressing the link between East Greenlandic and Faroese sediments are relatively sparse (e.g. Whitham & Morton 2001; Morton & Whitham 2002; Pickles & Sherlock 2002; Whitham et al. 2004,). Furthermore, these studies (based on provenance sensitive heavy mineral ratios (Morton & Whitham, 2002), $^{40}Ar/^{39}Ar$ dating of detrital micas (Pickles & Sherlock 2002) and U-Pb dating of zircons (Whitham et al. 2004)) have not conclusively established whether there is a link between the two regions.

The seven contributions presented in this volume summarise the results obtained in the research project “Linking the Faroese area and Greenland: an innovative, integrated provenance study” jointly conducted by the Geological Survey of Denmark and Greenland (GEUS) and the Cambridge Arctic Shelf Programme (CASP). This project forms a part of the SINDRI programme (Future Exploration Issues Programme of the Faroese Continental Shelf established by the Faroese Ministry of Petroleum) and was funded by the SINDRI group. The current licensees of the SINDRI group are: Agip Denmark BV, Amerada Hess (Faroes) Ltd., Anadarko Faroes Company, P/F Atlantic Petroleum, BP Amoco Exploration Faroes Ltd., British Gas International BV, DONG Føroyar P/F, Enterprise Oil Exploration Ltd., Føroya Kolvetni P/F, Petro-Canada Faroes GmbH, Phillips Petroleum Europe Exploration Ltd., Shell (UK) Ltd., and Statoil Færøyene AS.

The aim of this project was to improve our understanding of the link between the Faroese area and East Greenland using a modern, multianalysis approach. To this end, a plethora of data based on conventional and novel provenance analysis techniques have been acquired for a wide range of samples including sediments from wells and outcrops in three main areas comprising: (1) Cretaceous, Paleocene and Eocene sediments from outcrops in the Kangerlussuaq region; (2) cuttings from wells in the UK sector of the Faroe-Shetland region; and (3) samples from outcrops on the Orkney Islands. The geographical position of the investigated areas is illustrated in Fig. 1. All samples investigated in this study are reported in Table 1 in Appendix B (including locality, stratigraphic position and types of analy-

sis). Preliminary results based on a limited data base have already been published by Whitham et al. (2004) and Frei et al. (2005a).

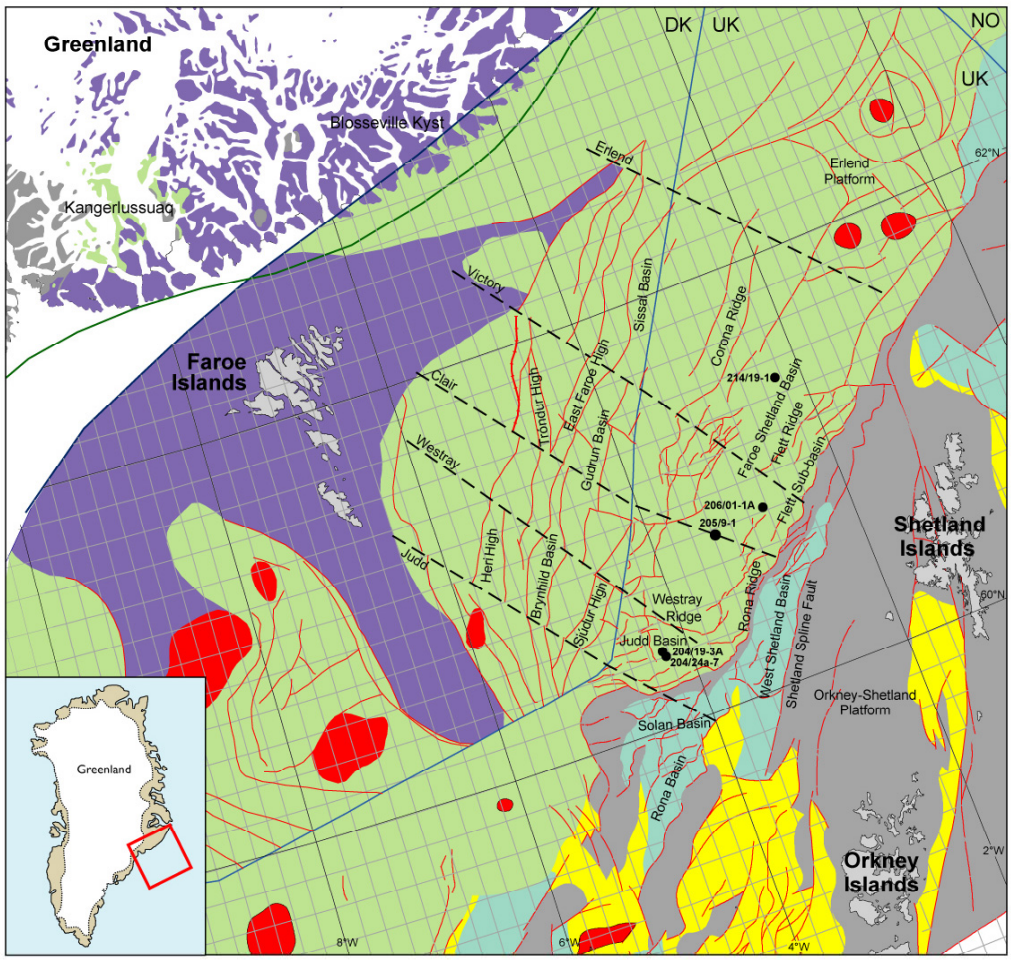

Figure 1. *Location map of East Greenland and the Faroe-Shetland region depicting the geographical position of the areas investigated in this study. Also shown are on- and offshore geology, main structural elements, transfer zones and position of the wells investigated in this study. Note that the position of Greenland is shown prior to Paleogene seafloor spreading (modified from Larsen et al. 2005).*

In the first contribution of this volume, Morton et al. (2005) present the results of a detailed provenance study based on conventional petrographic and mineral chemical techniques applied to samples of all three regions. This study establishes an excellent framework for the interpretation of the source characteristics of sediments in the Kangerlussuaq area and the UK sector of the Faroe-Shetland Basin.

A major goal of this project was to develop, test and refine new and relatively inexpensive techniques of general interest to hydrocarbon exploration, especially analysis of the frequency and chemistry of heavy minerals by computer controlled scanning electron microscopy (CCSEM) and zircon dating by laser ablation – inductively coupled plasma – mass spectrometry (LA-ICP-MS). The results of these studies are presented in three contributions by Frei et al. (2005b, 2005c, and 2005d).

The quantitative and qualitative analysis of the age distributions of detrital zircon populations is undoubtly one of the most powerful tools available for sedimentary provenance studies. In the past, the full potential that detrital zircon age distributions may offer for provenance studies has not been realised. This is mainly due to the high costs involved with SHRIMP/SIMS analysis of the large number of grains necessary to detect all age components with sufficient confidence. During the last decade, LA-ICP-MS has been established as an inexpensive alternative to SHRIMP/SIMS, and the application of new state-of-the-art equipment allows the determination of zircon ages with precision and accuracy comparable to those of SHRIMP/SIMS. Frei et al. (2005e) describe the constraints on sediment provenance in the Kangerlussuaq area and the UK sector of the Faroe-Shetland Basin based on more than 4000 individual zircon LA-ICP-MS age determinations.

The variation in major element geochemistry of garnet has been proved over the last decade to be a very useful provenance indicator, mainly by the pioneering work of Morton and co-workers. The enormous progress in the development of LA-ICP-MS techniques for the determination of a wide range of geochemically important trace elements in *in-situ* in minerals has made it feasible to explore the trace element variation in garnet for fingerprinting their source region. In the course of this project, > 2500 hand-picked garnets have been analysed for their major and trace element contents. The contribution by Frei et al. (2005f) briefly evaluates the potential of the trace element signatures to constraint the sources of detrital garnets. Finally, Knudsen (2005) describes the major and trace element chemostratigraphy of sediments from Kangerlussuaq and wells in the UK sector of the Faroe-Shetland Basin and its use for the correlation of sedimentary successions.

References

Frei, D., Rasmussen, T., Knudsen, C., Larsen, M., Whitham, A.G., Morton, A. C. 2005a: New methods and techniques for innovative, integrated provenance studies. Annales Societatis Færoensis, Supplementum **43**, 96-108.

Frei, D., Frei, M., Hansen Klünder, M., Rasmussen, T., Knudsen, C., Morton, A.C., Whitham, A.G. 2005b: Evaluation of novel analytical techniques for provenance studies I: CCSEM. Danmarks og Grønlands Geologiske Undersøgelse Rapport **2005/54** *(this volume).*

Frei, M., Frei, D., Rasmussen, T., Knudsen, C., Morton, A.C., Whitham, A.G. 2005c: Evaluation of novel analytical techniques for provenance studies II: U-Th age dating of detrital zircons using LA-ICP-MS techniques. Danmarks og Grønlands Geologiske Undersøgelse Rapport **2005/54** *(this volume).*

Frei, D., Frei, M., Hansen Klünder, M., Rasmussen, T., Knudsen, C. 2005d: Heavy mineral characteristics of Cretaceous-Eocene sandstones in the Kangerlussuaq Basin, East Greenland – results from CCSEM. Danmarks og Grønlands Geologiske Undersøgelse Rapport **2005/54** *(this volume).*

Frei, D., Rasmussen, T., Frei, M., Knudsen, C., Larsen, M. 2005e: Detrital zircon age constraints on provenance of Paleocene-Eocene sandstones in the Faroe-Shetland Basin. Danmarks og Grønlands Geologiske Undersøgelse Rapport **2005/54** *(this volume).*

Frei, M., Frei, D., Hansen Klünder, M., Rasmussen, T. Knudsen, C., 2005f: Trace element geochemistry of detrital garnets – a useful provenance indicator? Danmarks og Grønlands Geologiske Undersøgelse Rapport **2005/54** *(this volume).*

Knudsen, C. 2005: Chemostratigraphy and chemical characteristics of Cretaceous-Paleocene-Eocene sandstones and mudstones in the Kangerlussuaq area, East Greenland, and in the Faroe-Shetland Basin. Danmarks og Grønlands Geologiske Undersøgelse Rapport **2005/54** *(this volume).*

Larsen, M., Nøhr-Hansen, H., Whitham, A.G., Kelly, S.R.A. 2005: Stratigraphy of the prebasaltic sedimentary succession of the Kangerlussuaq Basin. Volcanic basins of the North Atlantic. Danmarks og Grønlands Geologiske Undersøgelse Rapport **2005/62**.

Morton, A.C., Whitham, A.G. 2002: A provenance study of Aptian-Eocene sandstones from the Kangerlussuaq region, SE Greenland - II. CASP East Greenland Series, Greenland Faroe Provenance Project Report **2**.

Morton, A.C., Hallsworth, C.R., Whitham, A. G. 2005: Heavy mineral provenance of Paleocene-Eocene sandstones in the Faroe-Shetland Basin – results from conventional petrographic and mineral-chemical techniques. Danmarks og Grønlands Geologiske Undersøgelse Rapport **2005/54** *(this volume).*

Pickles, C.S. and Sherlock, S. 2002: Late Cretaceous-Paleocene cross rift sediment transported from Greenland to the Faroe-Shetland region identified by $^{40}Ar/^{39}Ar$ dating of white micas. CASP East Greenland Series, unpublished report, pp 62.

Whitham, A.G. and Morton, A.C. 2001: Insights into Paleocene sediment transport paths and basin evolution in the North Atlantic from a heavy mineral study of sandstones from southern East Greenland. Palaeogene Stratigraphy, Tectonis and Petroleum. Geology of North West Europe, 18. – 19. September 2001, Programme and Abstracts.

Whitham, A.G., Morton, A.C., Fanning, C.M. 2004: Insights into Paleocene sediment transport paths and basin evolution in the North Atlantic from a heavy mineral study of sandstones from southern East Greenland. Petroleum Geoscience **10**, 61-72.

Heavy mineral provenance of Paleocene-Eocene sandstones in the Faroe-Shetland Basin – results from conventional petrographic and mineral-chemical techniques

Andrew C. Morton[1], Claire Hallsworth[1], Andrew G. Whitham[2]

[1]HM Research Associates, 100 Main Street, Woodhouse Eaves, Leicestershire, LE12 8RZ, UK
[2]CASP, Dept. of Earth Sciences, University of Cambridge, West Building, 181a Huntingdon Road, Cambridge, CB3 ODH, UK

Introduction

This contribution presents the present state of knowledge of heavy mineral provenance of Paleocene-Eocene sandstones in the Faroe-Shetland Basin. The information presented herein includes new data acquired during the SINDRI programme, together with a synthesis of published heavy mineral data and released but, as yet, unpublished data. The rationale involved in the application of heavy mineral analysis for provenance and correlation studies of sandstones is discussed in the Appendix, together with details of analytical methods.

The new data acquired during the SINDRI project “Linking the Faroese and Greenland: an innovative, integrated provenance study” fall into three parts. Most of the new data are from Cretaceous - Eocene sandstone samples from outcrops in the Kangerlussuaq area of East Greenland (Tables 1 and 2), and supplement two previous batches of data from the same area, one published by Whitham et al. (2004) and one included in an unpublished CASP report (Morton and Whitham 2002).

The second set of data is from the Devonian Old Red Sandstone (ORS) of Orkney (Tables 3 and 4). These data were collected to fill a gap in knowledge of possible source materials for the Paleocene-Eocene of the Faroe-Shetland Basin. The ORS outcrops extensively over the Orkney-Shetland Platform, which forms the western margin of the Faroe-Shetland Basin, yet there are virtually no published heavy mineral data available from this succession. The only exception is the Clair Group in the Clair Field, which has been studied by Allen and Mange-Rajetzky (1992) and Morton et al. (2003). However, Allen and Mange-Rajetzky (1992) and Nichols (in press) consider the Clair Basin to be a small endorheic (internal drainage) basin. In that case, the Clair Basin would be disconnected from the main Orcadian Basin, implying a different provenance for the Devonian succession in the two basins. Heavy mineral characteristics of other potential source materials on the Orkney-Shetland Platform are comparatively well known: garnet geochemical data are available for Lewisian, Moine and Dalradian basement rocks of northern Scotland and Shetland (Morton et al. 2004), and both conventional and garnet data are available from the Triassic of the Strathmore Field (Morton et al. in press). The acquisition of the data set from the ORS of

the Orcadian Basin enables a more complete assessment of the contributions of the various potential sediment contributors on the UK margin of the Faroe-Shetland Basin.

The third batch of data is from Paleocene-Eocene sandstones recovered during hydrocarbon exploration activities in the UK sector of the Faroe-Shetland Basin (Tables 5 and 6). These data were acquired to infill gaps in regional and stratigraphic coverage in the wake of hydrocarbon industry-funded projects, which tend to concentrate on stratigraphic intervals and geographical areas that have the greatest economic interest. See Lamers and Carmichael (1999), Naylor et al. (1999) and Mudge and Bujak (2001) for details of Early Tertiary stratigraphy in the Faroe-Shetland Basin. The published heavy mineral data from the Paleocene of the Foinaven sub-basin, located in the southern part of the Faroe-Shetland Basin (Morton et al. 2002), concentrate on the earlier part of the interval (Vaila and Sullom Formations), with little or no coverage of the overlying Lamba and Flett Formations. The new data from this region therefore aimed to extend the stratigraphic coverage to these younger intervals. Data have also been acquired during industry-funded projects on the Flett sub-basin, further to the north, but these have not yet been published. However, since permission to publish has been given in principle, the data from this area are also discussed herein. As with the Foinaven sub-basin, the existing data are from the earlier part of the Paleocene (Vaila Formation). The new data therefore concentrate on the younger Lamba and Flett Formations, although data have also been acquired from the Vaila Formation in well 214/19-1 in order to extend the geographic coverage of the heavy mineral data set.

Most of the new data collected in this study are from conventional (petrographic) analysis, although a limited number of garnet populations have been characterised by electron microprobe. Garnet data are interpreted using the framework acquired during river sediment studies of Scotland and Norway (Morton et al. 2004), in which three main types of garnet assemblages were recognised. Type A garnets (low Ca, high Mg) are believed to be derived from high-grade granulite facies metasediments or charnockites; Type C garnets (high Ca, high Mg) are from metabasic rocks; and Type B garnets (low Mg, variable Ca and Mn) are predominantly from low- to medium-grade metasediments, although garnets derived from intermediate-acidic gneisses and granites would also fall into this field. The type A field has been further subdivided into Ai (X_{Mg} < 30 %) and Aii (X_{Mg} = 20-30 %) following the recognition of differences in the relative abundance of these two subtypes in Paleocene sandstones of the Flett sub-basin (see below).

Kangerlussuaq region

Summary of existing data

In previous studies of the Cretaceous-Tertiary succession of Kangerlussuaq, three distinct heavy mineral stratigraphic units have been recognised. Rutile:zircon (RuZi) and apatite:tourmaline (ATi) ratios proved to be the most useful conventional heavy mineral parameters for interpretation of provenance in the Cretaceous-Early Eocene succession in Kangerlussuaq, with subsidiary support from garnet compositions and zircon U-Pb isotopic data. The use of garnet:zircon (GZi) and garnet compositional data is hampered by postde-

positional diagenetic activity, which has caused variable lowering of GZi and modification of garnet compositional ranges through garnet dissolution. However, there are significant variations in the stable (low Ca) component of the garnet populations (X_{Ca} < 10 %), particularly in the abundance of type Ai (low-Ca garnets with X_{Mg} > 30 %). Variations in provenance can therefore be evaluated using ATi - RuZi and RuZi - % type Ai garnet plots (Figs 1 and 2).

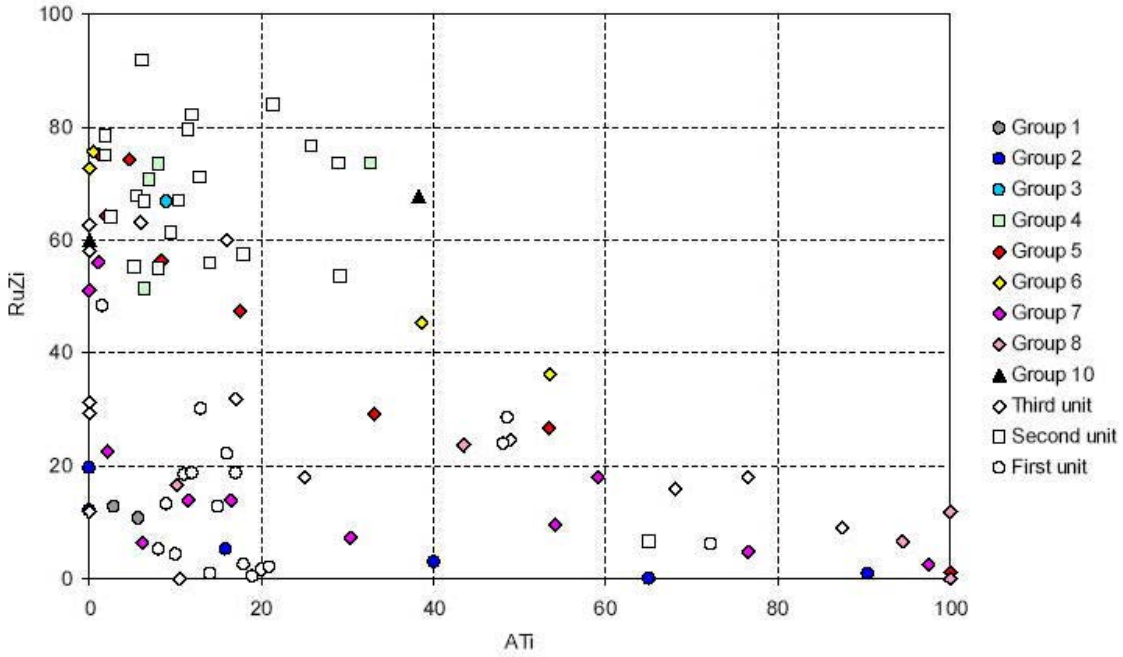

Figure 1. *RuZi – ATi plot comparing Cretaceous-Tertiary sandstones of the Kangerlussuaq area. First, second and third units are as defined by Whitham et al. (2004). Groups 1-10 refer to stratigraphic assignations of samples analysed during the SINDRI project: see text for further information.*

The three units have been informally termed 'first unit', 'second unit' and 'third unit' (Whitham et al. 2004). The first unit, which covers the Aptian-Late Coniacian, is characterised by relatively low RuZi, which is <30 in all samples except P5490 (Turonian). ATi values are generally low (mostly <20), but a small number of samples have higher values (up to c. 70). Type Ai garnets are scarce (even in sample P5490, which has anomalously high RuZi). Zircons from a typical sample (W4629, Albian) show that sand was supplied almost exclusively from Archaean basement, and local sourcing is therefore envisaged.

The second unit (Campanian-Maastrichtian) contains sandstones with high RuZi (>50) and low ATi (<30), conspicuous chloritoid, and garnet populations with abundant type Ai garnets. The zircon population is diverse, dominated by Proterozoic grains (covering a wide range from 1000-2000 Ma), with comparatively few Archaean and a small but significant group of Early Paleozoic (Caledonian-age) grains. The high RuZi, the presence of chloritoid, and the high-Mg garnet assemblages indicate that these sandstones were derived from a source area comprising widespread metasedimentary rocks, including some at high metamorphic grade (granulite facies). The presence of Grenvillian (c. 1000 Ma) and Caledonian zircons requires a source to the north or northeast, since the area to the south was

not affected by either of these orogenic events (Escher and Pulvertaft 1995). The most likely source of the sediment in the second unit is therefore considered to be Proterozoic metasediments such as the Krummedal succession or the Eleanore Bay Supergroup.

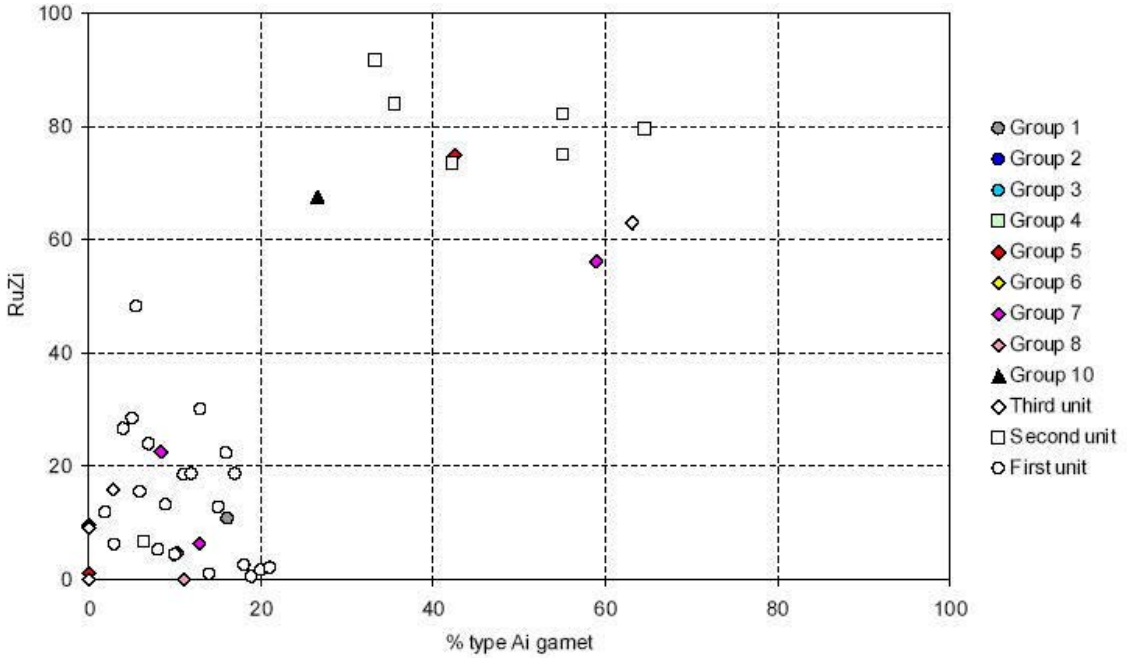

Figure 2. *RuZi – % type Ai garnet plot comparing Cretaceous-Tertiary sandstones of the Kangerlussuaq area. Type Ai garnets have X_{Mg} > 30% and X_{Ca} <10% First, Second and Third units are as defined by Whitham et al. (2004). Groups 1- 10 refer to stratigraphic assignations of samples analysed during the SINDRI project: see text for further information.*

One sample from the second unit (K10343) has anomalous mineralogy, with low RuZi, high ATi, and low abundances of type Ai garnet (Figs 1-2). This sample plots within the range shown by typical sandstones from the first unit, and is interpreted as having a local provenance. The data from K10343 therefore shows that although the vast majority of sandstones in second unit were not locally derived, local Archaean basement continued to play a significant role in sediment sourcing.

The third unit (Early Eocene) is dominated by sandstones similar to those of the first unit, with low RuZi (<30), variable ATi (0-88), and garnet assemblages with low abundances of type Ai (Figs 1-2). Zircon ages were determined from one Early Eocene sample (P5219) with these mineralogical characteristics, confirming a return to predominantly local sourcing from Archaean basement. However, some samples from this unit have mineralogical characteristics akin to those of the second unit, implying that supply from metasedimentary sources to the north or northeast continued to take place at this time. A small number of Early Eocene sandstones from J C Jacobsens Fjord (P5216, P5224, P5225) have different characteristics, with high RuZi (62-70), moderate ATi (45-52), and garnet assemblages dominated by high Ca types with variable Mg, indicating supply from basic gneisses. This subgroup probably represents sediment derived from local basic gneisses within the adjacent Archaean.

The three heavy mineral stratigraphic units are separated by two major unconformities, one spanning the Late Coniacian to Late Campanian interval, and the other spanning the Late Maastrichtian to Early Eocene interval. Rifting during the deposition of the first unit (Aptian-Late Coniacian) led to rift flank uplift and resulted in the local sourcing of sediment. Thermal subsidence during the deposition of the second unit (Late Campanian-Late Maastrichtian) led to rift flank subsidence and sediment sourcing from outside the immediate region. Renewed rifting immediately preceding the third unit (Early Eocene) resulted in a return to local sediment sourcing (Whitham et al. 2004).

New data

The samples analysed during the SINDRI project have been assigned to 10 stratigraphic groups, as follows:

Group 1: Early Cretaceous, pre-volcanic, Watkins Fjord Fm., Torsukáttak Mb., fluvial.
Group 2: Early Cretaceous, pre-volcanic, Watkins Fjord Fm., Suunigajik Mb., shallow marine.
Group 3: Early Cretaceous, pre-volcanic, Sorgenfri Fm., shelf.
Group 4: Late Cretaceous, pre-volcanic, Christian IV Fm. ('Lower Ryberg'), shelf.
Group 5: Early Paleocene, pre-volcanic, Sediment Bjerge Fm., Fairy Tale Valley Mb., ('Upper Ryberg'), deep marine.
Group 6: Late Paleocene, pre-volcanic, Sediment Bjerge Fm., Klitterhorn Mb. ('Upper Ryberg'), deltaic.
Group 7: Late Paleocene, pre/syn-volcanic, Vandfaldsdalen Fm., Schjelderup Mb. ('Ryberg Sandstone Bed' *s. s.)*, fluvial.
Group 8: Paleocene-Eocene, syn-volcanic, Vandfaldsdalen Fm., Willow Pass Mb., fluvial.
Group 9: Paleocene-Eocene, syn-volcanic, Vandfaldsdalen Fm., Kulhøje Mb., intra basalt layer.
Group 10: Eocene, post-volcanic, Bopladsdalen Fm., Kap Dalton, Savoia Halvø, post-basalt, (outside the Kangerlussuaq Basin).

The heavy mineral data (Tables 1-2) are closely comparable to those acquired in previous studies of the area, with a large number of minerals identified and major variations in relative mineral abundance. The most abundant phases overall are zircon (mean 38 %), garnet (mean 16 %) rutile (mean 16 %), epidote (mean 11 %), apatite (mean 6 %) and tourmaline (mean 5 %). All these minerals show wide variations in abundance (zircon <0.5 % - 89 %, garnet 0 % - 77 %, rutile 0 % - 63 %, epidote 0 % - 91 %, apatite 0 % - 78 %, tourmaline 0 % - 36 %). Other minerals that occur in significant amounts are clinopyroxene, which forms over 90 % of the assemblage in two samples, and calcic amphibole, which forms up to 15 %.

The large variations seen within the data are the result of several factors, including differences in provenance, differences in the extent of weathering during the sedimentation cycle, variations in hydraulic conditions at the time of deposition, and the extent of postdepositional diagenetic modification. Other than provenance, the most significant factor is diagenesis, which has removed unstable minerals (clinopyroxene, amphibole, epidote, ti-

tanite, kyanite, staurolite and garnet in increasing order of stability) to varying degrees. The effects of diagenetic modification, and the effects of variable hydrodynamic conditions, are eliminated by the use of provenance-sensitive ratio parameters and mineral chemical data. As discussed above, the most useful parameters are rutile:zircon (RuZi) and apatite:tourmaline (ATi), together with garnet geochemical data. The use of the garnet geochemistry is limited to samples where garnet has not been entirely dissolved: furthermore, interpretation of garnet data relies on variations in the stable (low Ca) component of the garnet populations (X_{Ca} < 10 %), since high-Ca garnets are selectively removed during diagenesis due to their relative instability (Morton 1987, Morton and Hallsworth in press). Variations in provenance within the new data set have therefore been evaluated using ATi - RuZi and RuZi - % type Ai garnet plots, and are compared with existing data in Figs 1 and 2. Garnet ternary plots for samples analysed during the SINDRI project as shown in Fig. 3.

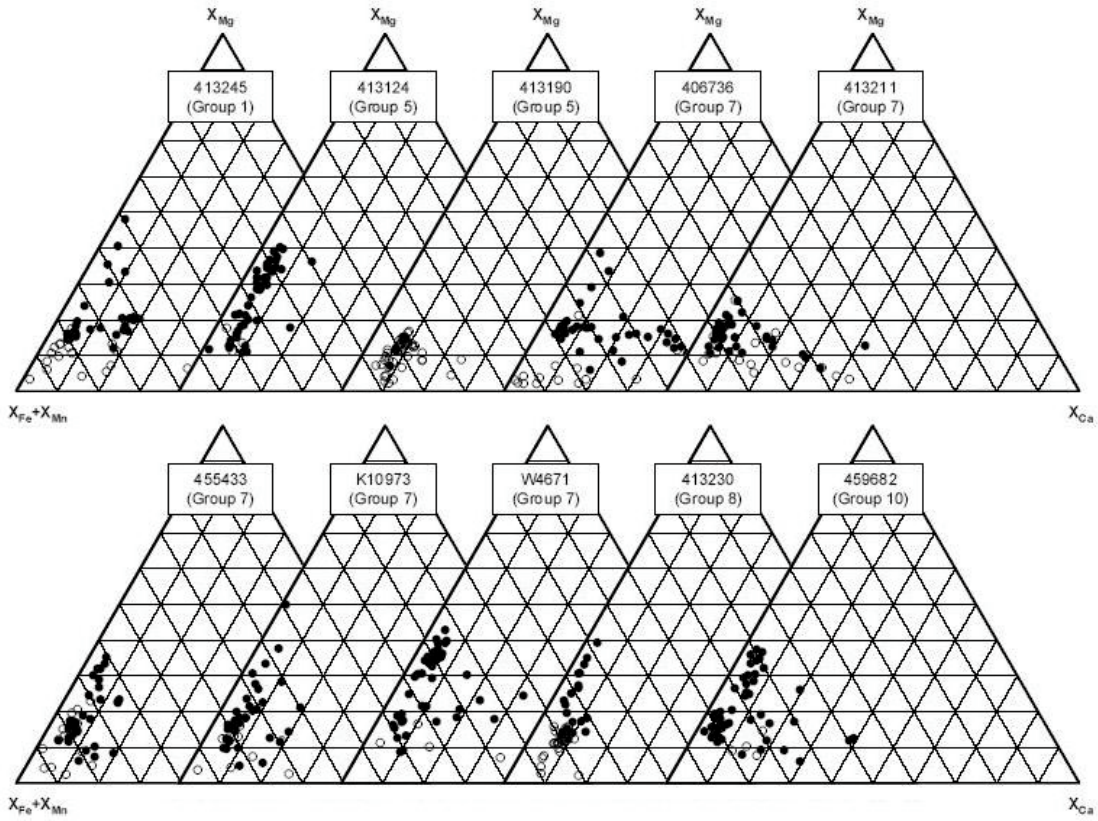

Figure 3. *Garnet compositions in samples from Kangerlussuaq analysed duing the SINDRI project. X_{Fe}, X_{Mg}, X_{Ca}, X_{Mn} = molecular proportions of Fe, Mg, Ca and Mn. All Fe calculated as Fe^{2+}. Solid symbols = X_{Mn} < 5%. Open symbols = X_{Mn} > 5%.*

Group 1 samples (Watkins Fjord Fm., Torsukáttak Mb, Early Cretaceous, fluvial) have low RuZi, low ATi, and low abundances of high-Mg garnet (Figs 1 and 2). They therefore fall within the cluster previously defined by Early Cretaceous samples, and local sourcing from Archaean basement is inferred.

All the Group 2 samples (Watkins Fjord Fm., Suunigajik Mb, Early Cretaceous, shallow marine) have low RuZi similar to Group 1, but have a wider range of ATi values, up to c. 90.

They are therefore interpreted as being largely derived from local Archaean basement, although this has not been tested by garnet geochemical analysis. The wider range of ATi indicates that weathering during the sedimentation cycle was less prolonged or intensive than for the fluvial Group 1 sample. This suggests shorter fluvial transport, consistent with the shallow marine depositional environment.

The single Group 3 sample (413270, Sorgenfri Fm., Early Cretaceous, shelf) has anomalously high RuZi compared with the other Early Cretaceous samples. Garnet geochemistry was not undertaken on this sample, although it would be possible to undertake microprobe analysis since garnet has not been thoroughly depleted. The data suggest either that the northern/northeastern provenance supplied sediment to the Kangerlussuaq area at an earlier stage than was previously recognised, or it was derived from local Archaean with unusually high RuZi.

All the Group 4 samples (Christian IV Fm., 'Lower Ryberg', Late Cretaceous, shelf) have high RuZi and low ATi. None of the samples have sufficient garnet to enable mineral chemical calibration. The available data therefore indicate sediment was supplied from the distal northern/northeastern source, in common with samples analysed during previous studies of the area.

The Group 5 samples (Sediment Bjerge Fm., Fairy Tale Valley Mb., 'Upper Ryberg', Early Paleocene, deep marine) show a wide range in composition. Five of the samples (412778, 413123, 413124, 413143, W4768) have high RuZi and low ATi, and garnet data on one of these four (413124) shows the presence of abundant high-Mg garnet. These samples were therefore supplied by the northern/northeastern source. However, it is possible that they were reworked from the Christian IV Fm rather than representing direct supply from the distal source. Another sample (413190) has very low RuZi, high ATi, and lacks type Ai garnet, and appears to have local Archaean basement sourcing. The other two Group 5 samples (412773, 413276) have moderate RuZi and moderate ATi. They fall within the overall range of sediment supplied by the local Archaean basement, but it is possible that they represent a mixture of locally-derived basement and more distally-sourced detritus, the latter probably having been reworked from the Christian IV Fm.

The Group 6 samples (Sediment Bjerge Fm., Klitterhorn Member, 'Upper Ryberg', Late Paleocene, deltaic) show the same pattern as the Group 5 samples. Two samples (413146, 455499) have high RuZi and low ATi, suggesting a northern/northeastern provenance. One sample (412725) has low RuZi and high ATi (not plotted on Fig. 1 because of a low count for the ATi determination), suggesting local Archaean basement sourcing. The other two samples (455423, 455537) have intermediate ATi and RuZi values that suggest they may have a mixed provenance.

Most of the Group 7 samples (Vandfaldsdalen Fm., Schjelderup Mb, 'Ryberg Sandstone Bed' *sensu stricto*, Late Paleocene, fluvial) have low RuZi, variable ATi and scarce high-Mg garnets. A local Archaean basement source is therefore indicated. However, two samples (455516, W4671) have high RuZi, and W4671 contains common type Ai garnets. These two samples therefore appear to have been supplied from the northern/northeastern source. Given that W4671 rests immediately above the Christian IV Fm, it seems most

likely that these anomalous samples originated by reworking, rather than being supplied directly from the northern/northeastern source.

All the Group 8 samples (Vandfaldsdalen Fm., Willow Pass Mb, Late Paleocene, fluvial) have low RuZi. ATi values are variable, several being very high (>90). Where data are available, type Ai garnets are scarce. Local Archaean basement sourcing is implied. One sample (455613) is dominated by clinopyroxene, indicating that basic igneous rocks formed a major component of the hinterland.

Only one Group 9 sample (Vandfaldsdalen Fm., intra basalt layer, Paleocene-Eocene) was included in the sample set. Recovery of detrital non-opaque heavy minerals was poor from this sample, precluding accurate determination of ratio values, and consequently the sample is not plotted on Figs 1 and 2. The ATi value is high (79), and RuZi values appear to be low, and a local Archaean basement sourcing is tentatively proposed.

The three Group 10 samples (Bopladsdalen Fm., Kap Dalton, Savoia Halvø, post-basalt, Eocene) have high RuZi and low-moderate ATi, suggesting derivation from the northern/northeastern source. This is supported by the presence of common type Ai garnets in sample 459682. One sample (459717) has very high abundances of clinopyroxene and chrome spinel (CZi = 49.4), both features consistent with derivation from the immediately preceding basic volcanic rock succession.

Old red sandstone

The Devonian Old Red Sandstone (ORS) is widespread over the Orkney-Shetland Platform, which forms the eastern margin of the Faroe-Shetland Basin. The ORS is therefore a significant potential sediment source for the Paleocene of the Faroe-Shetland Basin. However, there are no modern heavy mineral data from this succession to use for comparison with the data from the basinal areas. This has been rectified as part of the SINDRI project, with 32 samples of the ORS succession on Orkney having been analysed (Tables 3 and 4).

The samples cover the Yesnaby and Harra Ebb Ssts, Eday Group (Passage Beds, Lower Eday Sst, Eday Flags, Middle Eday Sst, Upper Eday Sst), and the Hoy Sst (Fig. 4). According to Trewin and Thirlwall (2002), the Yesnaby and Harra Ebb Ssts belong to the Lower ORS, the Eday Group belongs to the Middle ORS, and the Hoy Sst belongs to the Upper ORS. However, Marshall and Hewitt (2003) consider that the Hoy Sst is the lateral equivalent of the Eday succession, with the two being deposited by separate river systems, one (depositing the Eday succession) coming in from the north and the other (depositing the Hoy Sst) from the west (Marshall, pers. comm.).

The ORS on Orkney is characterised by low-diversity heavy mineral assemblages. Only ten species have been recognised, and three of these (calcic amphibole, clinopyroxene and garnet) are extremely scarce. Two species, apatite and zircon, form the large majority of the assemblages, mean apatite and zircon contents being 32.6 % and 55.7 % respectively. Of the other minerals, mean rutile and tourmaline contents are 4.6 % and 5.5 %: anatase, chrome spinel and monazite are comparatively scarce. The low diversity of the assem-

blages, and the fact that all the minerals present in significant amounts are stable during burial diagenesis (Morton and Hallsworth, in press), indicates that the succession has experienced advanced burial diagenetic conditions, which has caused virtually complete dissolution of all unstable species. High-temperature pore waters (>80°C) are believed to be responsible for garnet dissolution (Hansley, 1987), implying that the ORS sandstones on Orkney were flushed by pore waters of at least this temperature. This supports the study of thermal maturation in the Orcadian Basin by Hillier and Marshall (1992), who suggested that the succession on Orkney was subjected to temperatures exceeding 100°C. Although the heavy mineral study focussed only on Orkney, the data presented by Hillier and Marshall (1992) indicate that the same conditions extended across the Orcadian Basin from Caithness to Shetland. Consequently, the ORS is likely to contain low-diversity heavy mineral assemblages, characterised by extremely low GZi values, across the entire Orkney-Shetland Platform.

Because of the advanced burial diagenetic conditions, GZi values are without exception extremely low, and therefore fail to reveal any information on changes in provenance through the succession. MZi and CZi values are also low throughout, due to the scarcity of monazite and chrome spinel in the source regions. The only parameters to show any appreciable variation through the ORS on Orkney are the ATi and RuZi (Fig. 4). Of these, ATi is very low in the Lower ORS and in some samples of the Hoy Sst. However, in the latter case, this is an outcrop-induced feature, the samples being evidently weathered, and their original ATi values are interpreted as being high like those elsewhere in the Hoy Sst. There are some minor excursions in the ATi profile within the Eday Group that might be useful for correlation, but these are unlikely to represent significant differences in provenance. There are only minor variations in RuZi values, the succession having relatively low values throughout (Fig. 4), although some values are higher in the Eday Group. Paleogeographic reconstructions (Trewin and Thirlwall 2002) indicate that local sources were predominant during the Lower ORS, with an uplifted area to the northwest supplying sediment during the Middle and Upper ORS. There is minor heavy mineral evidence for a change in provenance at the Lower-Middle ORS boundary (change in ATi), which might correspond to the switch from local sourcing to sourcing from the northwest. There is no evidence for any change between the Eday Group and the Hoy Sst, indicating that the two have a common provenance and supporting the suggestion that the two are laterally equivalent (Marshall and Hewitt 2003).

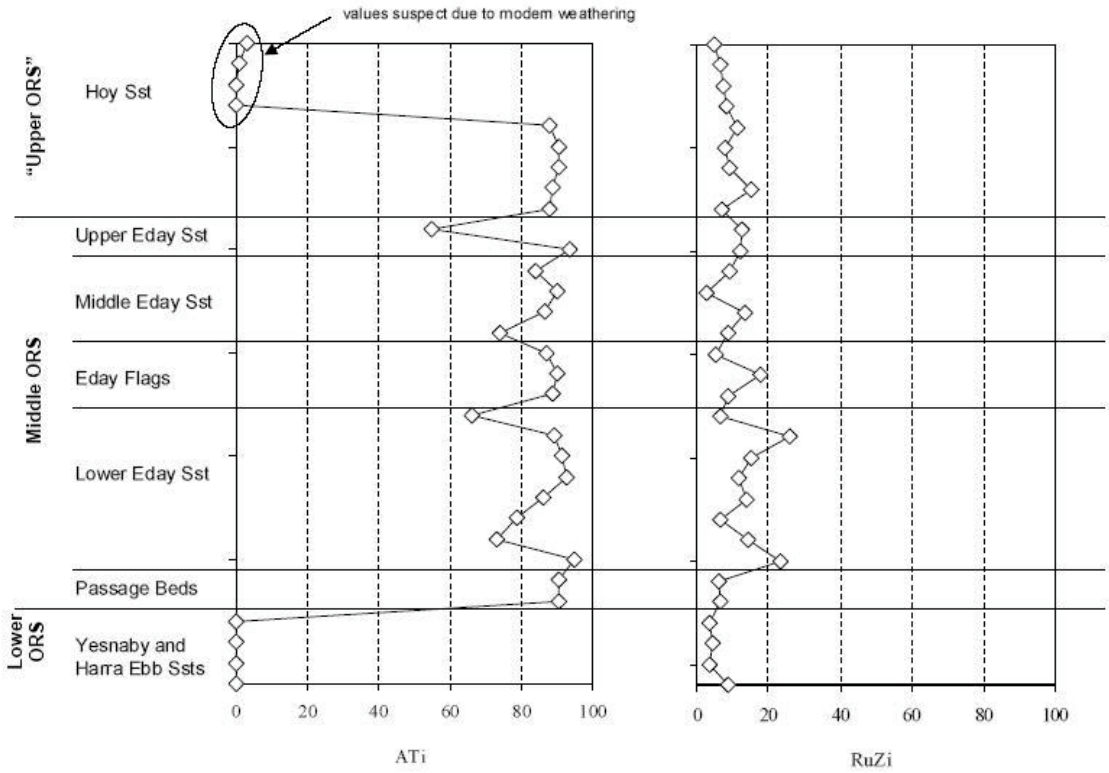

Figure 4. *Stratigraphic variations in ATi and RuZi values in the Devonian ORS succession of Orkney. Note that the stratigraphy (taken from Trewin and Thirlwell 2002) is subject to debate since the Hoy Sandstone may be Middle ORS (Marshall and Hewitt, 2003). The Y-axis shows samples in their stratigraphic order, but has no significance in terms of thickness.*

The ORS on Orkney is compared with the Clair Group succession in Fig. 5. The succession in the Clair Field has been subdivided into two major parts, the Upper Clair Group and the Lower Clair Group (Allen and Mange-Rajetzky 1992), with a major change in provenance observed at the boundary. The precise age of the succession in the Clair Field is uncertain: it is generally accepted that the top of the Lower Clair Group is Givetian (Middle ORS) on the basis of miospores, but the age of the lower part is not constrained biostratigraphically. The very top of the Upper Clair Group is Visean in age, but no evidence exists for the age of the underlying part of the Upper Clair.

The ORS on Orkney shows strong similarities with the Lower Clair Group, both successionsfalling in the same area of the ATi-RuZi crossplot (Fig. 5). There is a marked difference in GZi, but this is due to garnet dissolution in the Orkney succession. The ORS in Orkney therefore appears to have the same provenance as the Lower Clair Group, being derived from the uplifted area to the northwest. Derivation of the Lower Clair Group from the northwest is in accord with the interpretation of Nichols (in press), although it is unlikely that the Lewisian was the main contributor: metasediments of Moine/Dalradian aspect are more likely to have been predominant (Allen and Mange-Rajetzky 1992). The similarity in provenance suggests that the Clair Basin may have been connected to the main Orcadian Basin, rather than being a separate endorheic basin. The Upper Clair Group is clearly dif-

ferentiated from the Lower Clair Group on the basis of ATi, RuZi and GZi values, and has no counterpart in the succession on Orkney.

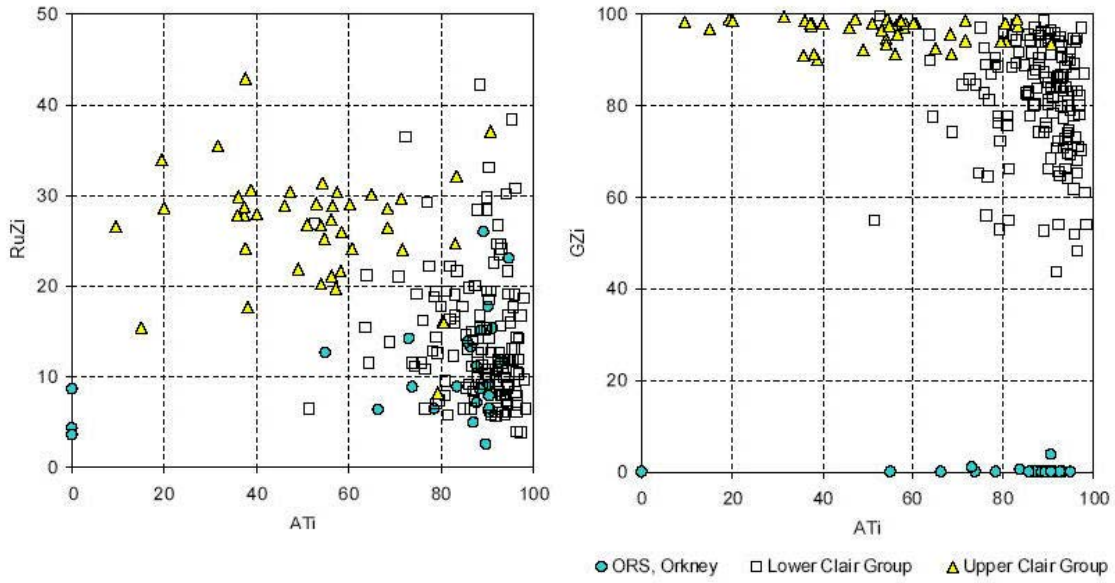

Figure 5. *Ratio crossplots comparing the Devonian succession of Orkney with sandstones from the Clair Field.*

Paleocene-Eocene, Faroe-Shetland Basin

The Paleocene-Eocene provenance patterns in the Faroe-Shetland Basin are discussed using five key wells, 204/19-3a, 204/24a-7, 205/9-1, 214/19-1 and 206/1-1a. Two of these (204/19- 3a, 204/24a-7) are in the Foinaven sub-basin and three (205/9-1, 214/19-1, 206/1-1a) in the Flett sub-basin. Wells 204/19-3a and 204/24a-7 cover the full stratigraphic range (Sullom to Flett Formations), with 205/9-1 covering the Vaila-Flett interval. Only the Vaila has been analysed in 214/19-1, and only the Flett in 206/1-1a.

Well 204/19a-3

Stratigraphic changes in key heavy mineral parameters in 204/19-3a are shown in Fig. 6, with garnet geochemical data in Figs 7 and 8. RuZi and GZi values show comparatively little change throughout, with the major changes being shown by ATi and garnet geochemistry.

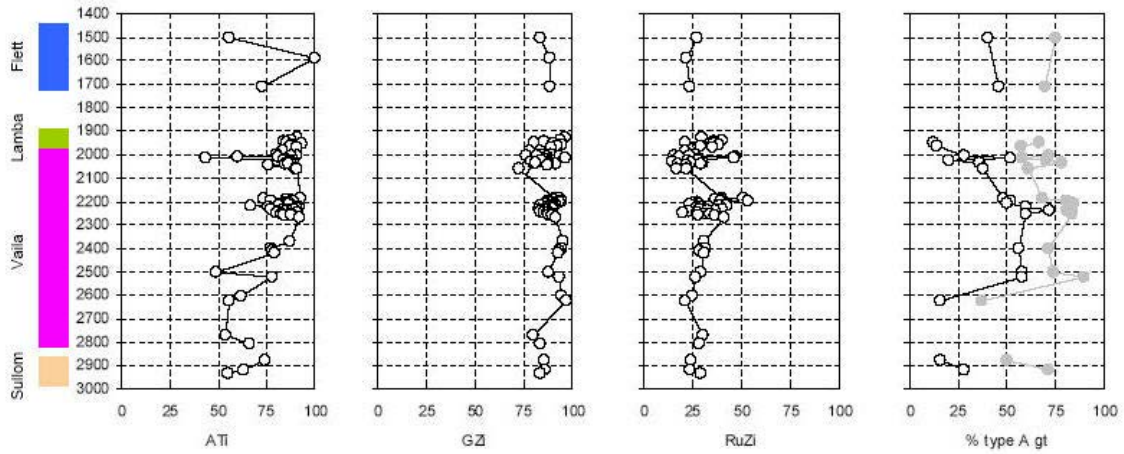

Figure 6. *Downhole variations in key mineral parameters in the Paleocene-Eocene of 204/19-3a. Grey trace on the garnet plot refers to the ratio of type Ai to type Aii garnet (Ai = low Ca garnet with X_{Mg} > 30%, Aii = low Ca garnet with X_{Mg} 20-30%).*

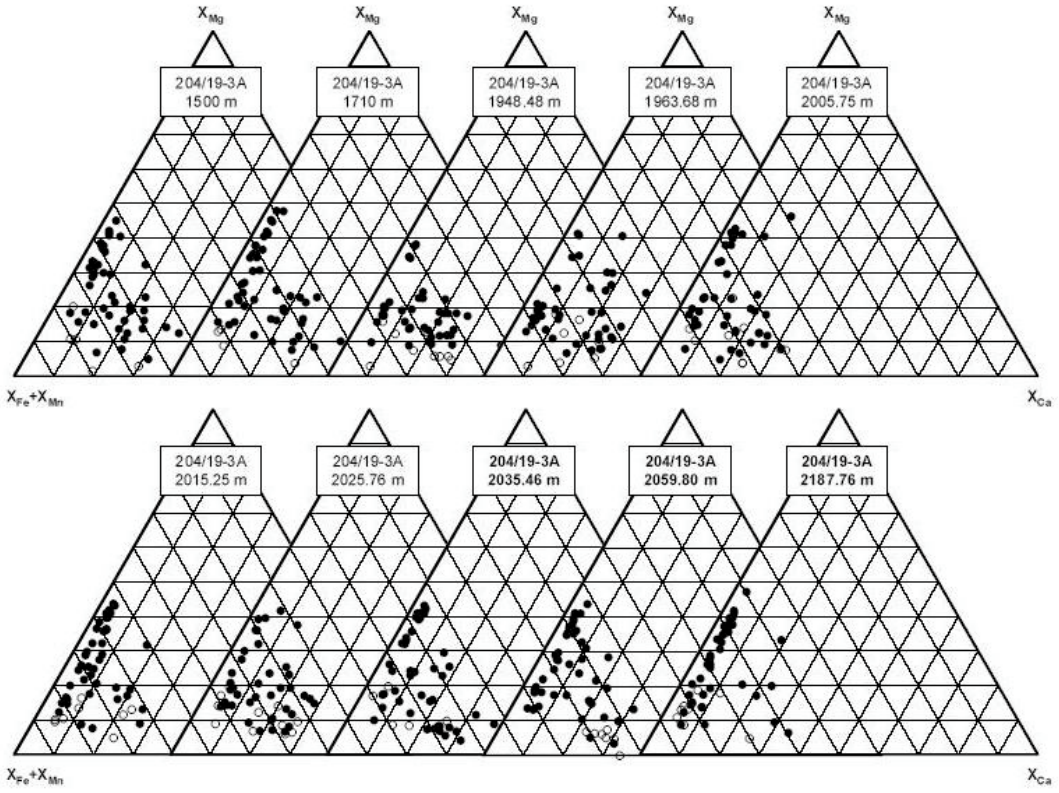

Figure 7. *Garnet compositions in samples from 204/19-3A (upper part), Foinaven sub-basin. X_{Fe}, X_{Mg}, X_{Ca}, X_{Mn} = molecular proportions of Fe, Mg, Ca and Mn. All Fe calculated as Fe^{2+}. Solid symbols = X_{Mn} < 5%. Open symbols = X_{Mn} > 5%.*

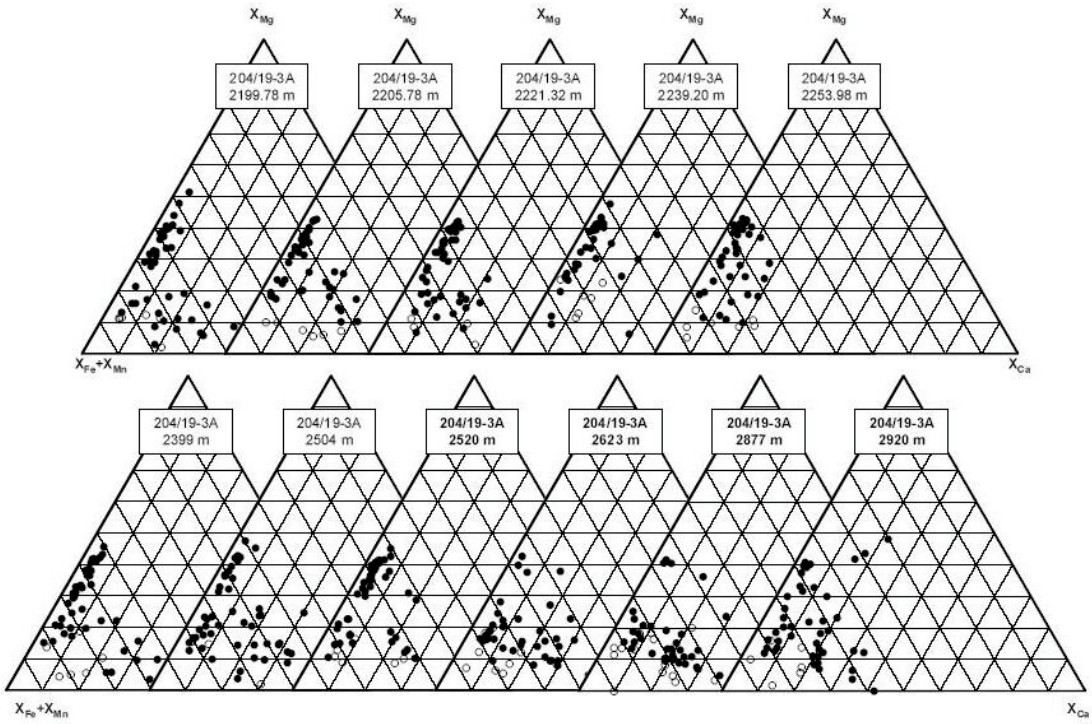

Figure 9. *Garnet compositions in samples from 204/19-3A (lower part), Foinaven sub-basin. X_{Fe}, X_{Mg}, X_{Ca}, X_{Mn} = molecular proportions of Fe, Mg, Ca and Mn. All Fe calculated as Fe^{2+}. Solid symbols = X_{Mn} < 5%. Open symbols = X_{Mn} > 5%.*

The lower part of the succession (Sullom and lower Vaila) is characterised by relatively low ATi values. Garnet assemblages at this level are rich in type B and have comparatively few types A and C. There is a change in provenance in the mid-Vaila, shown by marked increases in ATi and abundances of type A garnet. Towards the top Vaila, type A garnet abundances decline, to be replaced by predominantly type B. This trend continues into the Lamba Formation. Type A garnet reappears in abundance in the Flett Formation, with ATi values showing a distinct fall at the top of the unit.

Well 204/24a-7

Stratigraphic changes in key heavy mineral parameters in 204/24a-7 are shown in Fig. 9, with garnet geochemical data in Figs 10 and 11. The profile in 204/24a-7 is generally similar to that seen in 204/19-3a. ATi values and type A garnet abundances are low in the Sullom Formation, although ATi values are lower than in 204/19-3a, and GZi values are also distinctively low in some cases. The Vaila sandstones have high ATi and high type A

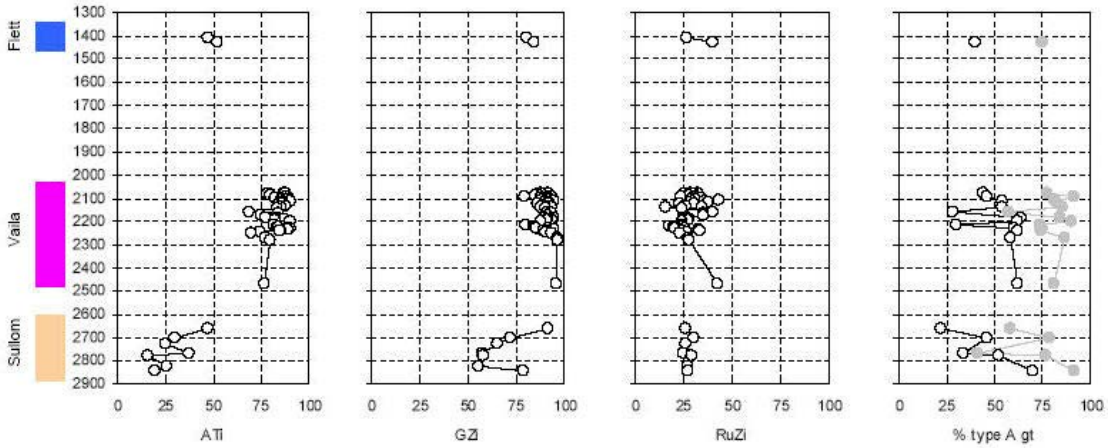

Figure 9. *Downhole variations in key mineral parameters in the Paleocene-Eocene of 204/24a-7 Grey trace on the garnet plot refers to the ratio of type Ai to type Aii garnet (Ai = low Ca garnet with X_{Mg} > 30%, Aii = low Ca garnet with X_{Mg} 20-30%).*

garnet abundances, similar to the middle part of the Vaila in 204/19-3a. The trend of decreasing type A garnets in upper part of the Vaila and the Lamba seen in 204/19-3a has not been seen in 204/24a-7, due to a lack of sand in the relevant stratigraphic interval. The Flett Formation has similar characteristics to the topmost Flett in 204/19-3a, with low ATi and moderate type A garnet abundances.

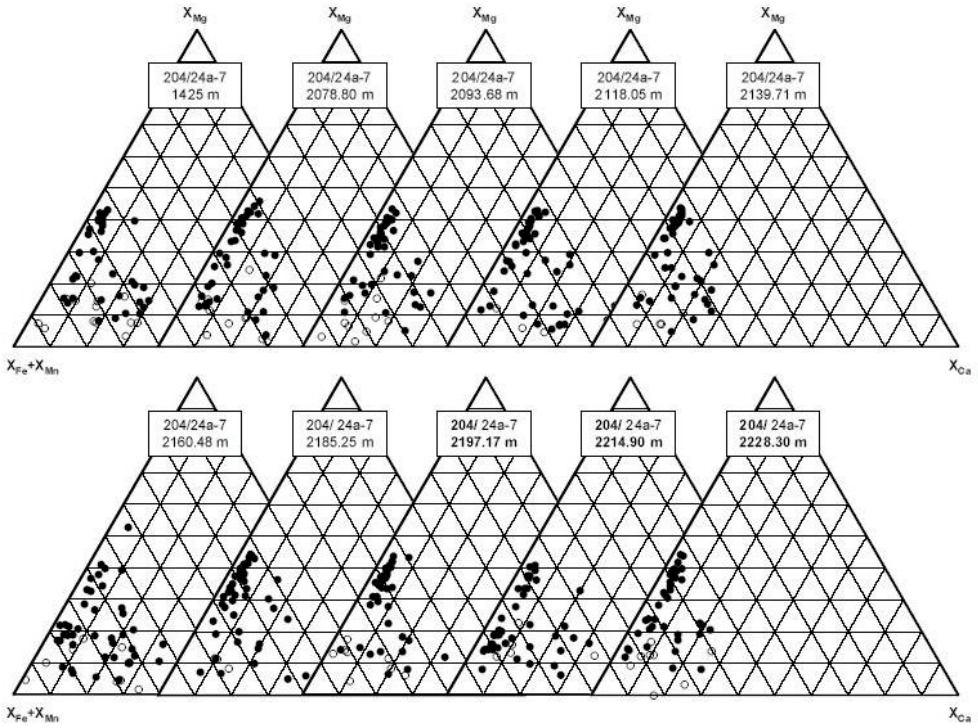

Figure 10. *Garnet compositions in samples from 204/24a-7 (upper part), Foinaven sub-basin. X_{Fe}, X_{Mg}, X_{Ca}, X_{Mn} = molecular proportions of Fe, Mg, Ca and Mn. All Fe calculated as Fe^{2+}. Solid symbols = X_{Mn} < 5%. Open symbols = X_{Mn} > 5%.*

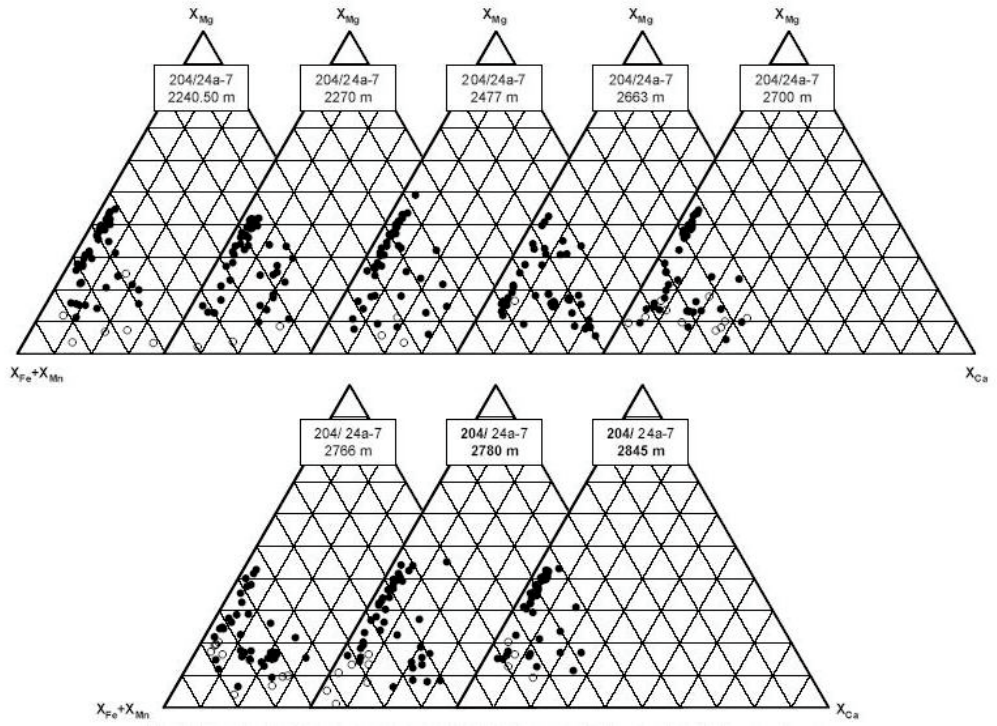

Figure 11. *Garnet compositions in samples from 204/24a-7 (lower part), Foinaven sub-basin. X_{Fe}, X_{Mg}, X_{Ca}, X_{Mn} = molecular proportions of Fe, Mg, Ca and Mn. All Fe calculated as Fe_{2+}. Solid symbols = X_{Mn} < 5%. Open symbols = X_{Mn} > 5%.*

Well 205/9-1

Stratigraphic changes in key heavy mineral parameters in 205/9-1 are shown in Fig. 12, with garnet geochemical data in Fig. 13. The profile in this well shows the existence of significant variations in the RuZi value, which is distinctively low in the Kettla Member. The sandstones in the Kettla of 205/9-1 therefore have a different provenance to the other sandstones in the well, and have no counterpart in any other samples in the Faroe-Shetland Basin analysed to date. The Kettla Member in 205/9-1 is also distinctive in that some sandstones have high abundances of clinopyroxene, indicating that basic igneous rocks were present in the source of the low-RuZi material.

The Vaila Formation has similar characteristics to the mid-Vaila in 204/19-3a and the Vaila in 204/24a-7, with high ATi, high GZi, moderate RuZi and high abundances of type A garnet. Garnet surface textures in the Vaila samples show extensive corrosion, indicating ongoing dissolution. It is known from other basins that high-Ca garnets are less stable than low-Ca garnets during deep burial (Morton 1987; Morton and Hallsworth, in press), and since the compositional range shown by the garnet population in the Vaila Formation is much more restricted than higher in the well (Fig. 13), the abundance of type A garnets has almost certainly been boosted by the effects of burial diagenesis.

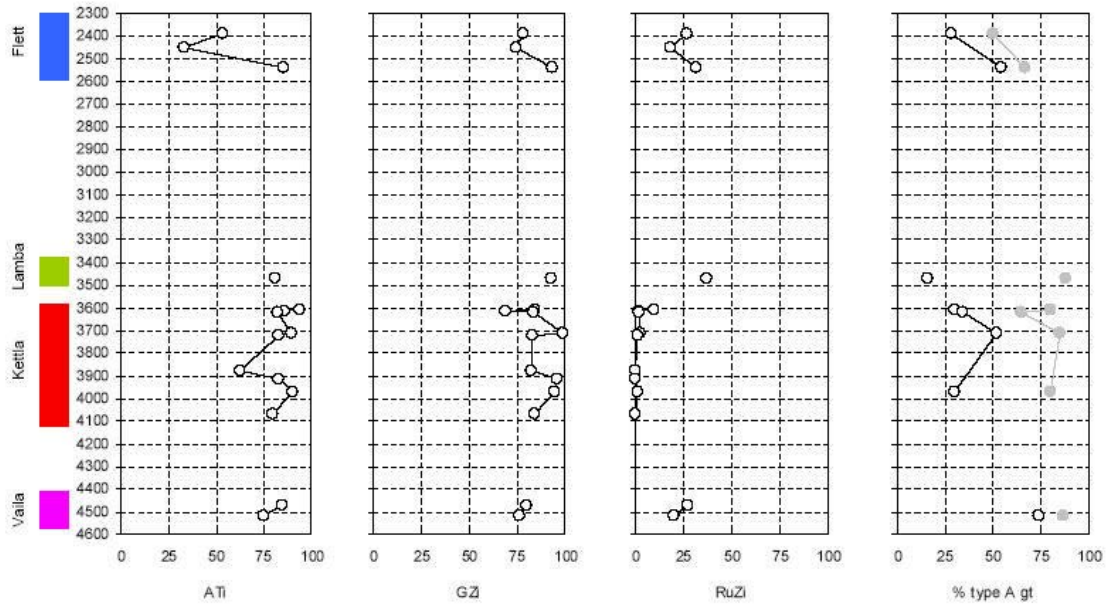

Figure 12. *Downhole variations in key mineral parameters in the Paleocene-Eocene of 205/9-1. Grey trace on the garnet plot refers to the ratio of type Ai to type Aii garnet (Ai = low Ca garnet with X_{Mg} > 30%, Aii = low Ca garnet with X_{Mg} 20-30%).*

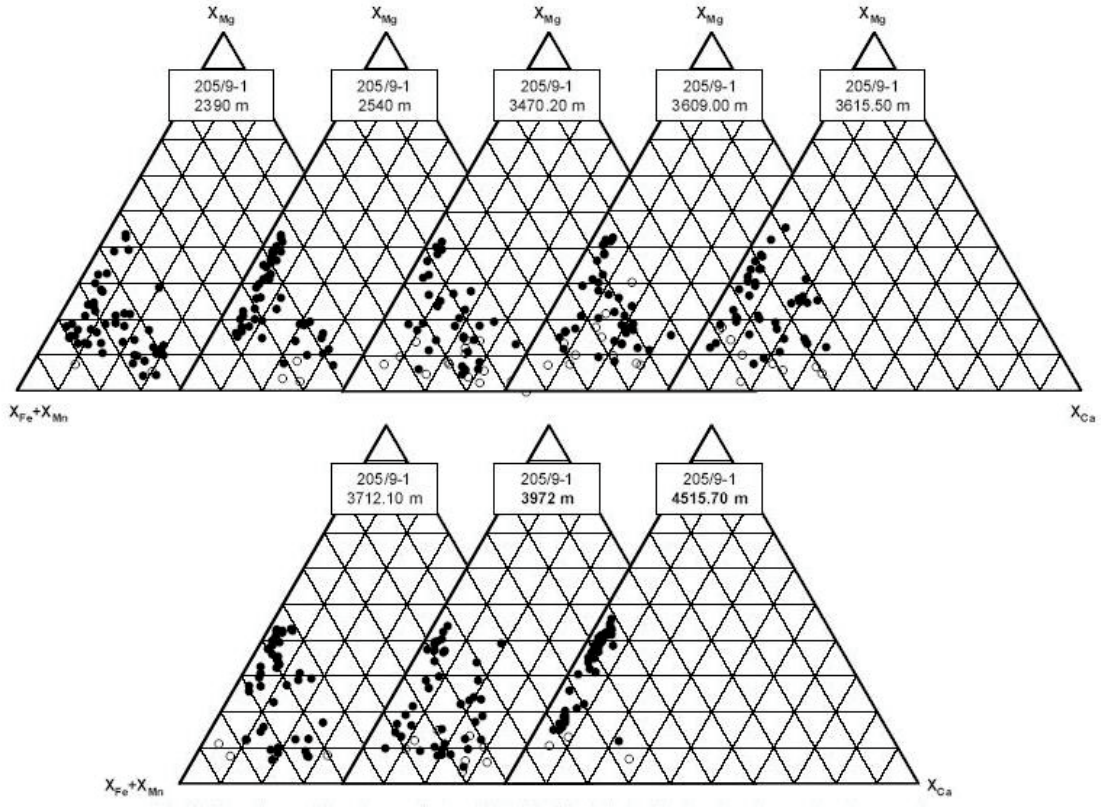

Figure 13. *Garnet compositions in samples from 205/9-1, Flett sub-basin. X_{Fe}, X_{Mg}, X_{Ca}, X_{Mn} = molecular proportions of Fe, Mg, Ca and Mn. All Fe calculated as Fe^{2+}. Solid symbols = X_{Mn} < 5%. Open symbols = X_{Mn} > 5%.*

There is a marked change in provenance at the base of the Lamba Formation, with a reversion to 'typical' RuZi values and a decrease in abundance of type A garnet. The assemblage in the Lamba Formation in 205/9-1 is closely comparable to that found at the same level in 204/19- 3a.

The Flett Formation sees a return to assemblages with moderately high abundances of type A garnet, and the occurrence of sandstones with low ATi, similar to those at the top of the Flett in 204/19-3a and 204/24a-7.

Well 214/19-1

The data from 214/19-1 cover a relatively short part of the succession, being confined to the Vaila Formation (Fig. 14). The samples are from considerable depth and consequently burial diagenesis has caused modification of the garnet geochemistry. This is manifested by the predominantly low-Ca nature of the assemblages (Fig. 15), which is inferred to be the result of preferential dissolution of the high-Ca component of the garnet population. It is also likely that GZi values have been reduced to some extent.

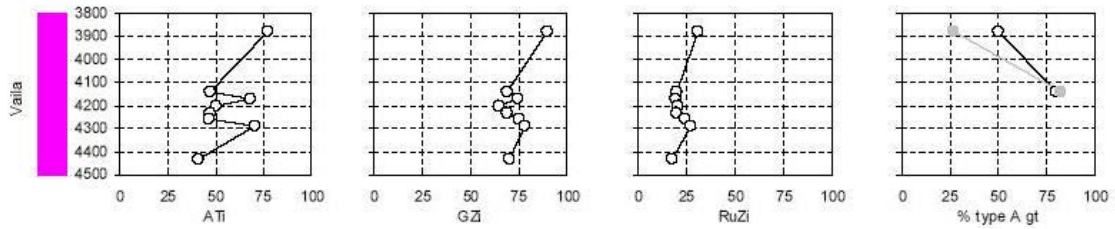

Figure 14. *Downhole variations in key mineral parameters in the Paleocene of 214/19-1. Grey trace on the garnet plot refers to the ratio of type Ai to type Aii garnet (Ai = low Ca garnet with X_{Mg} > 30%, Aii = low Ca garnet with X_{Mg} 20-30%).*

ATi values are variable in the analysed interval. Unlike the other analysed wells, this is considered to be an artefact of the drilling process. All the samples from this well are ditch cuttings, and in such material apatite abundances can be preferentially reduced by the crushing action of the drill bit, especially if a PDC drill bit was used in preference to a conventional rotary bit.

Despite the adverse drilling and burial conditions, garnet geochemistry shows that there is a marked change in the provenance in the analysed interval. This is manifested by an upward change from assemblages dominated by type Ai garnet in the lower part of the Vaila (comparable to the Vaila in 205/9-1, for example) to assemblages dominated by type Aii garnet (Figs 14 and 15). Assemblages dominated by Aii garnets are not present in any of the other analysed wells, but are known to be present elsewhere in the Flett sub-basin at the same stratigraphic level (HM Research Associates unpublished data).

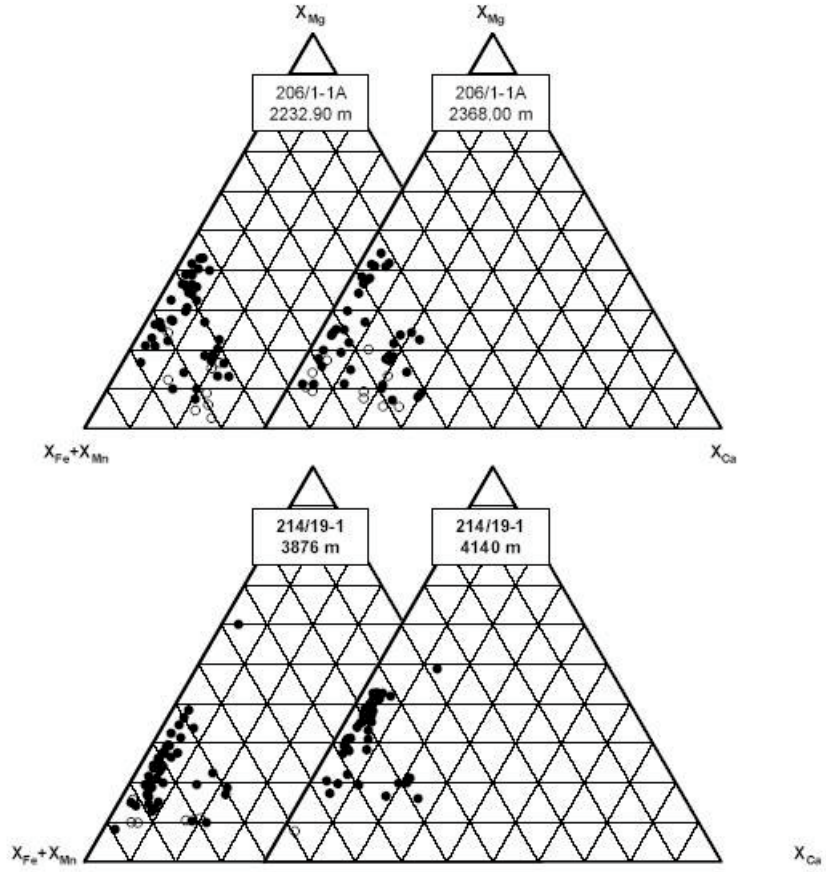

Figure 15. *Garnet compositions in samples from 206/1-1A and 214/19-1, Flett sub-basin. X_{Fe}, X_{Mg}, X_{Ca}, X_{Mn} = molecular proportions of Fe, Mg, Ca and Mn. All Fe calculated as Fe^{2+}. Solid symbols = X_{Mn} < 5%. Open symbols = X_{Mn} > 5%.*

Well 206/1-1a

The data from 206/1-1a (Figs 15 and 16) cover a relatively short part of the succession, being confined to the Flett Formation. The samples have generally high ATi, although values decrease towards the top of the unit, as seen in other Flett Formation penetrations. Most samples have moderate RuZi, but two have distinctively high values. Garnet assemblages are similar to other Flett samples, with relatively high type A abundances.

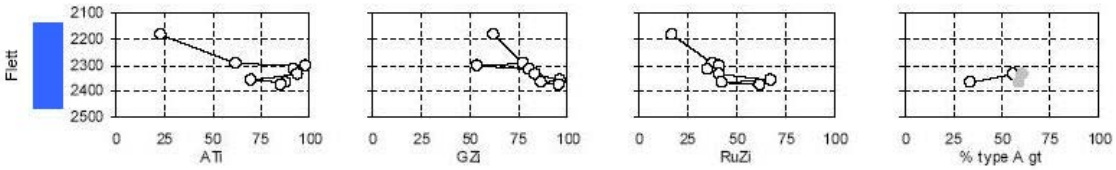

Figure 16. *Downhole variations in key mineral parameters in the Paleocene-Eocene of 206/1-1a. Grey trace on the garnet plot refers to the ratio of type Ai to type Aii garnet (Ai = low Ca garnet with X_{Mg} > 30%, Aii = low Ca garnet with X_{Mg} 20-30%).*

Provenance history

The Paleocene-Eocene sandstone data are compared on four crossplots (Figs 17-20) and on a ternary diagram of the relative abundance of garnet types A, B and C (Fig. 22). Also shown on these diagrams are the mean compositions from the most likely source lithologies on the Orkney-Shetland Platform (Lewisian and Moine/Dalradian basement, Old Red Sandstone and the Triassic Foula Fm).

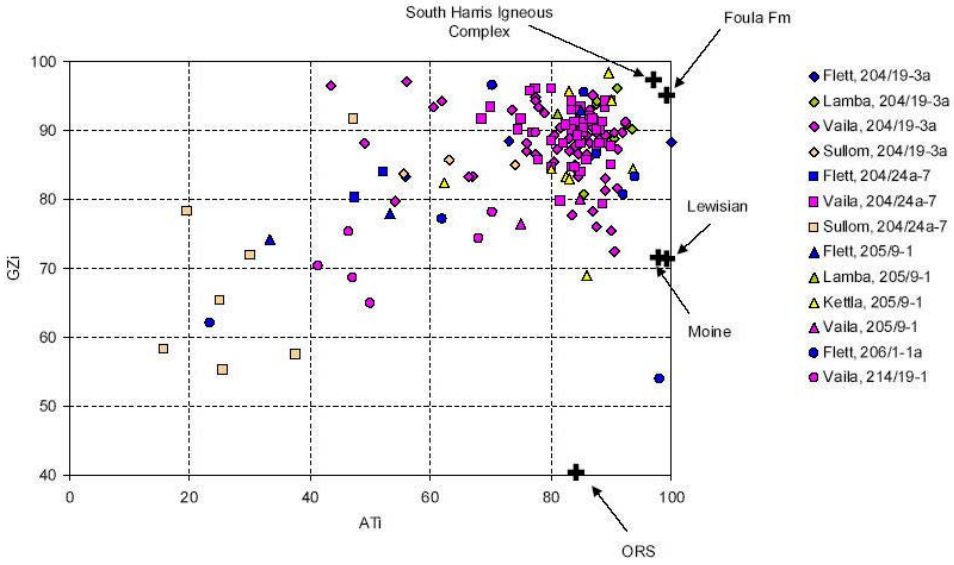

Figure 17. *GZi-ATi crossplot comparing heavy mineral assemblages in Paleocene-Eocene sandstones in the Faeroe-Shetland Basin*.

Sullom and lower Vaila Fm.

The data from the Sullom and lower Vaila in the Foinaven sub-basin form a well-defined linear mixing trend on the GZi – RuZi and ATi – type A garnet crossplots (Figs 18 and 20), and similar, but more scattered, trends on the GZi – ATi crossplot and GZi – type A garnet crossplots (Figs 17 and 21). They also form a linear trend on the garnet ternary plot, trending away from the type A pole towards a point on the type B – type C tieline.

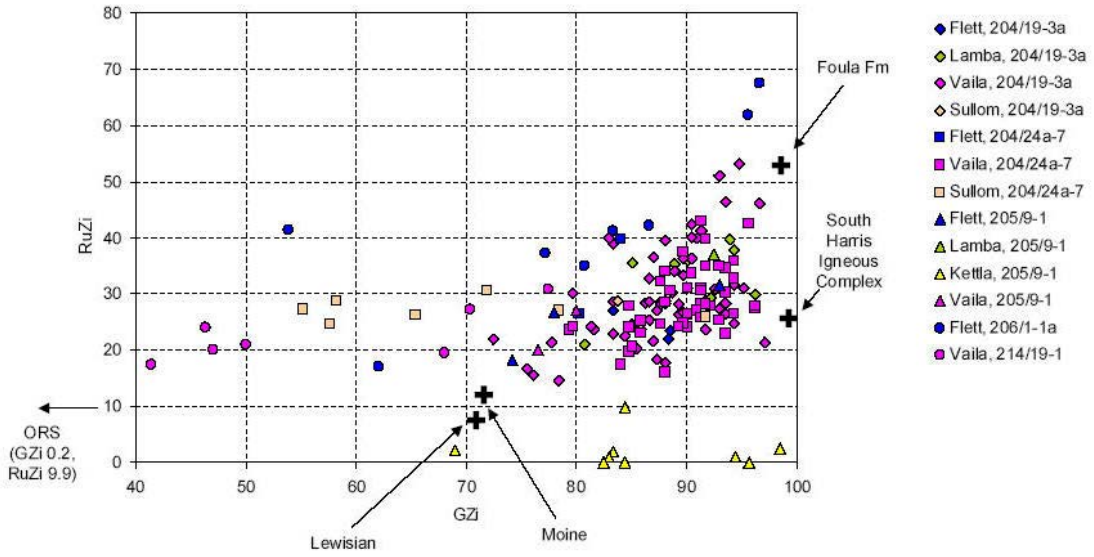

Figure 18. *GZi-RuZi crossplot comparing heavy mineral assemblages in Paleocene-Eocene sandstones in the Faeroe-Shetland Basin.*

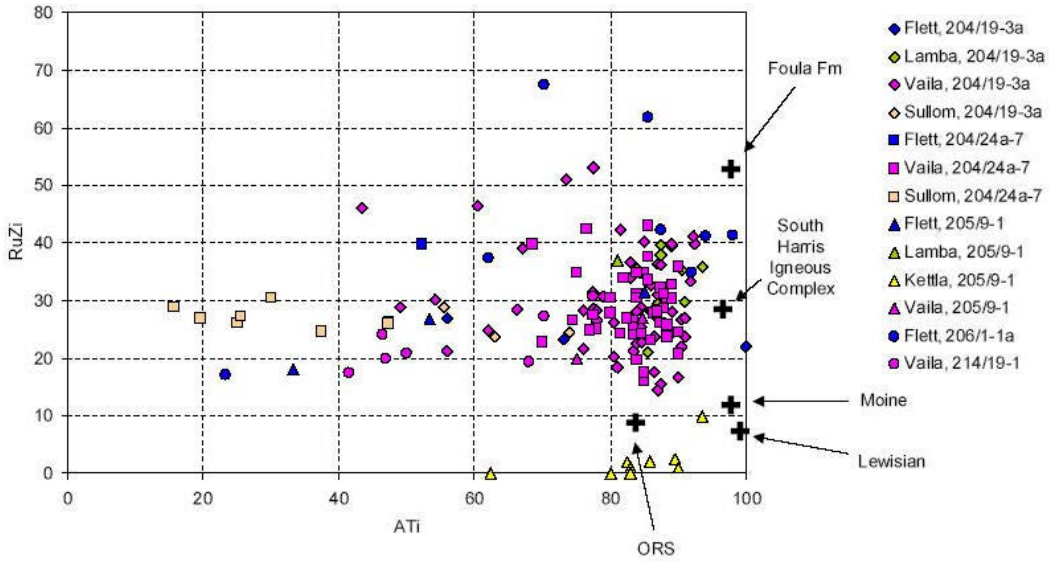

Figure 19. *ATi-RuZi crossplot comparing heavy mineral assemblages in Paleocene-Eocene sandstones in the Faeroe-Shetland Basin.*

These trends suggest the sandstones in this interval represent mixing of two main components. One end member (source I) has high type A garnet contents, moderate GZi and very low ATi, with the other (source II) having high ATi, high GZi, and low type A garnet abundance. By comparison with existing data on possible sources, source B is most likely to comprise metamorphic basement, including metasediment of Moine/Dalradian aspect plus Lewisian basement gneisses (both metabasic rocks and more typical intermediate-acidic gneisses). Source I, by contrast, has no obvious immediate origin, since none of the likely sources have very low ATi. However, ATi is not only sensitive to source lithology, but also

to weathering history. Consequently, source A is interpreted as representing heavily weathered material. This could also account for the lowered GZi, since garnet is also susceptible to weathering, although to a lesser extent than apatite. Given that the samples with the lowest ATi tend to occur at the base of the Sullom Fm. (in 204/24a-7, Fig. 9), source I is interpreted as representing the erosional product of the Late Cretaceous land surface (Morton et al. 2002). The high type A garnet abundance suggests that weathered Foula Fm. was present, but other components (basement, ORS) could also be present.

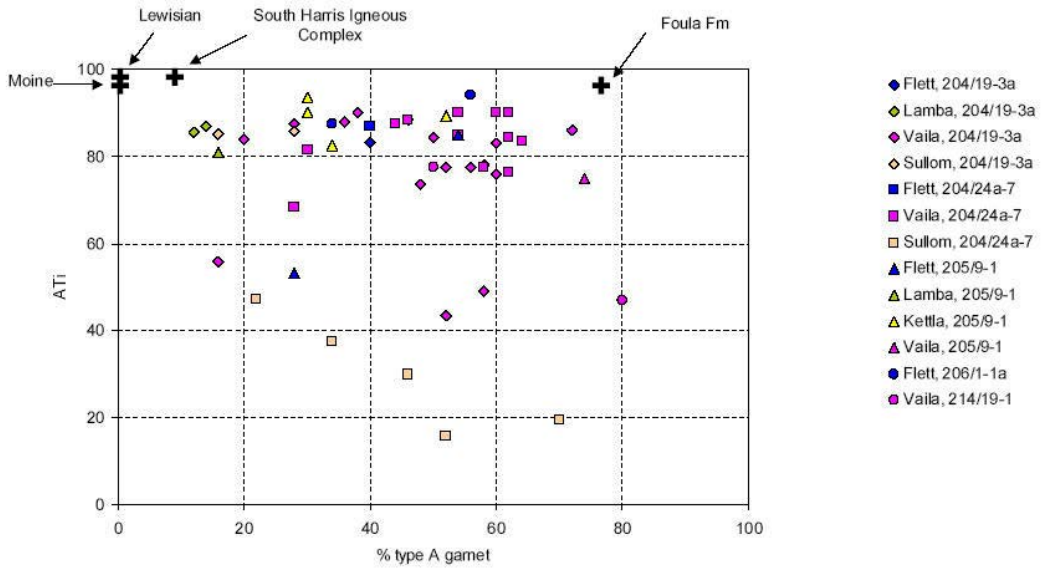

Figure 20. *ATi-type A garnet crossplot comparing heavy mineral assemblages in Paleocene-Eocene sandstones in the Faeroe-Shetland Basin.*

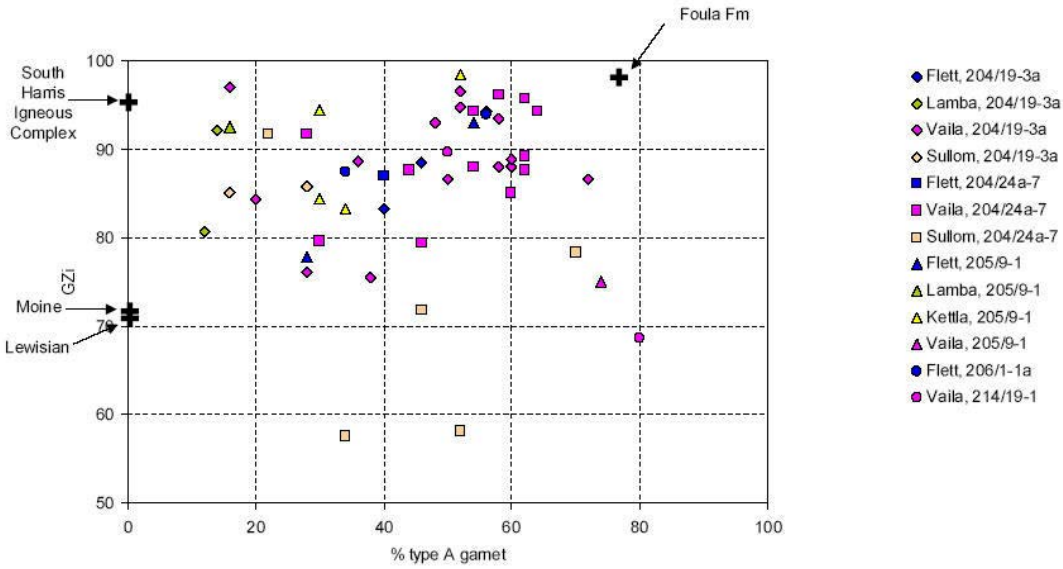

Figure 21. *GZi-type A garnet crossplot comparing heavy mineral assemblages in Paleocene-Eocene sandstones in the Faeroe-Shetland Basin.*

Middle-upper Vaila

There is a marked change in provenance in the middle part of the Vaila Fm. in the Foinaven sub-basin, with a switch to sand with high ATi, high GZi, moderate-high RuZi, and high abundances of type A garnet. Sandstones with these characteristics are found in both 204/19- 3a and 204/24a-7 (Figs 6 and 9), and clearly have a different source component to either end member found in the Sullom and lower Vaila. This component is termed source III.

Consideration of the crossplots and ternary diagram in Figs 17-22 shows that the Foula Fm. represents source III, since the mean Foula Fm. plots close to the data array shown by the Vaila Fm. on all plots. However, other sources are also involved, since the middle-upper Vaila shows a spread of data away from the Foula Fm. end member. Garnet data (Figs 20-22) indicates the presence of detritus derived from source II, since many samples have relatively igh abundances of type B garnets. This component becomes more significant in the uppermost part of the Vaila in 204/19-3a. The GZi – RuZi plot (Fig. 18) shows that the Vaila Fm. data array in 204/19-3a and 204/24a-7 requires significant input from a source with low RuZi and low GZi, termed source IV: this is likely to represent the ORS.

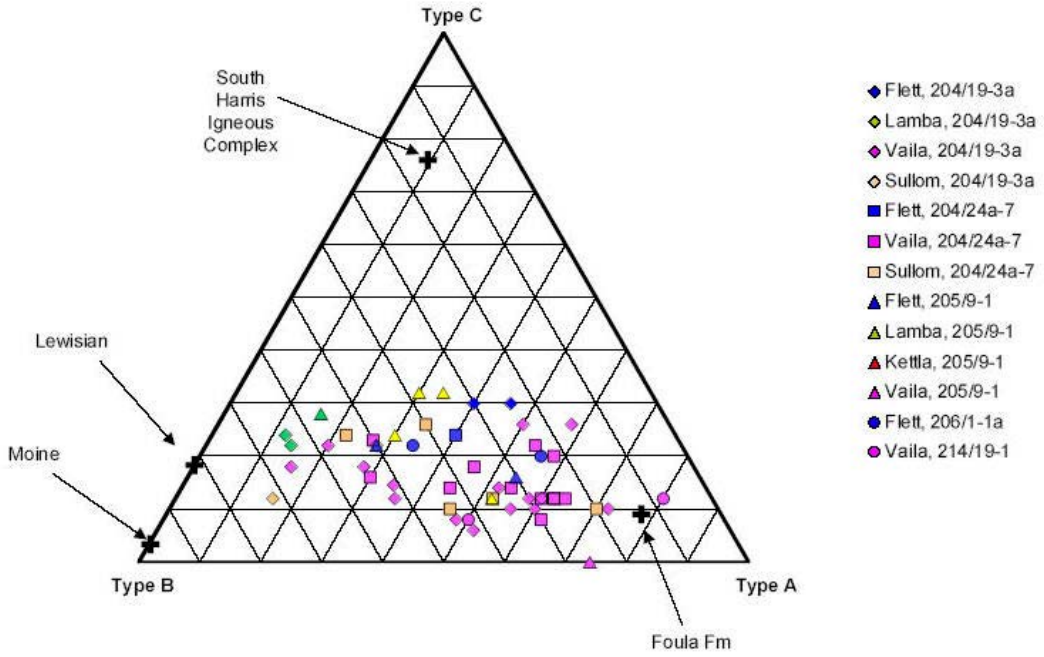

Figure 22: *Comparison of garnet assemblages in Paleocene-Eocene sandstones from the Faeroe-Shetland Basin. Also shown are mean garnet assemblages from potential sources on the UK margin. Moine, Lewisian and South Harris Igneous complex data are from river sediments described by Morton et al. (2004).*

Moving north to the Flett sub-basin, sediment in the Vaila in 205/9-1 and in the lower part of the Vaila analysed from 214/19-1 have similar characteristics to those in the Vaila of 204/19- 3a and 204/24a-7, dominated by the Foula Fm. with subsidiary input from metamorphic basement and the ORS. Some data from the Vaila in these two wells plot in aber-

rant positions on the plots because of diagenetic depletion of garnet and mechanical loss of apatite. Although they share similar source lithologies, it is unlikely that the Vaila in the Flett subbasin was deposited by the same depositional system as those supplying the Foinaven subbasin, since seismic data indicate different entry points (Lamers and Carmichael 1999).

Garnet data indicate a significant shift in provenance in the upper part of the Vaila in 214/19- 1, with a change from sandstones dominated by the Ai component to garnets dominated by the Aii component. The sandstones at the top of the Vaila in the Flett subbasin was therefore influenced by a fifth source, termed source V. Unpublished data indicates that Clair Group sandstones are likely to represent source V, since garnet assemblages, particularly from the Upper Clair Group (Fig. 23), are also dominated by Aii garnets.

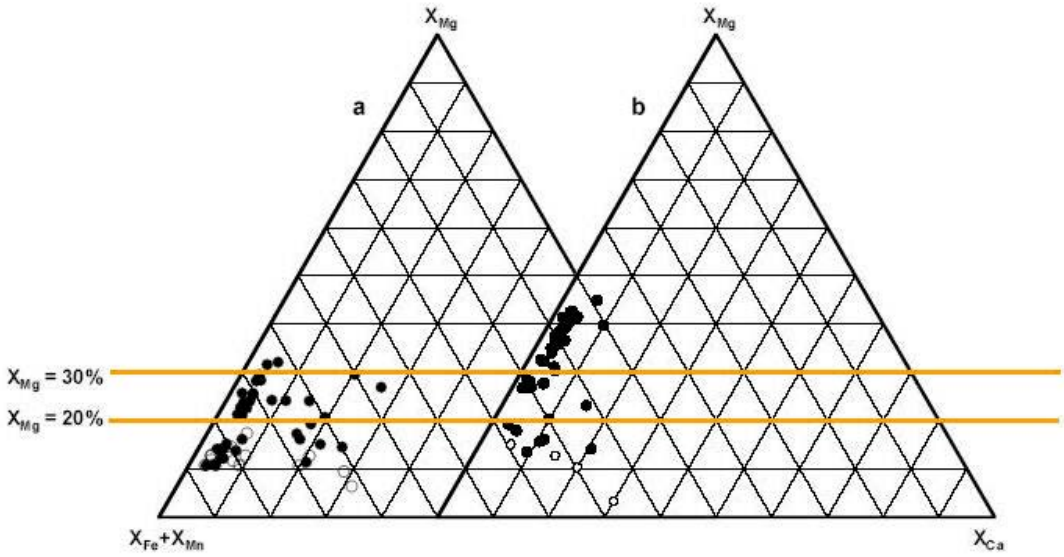

Figure 23: *Typical garnet population from (a) the Upper Clair Group, Clair Field, and (b) the Foula Fm., Strathmore Field. Lines show X_{Mg} = 20% and X_{Mg} 30%, dividing Ai and Aii garnet subfields X_{Fe}, X_{Mg}, X_{Ca}, X_{Mn} = molecular proportions of Fe, Mg, Ca and Mn. All Fe calculated as Fe^{2+}. Solid symbols = X_{Mn} < 5%. Open symbols = X_{Mn} > 5%.*

Kettla Member

The only well with a thick sandstone development in the Kettla Member is 205/9-1. The sandstones from the Kettla in this well have distinctively low RuZi values, markedly lower than any other well in the study (Figs 18 and 19). They were clearly derived from another source, termed source VI. The low RuZi suggests this source comprised metamorphic basement similar to either Moine/Dalradian metasediments or Lewisian gneisses. Garnet data indicate the presence of relatively high amounts of type C garnet, implying involvement of metabasic rocks, although both type A and type B garnets are also present.

It is unlikely that the Kettla sandstones in 205/9-1 were derived from the Orkney-Shetland Platform, since some of the samples contain high abundances of clinopyroxene, indicating that source F includes basic igneous rocks, and such rocks are not present to the east of

the Faroe-Shetland Basin. By contrast, the area to the west was the locus for extensive basic magmatism during the Paleocene-Eocene, including widespread flood basalts (e.g. Kiørboe 1999). Consequently, source VI is interpreted as lying to the west, and comprised a combination of basic igneous rocks and basement gneisses. Lithologies supplying type A garnets are also required: however, the low RuZi suggests that the Foula Fm. was not involved. In this instance, therefore, it may be that the type A garnets are directly derived from high-grade metasediments within the gneissic basement, as found locally within the Lewisian, for instance in Tiree (Cartwright 1992).

Lamba Formation

The Lamba Formation is relatively sand-poor, with data available only from 204/19-3a (Foinaven sub-basin) and 205/9-1 (Flett sub-basin). The plots comparing sandstones in the Faroe-Shetland Basin (Figs 17-22) show strong similarities between the available Lamba sandstone data. All have low abundances of type A garnet, high ATi, high GZi and moderate RuZi, and are interpreted as being derived predominantly from source B (metamorphic basement, including metasediment of Moine/Dalradian aspect plus Lewisian basement gneisses).

Flett Formation

The Flett Formation sandstones show strong overlap with the Vaila Fm. data set on all of the comparative plots (Figs 17-22), and a similar combination of sources, including source II (Moine/Dalradian and/or Lewisian basement), source III (Foula Formation) and source IV (ORS) is inferred. Garnet data suggest that the Foula Fm. is less influential than was the case in the Vaila Fm., although two samples from 206/1-1a have distinctly high RuZi that must be attributable to this source type. In all wells, there is a clear trend towards decreasing ATi and, to a lesser extent, GZi towards the top of the succession. This is considered to be the result of increased weathering during the Flett sedimentation cycle, rather than to source area weathering. The latter is unlikely considering the amount of sediment shed from the hinterland during the preceding phases of deposition. The Flett Fm. was the period of lowest sea level during the interval under consideration (Naylor et al. 1999), and consequently saw widespread development of coastal plain and delta top facies. Such conditions promote apatite dissolution, since there is much greater chance of prolonged alluvial storage and subaerial weathering.

Conclusions

Heavy mineral data have identified influx from six distinct sources to the Paleocene-Eocene successions in the UK sector of the Faroe-Shetland Basin. Of these, five are interpreted as lying on the eastern margin, with only one considered to be from the west (source VI).

Source I: heavily weathered material comprising the late Cretaceous land surface. This source was a major contributor to the earliest Paleocene (Sullom and early Vaila), especially in 204/24a-7. The weathered natire of the detritus causes problems in identifying the

source lithologies: the high type A garnet abundance suggests that the Foula Fm. was involved, but other components (basement, ORS) were probably also present.

Source II: metamorphic basement on the UK margin (Moine/Dalradian metasediment, Lewisian gneiss). This was a major source during the Sullom and early Vaila, the late Vaila, and the Lamba, and was of subsidiary importance during the mid-Vaila and the Flett.

Source III: the Triassic Foula Formation was a major source in the mid-Vaila and the Flett, and was of minor importance during the Sullom, early Vaila, late Vaila and Lamba.

Source IV: the ORS of the Orcadian Basin was a significant contributor throughout, although its contribution is most obvious in the mid Vaila.

Source V: the Devonian-Carboniferous Clair Group was a major source of sediment in the later part of Vaila deposition in the Flett sub-basin.

Source VI: a source lying on the western side of the basin, comprising basic igneous material plus metamorphic basement, supplied sediment to the Kettla Member in one well in the Flett sub-basin. It is possible that the basement component present in source VI could have lain on the UK margin, since the detritus shows similarities with sediment sourced from the Lewisian or Moine/Dalradian, but basic igneous rocks do not occur in association with these basement units on the Orkney-Shetland Platform.

New data from the Kangerlussuaq area confirm the involvement of two distinct sources as identified previously by Whitham et al. (2004) and Morton and Whitham (2002). Local sources dominate the Early Cretaceous and Early Tertiary parts of the succession, whereas a more distal source to the north or northeast supplied the majority of sediment in the intervening Late Cretaceous. Comparison of Figs 1 and 19 (RuZi-ATi crossplots for the two areas) shows there are marked differences in sediment composition between the two areas. The only overlap that occurs is between detritus derived from the local source in Kangerlussuaq area and that derived from source VI in the Faroe-Shetland Basin. Both of these sediment groups have low RuZi, but there are also some differences, notably in terms of garnet composition. The relationship between these two sources can be further evaluated on the basis of detrital zircon age data, presently being acquired by GEUS.

References

Allen, P.A., Mange-Rajetzky, M.A., 1992: Sedimentary evolution of the Devonian- Carboniferous Clair Field, offshore northwestern UK: impact of changing provenance. Marine and Petroleum Geology **9**, 29-52.

Cartwright, I. 1992: Archaean granulite facies metamorphism of the Lewisian of Tiree, Inner Hebrides, north-west Scotland. Journal of Metamorphic Geology **10**, 727-744.

Escher, J.C., Pulvertaft, T.C.R. 1995: Geological Map of Greenland. Scale 1:2 500 000. Scale 1:2,500,000. Geological Survey of Greenland, Copenhagen.

Hansley, P.L. 1987: Petrologic and experimental evidence for the etching of garnets by organic acids in the Upper Jurassic Morrison Formation, northwestern New Mexico. Journal of Sedimentary Petrology **57,** 666-681.

Hillier, S., Marshall, J.E.A. 1992: Organic maturation, thermal history and hydrocarbon generation in the Orcadian Basin, Scotland. Journal of the Geological Society, London **149**, 491-502.

Kiørboe, L. 1999: Stratigraphic relationships of the Lower Tertiary of the Faroe basalt plateau and the Faroe-Shetland Basin. In: Fleet, A.J. and Boldy, S.A.R. (eds) Petroleum Geology of Northwest Europe: Proceedings of the 5th Conference. Geological Society, London, 559-572.

Lamers, E., Carmichael, S.M.M. 1999: The Paleocene deepwater sandstone play west of Shetland. In: Fleet, A.J. and Boldy, S.A.R. (eds) Petroleum Geology of Northwest Europe: Proceedings of the 5th Conference. Geological Society, London, 645-659.

Marshall, J.E.A., Hewitt, A.J. 2003: Devonian. In: Evans, D., Graham, C., Armour, A. and Bathurst, P. (eds) The Millenium Atlas: Petroleum Geology of the Central and Northern North Sea. Geological Society, London, 65-81.

Morton, A.C., 1987: Influences of provenance and diagenesis on detrital garnet suites in the Forties sandstone, Paleocene, central North Sea. Journal of Sedimentary Petrology **57**, 1027- 1032.

Morton, A.C., Boyd, J.D., Ewen, D.F. 2002: Evolution of Paleocene sediment dispersal systems in the Foinaven Sub-Basin, West of Shetland. In: Jolley, D.W. and Bell, B.R. (eds) The North Atlantic Igneous Province: Stratigraphy, tectonics, volcanic and magmatic processes. Geological Society, London, Special Publication **197**, 69-93.

Morton, A.C., Hallsworth, C.R. in press: Stability of detrital heavy minerals during burial diagenesis. In: Mange, M. and Wright, D.K. (eds), Heavy Minerals In Use. Developments in Sedimentology.

Morton, A.C., Hallsworth, C.R., Chalton, B. 2004: Garnet compositions in Scottish and Norwegian basement terrains: a framework for interpretation of North Sea sandstone provenance. Marine and Petroleum Geology **21**, 393-410.

Morton, A.C., Herries, R., Fanning, C.M. in press: Correlation of Triassic sandstones in the Strathmore Field, west of Shetland, using heavy mineral provenance signatures. In: Mange, M. and Wright, D.K. (eds), Heavy Minerals In Use. Developments in Sedimentology

Morton, A.C., Spicer P.J., Ewen, D.F., 2003: Geosteering of high-angle wells using heavy mineral analysis: the Clair Field, West of Shetland. In: Carr, T.R., Mason, E.P., and Feazel, C.T. (eds) Horizontal Wells: Focus on the Reservoir. American Association of Petroleum Geologists, Methods in Exploration **14**, 249-260.

Morton, A.C., Whitham, A.G. 2002: A provenance study of Aptian-Eocene sandstones from the Kangerlussuaq region, SE Greenland - II. CASP Greenland Faroe Provenance Project, Report **2**.

Mudge, D.C., Bujak, J.P. 2001: Biostratigraphic evidence for evolving palaeoenvironments in the lower Palaeogene of the Faroe-Shetland Basin. Marine and Petroleum Geology **18**, 577-590.

Naylor, P.H., Bell, B.R., Jolley, D.W., Durnall, P., Fredsted, R. 1999: Palaeogene magmatism in the Faroe-Shetland Basin: influences on uplift history and sedimentation. In: Fleet, A.J. and Boldy, S.A.R. (eds) Petroleum Geology of Northwest Europe: Proceedings of the 5th Conference. Geological Society, London, 545-558.

Nichols, G.J. in press: Sedimentary evolution of the Lower Clair Group, Devonian, west of Shetland: climate and sediment supply controls on fluvial, aeolian and lacustrine deposition. In: Doré, A.G. and Vining, B.A. (eds) Petroleum Geology: North-west Europe and Global Perspectives – Proceedings of the 6th Petroleum Geology Conference. Geological Society, London.

Trewin, N.H., Thirlwall, M.F. 2002: Old Red Sandstone. In: Trewin, N.H. (ed.) The Geology of Scotland. Geological Society, London, 213-249.

Whitham, A.G., Morton, A.C., Fanning, C.M. 2004: Insights into Paleocene sediment transport paths and basin evolution in the North Atlantic from a heavy mineral study of sandstones from southern East Greenland. Petroleum Geoscience **10**, 61-72.

Table 1. Conventional heavy mineral data from Kangerlussuaq samples analysed in the SINDRI study. Data are expressed as frequency % of the non-opaque detrital component in the 63-125 μm fraction.

Sample	Strat Group	Ae	At	Ap	Br	Ca	Cp	Cr	Ct	Ep	Gh	Gt	Ky	Mo	Op	Ru	Sl	Sp	St	To	Zr	Total
413245	1		4.0	R		3.0	R			1.0		37.5		1.0		5.5		1.0		6.5	40.5	200
413255	1			1.0		1.0	1.0			3.5		3.5	R	3.0		R			R	R	87.0	200
455107	1			0.5		2.0		0.5		1.5		1.5		0.5		11.0				10.0	72.5	200
413284	2			0.5		2.0				2.0		45.5	R							1.0	49.0	200
413288	2			0.5		0.5				85.5		4.0				R				R	9.5	200
455117	2					0.5		0.5		0.5		2.0		R		18.5				1.5	76.5	200
455118	2					9.0	R			1.5		1.5		1.0		10.0				4.0	73.0	200
455672	2									1.0		27.5		1.0		0.5				2.0	68.0	200
455677	2		1.5	1.5						3.0		9.5		6.5		2.0				6.0	70.0	200
W4678	2		0.6	4.0						0.5		7.3		2.8		3.4				20.9	61.0	177
413270	3		2.0	2.0		0.5		R		1.0		26.0		2.0		33.0				18.5	15.0	200
406752	4		0.5	0.5		1.0	R		R	R		77.0		R		10.5			R	8.0	2.5	200
455636	4			0.5				R				2.5		4.0		57.0				12.0	24.0	200
455648	4			0.5		1.0		R	R	R		41.5		1.0		32.5				6.0	17.5	200
W4685	4		R	1.5						46.5		40.5				1.0		1.0		8.5	1.0	200
412773	5		7.0	5.0		R		R						4.0		24.5				6.0	53.5	200
412778	5		0.5	1.0		R			0.5	R						49.5				9.5	39.0	200
413123	5			0.5				R				17.0		1.0		49.0				4.5	28.0	200
413124	5			R				R				33.5		1.0		46.5				3.5	15.5	200
413143	5		R	R		R						41.5		R		30.0		12.5		2.5	13.5	200
413190	5		R	50.0		1.0				27.5		4.5		2.0		R		0.5			14.5	200
413276	5		3.0	6.0		0.5								3.0		20.5				2.0	65.0	200
W4768	5		6.0	2.0						0.5		1.5		3.0		39.5				7.0	40.5	200
412725	6		3.5	7.9	1.7	14.9	1.7			18.4		5.3		0.9		1.7		2.6		1.7	39.7	114
413146	6		0.5									R		2.0		63.0				11.0	23.5	200
455423	6			2.0		0.5	R	R				R		1.0		41.0				5.0	50.5	200
455499	6		R	R		1.0				R		4.0		0.5		44.0				36.0	14.5	200
455537	6		R	4.0										1.0		34.5				2.0	58.5	200
406736	7		R	R		0.5			R	66.5		10.5		0.5	R	4.0		0.5		1.0	16.5	200
412733	7		1.0	12.5		15.5				5.0		4.5		3.0		0.5		1.5		0.5	56.0	200
412784	7		1.0	3.5		6.0	0.5	R		1.5		9.0		4.5		12.0		0.5	0.5	5.5	55.5	200
413148	7		1.5	R		1.0						0.5		24.5		10.5				1.0	61.0	200
413166	7			0.5		R						14.5				0.5				R	84.5	200
413211	7			R				R		91.0		2.5				1.0		2.0		0.5	3.0	200
437815	7			R		1.0	R	R		1.0				1.0		7.0				1.0	89.0	200
455433	7			R		R				0.5		20.0		0.5		5.0				1.5	72.5	200
455516	7							R				2.0		5.5		44.5				5.0	43.0	200
455539	7		1.0	2.0		1.5				1.5				3.5		13.5		0.5		6.5	70.0	200
K10793	7		1.0	30.0			R					31.5		R		5.0				4.0	28.5	200
W4671	7		0.5	R				R		53.5		28.0				7.5		1.5		4.0	5.0	200
413192	8			1.5		4.5	R			22.5		51.5				1.5		R		1.0	17.5	200
413230	8			6.5		0.5				67.5		15.5						3.5			6.5	200
455438	8		1.0	13.0		1.0		R	R			11.5		2.0		13.5				14.0	44.0	200
455444	8		R	1.0		9.0	R			2.0		8.5		0.5		12.0	R	1.0		6.0	60.0	200
455550	8			78.5								6.0				2.0					13.5	200
455613	8					1.0	98.5			0.5		R									R	200
455462	9		1.4	48.6		2.9						22.9								12.9	11.3	70
459670	10							R		13.0		69.5	7.0	R		1.0		1.5	5.0	2.5	0.5	200
459682	10		R	0.5		R	R	R		14.5		72.0	2.0	1.0		2.0		3.0	2.0	2.0	1.0	200
459717	10	R		R		4.5	91.5	R	R	0.5		2.5	R			R		1.0		R	R	200

Ae – aegirine, At – anatase, Ap – apatite, Br – brookite, Ca – calcic amphibole, Cp – clinopyroxene, Cr – chrome spinel, Ct – chloritoid, Ep – epidote, Gh – gahnite, Gt – garnet, Ky – kyanite, Mo – monazite, Op – orthopyroxene, Ru – rutile, Sl – sillimanite, Sp – titanite, St – staurolite, To – tourmaline, Zr – zircon

R – rare (<0.5%)

Table 2. Heavy mineral ratio data from Kangerlussuaq samples analysed in the SINDRI study. Data in parentheses refer to raw grain counts for samples with poor recovery.

Sample	Strat Group	ATi	Total	GZi	Total	RuZi	Total	MZi	Total	CZi	Total
413245	1	5.7	53	42.4	236	10.7	224	2.4	205	0.0	200
413255	1	(3/4)		3.8	292	0.4	282	3.4	291	0.0	281
455107	1	2.9	35	2.2	236	12.8	265	0.4	232	0.4	232
413284	2	65.0	20	49.2	394	0.0	200	0.0	200	0.0	200
413288	2	90.5	21	37.1	318	1.0	202	0.0	200	0.0	200
455117	2	0.0	97	2.7	257	19.6	311	0.4	251	0.8	252
455118	2	0.0	53	1.8	220	12.0	250	3.5	228	0.0	220
455672	2	(0/5)		28.6	259	0.5	186	1.6	188	0.0	185
455677	2	40.0	20	10.2	216	3.0	202	8.1	211	0.0	194
W4678	2	15.9	44	10.7	121	6.1	115	5.3	114	4.4	113
413270	3	9.0	200	59.2	395	66.7	312	9.9	222	1.5	203
406752	4	32.8	67	96.0	272	73.6	110	3.3	30	0.0	29
455636	4	7.0	200	12.6	206	70.6	378	16.3	246	0.5	207
455648	4	6.5	107	65.0	311	51.2	410	3.4	207	0.5	201
W4685	4	8.0	125	96.6	207	73.3	60	(0/16)		(0/16)	
412773	5	33.0	200	0.0	200	29.2	212	7.4	216	0.5	201
412778	5	8.3	252	0.0	242	56.2	552	0.0	242	0.0	242
413123	5	1.9	206	39.8	339	64.2	380	6.1	213	0.5	201
413124	5	1.0	200	64.7	357	75.1	281	6.4	220	0.5	207
413143	5	4.7	64	77.2	259	74.3	269	1.5	203	0.0	200
413190	5	100.0	200	25.5	200	1.1	177	12.5	200	0.0	175
413276	5	53.3	107	0.0	200	26.7	273	4.3	209	0.0	200
W4768	5	17.5	200	2.9	206	47.4	211	6.5	214	0.0	200
412725	6	(9/11)		11.8	51	4.3	47	2.2	46	0.0	45
413146	6	0.0	100	0.9	222	72.7	560	9.1	242	0.0	220
455423	6	38.5	200	0.4	250	45.3	455	2.3	261	0.4	250
455499	6	0.5	200	25.8	291	75.6	291	3.6	224	0.0	216
455537	6	53.5	170	0.0	211	36.3	331	1.9	215	0.0	211
406736	7	2.1	47	41.0	200	22.5	258	1.0	202	0.0	200
412733	7	97.4	39	6.7	165	2.5	158	4.3	161	0.0	154
412784	7	59.1	88	14.2	233	18.0	244	7.8	217	0.5	201
413148	7	11.5	26	1.5	203	13.8	232	26.7	273	0.0	200
413166	7	(4/6)		14.7	327	0.7	281	0.4	280	0.0	279
413211	7	54.1	37	46.5	200	9.5	221	0.0	200	0.5	201
437815	7	30.4	23	0.0	267	7.3	288	1.1	270	0.4	268
455433	7	6.1	49	21.7	286	6.3	239	2.6	230	0.0	224
455516	7	0.0	200	3.8	208	51.1	409	11.1	226	1.0	202
455539	7	16.4	55	0.0	200	13.8	232	4.8	210	0.0	200
K10793	7	76.5	200	49.5	200	4.8	210	1.0	202	0.0	200
W4671	7	1.0	200	79.4	252	56.1	228	0.0	200	1.0	202
413192	8	94.4	36	74.8	270	6.5	263	0.0	246	0.0	246
413230	8	100.0	28	69.4	98	0.0	30	0.0	30	0.0	30
455438	8	43.5	200	20.6	252	23.7	262	5.2	211	0.5	201
455444	8	10.2	49	12.3	228	16.7	240	1.0	202	0.0	200
455550	8	100.0	244	29.7	64	11.8	51	0.0	45	0.0	45
455462	9	79.1	43	66.7	24	(0/8)		(0/8)		(0/8)	
459670	10	0.0	126	96.9	227	59.8	276	1.8	113	0.9	112
459682	10	38.3	120	97.5	279	67.6	222	18.2	99	49.4	160
459717	10	(1/3)		93.7	63	(1/5)		(0/4)		(1/5)	

ATi – apatite:tourmaline index, GZi – garnet:zircon index, RuZi – rutile:zircon index, MZi – monazite:zircon index, CZi – chrome spinel:zircon index

(see Appendix for definitions)

Table 3. Conventional heavy mineral data from Devonian Old Red Sandstone samples from Orkney, analysed in the SINDRI study. Data are expressed as frequency % of the non-opaque detrital component in the 63-125 μm fraction.

Sample	Stratigraphy	Grid Ref	At	Ap	Ca	Cp	Cr	Gt	Mo	Ru	To	Zr	total
ORK 29	Hoy Sst	207 978	0.5	0.5			0.5		0.5	4.5	4.5	89.0	200
ORK 30	Hoy Sst	207 980	0.5				0.5			6.0	4.5	88.5	200
ORK 31	Hoy Sst	208 982	0.5				0.5		0.5	6.5	9.0	83.0	200
ORK 32	Hoy Sst	207 976	1.0				0.5		0.5	7.5	4.5	86.0	200
ORK 25	Basal Hoy Sst	260 888	0.5	29.5			1.5		1.0	7.0	4.5	56.0	200
ORK 26	Basal Hoy Sst	259 886		35.0			1.0		0.5	4.5	4.0	55.0	200
ORK 27	Basal Hoy Sst	256 883	R	41.5			0.5		0.5	5.0	4.5	48.0	200
ORK 28	Basal Hoy Sst	255 884	0.5	38.5			1.0		0.5	8.0	5.0	46.5	200
ORK 33	Tuffaceous UORS Sst	196 990		25.5					0.5	5.0	3.5	65.5	200
ORK 35	Upr Eday Sst (middle-upper)	549 368		62.5					0.5	3.5	4.5	29.0	200
ORK 36	Upr Eday Sst (middle-upper)	549 368	0.5	58.5					0.5	4.5	4.0	32.0	200
ORK 11	Middle Eday Sst	431 891	0.5	39.5			0.5	0.5	0.5	4.5	7.5	46.5	200
ORK 12	Middle Eday Sst	430 891		19.0			0.5		1.5	2.0	2.0	75.0	200
ORK 13	Middle Eday Sst	428 891	0.5	42.0			0.5		1.0	6.5	6.5	43.0	200
ORK 14	Middle Eday Sst	428 892		28.0			R		0.5	5.5	9.5	56.5	200
ORK 16	Sst in Eday flags	563 032		22.0			2.5		R	4.0	2.5	69.0	200
ORK 17	Sst in Eday flags	566 034	0.5	66.0			1.0		0.5	3.0	7.0	22.0	200
ORK 18	Sst in Eday flags	568 039	0.5	28.5			0.5		0.5	5.5	3.5	61.0	200
ORK 8	Lr Eday Sst	458 868		37.0						2.5	19.0	41.5	200
ORK 9	Lr Eday Sst	460 868		77.5			0.5			1.5	9.0	11.5	200
ORK 10	Lr Eday Sst	463 867	2.0	64.5			0.5			4.0	6.0	23.0	200
ORK 15	Lr Eday Sst	559 032	0.5	47.0			R			5.0	3.5	44.0	200
ORK 19	Lr Eday Sst	561 032		68.0			1.0			2.5	11.0	17.5	200
ORK 20	Lr Eday Sst	559 032		16.0			1.5		0.5	5.0	4.0	73.0	200
ORK 21	Lr Eday Sst	554 035		38.5			0.5	0.5	0.5	6.5	14.0	39.5	200
ORK 22	Lr Eday Sst	554 034		87.0						1.5	4.5	7.0	200
ORK 23	Sst in passage beds	553 036		19.0			0.5		0.5	4.5	2.0	73.5	200
ORK 24	Sst in passage beds	552 036		51.0	R	R	1.5	1.5		2.0	5.5	38.5	200
ORK 1	Yesnaby Sst	220 155					2.0		0.5	3.0	1.5	93.0	200
ORK 4	Harra Ebb SSt	217 147	1.5				1.5		2.0	4.5	1.0	89.5	200
ORK 5	Harra Ebb SSt	217 148	1.7						1.1	3.4	0.6	93.2	179
ORK 7	Harra Ebb SSt	220 154	0.5				1.0		0.5	8.0	4.0	86.0	200

At – anatase, Ap – apatite, Ca – calcic amphibole, Cp – clinopyroxene, Cr – chrome spinel, Gt – garnet, Mo – monazite, Ru – rutile, To – tourmaline, Zr – zircon

R – rare (<0.5%)

Table 4. Heavy mineral ratio data from Devonian Old Red Sandstone samples from Orkney, analysed in the SINDRI study. Data in italics (ATi information for Harra Ebb and Yesnaby Ssts) are pooled from the four samples, since none contain sufficient apatite and tourmaline for a valid individual analysis.

Sample	Stratigraphy	Grid Ref	ATi	total	GZi	total	RuZi	total	MZi	total	CZi	total
ORK 29	Hoy Sst	207 978	3.1	162	0.0	300	4.8	315	0.3	301	0.3	301
ORK 30	Hoy Sst	207 980	0.8	125	0.0	272	6.5	291	0.0	272	0.7	274
ORK 31	Hoy Sst	208 982	0.0	100	0.0	361	7.4	390	0.5	363	0.3	362
ORK 32	Hoy Sst	207 976	0.0	100	0.0	288	8.0	313	0.3	289	0.3	289
ORK 25	Basal Hoy Sst	260 888	87.7	204	0.0	216	11.1	243	13.7	219	2.7	222
ORK 26	Basal Hoy Sst	259 886	90.5	200	0.0	222	7.9	241	0.4	223	2.2	227
ORK 27	Basal Hoy Sst	256 883	90.5	388	0.0	410	9.1	451	1.0	414	1.2	415
ORK 28	Basal Hoy Sst	255 884	88.9	216	0.0	202	15.1	238	1.0	204	1.9	206
ORK 33	Tuffaceous UORS Sst	196 990	87.9	58	0.0	130	7.1	140	0.8	131	0.0	130
ORK 35	Upr Eday Sst (middle-upper)	549 368	55.0	262	0.0	200	12.7	229	1.0	202	0.0	200
ORK 36	Upr Eday Sst (middle-upper)	549 368	93.3	239	0.0	200	11.9	227	0.5	201	0.0	200
ORK 11	Middle Eday Sst	431 891	83.7	209	0.5	206	8.9	225	1.4	208	1.4	208
ORK 12	Middle Eday Sst	430 891	89.9	307	0.0	308	2.5	316	1.9	314	0.6	310
ORK 13	Middle Eday Sst	428 891	86.5	237	0.0	208	13.3	240	2.8	214	1.4	211
ORK 14	Middle Eday Sst	428 892	73.9	211	0.0	228	8.8	250	0.9	230	0.4	229
ORK 16	Sst in Eday flags	563 032	87.1	224	0.0	207	5.0	218	0.0	207	3.7	215
ORK 17	Sst in Eday flags	566 034	90.2	244	0.0	200	17.7	243	0.5	201	4.8	210
ORK 18	Sst in Eday flags	568 039	88.5	226	0.0	222	8.6	243	0.4	223	0.4	223
ORK 8	Lr Eday Sst	458 868	66.3	163	0.0	120	6.3	128	0.0	120	0.0	120
ORK 9	Lr Eday Sst	460 868	89.3	281	0.0	203	25.9	274	0.5	204	3.3	210
ORK 10	Lr Eday Sst	463 867	91.3	219	0.0	200	15.3	236	0.5	201	3.4	207
ORK 15	Lr Eday Sst	559 032	92.7	205	0.0	208	11.5	235	0.0	208	0.5	209
ORK 19	Lr Eday Sst	561 032	85.9	241	0.0	125	13.8	145	0.0	125	3.8	130
ORK 20	Lr Eday Sst	559 032	78.5	200	0.0	229	6.5	245	0.4	230	2.1	234
ORK 21	Lr Eday Sst	554 035	73.1	268	1.0	202	14.2	233	0.5	201	1.5	203
ORK 22	Lr Eday Sst	554 034	94.9	296	0.0	30	23.1	39	0.0	30	0.0	30
ORK 23	Sst in passage beds	553 036	90.5	231	0.0	232	6.1	247	0.4	233	0.9	234
ORK 24	Sst in passage beds	552 036	90.5	221	3.8	208	6.5	214	0.0	200	2.4	205
ORK 1	Yesnaby Sst	220 155	*0.0*	*44*	0.0	260	3.5	269	0.8	262	1.9	260
ORK 4	Harra Ebb SSt	217 147	*0.0*	*44*	0.0	200	4.3	209	2.0	204	2.0	204
ORK 5	Harra Ebb SSt	217 148	*0.0*	*44*	0.0	167	3.5	173	1.2	169	0.0	167
ORK 7	Harra Ebb SSt	220 154	*0.0*	*44*	0.0	265	8.6	290	0.4	266	1.1	268

ATi – apatite:tourmaline index, GZi – garnet:zircon index, RuZi – rutile:zircon index, MZi – monazite:zircon index, CZi – chrome spinel:zircon index

(see Appendix for definitions)

Table 5. Conventional heavy mineral data from Faeroe-Shetland Basin samples analysed in the SINDRI study. Data are expressed as frequency % of the non-opaque detrital component in the 63-125 μm fraction.

Well	Depth (m)	type	Litho unit	Al	At	Ap	Ca	Cp	Cr	Ct	Ep	Gh	Gt	Ky	Mo	Op	Ru	Sp	St	To	Zr	Total
204/19-3a	1500	uwc	Flett		0.5	1.5	10.0	0.5	R		48.0		25.5	2.0	R		2.5	3.5	0.5	1.0	4.5	200
	1590	uwc	Flett			5.5	20.0				31.5		27.0	2.0	R		2.0	4.5	R		7.5	200
	1710	uwc	Flett		R	4.0	11.5		R		31.5		36.5	3.5			1.0	7.0	R	R	5.0	200
204/24a-7	1405	uwc	Flett		R	1.0	51.5		R		28.0		7.0	3.0	R		2.0	3.5	0.5	0.5	3.0	200
	1425	uwc	Flett			0.5	25.0	R	R		48.0		15.5	1.0	R	0.5	1.0	3.0		0.5	5.0	200
205/9-1	2390	uwc	Flett			2.5	1.5			0.5	2.5		62.0		0.5		8.0	1.5	1.5	2.0	17.5	200
	2450	uwc	Flett			2.0	14.0			0.5	4.5		54.5		R		3.0		3.5	2.0	16.0	200
	2540	uwc	Flett			6.5	1.0			R	R		82.0		0.5		0.5		R	2.5	7.0	200
	3470.2	core	Lamba		0.5	9.0	0.5			R	77.5		10.0		R		1.0	1.0		R	0.5	200
	3712.1	core	Lamba			6.0					75.0		13.5				R	5.5		R	R	200
206/1-1A	2185	uwc	Flett			1.5	0.5			1.5	1.0		50.5				6.5	4.5	0.5	3.0	30.5	200
	2293.5	core	Flett	0.5	2.0	4.0				1.0		R	64.5		R		9.5		2.5	2.0	14.0	200
	2303.7	core	Flett	1.0	1.0	24.5				R			27.5		0.5		18.5		1.5	R	25.5	200
	2313.9	core	Flett	0.5	0.5	41.5				R		R	41.0		0.5		6.5		0.5	2.5	6.5	200
	2332.9	core	Flett	R	1.5	38.5				1.0			43.5		R		3.5		R	3.0	9.0	200
	2359.2	core	Flett		0.5	0.5				R			87.0		R		9.0		R	0.5	2.5	200
	2368.0	core	Flett		1.0	15.5							67.5		R		5.5			2.0	8.5	200
	2374.1	core	Flett		1.5	37.0		0.5		R			47.0		R		4.0		R	9.5	0.5	200
214/19-1	3876	uwc	Vaila		0.5	14.0	1.0	0.5	0.5	R	1.5		65.5				3.5		0.5	6.5	6.0	200
	4140	uwc	Vaila		1	5.0							54.0		R		8.0			5.0	27.0	200
	4170	uwc	Vaila		R	8.5							63.5				7.0			1.5	19.5	200
	4200	uwc	Vaila		0.5	5.0							54.5		0.5		6.0			5.0	28.5	200
	4230	uwc	Vaila		1.0	5.0							54.0		R		8.0			5.0	27.0	200
	4260	uwc	Vaila			5.0			R		R		61.0		R		9.0			4.0	21.0	200
	4290	uwc	Vaila			5.5			R		R		68.5		R		5.0			2.0	19.0	200
	4431	uwc	Vaila		R	2.5			R		R		62.5				6.0			2.5	26.5	200

Al – allanite, At – anatase, Ap – apatite, Ca – calcic amphibole, Cp – clinopyroxene, Cr – chrome spinel, Ct – chloritoid, Ep – epidote, Gh – gahnite, Gt – garnet, Ky – kyanite, Mo – monazite, Ru – rutile, Sp – titanite, St – staurolite, To – tourmaline, Zr – zircon

R – rare (<0.5%)

Table 6. Heavy mineral ratio data from Faeroe-Shetland Basin samples analysed in the SINDRI study.

Well	Depth (m)	type	Litho unit	ATi	Total	GZi	Total	RuZi	Total	MZi	Total	CZi	Total
204/19-3a	1500	uwc	Flett	55.9	68	83.3	240	27.0	274	1.0	202	0.5	201
	1590	uwc	Flett	100.0	29	88.3	214	21.9	32	7.4	27	0.0	25
	1710	uwc	Flett	73.1	78	88.5	226	23.4	197	0.0	151	0.7	152
204/24a-7	1405	uwc	Flett	47.4	38	80.3	249	26.4	121	3.3	92	1.1	90
	1425	uwc	Flett	52.2	46	84.0	238	39.8	249	1.7	175	0.6	173
205/9-1	2390	uwc	Flett	53.3	30	77.9	263	26.7	273	1.0	202	2.0	204
	2450	uwc	Flett	33.3	45	74.2	310	18.1	188	1.3	156	1.9	157
	2540	uwc	Flett	85.0	200	93.0	215	31.5	292	2.4	205	0.5	201
	3470.2	core	Lamba	81.0	200	92.5	200	37.0	200	2.0	204	4.8	210
	3712.1	core	Lamba	89.5	200	98.5	203	2.4	127	0.0	124	0.0	124
206/1-1A	2185	uwc	Flett	23.3	30	62.1	322	17.0	241	0.0	200	3.8	208
	2293.5	core	Flett	62.0	200	77.2	259	37.3	319	1.0	202	3.9	208
	2303.7	core	Flett	98.0	200	53.9	217	41.4	341	1.5	203	1.0	202
	2313.9	core	Flett	92.0	200	80.7	248	34.9	307	1.5	203	1.0	202
	2332.9	core	Flett	94.0	200	83.3	240	41.2	340	1.0	202	2.9	206
	2359.2	core	Flett	70.2	161	96.6	207	67.5	308	1.0	202	2.0	204
	2368.0	core	Flett	87.5	200	86.6	231	42.2	346	2.0	204	0.0	200
	2374.1	core	Flett	85.5	200	95.6	209	61.8	262	0.6	173	2.8	177
214/19-1	3876	uwc	Vaila	77.5	200	89.7	223	30.8	172	0.0	119	1.7	121
	4140	uwc	Vaila	47.0	200	68.7	291	20.0	250	0.5	201	0.0	200
	4170	uwc	Vaila	68.0	200	74.3	269	19.4	248	0.0	200	0.0	200
	4200	uwc	Vaila	50.0	200	64.9	231	20.9	253	1.0	202	0.0	200
	4230	uwc	Vaila	47.0	200	68.7	291	20.0	250	0.5	201	0.0	200
	4260	uwc	Vaila	46.4	110	75.3	288	24.1	266	0.5	201	0.5	201
	4290	uwc	Vaila	70.3	148	78.2	262	27.3	275	0.5	201	1.0	202
	4431	uwc	Vaila	41.4	29	70.3	354	17.4	242	0.0	200	0.5	201

ATi – apatite:tourmaline index, GZi – garnet:zircon index, RuZi – rutile:zircon index, MZi – monazite:zircon index, CZi – chrome spinel:zircon index

(see Appendix for definitions)

Evaluation of novel analytical techniques for provenance analysis I: CCSEM

Dirk Frei[1], Martina Frei[1], Maiken Hansen Klünder[1], Thomas Rasmussen[1], Christian Knudsen[1], Andrew C. Morton[2]

[1]Geological Survey of Denmark and Greenland, Øster Voldgade 10, DK-1350 Copenhagen K, Denmark
[2]HM Research Associates, 100 Main Street, Woodhouse Eaves, Leicestershire, LE12 8RZ, UK

Introduction

Mineralogical analysis of the heavy mineral fraction of clastic sediments is a powerful approach to constrain provenance. Provenance sensitive heavy mineral ratios and geochemistry of detrital garnets helps to characterize the lithology of source areas and to correlate sedimentary successions (e.g. Morton & Hallsworth 1994; 1999) Therefore, combination of the two approaches helps to identify the nature of sedimentary source areas.

The major drawback of both approaches is that they are based on tedious and time consuming sample preparation and analytical procedures, such like point counting by optical microscopy and electron microprobe analysis (EMPA), resulting in comparatively high costs. Hence, in many cases the application of these conventional techniques is prohibitively expensive, especially if large sets of samples have to be considered. The development of alternative analytical techniques which are more cost-efficient is therefore highly desirable.

Computer controlled scanning electron microscopy (CCSEM) has the potential to provide the same, or even more detailed information with sufficient precision more rapidly and economically. One of the major goals of the research project “Linking the Faroese and Greenland: an innovative, integrated provenance study” was to test the results obtained by CCSEM against those obtained by optical microscopy and EMPA. In the following, we present the results of a very detailed comparative study and we shall demonstrate that CCSEM is indeed a reliable, cost-efficient technique for advanced provenance studies.

Comparison of CCSEM and conventional techniques for chemical characterisation of heavy minerals

CCSEM is used for the rapid determination of modal abundances, average chemical compositions, grain size distributions, and grain shape parameters of individual heavy mineral species. Furthermore, the maturity of the Ti-minerals (i.e. the average Ti-content of ilmenite, leucoxene and rutile) is determined. For a detailed description of the CCSEM technique and its application in provenance analysis and heavy mineral exploration the reader is addressed to Frei et al. (2005a) and Frei et al. (2005b).

Ideally, for CCSEM analysis no mineral grains should be in grain-to-grain contact. Consequently, CCSEM technique is vulnerable to poor liberation of mineral grains especially when dealing with highly indurated rocks such as sandstones. Originally, it was planned to obtain all CCSEM data on processed whole-rock samples. However, reconnaissance CCSEM analysis for a total of 18 whole rock samples proved that the degree of liberation was insufficient for the purposes of this study (Fig. 1).

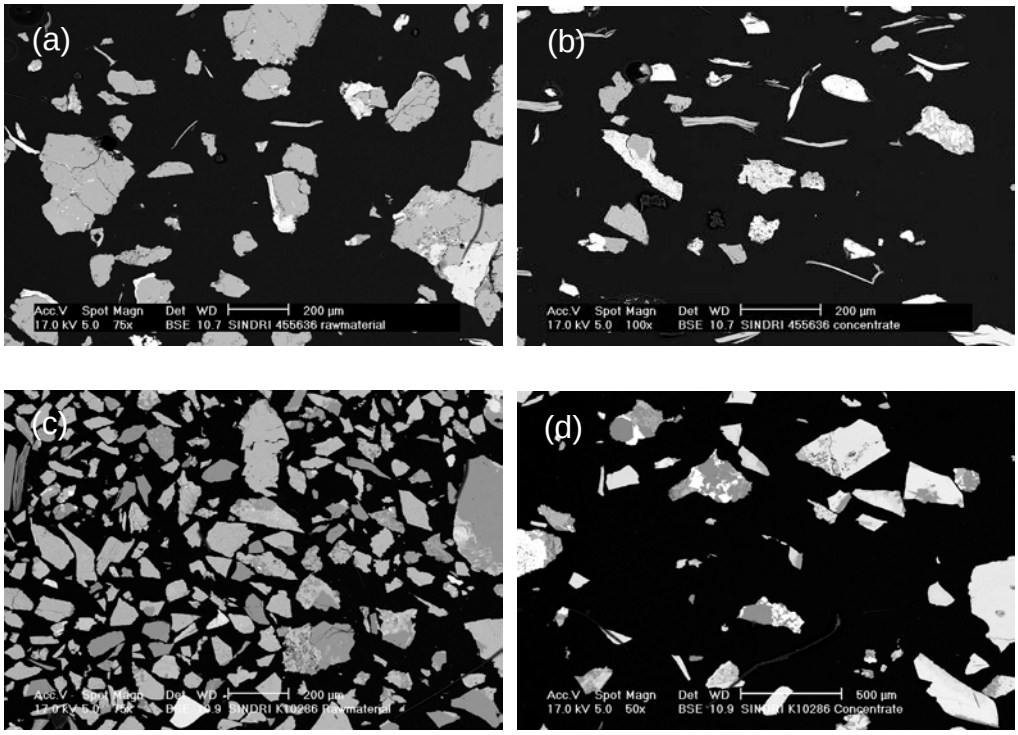

Figure 1. *Backscattered electron images of whole rock samples 455636 (top) and K 10286 (bottom) prepared for CCSEM analysis (**a** & **c**: whole rock sample; **b** & **d**: heavy mineral fraction obtained from the whole rock sample by mineral separation using heavy liquids). Note the poor liberation of individual mineral grains in both the whole rock sample and, especially critical for CCSEM, the heavy mineral fraction obtained by heavy liquid separation.*

The modal abundances of the major rock-forming and heavy minerals as determined by CCSEM for whole rock samples and their corresponding heavy mineral fractions are depicted in Fig. 2. A very high proportion of undifferentiated silicates (consisting mainly of quartz, feldspar and mica) and unclassified mineral grains (most likely mixed analysis of poorly liberated, agglomerated grains; *cf.* Fig. 1) are determined for both whole rock samples and heavy mineral fractions. Especially for the heavy mineral fraction, the amount of heavy minerals counted is dissapointingly low. Based on these reconnaissance experiments, we concluded that the data obtained in this fashion is not representative and insufficient for statistical treatment.

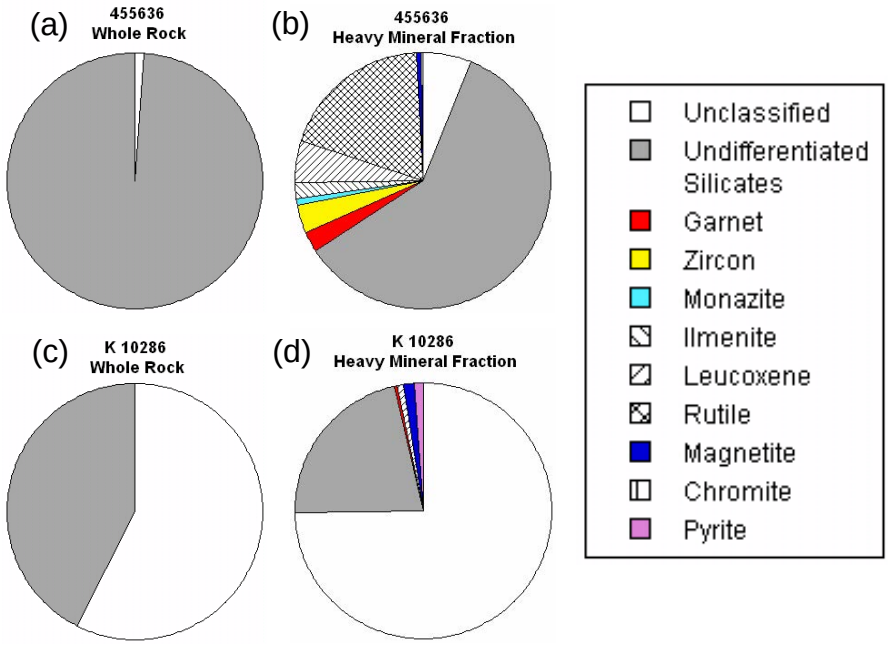

Figure 2. *Mineral modal abundances of whole rock samples 455636 (top) and K 10286 (bottom) determined by CCSEM analysis (**a** & **c**: whole rock sample; **b** & **d**: heavy mineral fraction obtained from the whole rock sample by mineral separation using heavy liquids). The poor liberation leads to high modal abundances of undifferentiated silicates (mainly quartz, feldspar and mica) and unclassified grains especially in the fraction obtained by heavy liquid separation.*

Therefore, we tested with a number of preparation techniques to find a method that ensures as good liberation of the heavy mineral fraction as possible. We found that the sample preparation method that yields the highest amount of liberated heavy mineral grains (apart from hand-picking) is closely following the method routinely employed by Morton et al. (this volume; *cf.* Appendix A). Here, samples are gently diaggregated without grinding using a pestle and mortar, and the heavy mineral fraction is obtained by heavy liquid separation from the 63 to 125 µm grain size fraction. We therefore altered our experimental strategy and used two different sets of samples for all subsequent CCSEM analyses: (1) heavy mineral residues obtained from whole rocks by heavy liquid separation from the 63 to 125 µm grain size fraction (prepared by Andrew Morton, HM Research Associates) and garnet separates obtained by hand-picking. The basic principles of CCSEM analysis, as well as all analytical and sample preparation details are reported in Appendix B. The results for all investigated samples are presented in ternary diagrams in Plates 1 and 2 in Appendices A and B. All data obtained by CCSEM and EMPA are reported in Excel based spreadsheets in the attached data CD-ROM.

Garnet major element geochemistry

Detrital garnet is one of the most frequent heavy minerals in clastic sediments, especially in NW Europe. Because garnet has a wide range in potential major element compositions that are strongly dependent on paragenesis, garnet geochemical studies have proved particularly useful in identifying and characterising the provenance of clastic sediments (e.g. Morton 1985; Hutchison and Oliver 1998; Morton et al. 2004).

Garnet major element compositions are conventionally acquired from hand-picked grains by wavelength-dispersive (WDS) or energy-dispersive (EDS) X-ray electron microprobe analysis (EMPA). Data is usually acquired by spot analysis on grain surfaces of garnets mounted on sample stubs (e.g. Morton et al., 2004) or on embedded, sectioned, and polished grain mounts. In either way, analysis is tedious and time-consuming because all analysis have to be pre-set manually by an operator. In contrast, all data is acquired fully automatic in CCSEM analysis without the need for pre-setting analysis points manually. Consequently, CCSEM analyses is much more time and cost efficient compared to conventional analysis.

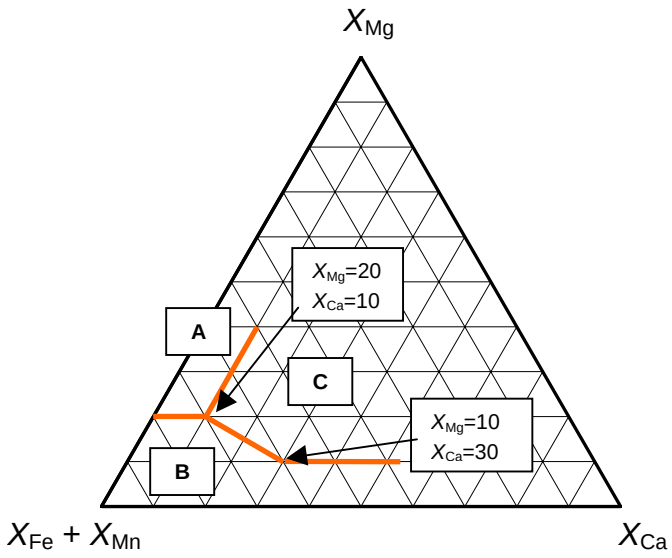

Figure 3. *Ternary plot showing the boundaries of the compositional fields for Type A, B and C garnets according to Morton et al. (2004). See text for further explanations.*

In order to test the reliability of the garnet major element data that CCSEM analysis provides, we have determined the major element chemistry of 2835 detrital garnets separated from 37 samples (collected in the Kangerlussuaq area and in wells in the UK sector of the Faroe-Shetland Basin) by EMP using WDS analysis. All samples were subsequently re-analysed by CCSEM using the same polished mounts prepared from garnet separates that were previously used for EMPA analyses. For all garnets analysed in this fashion, compositions are expressed in terms of the endmember molecules pyrope (Mg), almandine (Fe^{2+}), grossular (Ca) and spessartine (Mn). The compositional variation of the garnet assemblages is depicted in ternary diagrams using the molecular proportions of Fe + Mn, Mg, and Ca (i.e. X_{Fe}+X_{Mn}, X_{Mg} and X_{Ca}, respectively) as poles. All garnet compositional data is dis-

cussed using the interpretative framework of Morton et al. (2004) that subdivides the ternary compositional space into three different garnet assemblages (Fig. 3): Type A garnets (low Ca, high Mg) are believed to be derived from high-grade granulite facies metasedimentary rocks or charnockites; Type C garnets (high Ca, high Mg) are from metabasic rocks; and Type B garnets (low Mg, variable Ca and Mn) are predominantly from low- to medium-grade metasediments or from intermediate to acidic gneisses and granites.

In the following, we will discuss the results for garnets populations in five samples that show a characteristic and distinctive variation in the ternary composition space (samples 459682, W4629 and 459679 from East Greenland as well as samples 204/19-3a 2251,3 and 206/1-1a 7558) and are representative for the entire range in compositions observed. The results for all 37 samples analysed are graphically displayed in Plates A1 to A9 in Appendix B.

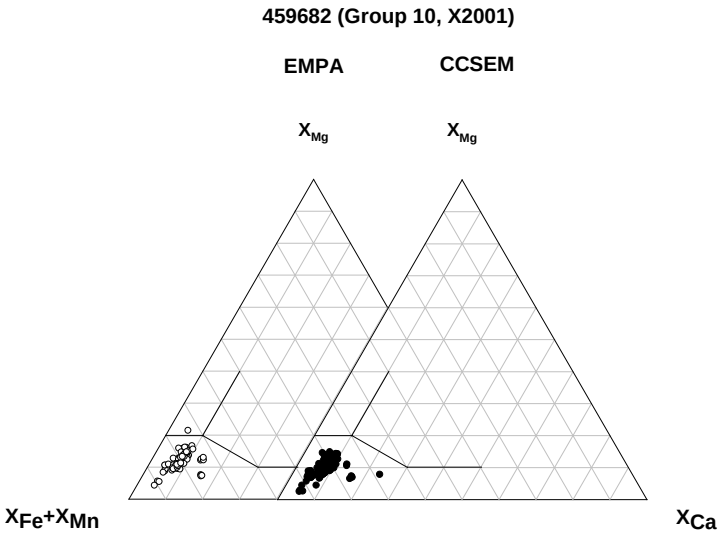

Figure 4. *Garnet compositions in sample 459682 as determined by EMPA (open symbols; left hand side) and CCSEM (solid symbols; right hand side). X_{Fe}, X_{Mn}, X_{Mg} and X_{Ca} are molecular proportions of Fe, Mn, Mg, and Ca, respectively. All Fe was calculated as Fe^{2+}. The group indicated refers to the stratigraphic subdivision of the Cretaceous-Tertiary sucession of Kangerlussuaq and Kap Dalton in ten groups according to Larsen et al. (2005). The sample location (i.e. X2001) refers to the sample locations given in the sample list in Table 1 in Appendix B.*

The garnet population from sample 459682, an Eocene sandstone from Kap Dalton, East Greenland, shows a very uniform distribution. Virtually all garnets are Fe-Mn rich and Mg-Ca poor and fall into field A of the ternary plot. The results from EMPA (open symbols) and CCSEM (solid symbols) are in excellent agreement (Fig. 4). The only minor differences are one single grain with slightly higher Mg content detected by EMPA and one single grain with slightly higher Ca-content detected by CCSEM.

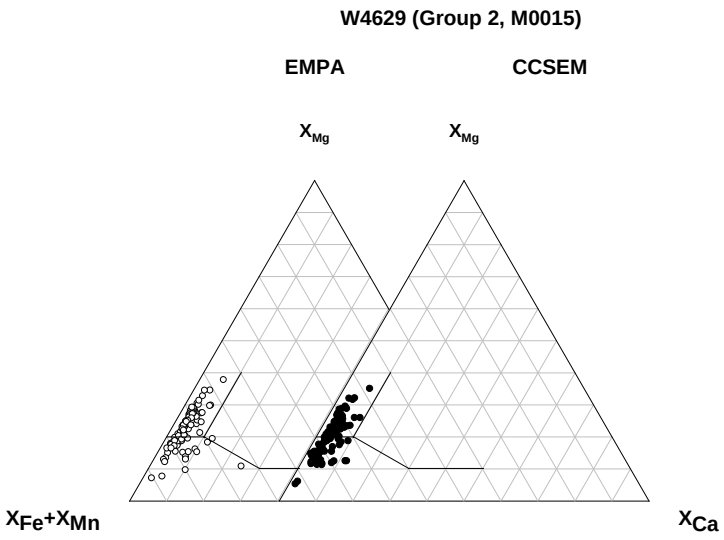

Figure 5. *Garnet compositions in sample W4629 as determined by EMPA (open symbols; left hand side) and CCSEM (solid symbols; right hand side). X_{Fe}, X_{Mn}, X_{Mg} and X_{Ca} are molecular proportions of Fe, Mn, Mg, and Ca, respectively. All Fe was calculated as Fe^{2+}. The group indicated refers to the stratigraphic subdivision of the Cretaceous-Tertiary sucession of Kangerlussuaq and Kap Dalton in ten groups according to Larsen et al. (2005). The sample location (i.e. M0015) refers to the sample locations given in the sample list in Table 1 in Appendix B.*

The garnets in sample W4629, an Albian sandstone from Kangerlussuaq, East Greenland, are continuously distributed along the Fe rich part of the pyrope – almandine+spessartine join with Mg contents varying between ~10 and 40 %, and Ca contents that are generally below 10 % (Fig. 5). Virtually all garnets plot into fields A or B of the ternary diagram. The results from EMPA (open symbols) and CCSEM (solid symbols) for this slightly more complex population are in remarkable agreement and only insignificant differences are observed. In sample 459679, again an Eocene sandstone from Kap Dalton, East Greenland, the compositional distribution resembles those observed in sample W4629, with the majority of garnets plotting with Mg contents between 10 and 40 % along the pyrope – almandine+spessartine join (Fig.6). However, a small additional population of garnets with elevated Ca contents (between 10 and 20 % Ca) plotting into field C of the ternary diagram is present. The presence of this small garnet fraction with elevated Ca contents is confidently detected by CCSEM.

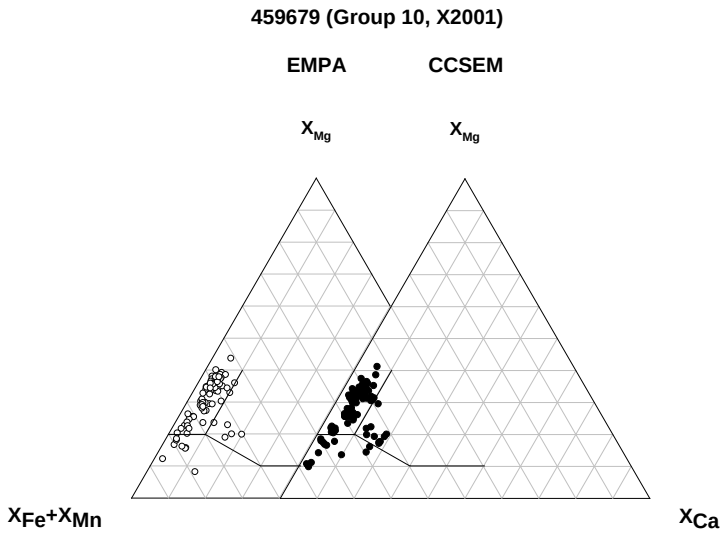

Figure 6. *Garnet compositions in sample 459679 as determined by EMPA (open symbols; left hand side) and CCSEM (solid symbols; right hand side). X_{Fe}, X_{Mn}, X_{Mg} and X_{Ca} are molecular proportions of Fe, Mn, Mg, and Ca, respectively. All Fe was calculated as Fe^{2+}. The group indicated refers to the stratigraphic subdivision of the Cretaceous-Tertiary sucession of Kangerlussuaq and Kap Dalton in ten groups according to Larsen et al. (2005). The sample location (i.e. x2001) refers to the sample locations given in the sample list in Table 1 in Appendix B.*

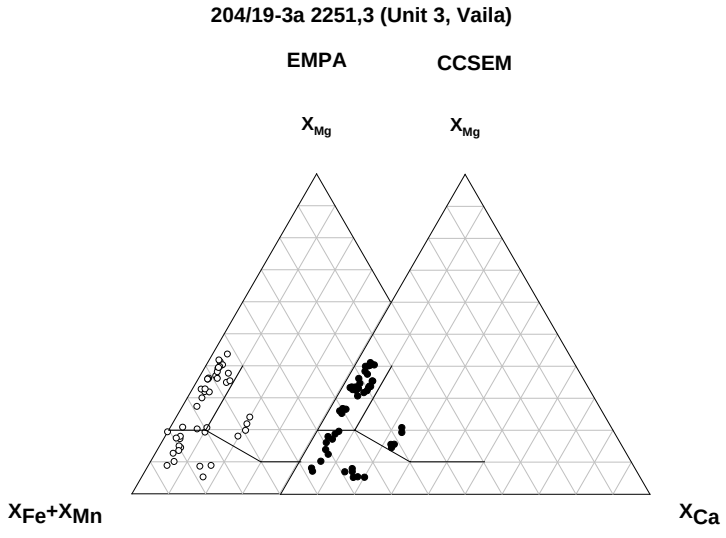

Figure 7. *Garnet compositions in sample 204/19-3a 2251,3 as determined by EMPA (open symbols; left hand side) and CCSEM (solid symbols; right hand side). X_{Fe}, X_{Mn}, X_{Mg} and X_{Ca} are molecular proportions of Fe, Mn, Mg, and Ca, respectively. All Fe was calculated as Fe^{2+}. The unit and formation indicated refers to the stratigraphic subdivision of the sedimentary sucessions drilled in the UK sector of the Faroe-Shetland Basin according to Larsen et al. (2005).*

In Fig. 7, the garnet compositions observed in a sample from the Late Paleocene Vaila Fm. (2004/19-3a 2251,3) are displayed. Compared to the three above discussed samples, the garnet distribution is more complex and consists of three relatively well defined groups: one group plotting along the pyrope – almandine+spessartine join, comparable to those observed in samples W4629 and 455682 (Figs 5 and 6, respectively), but slightly more discontinous; a second group that has elevated Ca contents (~20 % Ca) compared to group one; and a third group that has elevated Ca contents (~20 % Ca), but much lower Mg contents (~5 to 10 % Mg) compared to group one. Again, apart from minor differences, the agreement between EMPA and CCSEM is excellent and all groups are unequivocally determined by CCSEM.

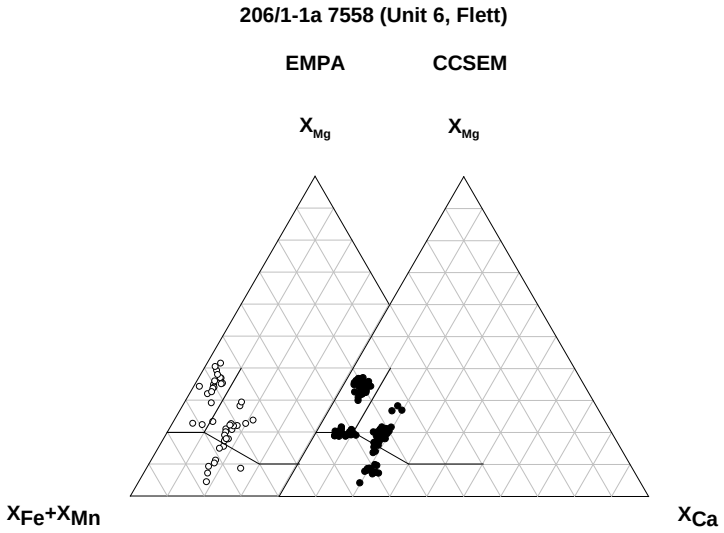

Figure 8. *Garnet compositions in sample 206/1-1a 7558 as determined by EMPA (open symbols; left hand side) and CCSEM (solid symbols; right hand side). X_{Fe}, X_{Mn}, X_{Mg} and X_{Ca} are molecular proportions of Fe, Mn, Mg, and Ca, respectively. All Fe was calculated as Fe^{2+}. The unit and formation indicated refers to the stratigraphic subdivision of the sedimentary sucessions drilled in the UK sector of the Faroe-Shetland Basin according to Larsen et al. (2005).*

The garnet compositions observed in a sample from the Late Paleocene Flett Fm. (206/1-1a 7558) are displayed in Fig. 8. The compositional distribution is complex and the garnet population can be divided in at least five different compositional clusters. Two groups with low Ca contents (< 10 % Ca) plot along the pyrope – almandine+spessartine join at ~20 and 30 to 40 % Mg, respectively. The three other groups plot at elevated Ca contents (~15 to 20 % Ca) parallel to the pyrope – alamandine+spessartine join at ~10, ~20 and 30 % Mg, respectively. However, with minor differences, CCSEM clearly differentiates between all groups present and accurately determines the locus of all five groups present. At this point it is worth to note that, because CCSEM analysis is carried out fully automatic without presetting of points for analysis, individual grains might be counted several times and hence the total number of analysis is higher compared to EMPA.

The apparent minor deviations observed between the results obtained by the EMPA and CCSEM methods might be explained with a fundamental analytical difference between the two techniques: All EMPA analysis were obtained by analysing a single spot in the core of each grain using a focussed beam with a spotsize of 1 µm. Hence, EMPA analysis neglects potential chemical zoning of garnet grains. In contrast, CCSEM analysis is obtained by scanning the complete grain and therefore represents a “bulk” composition for the entire garnet grain.

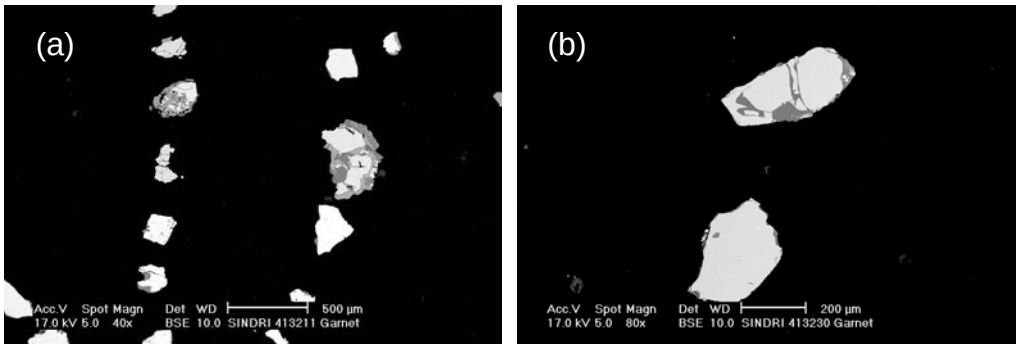

Figure 9. *Backscattered electron images of garnet separates obtained from samples 413211 (a) and 413233 (b) prepared for CCSEM analysis. Note the presence of intergrowths, inclusions and agglomerated grains that most likely cause the observed minor differences between EMPA and CCSEM results (see text for further explanation).*

Additionally, for EMPA analysis clean, inclusion and intergrowth free regions can be selected manually for spot analysis by the operator. The presence of inclusions, intergrowths and unliberated, agglomerated grains in the garnet separates prepared for this study is apparent (Fig. 9) and can not be avoided, even if outmost care is taken during hand-picking using a binocular. CCSEM does not resolve these features while scanning the entire garnet grain during EDS analysis and can be regarded as the most likely source for the minor differences between EMPA and CCSEM results.

Provenance sensitive heavy mineral ratios and CCSEM

Provenance sensitive heavy mineral ratios are very useful for correlation and provenance studies of clastic sediments, especially when environmentally stable minerals with similar hydraulic properties are used (e.g. Morton and Hallsworth 1999). The heavy mineral ratios that best reflect provenance characteristics and are the most frequently and succesful applied are apatite:tourmaline, garnet:zircon, rutile:zircon and chrome spinel:zircon (e.g. Morton et al. 2005). These ratios are conventionally determined by point-counting and the individual minerals are indentified on the basis of their optical properties using a petrographical microscope (see Appendix A for details).

It is, of course, tempting to obtain these ratios fully automatic by CCSEM, because point-counting using optical microscopy is extremely tedious, time-consuming and cumbersome. However, our preliminary results indicate a main obstacle that currently limits the applica-

tion of CCSEM for the determination of apatite:tourmaline, rutile:zircon and chrome spinel:zircon ratios. The obstacle is that all grains detected and analysed by CCSEM are subsequently classified by chemical typing algorithms. Hence, the abundances of individual mineral species are solely based on chemical information, neglecting any constraints from optical information. The implications for the determination of rutile:zircon ratios are straightforward: all TiO_2 polymorphs (i.e. rutile, anatase and brookite) will be classified as rutile, leading to higher ratios compared to those determined by optical microscopy. The implications for the determination of apatite:tourmaline and chrome spinel:zircon ratios are not as straightforward. The problem for accurate classification of these minerals is that a) both tourmaline and chrome spinel form intensive solid solution series, and b) tourmaline contains significant amounts of the light element Be, that is currently not amenable to EDS analysis. Our results indicate that the chemical typing algorithms need to be refined and fine tuned, and that synchronisation between optical and chemical properties is necessary in order to realize the potential of CCSEM for the fully automatic determination of the entire range of provenance sensitive heavy mineral ratios.

Conclusions

Our investigations have unequivocally demonstrated that the precision and accuracy of CCSEM is sufficient to determine the compositional variations of detrital garnets. Within the analytical errors and limitations of EDS analysis, the reults obtained by CCSEM are in excellent agreement with those obtained by EMPA. The apparent minor differences can be readily explained by the fact that the CCSEM analyses are performed as a scan across the whole grain, whereas EMPA analyses are usually conducted by analyzing a point in the core of a grain, with a much higher spatial resolution. For the determination of provenance sensitive heavy mineral ratios, the apparent differences between optically-based mineral classification (point-counting by petrographical microscope) and chemically-based mineral classification (CCSEM) leads to discrepancies between both methods. More research is needed in order to fine-tune and synchronise the chemical typing algorithms of CCSEM with classifications based on optical criteria. One of the advantages of CCSEM is that it provides information about the chemical maturity of the host sediment (in terms of the average TiO_2 content of the Ti-mineral fraction), the grain size distributions of individual mineral fractions and the modal abundances of individual heavy mineral species- additional data that might be very useful for the characterisation of sedimentary successions.

References

Frei, D., Rasmussen, T., Knudsen, C., Larsen, M., Whitham, A.G., Morton, A. C. 2005a: New methods and techniques for innovative, integrated provenance studies. Annales Societatis Færoensis, Supplementum **43**, 96-108.

Frei, D., Knudsen, C., McLimans, R.K., Bernstein, S. 2005b: Fully automated analysis of chemical and physical properties of individual mineral species in heavy mineral sands by Computer Controlled Scanning Electron Microscopy (CCSEM). Proceedings of the Heavy Minerals Conference *(in press).*

Hutchison, A.R., Oliver, G.J.H. 1998: Garnet provenance studies, juxtaposition of Laurentian marginal terranes and timing of the Grampian Orogeny in Scotland. Journal of the Geological Society, London **155**, 541-550.

Larsen, M., Nøhr-Hansen, H., Whitham, A.G., Kelly, S.R.A. 2005: Stratigraphy of the prebasaltic sedimentary succession of the Kangerlussuaq Basin. Volcanic basins of the North Atlantic. Danmarks og Grønlands Geologiske Undersøgelse Rapport **2005/62**.

Morton, A.C. 1985: A new approach in provenance studies: electron microprobe analysis of detrital garnets from Middle Jurassic sandstones of the northern North Sea. Sedimentology **32**, 553-566.

Morton, A.C., Hallsworth, C.R. 1994: Identifying provenance-specific features of detrial heavy mineral assemblages in sandstones. Sedimentary Geology **90**, 241-256.

Morton, A.C., Hallsworth, C.R. 1999: Processes controlling the composition of detrial heavy mineral assemblages in sandstones. Sedimentary Geology **124**: 3-29.

Morton, A.C., Hallsworth, C.R., Chalton, B. 2004: Garnet compositions in Scottish and Norwegian basement terrains: a framework for interpretation of North Sea sandstone provenance. Marine and Petroleum Geology **21**, 393-410.

Morton, A.C., Hallsworth, C.R., Whitham, A. G. 2005: Heavy mineral provenance of Paleocene-Eocene sandstones in the Faroe-Shetland Basin – results from conventional petrographic and mineral-chemical techniques. Danmarks og Grønlands Geologiske Undersøgelse Rapport **2005/54** *(this volume).*

Whitham, A.G., Morton, A.C., Fanning, C.M. 2004: Insights into Cretaceous-Paleocene sediment transport paths and basin evolution in the North Atlantic from a heavy mineral study of sandstones from southern East Greenland. Petroleum Geoscience **10**, 61-72.

Evaluation of novel analytical techniques for provenance analysis II: U-Th age dating of detrital zircons using LA-ICP-MS techniques

Martina Frei[1], Dirk Frei[1], Thomas Rasmussen[1], Christian Knudsen[1], Andrew C. Morton[2], Andrew G. Whitham[3]

[1]Geological Survey of Denmark and Greenland, Øster Voldgade 10, DK-1350 Copenhagen K, Denmark
[2]HM Research Associates, 100 Main Street, Woodhouse Eaves, Leicestershire, LE12 8RZ, UK
[3]CASP, Dept. of Earth Sciences, University of Cambridge, West Building, 181a Huntingdon Road, Cambridge, CB3 ODH, UK

Introduction

Analysis of the crystallisation ages of detrital zircon grains in clastic sediments has proved to be a powerful tool in sedimentary provenance studies (e.g. Fedo et al. 2003). Zircon is very resistant to physical and chemical alteration, and U-Pb dating of detrital zircons can therefore yield the age of their sources, even after metamorphism and deformation. Previous studies have demonstrated that accurate and precise U-Pb ages of about 60-100 zircon grains in a sample are sufficient to detect all major sedimentary source components with statistical confidence (Dodson et al. 1988; Vermeesch 2004; Andersen 2005).

The currently most widely accepted and used techniques for the determination of U-Pb ages are isotope dilution – thermal ionisation mass spectrometry (ID-TIMS), sensisitve high resolution ion microprobe (SHRIMP) and secondary ion mass spectrometry (SIMS). When combined with air abrasion and low analytical blanks, ID-TIMS yields the most precise and accurate ages for single zircon grains or domains of single grains (Krogh 1973; 1982). However, achieving the large numbers of individual analysis needed in provenance studies by ID-TIMS is prohibitively expensive. Therefore, analysis of the large numbers of detrital zircons needed for provenance studies is generally the domain of ion microprobe techniques (SHRIMP or SIMS), where relatively rapid *in-situ* analysis can be achieved. The major drawback of these techniques are the very high purchasing and operating costs of the equipment and the need for highly specialised personnel. Therefore, ion microprobes are limited to very few laboratories world-wide.

The potential of laser ablation – inductively coupled plasma – mass spectrometry (LA-ICP-MS) as a low cost alternative for U-Pb zircon dating was recognized relatively early (e.g. Feng et al. 1993; Fryer et al. 1993), but its application was hampered by the inability to yield U-Pb ages with the same precision and accuracy as those derived by SHRIMP or SIMS. Although this drawback has been overcome by recent technical developments (e.g. Horn et al. 2000; Košler et al. 2002; Tiepolo 2003), one of the most attractive features of LA-ICP-MS with respect to provenance studies is its ability to produce ^{207}Pb-^{206}Pb ages of detrital zircon grains with sufficient precision (usually in the 5-20 % range), minimal sample preparation, high sample throughput and low costs (Machado and Gauthier, 1996). It is therefore surprising that its application in sedimentary provenance studies is still in its in-

fancy. This might be partly due to the absence of studies that compare age information derived by ^{207}Pb-^{206}Pb and U-Pb dating using LA-ICP-MS with those derived by conventional U-Pb dating using SHRIMP or ID-TIMS in order to document the reliability of the age information derived by LA-ICP-MS. To date, the only available study that compares LA-ICP-MS and SIMS U-Pb dating techniques for detrital zircons is the contribution by Košler et al. (2002). They report excellent agreement between concordant LA-ICP-MS and SIMS analyses. However, the study by Košler et al. is based on results from only one zircon population extracted from a Lower Silurian metasandstone from the Ulven Group, Skarfjell Formation, Norway.

LA-ICP-MS techniques using high resolution double focussing magnetic sectorfield mass spectrometers as mass analysers are fastly emerging as an alternative to SHRIMP and SIMS for the *in-situ* U-Pb dating of detrital zircons (Tiepolo et al. 2003; Tiepolo 2003). Compared to the traditionally used quadrupole mass analysers, high resolution magnetic sectorfield mass analysers offer supreme sensitivity and enhanced precision for the determination of isotope ratios. As a result, this technique offers the determination of U-Pb isotopic ratios with a precision and accuracy that is in the same order of magnitude compared to SHRIMP and SIMS, but has an at least five-fold higher sample throughput and substantially lower acquisition and operating costs.

Here we present the results of a detailed study that compares ^{207}Pb-^{206}Pb zircon age dating using LA-quadrupole-ICP-MS (LA-Q-ICP-MS) with U-Pb zircon age dating using SHRIMP and high-resolution LA – magnetic sectorfield – ICP-MS (LA-SF-ICP-MS). The SHRIMP analysis have been performed at the Australian National University in Canberra, whereas the LA-SF-ICP-MS analysis were performed at the newly established facility at the Geological Survey of Denmark and Greenland (GEUS) using an ELEMENT2 high resolution double focussing magnetic sectorfield mass spectrometer. In total, 607 individual zircon grains (obtained from samples from the Kangerlussuaq area, East Greenland and from wells in the UK sector of the Faroe-Shetland Basin) have been analysed at least twice by one of the different techniques. The results clearly demonstrate the reliability of LA-ICP-MS for detrital zircon geochronology. The experimental and analytical details for all methods employed are reported in Appendix B. A brief description of the principles of the different zircon age dating techniques is also provided in Appendix B. All zircon age dating results are reported in Excel-based spreadsheets in the attached data CD-ROM.

Comparison of ^{207}Pb-^{206}Pb dating using LA-Q-ICP-MS and U-Pb dating using SHRIMP

The comparison of these two techniques is based on three Cretaceous to Paleogene sandstone samples from the Kangerlussuaq area, East Greenland. Two aliquots of zircons were separated from each sample by hand-picking from a heavy mineral concentrate: one aliquot was separated by CASP and a second aliquot was subsequently separated from the remaining residue by GEUS (by different personnel). For each sample, the zircon aliquot prepared by CASP was analysed by U-Pb dating employing SHRIMP whereas the aliquot prepared by GEUS was analysed by ^{207}Pb-^{206}Pb dating employing LA-Q-ICP-MS. This approach allows to check if the hand-picking separation step introduces any bias to the re-

sulting age distributions. A detailed description of the samples, as well as the SHRIMP methodology and SHRIMP results are given by Whitham et al. (2004). The LA-Q-ICP-MS methodology was described in detail by Frei et al. (2005).

The results obtained are displayed in histograms in Figs 1-3. The most important result is that, within analyical error, the age distributions of the zircon populations determined by the two methods are in good agreement. For all three investigated samples, the overall patterns are reassuringly similar, and all significant age groups identified by SHRIMP are also recognized by LA-Q-ICP-MS. Moreover, the relative frequency of occurence in each age group is, apart from minor deviations, strikingly similar.

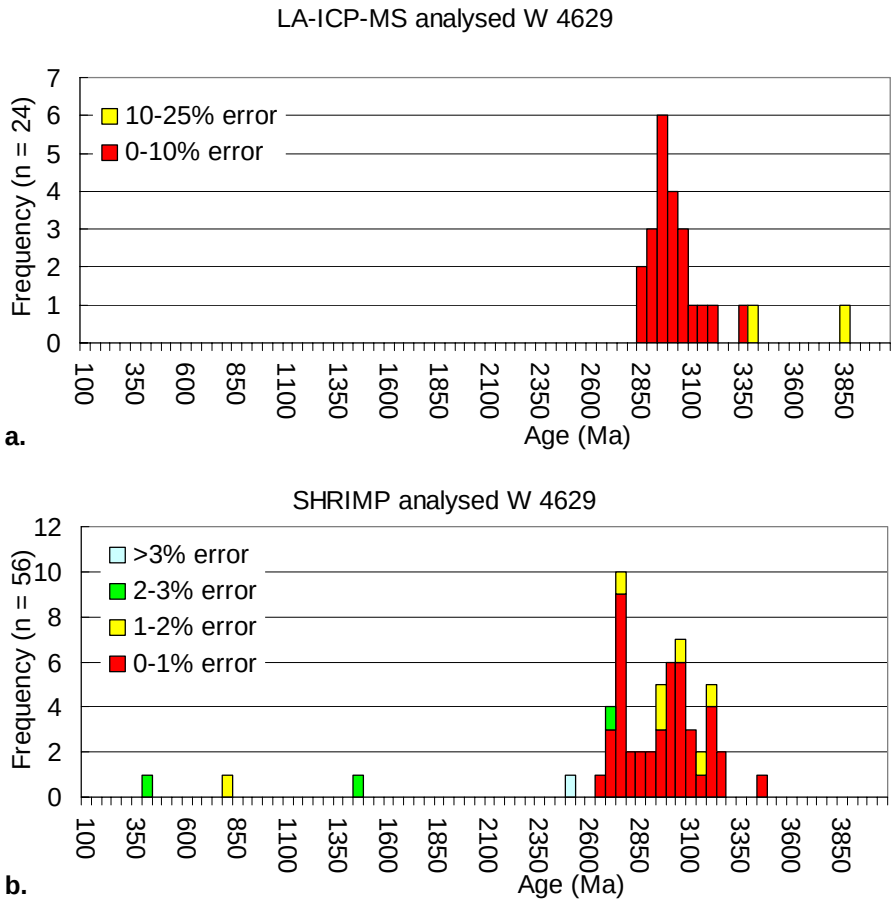

Figure 1. *Histograms displaying the distribution of ^{207}Pb-^{206}Pb zircon ages from Albian sandstones (sample W4629) from Kangerlussuaq, East Greenland, (**a**) determined by LA-ICP-MS, and (**b**) determined by SHRIMP.*

The zircon ages in the Albian sandstone (sample W 4629; Fig. 1) all fall in one large age group between 2600 Ma to 3300 Ma. Within this group, three minor clusters at 2720 Ma, 2960 Ma to 3120 Ma, and 3180 Ma can be distinguished in the SHRIMP determinations. Additionally, the SHRIMP method reveals individual occurences of younger zircons including a single zircon with a Paleoproterozoic age undetected by LA-ICP-MS. This is probably

due to the small number of zircon grains (total number = 24) that could be separated and analysed by LA-ICP-MS.

In contrast, the observed zircon age distribution in the Maastrichtian sandstone (sample W 4627; Figure 2) is relatively complex. However, the same five groups of zircon ages (900-1300 Ma, 1450-1500 Ma, 1600-2000 Ma, 2500-2600 Ma, and 2700-2800 Ma) are distinguished by both techniques. Furthermore, both techniques indicate the minor presence of young Caledonian (~500-600 Ma) and older Middle Archaean (~3100-3500 Ma) zircons.

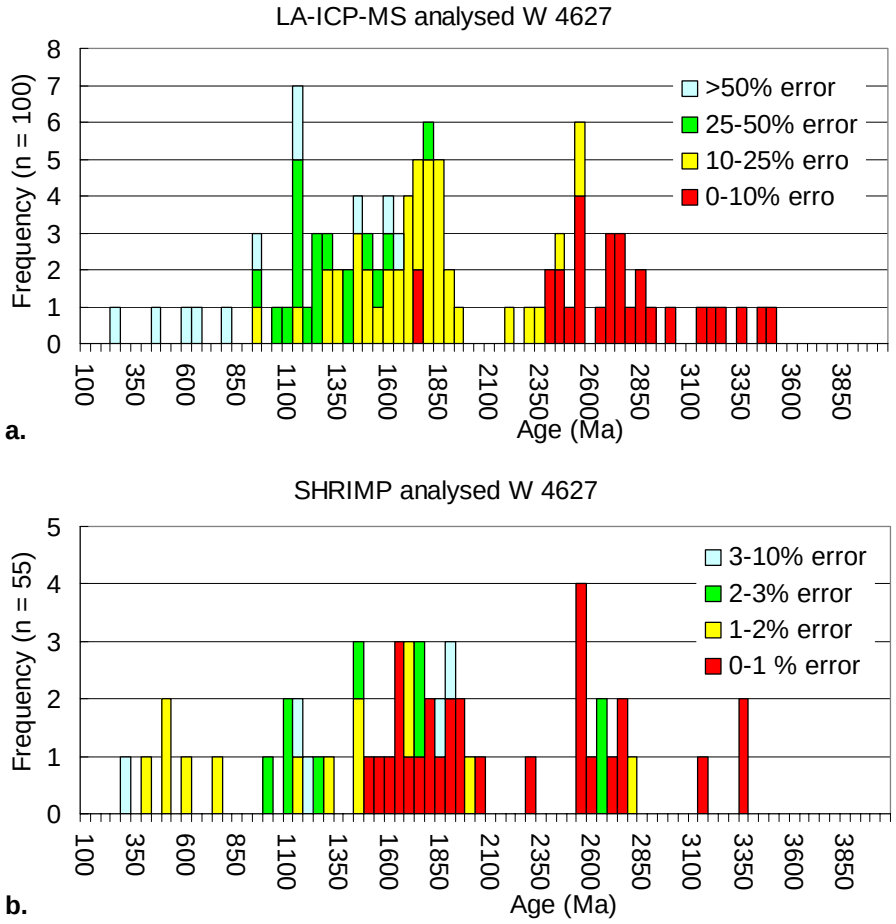

Figure 2. *Histograms displaying the distribution of ^{207}Pb-^{206}Pb zircon ages from Maastrichtian sandstones (sample W4627) from Kangerlussuaq, southern East Greenland, (**a**) determined by LA-ICP-MS, and (**b**) determined by SHRIMP.*

The zircon age distribution in the Early Eocene sandstone (sample P 5219; Fig. 3) is similar to the age distribution observed in the Albian sandstone (sample W 4629; *cf.* Fig. 1) with one large age group ranging from ~2600 Ma to ~3300 Ma that can be subdivided into three distinctive clusters around 2700-2750 Ma, 2950-3100 Ma, and 3200 Ma. Both methods reveal the presence of older, Paleoarchaean grains (~3700 Ma).

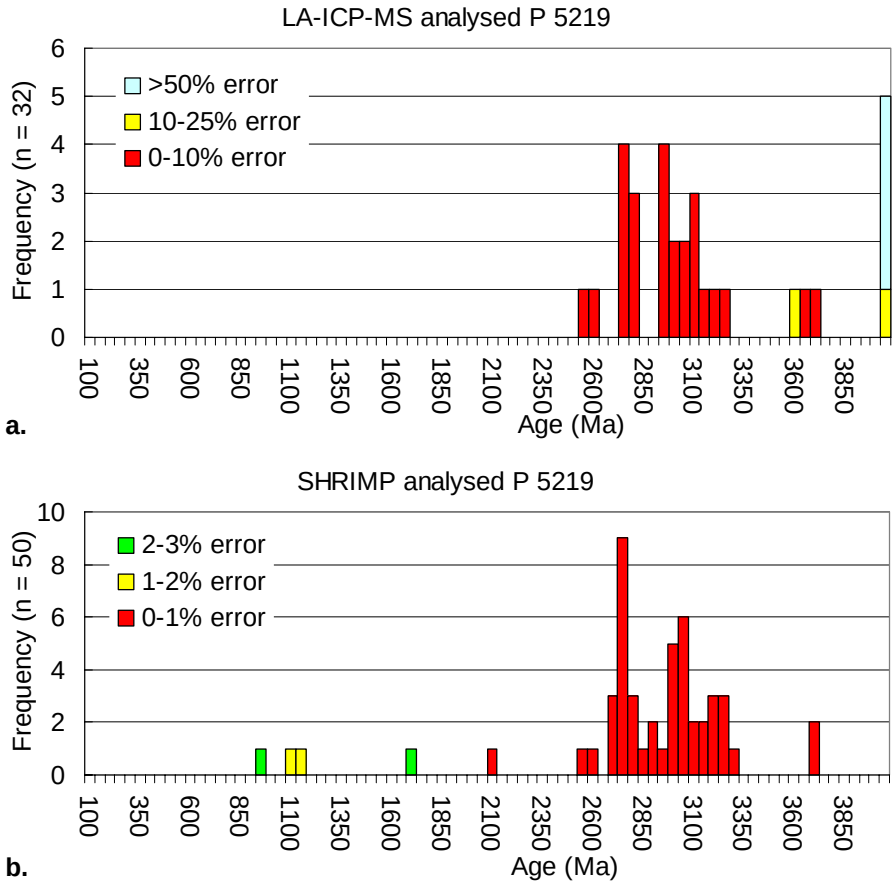

Figure 3. *Histograms displaying the distribution of ^{207}Pb-^{206}Pb zircon ages from Paleocene sandstones (sample P5219) from Kangerlussuaq, southern East Greenland, (**a**) determined by LA-ICP-MS; and (**b**) determined by SHRIMP.*

Comparison of ^{207}Pb-^{206}Pb dating using LA-Q-ICP-MS and U-Pb dating using LA-SF-ICP-MS

The comparison of ^{207}Pb-^{206}Pb dating using LA-Q-ICP-MS and U-Th dating using LA-SF-ICP-MS is based on four Cretaceous to Paleogene sandstone samples (samples 406736, 413245, 412784 and 455112) from the Kangerlussuaq area, East Greenland, and one Late Paleocene sample from the Lamda Fm. in well 204/19-3a (sample 1944.21) drilled in the UK sector of the Faroe-Shetland Basin. Detrital zircons were separated from each sample by hand-picking to optical clearness from a heavy mineral concentrate ontained by standard mineral separation techniques at GEUS. For ^{207}Pb-^{206}Pb dating by LA-Q-ICP-MS, zircons were mounted on double-sided adhesive tape and analysed with a single line scan on each individual grain. All zircon mounts were subsequently embedded in resin, ground and polished for U-Pb dating by LA-SF-ICP-MS. Prior to analysis, each individual grain was checked for internal growth structures by backscattered electron imaging. Analyses were acquired on a single spot on each individaul ziron.

The results obtained are displayed in histograms in Figs 4, 6, 8, 10, and 12. All concordant grains (concordance filtered at 95–105 %) determined by LA-SF-ICP-MS are displayed in a histogram combined with a probability density distribution plot (using AgeDisplay; Sircombe, 2004) in Figs 5, 7, 9, 11, and 13. The most important result is that apart from minor deviations, the age distributions of the zircon populations determined by the two methods are in excellent agreement. For all three investigated samples, the overall patterns are reassuringly similar and all significant age groups identified by LA-SF-ICP-MS are also recognized by LA-Q-ICP-MS. Furthermore, the relative frequency of occurence in each age group is generally in very good agreement.

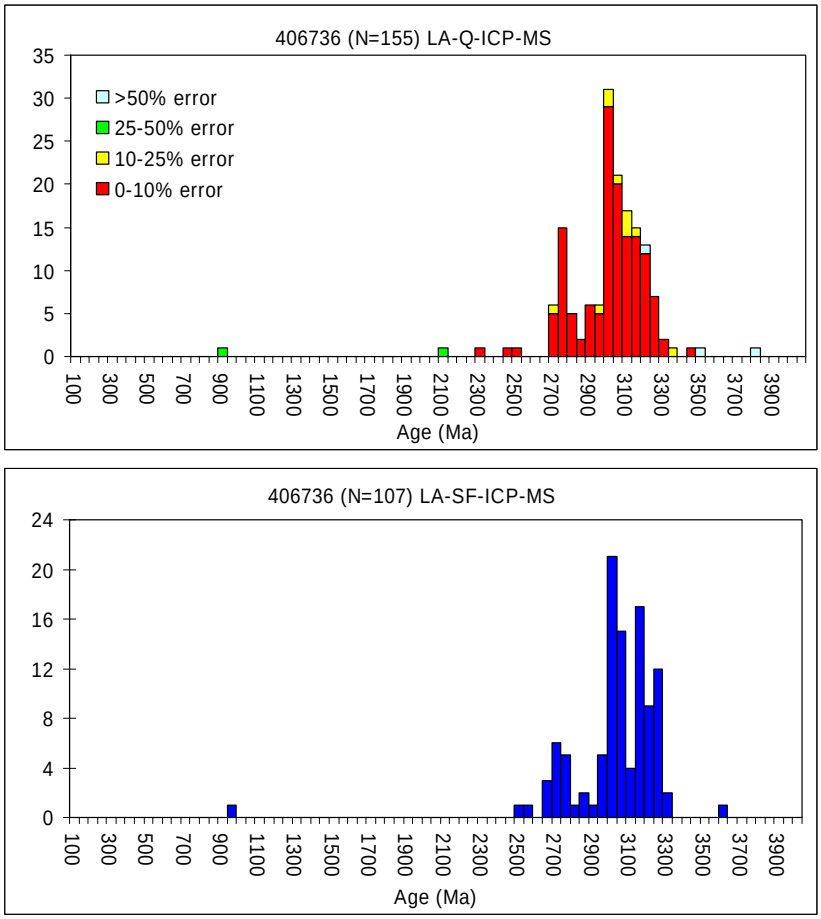

Figure 4. *Histograms displaying the distribution of detrital zircon ages in a Late Paleocene sandstone (sample 406736) determined by LA-Q-ICP-MS (top) and determined by LA-SF-ICP-MS (bottom).*

The zircon age distribution in a Late Paleocene sandstone (sample 406736) determined by ^{207}Pb-^{206}Pb dating (LA-Q-ICP-MS; Fig. 4, top) is characterised by one minor age group at 2750 Ma and one large age group between 3000 Ma and 3300 Ma with a pronounced peak at 3000 Ma. Additionally, single grains that fall outside these two age groups are detected; the two most prominent ones are a grain with a Grenvillian age (~900 Ma) and a grain with an Early Archaean age (3800 Ma). The zircon age distribution determined by U-Pb dating (LA-SF-ICP-MS; Fig. 4, bottom and Fig. 5) is strikingly similar. However, the superior precision and accuracy of this method is capable of resolving three distinctive peaks at in the

large age group at 3000 Ma, 3150 Ma and 3250 Ma. The absence of some of the single grains that plot outside these two major groups is probably due to the loss of grains during re-mounting and polishing of the zircon mount (see above).

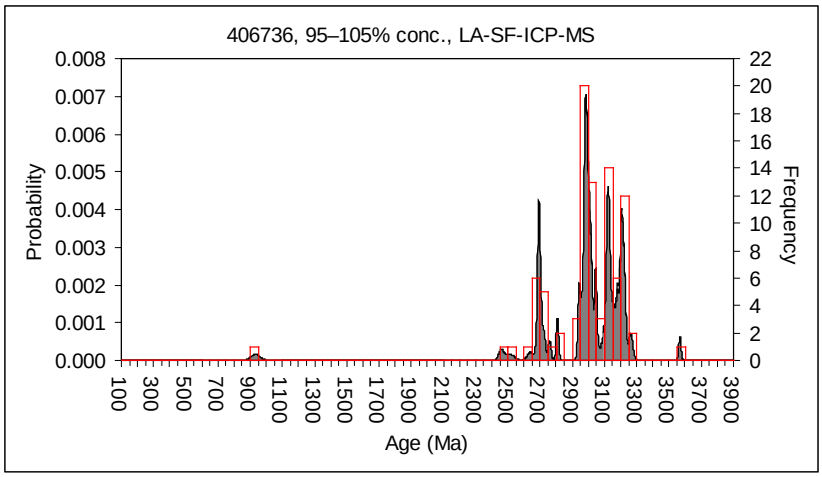

Figure 5. *Detrital zircon ages in sample 406736 determined by LA-SF-ICP-MS, displayed in a combined histogram and probability density distribution diagram. All data have been concordance filtered at 95–105 %.*

The zircon age distribution in an Early Cretaceous sandstone (sample 413245) as determined by ^{207}Pb-^{206}Pb dating (LA-Q-ICP-MS; Fig. 6, top) is characterised by a strong bimodal distribution with two main age groups. One age group is distributed between 2700-2800 Ma with a peak at 2800 Ma, the second age group shows a broader distribution between 2900 Ma and 3250 Ma with a peak at 3000 Ma. Like in sample 406736, a few single grains that fall outside these two age groups are detected. The zircon age distribution determined by U-Pb dating (LA-SF-ICP-MS; Fig. 6, bottom and Fig. 7) is in very good agreement. However, the relative frequencies observed in the second age group show minor deviations. Again, these deviations and the absence of some of the single grains outside these two major groups can be readily explained the loss of grains during re-mounting and polishing of the zircon mounts (see above).

The zircon age distribution in a Late Paleocene sandstone (sample 412784) determined by ^{207}Pb-^{206}Pb dating (LA-Q-ICP-MS; Fig. 8, top) indicates the presence of three major age groups with peaks at 2800, 3000 and 3150 Ma. A few single grains fall outside these major groups, most notably some Early Archaean grains. The zircon age distribution determined by U-Pb dating (LA-SF-ICP-MS; Fig. 8, bottom and Fig. 9) is in excellent agreement. The most prominent deviation is a small displacement of the Early Archaean grains.

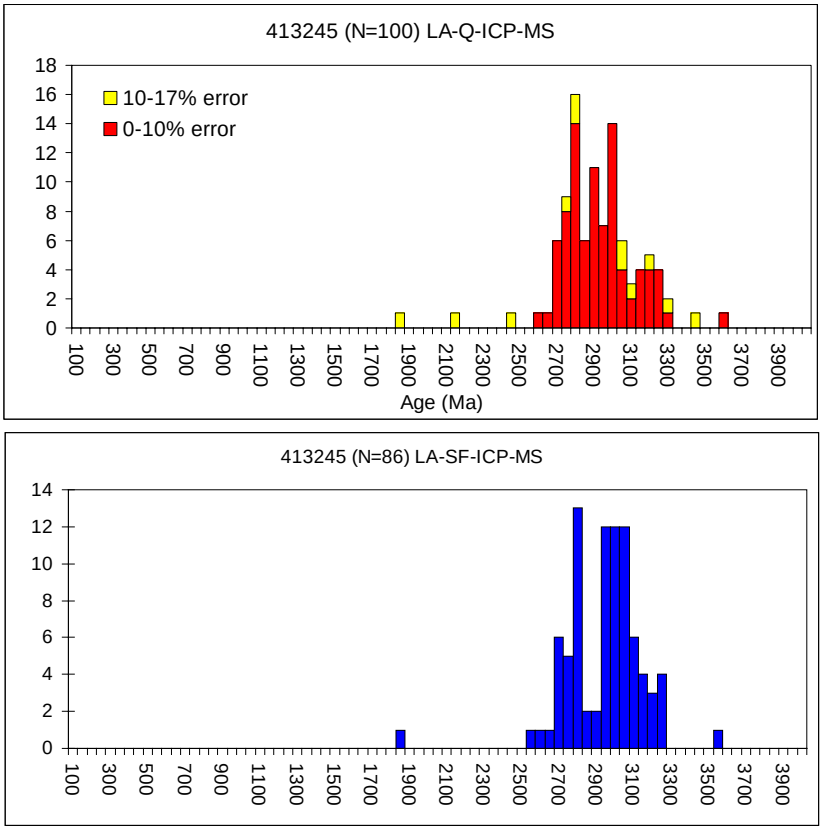

Figure 6. *Histograms displaying the distribution of detrital zircon ages in an Early Cretaceous sandstone (sample 413245) determined by LA-Q-ICP-MS (top) and LA-SF-ICP-MS (bottom).*

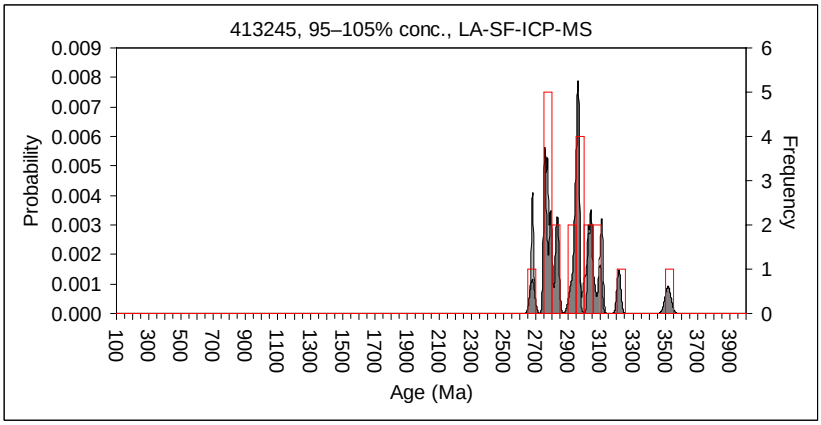

Figure 7. *Detrital zircon ages in sample 413245 determined by LA-SF-ICP-MS displayed in a combined histogram and probability density distribution diagram. All data have been concordance filtered at 95–105 %.*

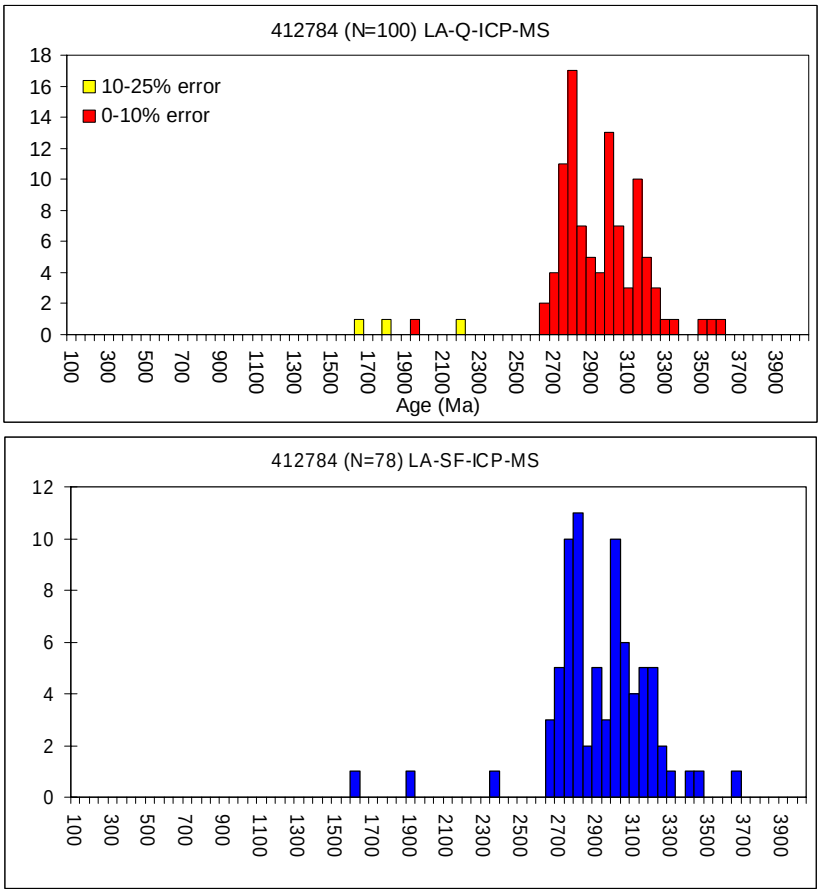

Figure 8. *Histograms displaying the distribution of detrital zircon ages in a Late Paleocene sandstone (sample 412784) determined by LA-Q-ICP-MS (top) and LA-SF-ICP-MS (bottom).*

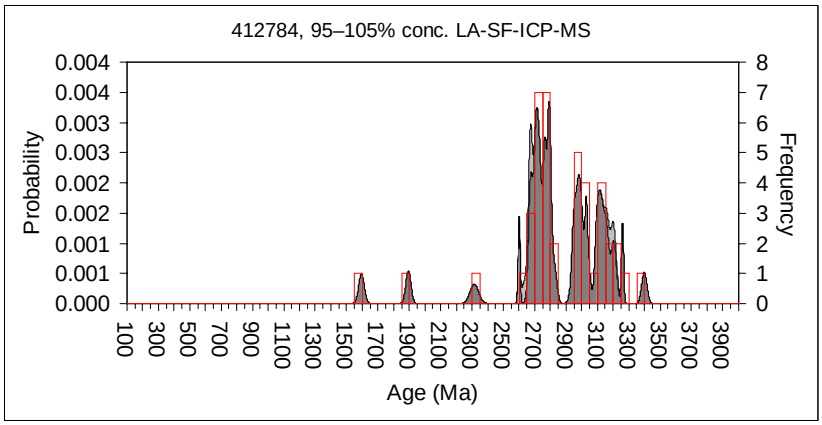

Figure 9. *Detrital zircon ages in sample 412784 determined by LA-SF-ICP-MS displayed in a combined histogram and probability density distribution diagram. All data have been concordance filtered at 95–105 %.*

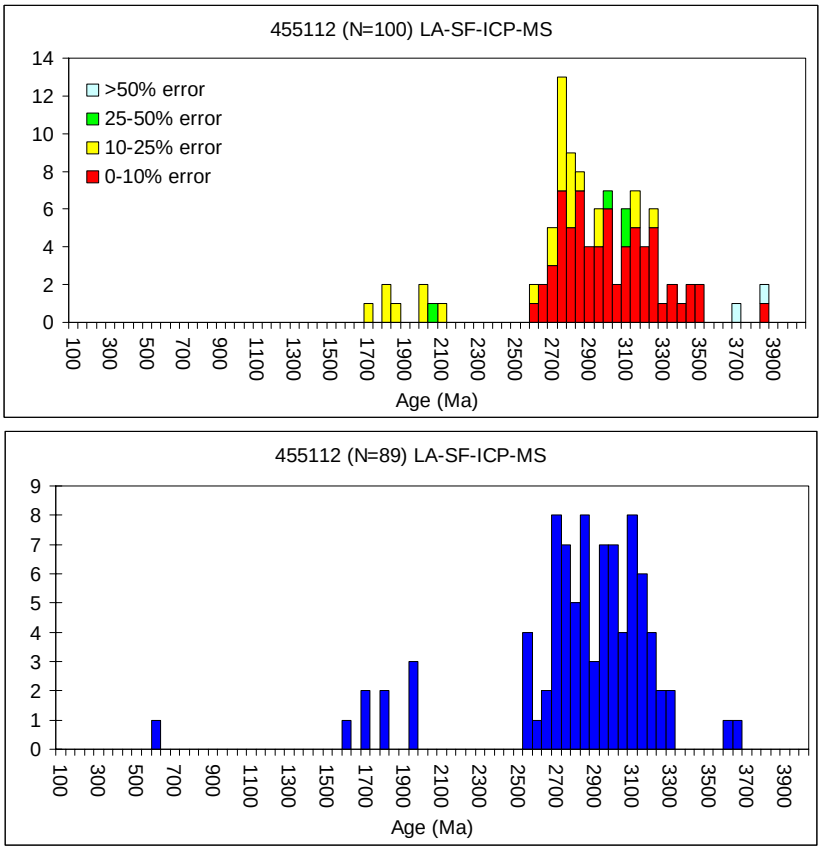

Figure 10. *Histograms displaying the distribution of detrital zircon ages in an Early Cretaceous sandstone (sample 455112) determined by LA-Q-ICP-MS (top) and LA-SF-ICP-MS (bottom).*

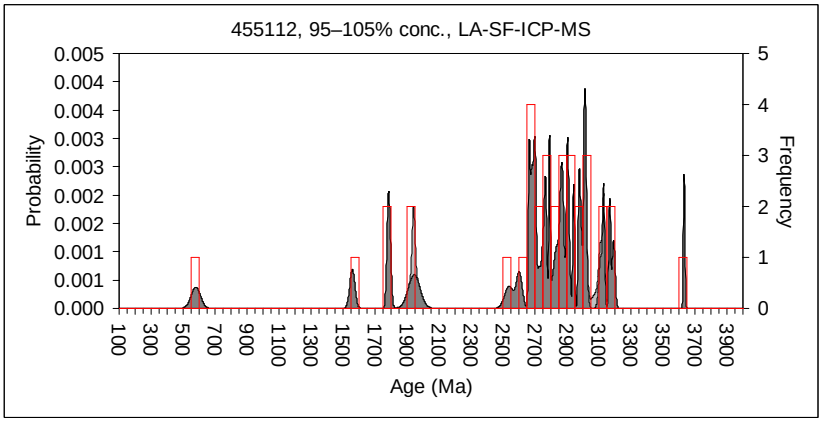

Figure 11. *Detrital zircon ages in sample 45512 determined by LA-SF-ICP-MS displayed in a combined histogram and probability density distribution diagram. All data have been concordance filtered at 95–105 %.*

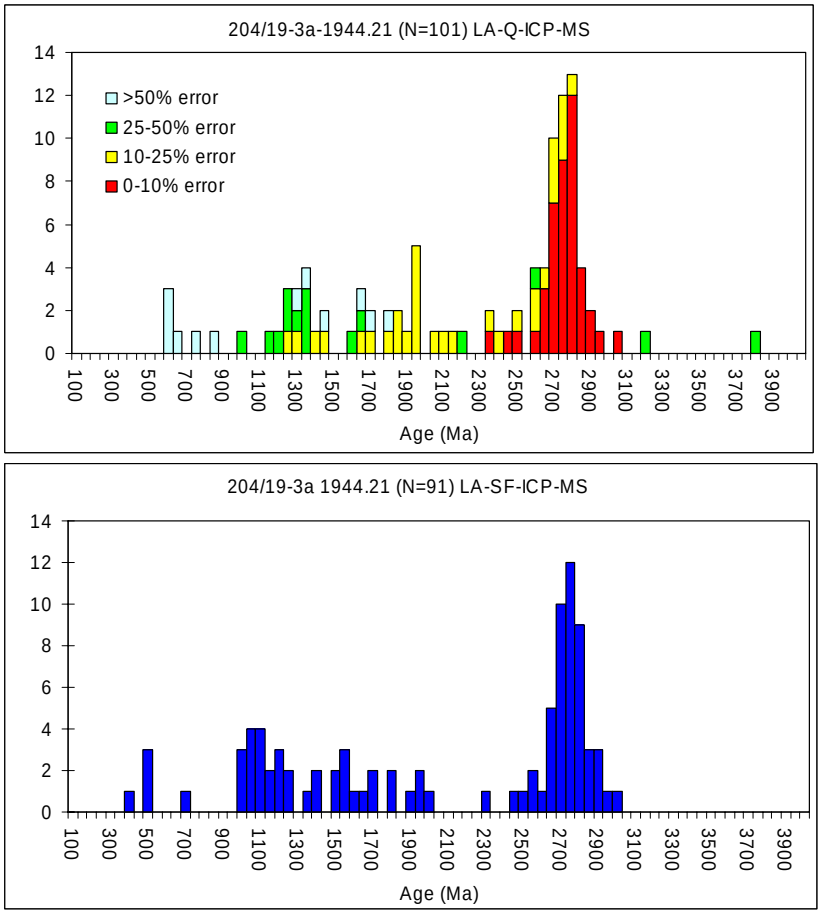

Figure 12. *Histograms displaying the distribution of detrital zircon ages in a Late Paleocene clastic sediment from (sample 204/19-3a 1944.21) determined by LA-Q-ICP-MS (top) and LA-SF-ICP-MS (bottom).*

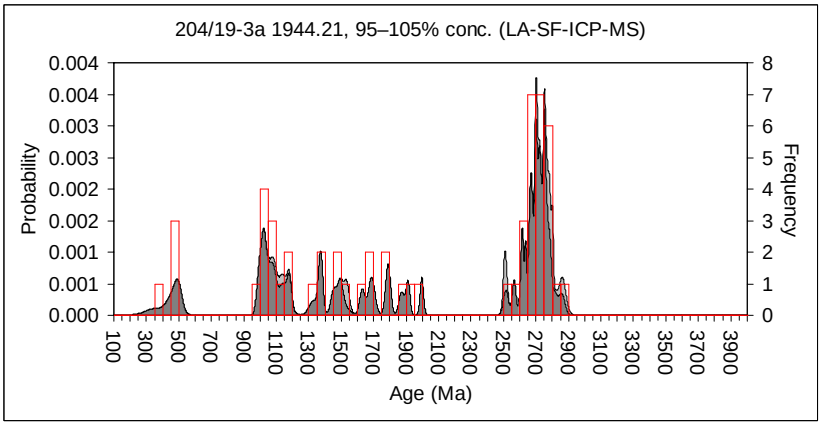

Figure 13. *Detrital zircon ages in sample 45512 determined by LA-SF-ICP-MS displayed in a combined histogram and probability density distribution diagram. All data have been concordance filtered at 95–105 %.*

The zircon age distribution in an Early Cretaceous sandstone (sample 455112) determined by ^{207}Pb-^{206}Pb dating (LA-Q-ICP-MS; Fig. 4 a) is characterised by one large, but strongly polymodal age group in the range 2500-3300 Ma with one major peak at 2750 Ma and two minor peaks at 3000 Ma and 3150 Ma. Additionally, a few Early Archaean and Proterozoic grains are present. The general age distribution pattern determined by LA-SF-ICP-MS is similar; however, an additional peak at 2500 Ma is detected and the peaks at 2750 Ma, 3000 Ma, and 3150 Ma appear with similar frequency. Furthermore, a single grain of Caledonian age is detected.

In contrast to the four samples investigated from the Kangerlussuaq area, the Late Paleocene sample (204/19-3 1944.21) from the well in the UK sector of the Faroe-Shetland Basin is characterised by a strongly polymodal age distribution. One very prominent age group ranging from 2500 Ma to 3000 Ma years, with a clear peak at 2800 Ma, is accompanied by a few small groups with Caledonian, Grenvillian and Early Proterozoic age. The most striking difference is the almost complete absence of Middle Archaean (3100-3600 Ma) rocks. The age distribution determined by LA-SF-ICP-MS is again in excellent agreement with that determined by LA-Q-ICP-MS.

Conclusions

One of the most important results of this study is that within analyical error, the age distributions of the zircon populations determined by ^{207}Pb-^{206}Pb dating using LA-Q-ICP-MS are in excellent agreement with those determined by U-Pb-dating using SHRIMP or LA-SF-ICP-MS. Clearly, both SHRIMP and LA-SF-ICP-MS offer a much higher precision compared with LA-Q-ICP-MS (and the additional advantage to check for concordance). However, the age distributions determined by the ^{207}Pb-^{206}Pb method are reassuringly similar compared with those obtained by U-Pb dating by SHRIMP or LA-SF-ICP-MS for all investigated samples. All significant age groups identified by SHRIMP and LA-SF-ICP-MS are also accurately recognized by LA-Q-ICP-MS and the relative frequency of each age group is correctly determined. These results give us every confidence that ^{207}Pb-^{206}Pb dating using LA-Q-ICP-MS is a reliable method for the determination of detrital zircon age distributions.

However, our results clearly demonstrate the enormous potential that LA-SF-ICP-MS offers for provenance studies based on detrital zircon geochronology. LA-SF-ICP-MS achieves the same precision and accuracy compared to SHRIMP and SIMS, but the sample throughput of LA-SF-ICP-MS is at least three- to four-fold higher at considerably lower costs. It is expected that the use of advanced sample cells may allow an even higher sample throughput in the near future. Because all analyses can be pre-set, only minimal operator presence is necessary. Furthermore, LA-SF-ICP-MS uses simpler and more robust equipment and the purchasing and operation costs are only a fraction of the costs of SHRIMP and SIMS. We therefore conclude that U-Pb dating by LA-SF-ICP-MS is the cost-saving technique of the future for advanced provenance studies using geochronology of detrital zircons.

References

Andersen, T. 2005. Detrital zircons as tracers of sedimentary provenance: limiting conditions from statistics and numerical simulation. Chemical Geology **216**, 249-270.

Dodson, M.H., Compston, W., Williams, I.S., Wilson, J.F. 1988: A search for ancient detrital zircons in Zimbabwean sediments. Journal of the Geological Society, London **145**, 977–983.

Fedo, C.M., Sircombe, K.N., Rainbird, R.H. 2003: Detrital zircon analysis of the sedimentary record. In: Hanchar, J.M. and Hoskin, P.W.O. (Eds) Zircon. Reviews in Mineralog and Geochemistry **53**, 277-303.

Feng, R.; Machado, N., Ludden, J. 1993: Lead geochronology of zircon by LaserProbe - Inductively Coupled Plasma Mass Specrometry (LP-ICPMS). Geochimica et Cosmochimica Acta **57**, 3479-3486.

Frei, D., Rasmussen, T., Knudsen, C., Larsen, M., Whitham, A.G., Morton, A. C. 2005: New methods and techniques for innovative, integrated provenance studies. Annales Societatis Færoensis, Supplementum **43**, 96-108.

Fryer, B.J., Jackson, S.E., Longerich, H.P. 1993: The application of laser microprobe-inductively coupled plasma-mass spectrometry (LAM-ICP-MS) to in situ (U)-Pb geochronology. Chemical Geology **109**, 1-8.

Horn, I., Rudnick, R., McDonough, W.F. 2000: Precise elemental and isotopic ratio determination by simultaneous solution nebulisation and laser ablation ICP-MS: application to U-Pb geocronology. Chemical Geology **164**, 281-301.

Horstwood, M.S., Foster, G.L., Parrish, R.R., Noble, S.R. Nowell, G.M. 2003: Common-Pb corrected *in-situ* U-Pb accessory mineral geochronology by LA-MC-ICP-MS. Journal of Analytical Atomic Spectrometry **18**, 837-846.

Kősler, J., Fonneland, H., Sylvester, P., Tubrett, M., Pedersen, R.-B. 2002: U-Pb dating of zircons for sediment provenance studies - a comparison of laser ablation ICPMS and SIMS techniques. Chemical Geology **182**, 605-618.

Krogh, T.E. 1973: A low-contamination method for hydrothermal decomposition of zircon and extraction of U and Pd for isotopic age determination. Geochimica et Cosmochimica Acta **37**, 485-494.

Krogh, T.E. 1982: Improved accuracy of U-Pb ages by the creation of more concordant systems using an air abrasion techniques. Geochimica et Cosmochimica Acta **46**, 637-649.

Morton, A.C., Hallsworth, C.R., Whitham, A. G. 2005: Heavy mineral provenance of Paleocene-Eocene sandstones in the Faroe-Shetland Basin – results from conventional petrographic and mineral-chemical techniques. Danmarks og Grønlands Geologiske Undersøgelse Rapport **2005/54** *(this volume).*

Sircombe, K.N. 2004: AgeDisplay: An EXCEL workbook to evaluate and display univariat geochronological data using binned frequency histograms and probability density distributions. Computers and Geosciences **30**, 21-31.

Tiepolo, M., Botazzi, P., Palenzona, M., Vanucci, R. 2003: A laser probe coupled with inductively coupled plasma – double focusing –sector field – mass spectrometer for *in-situ* analysis of geological samples and U-Th dating of zircon. The Canadian Mineralogist **41**, 259-272.

Tiepolo, M. 2003: *In-situ* Pb geochronology of zircon with laser ablation – inductively coupled plasma – sector field – mass spectrometry. Chemical Geology **199**, 159-177.

Vermeesch, P. 2004: How many grains are needed for a provenance study? Earth and Planetary Science Letters **224**, 351-441.

Whitham, A.G., Morton, A.C., Fanning, C.M. 2004: Insights into Cretaceous-Paleocene sediment transport paths and basin evolution in the North Atlantic from a heavy mineral study of sandstones from southern East Greenland. Petroleum Geoscience **10**, 61-72.

Heavy mineral characteristics of Cretaceous-Eocene sandstones in the Kangerlussuaq Basin, East Greenland – results from CCSEM

Dirk Frei, Martina Frei, Maiken Hansen Klünder, Thomas Rasmussen, Christian Knudsen

Geological Survey of Denmark and Greenland, Øster Voldgade 10, DK-1350 Copenhagen K, Denmark

Introduction

The geochemical information recorded in heavy minerals might yield particularly useful insights into the geological history of clastic sediments. For example, the major element geochemistry of detrital minerals like garnet or tourmaline place constraints on the chemical and physical nature of their source rock, and hence their provenance (Henry and Guidotti 1985; Morton 1985; Morton et al. 2004). The TiO_2-distribution of the Ti-mineral fraction (i.e. ilmenite, rutile and leucoxcene) of a sediment is a very sensitive indicator of its maturity and is useful for correlation of sedimentary successions (e.g. Weibel 2003; Knudsen et al. 2005) and might even have the potential to place constraints on its source rock (Bernstein et al. 2005).

Usually, chemical properties of heavy mineral species (such like detrital garnet and Ti-minerals major element chemistry) are determined by analysing mineral separates (obtained by size, gravity, magnetic, and/or other separation methods) employing microscopy, XRF or electron microprobe analyses. Besides being cumbersome, this procedure is tedious, time-consuming and labour intensive resulting in high cost, especially if large sets of samples have to be considered. In contrast, computer controlled scanning electron microscopy (CCSEM) is an elegant, reliable and relatively economic alternative for the determination of chemical properties of individual heavy mineral species in sediments (e.g. Frei et al. 2005; and references therein). Here, we present the results of a study that investigated the major element geochemistry of detrital garnet and Ti-minerals in a large set of sandstones samples from the Kangerlussuaq area, East Greenland (garnet and Ti-mineral chemistry), and from wells in the UK sector of the Faroe-Shetland Basin (garnet chemistry) using CCSEM.

Garnet major element geochemistry

All garnet compositions determined by CCSEM have been recalculated into the endmember molecules pyrope (Mg), almandine (Fe^{2+}), grossular (Ca) and spessartine (Mn). The compositional variation of the garnet assemblages is depicted in ternary diagrams using the molecular proportions of Fe + Mn, Mg, and Ca (i.e. X_{Fe}+X_{Mn}, X_{Mg} and X_{Ca}, respectively) as poles. We will discuss the garnet compositional data using the interpretative framework of Morton et al. (2004) acquired during river sediment studies of Scotland and Norway that

subdivides the ternary compositional space almandine + spessartine – pyrope – grossular in three fields of typical garnet assemblages (Figure 1): Type A garnets (low Ca, high Mg) are believed to be derived from high-grade granulite facies metasedimentary rocks or charnockites; Type C garnets (high Ca, high Mg) are from metabasic rocks; and Type B garnets (low Mg, variable Ca and Mn) are predominantly from low- to medium-grade metasediments or from intermediate to acidic gneisses and granites. The type A field is further subdivided into Ai (X_{Mg} > 30 %) and Aii (X_{Mg} 20-30 %).

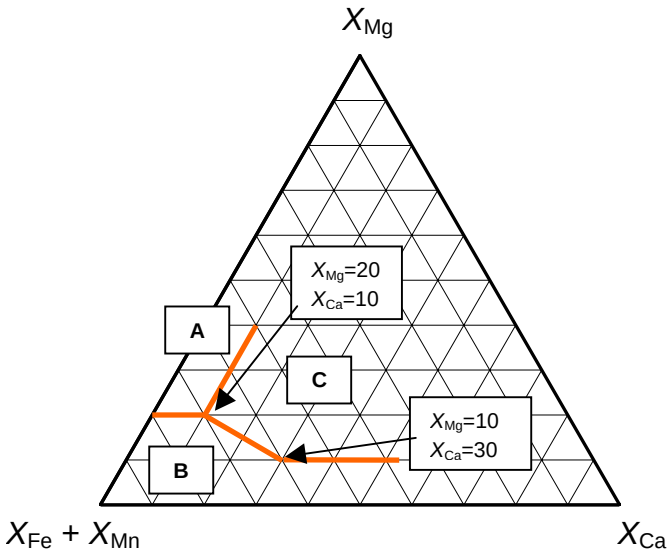

Figure 1. *Ternary plot showing the boundaries of the compositional fields for Type A, B and C garnets according to Morton et al. (2004). See text for further explanations.*

In the following, the results for representative stratigraphic profiles in the Cretaceous-Eocene succession in Kangerlussuaq, East Greenland, and in the Paleocene-Eocene successions drilled in the UK sector of the Faroe-Shetland Basin are discussed. A map depicting the stratigraphic position of all analysed samples from the Kangerlussuaq Basin and the respective garnet major element variation (depicted ternary diagrams) is provided in Enclosure 2. The results for all investigated samples are presented in ternary diagrams in Plates 1 and 2 in Appendix B. All data obtained by CCSEM is reported in Excel based spreadsheets in the attached data CD-ROM.

Kangerlussuaq Basin

The samples from the Kangerlussuaq Basin analysed in this SINDRI project have been assigned to the ten stratigraphic groups identified by Larsen et al. (2005):

Group 1: Early Cretaceous, pre-volcanic, Watkins Fjord Fm., Torsukáttak Mb., fluvial.
Group 2: Early Cretaceous, pre-volcanic, Watkins Fjord Fm., Suunigajik Mb., shallow marine.
Group 3: Early Cretaceous, pre-volcanic, Sorgenfri Fm., shelf.

Group 4: Late Cretaceous, pre-volcanic, Christian IV Fm. (‘Lower Ryberg’), shelf.

Group 5: Early Paleocene, pre-volcanic, Sediment Bjerge Fm., Fairy Tale Valley Mb., (‘Upper Ryberg’), deep marine.

Group 6: Late Paleocene, pre-volcanic, Sediment Bjerge Fm., Klitterhorn Mb. (‘Upper Ryberg’), deltaic.

Group 7: Late Paleocene, pre/syn-volcanic, Vandfaldsdalen Fm., Schjelderup Mb. (‘Ryberg Sandstone Bed’ *s. s.)*, fluvial.

Group 8: Paleocene-Eocene, syn-volcanic, Vandfaldsdalen Fm., Willow Pass Mb., fluvial.

Group 9: Paleocene-Eocene, syn-volcanic, Vandfaldsdalen Fm., Kulhøje Mb., intra basalt layer.

Group 10: Eocene, post-volcanic, Bopladsdalen Fm., Kap Dalton, Savoia Halvø, post-basalt, (outside the Kangerlussuaq Basin).

The position of these groups is shown in a sketch in Fig. 2 depicting the litho- and sequence stratigraphy of the Cretaceous-Paleogen succession of the Kangerlussuaq Basin including the major unconformities and hiatuses.

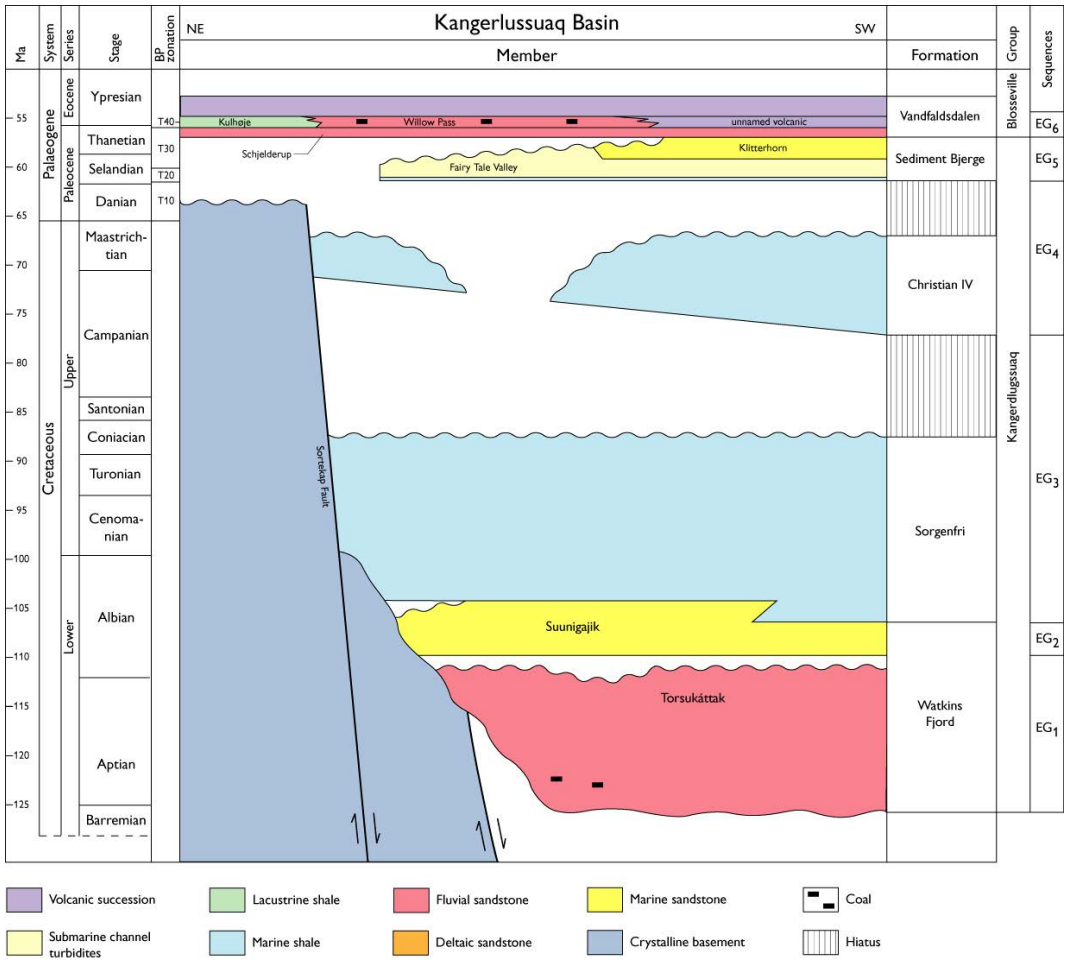

Figure 2. *Litho- and sequence stratigraphy of the Cretaceous-Paleogene succession in Kangerlussuaq, East Greenland (from Larsen et al. 2005).*

Based on detrital zircon age distribution patterns, the entire succession can be divided into three major units (*cf.* Whitham et al. 2004; Frei et al. 2005d): The first unit (Fig. 3) comprises sandstones from the Early Cretaceous stratigraphic groups 1, 2 and 3 that are predominantly derived from Archaean sources to the south or southwest; the second unit (Fig. 4) comprises sandstones from the Late Cretaceous to Late Paleocene groups 4, 5, and 6 and are predominantly derived from younger sources from the north/northeast (with subordinate sourcing from locally reworked material); and the third unit (Fig. 5) comprises sandstones from the Late Paleocene to Eocene groups 7, 8 and 9 that are again derived from Archaean sources to the north/northeast (for a detailed discussion, see Whitham et al. 2004; Morton et al. 2005; and Frei et al. 2005d).

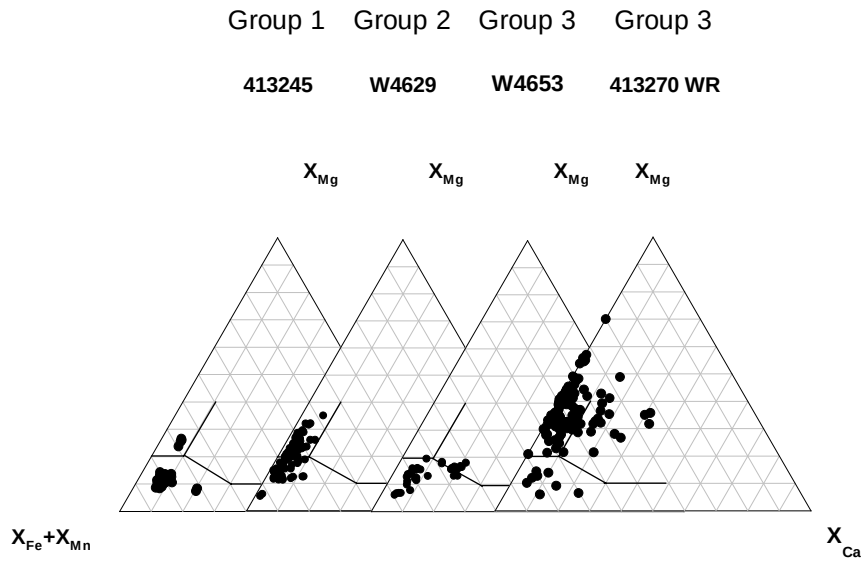

Figure 3. *Garnet compositions in Early Cretaceous sandstones (groups 1, 2, and 3 of Larsen et al. 2005) from Kangerlussuaq analysed by CCSEM. X_{Fe}, X_{Mn}, X_{Mg} and X_{Ca} are molecular proportions of Fe, Mn, Mg, and Ca, respectively. All Fe was calculated as Fe^{2+}.*

Garnets in samples from groups 1, 2, and 3 (Fig. 3) are typically low-Mg garnets and can be classified as Type Aii and Type B garnets. A few grains in sample W4653 plot close to the boundary that separates Type B and C garnets; however, the Ca-contents generally do not exceed 20 %. The observed dominance of low-Mg, low-Ca garnets in these groups agrees well with the low rutile:zircon index (RuZi; see Appendix A for further explanation) determined by Morton et al. (2005) and the observed detrital zircon age spectra (Whitham et al. 2004; Frei et al., 2005d) that suggest derivation from Archaean basement. The only exception is sample 413270 (group 3) that shows a very high abundance of Type Ai garnets, indicative for derivation from high grade, granulite facies metamorphic rocks. The exceptional nature of this sample was already identified by Morton et al. (2005) solely on the basis of an anomalously high RuZi. Morton et al. concluded that this sample was either sourced from high-grade metamorphic rocks to the north or northeast at an earlier stage than previously recognised, or that it was sourced from Archaean basement with unusual high RuZi. Our garnet data support derivation from a source to the north or northeast; this

assumption could be verified by detrital zircon age data, which unfortunately is not available for this sample.

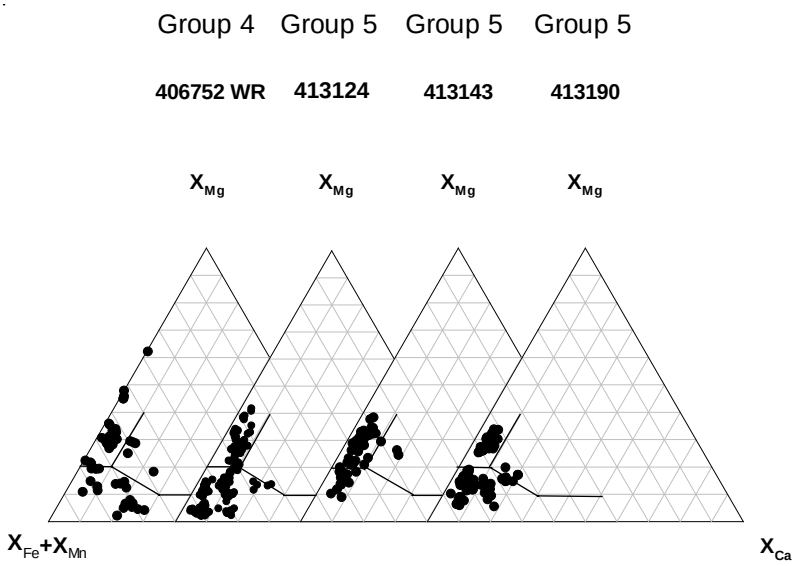

Figure 4. *Garnet compositions in Late Cretaceous to Late Paleocene sandstones (groups 4 and 5 of Larsen et al. 2005) from Kangerlussuaq analysed by CCSEM. X_{Fe}, X_{Mn}, X_{Mg} and X_{Ca} are molecular proportions of Fe, Mn, Mg, and Ca, respectively. All Fe was calculated as Fe^{2+}.*

Garnets in samples from groups 4 and 5 generally show the same low Ca contents observed for garnets in groups 1, 2, and 3. However, garnets in groups 4 and 5 are characterised by a higher proportion of Type Aii garnets (Fig. 4). This is especially true for samples 406752, 413124, and 413143 that contain garnets with up to 60 % Mg (sample 406752), suggesting derivation from a source containing significant proportions of high-grade metamorphic rocks. The high proportion of Ai garnets in these samples is in agreement with their high RuZi reported by Morton et al. (2005) and their north/northeast source inferred from detrital zircon age spectra (Whitham et al, 2004; Frei et al. 2005d). However, based on provenance sensitive heavy mineral ratios, Morton et al. (2005) suggests that group 5 samples were derived from reworked material from the Christian IV Fm (i.e. group 4) that was originally sourced from the north/northeast. The much less frequent occurrence of high-Mg garnets in sample 413190 from group 5 agrees with the very low RuZi and most likely indicates mixture of Archaean basement with minor amounts of reworked material from the Christian IV Fm.

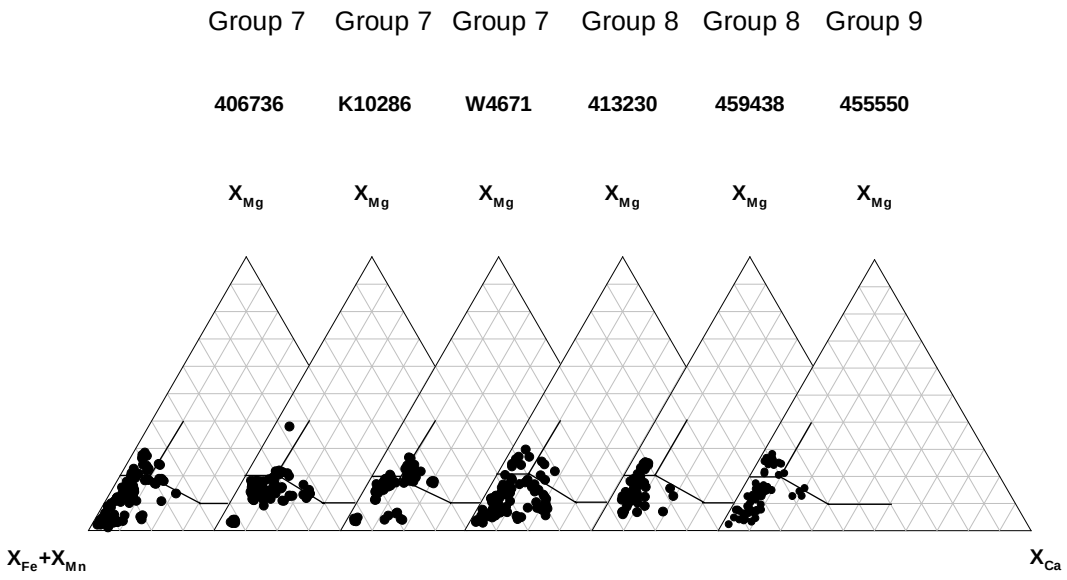

Figure 5. *Garnet compositions in Late Paleocene to Eocene sandstones (groups 7, 8, and 9 of Larsen et al. 2005) from Kangerlussuaq analysed by CCSEM. X_{Fe}, X_{Mn}, X_{Mg} and X_{Ca} are molecular proportions of Fe, Mn, Mg, and Ca, respectively. All Fe was calculated as Fe^{2+}.*

All samples from groups 7, 8, and 9 are typical low-Mg garnets and are classified as Type Aii and B garnets (Fig. 5). Only few grains plot in the field indicative for Type C garnets, and all grains are close to the boundary to field B with Ca-contents below 25 %. These observations agree with the generally low RuZi for these samples, pointing to source in Archaean basement to the south/southwest. Furthermore, the almost complete absence of Type Ai garnets from groups 7, 8, and 9 unequivocally excludes reworking of material from groups 4 and 5 and provides additional evidence for the exclusion of large-scale reworking indicated by detrital zircon age distributions (Frei et al. 2005d).

Paleocene-Eocene, Faroe-Shetland Basin

The samples from the Faroe-Shetland Basin analysed during the SINDRI project are from the Paleocene Sullom, Vaila, Lambda and Flett Fms. and the Eocene Balder and UPD Fms. from wells 204/19-3a and 204/24a-7 in the Foinaven sub-basin, and from wells 205/9-1, 206/1-1a and 214/19-1 in the Flett sub-basin. Samples have been assigned to the sedimentary succession using the stratigraphic units outlined by Larsen et al. (2005). The stratigraphic correlation of the early Paleogene successions West of Shetland, the Faroes and in Kangerlussuaq is shown in Fig. 6 (from Larsen et al. 2005). The samples analysed for detrital garnet major element compositions cover the sedimentary succession from Early-Middle Paleocene (Vaila Fm. V1; displayed in Fig. 7), Late Paleocoene (Kettla, Lambda,

and Flett Fms; displayed in Fig. 8) to the Early Eocene (Balder Fm. and Ypresian UPD Fm.; displayed in Fig. 9).

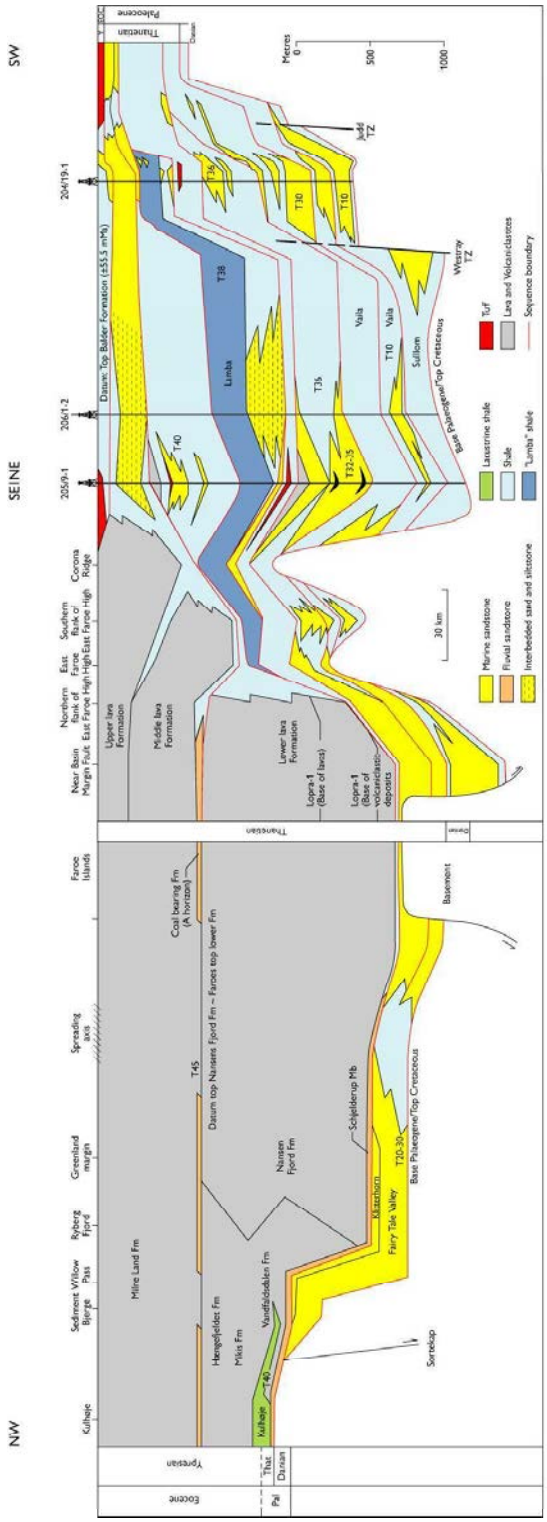

Figure 6. *Correlation of the early Paleogene successions West of Shetland, the Faroes and in Kangerlussuaq (from Larsen et al. 2005; right hand side of the diagramme from Ellis et al. 2002).*

Because CCSEM data on samples that cover continuous stratigraphic sucessions over a wide range within a single well are sparse, it is impossible to delineate compositional changes as a function of stratigraphic position and we will only briefly discuss the general features of the observed compositional variations. An in-depth discussion of the garnet compositional variations in these wells is given in Morton et al. (2005).

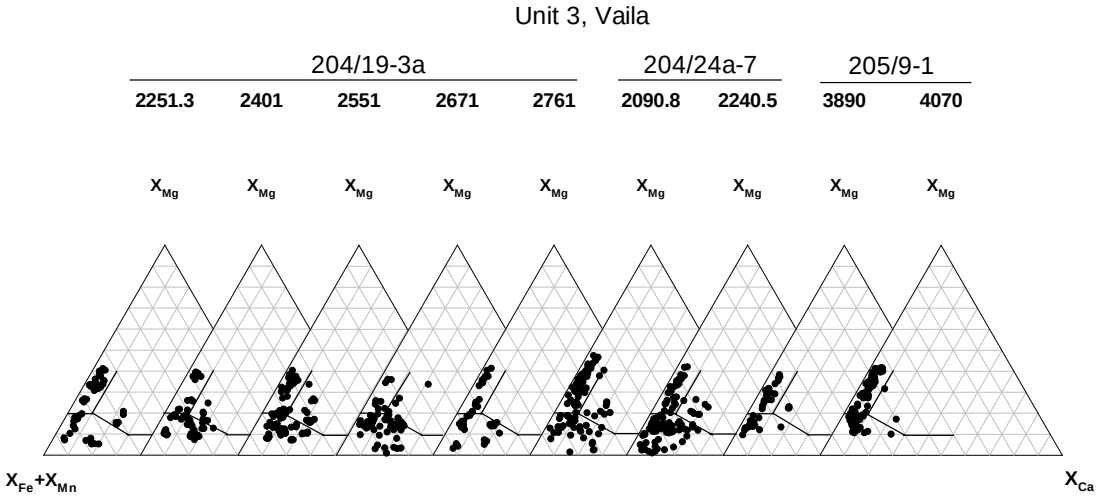

Figure 7. *Garnet compositions in Early-Middle Paleocene sandstones (unit 3, Vaila Fm.) from wells in the Foinaven (wells 204/19-3a and 204/24a-79 and Flett (well 205/9-1) sub-basin in the UK sector of the Faroe-Shetland Basin analysed by CCSEM. X_{Fe}, X_{Mn}, X_{Mg} and X_{Ca} are molecular proportions of Fe, Mn, Mg, and Ca, respectively. All Fe was calculated as Fe^{2+}.*

Garnets in the Early-Middle Paleocene Vaila Fm. (Fig. 7) are characterised by variable proportions of Type A and B garnets. Some samples show minor, but not substantial appearances of Type C garnets. Samples between 2251.3 and 2761 m in well 204/19-3a apparently indicate temporal variations in Type A to Type B ratios. Compared to the garnet compositions observed in samples in Kangerlussuaq, the most striking difference is the presence of significant amounts of high-Mg, Type Ai garnets in allmost all investigated samples, a feature also observed in all 51 samples from these wells investigated by Morton et al. (2005).

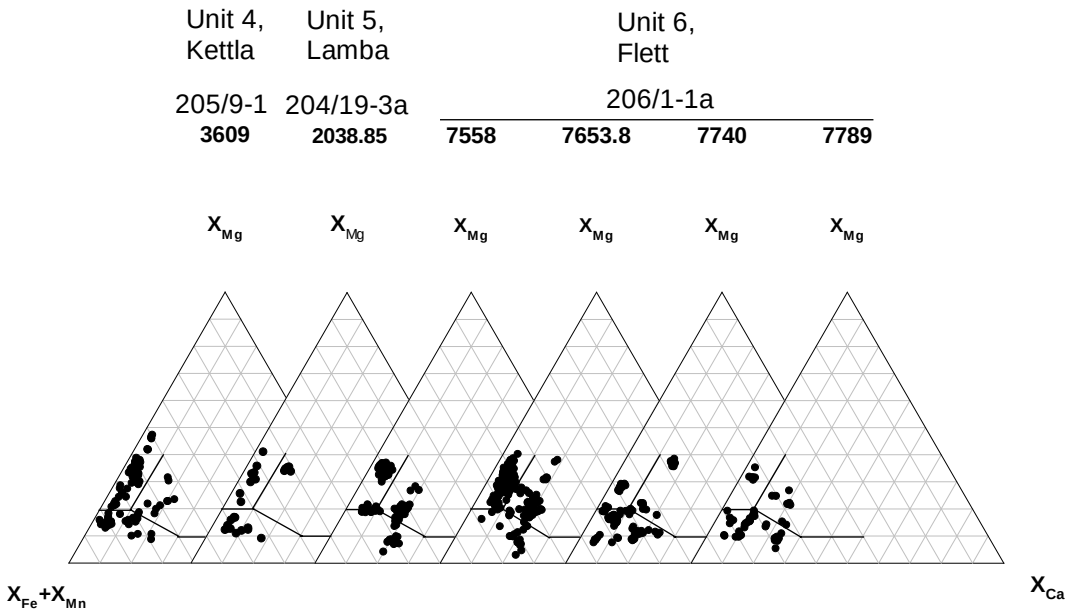

Figure 8. *Garnet compositions in Late Paleocene sandstones (unit 4, Kettla Fm; unit 5, Lambda Fm.; and unit 6, Flett Fm.) from wells in the Foinaven (well 204/19-3a) and Flett (wells 205/9-1 and 206/1-1a) sub-basin in the UK sector of the Faroe-Shetland Basin analysed by CCSEM. X_{Fe}, X_{Mn}, X_{Mg} and X_{Ca} are molecular proportions of Fe, Mn, Mg, and Ca, respectively. All Fe was calculated as Fe^{2+}.*

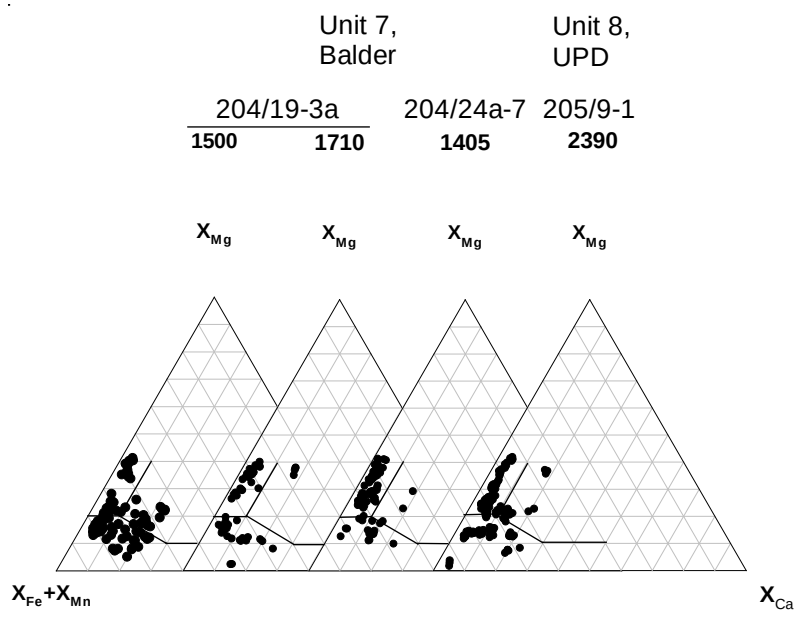

Figure 9. *Garnet compositions in Early Eocene sandstones (unit 7, Balder Fm; and unit 8, UPD Fm.) from wells in the Foinaven (wells 204/19-3a and 204/24a-7) and Flett (well 205/9-1) sub-basin in the UK sector of the Faroe-Shetland Basin analysed by CCSEM. X_{Fe}, X_{Mn}, X_{Mg} and X_{Ca} are molecular proportions of Fe, Mn, Mg, and Ca, respectively. All Fe was calculated as Fe^{2+}.*

In contrast to the Vaila Fm., garnets in the Late Paleocene Kettla, Lambda and Flett Fms (Fig. 8) are characterised by relatively low proportions of Type B garnets and the presence of significant amounts of Type C garnets in all samples analysed, indicating presence of material derived from mafic source rocks. All samples also show a significant proportion of Type Ai garnets.

The samples from the Early Eocene Balder and UPD Fms. (Fig. 9), are predominantely characterised by Type A and B garnets. However, Type C garnets are apparent in variable amounts and they are a significant component in sample 204/19-3a 1500. Like in samples from the Vaila, Kettla, Lambda and Flett Fms, all four samples from the Balder and UPD Fms investigated by CCSEM show a significant presence of Type Ai garnets.

TiO_2 distribution in Ti-minerals

The maturity of a sediment is reflected in the TiO2-distribution of the the Ti-mineral fraction. The continuous alteration of primary ilmenite (with a stochiometric TiO_2 content of 48-52.6 wt%; Deer et al., 1992) via pseudorutile to leucoxene by leaching of iron, leads to a significant increase in the TiO_2-grade of the Ti-mineral fraction in a mature sediment (e.g. Grey & Reid 1975; Frost et al. 1983; Grey et al. 1994; Mücke and Bhadra Chaudhuri 1991). Since CCSEM yields the average chemical compositions of all minerals present in a given sample, the TiO_2-distribution of the Ti-mineral fraction can be easily calculated without the need for tedious and time-consuming mineral separation.

The TiO_2-distributions in the Ti-mineral fractions (i.e. ilmenite, rutile and leucoxene) of sandstones from representative stratigraphic profiles in the Kangerlussuaq Basin and Kap Dalton obtained by CCSEM analysis are displayed in binned histograms in Figs. 10, 11, and 12. The samples have been assigned according to the stratigraphic groups discribed by Larsen et al. (2005).

Fig. 10 shows a vertical profile through the Kangerlussuaq Basin from Early Cretaceous to Early-Late Paleocene. The most striking feature is the very uniform, almost unimodal TiO_2-distribution in group 3 (sample 413270), group 4 (sample 455648), group 5 (sample 413123) and group 6 (sample 413146) with high average TiO_2 contents of the Ti-mineral fraction peaking at 94 to 98 wt% TiO_2; in all of these samples, ilmenite *sensu stricto* (with average stoichiometric TiO_2 contents of 48-52.6 wt%) has been completely transformed to very high grade leucoxene and pseudorutile requiring intensive leaching and recrystallisation. This very high degree of leaching, and hence maturity suggests a high porosity of the sandstones and a warm and humid climate during the deposition and maturation of the successions. Only sample 455550 (group 9; Paleocene-Eocene) from an intra-basalt layer does not show this uniform, highly enriched TiO_2-distribution and contains a significant fraction of unleached ilmenite. This unleached ilmenite fraction is most likely derived from unaltered basaltic country-rocks.

Further evidence for the derivation of this unleached ilmenite fraction from basaltic rocks comes from the observed TiO-distribution in two samples from the post-basaltic Eocene succession from Kap Dalton (Fig. 11) that are chracterised by the presence of a very large

fraction of ilmenite with a pronounced peak at TiO_2 contents characteristic for stoichiometric primary ilmenite.

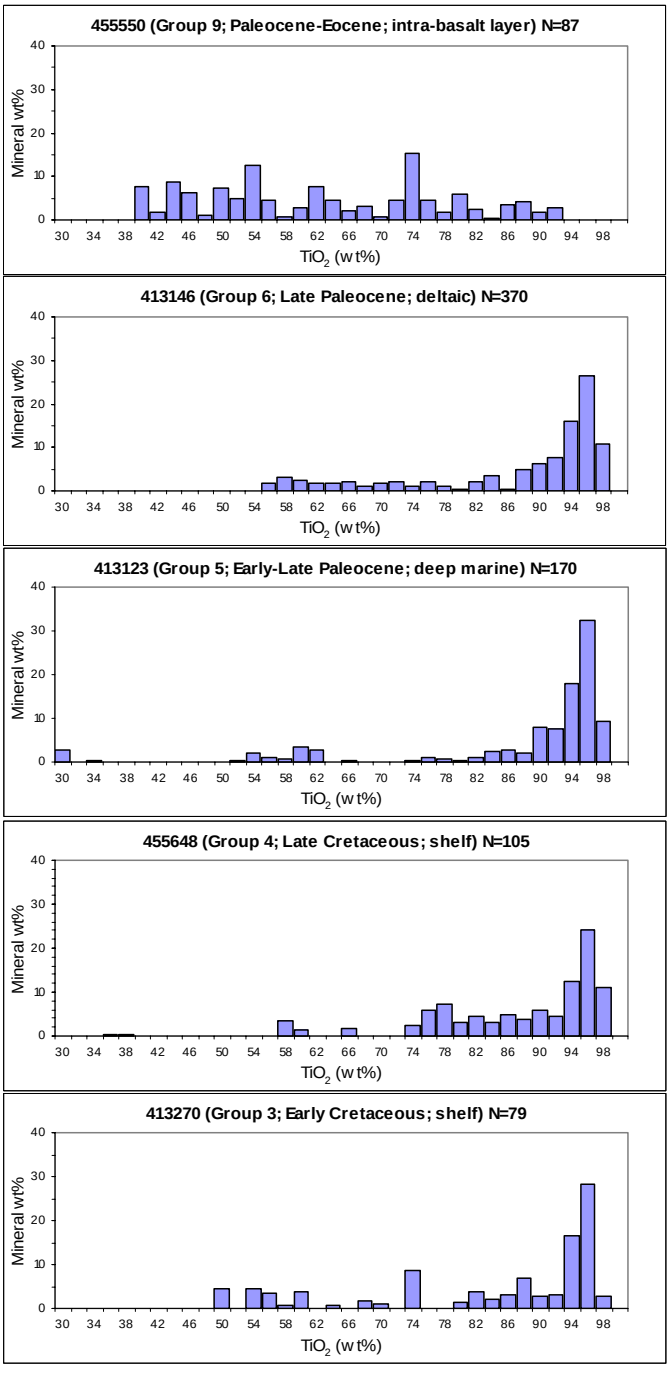

Figure 10. *TiO_2-distribution in the Ti-mineral fraction of sandstones from a vertical profile through the sedimentary succession in Kangerlussuaq, East Greenland (with the stratigraphically youngest sample on top).*

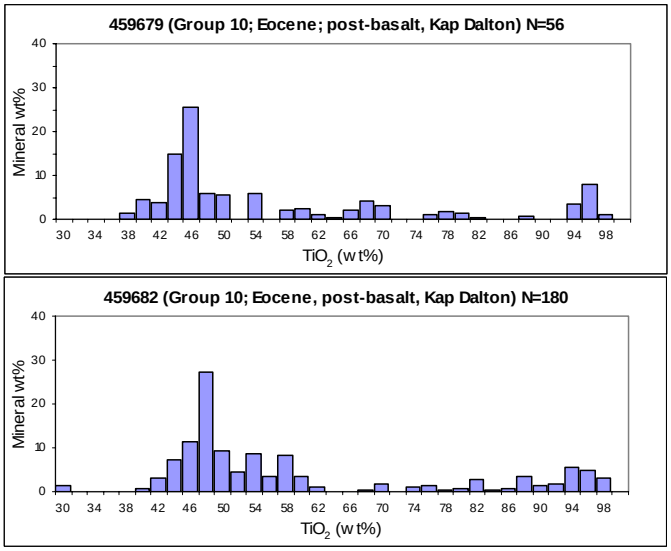

Figure 11. *TiO_2-distribution in the Ti-mineral fraction of sandstones from the Eocene, post-basaltic sedimentary succession at Kap Dalton, East Greenland. Note the sharp peak at TiO_2 contents around 48 wt%, characteristic for primary, stoichiometric ilmenite (Deer et al. 1992).*

In contrast to only minor lateral variations in detrital garnet major element composition (see above) and detrital zircon age distributions (Frei et al. 2005d), the TiO_2-distributions show marked lateral variations within stratigraphic groups. This can be exemplified by the lateral variation of the TiO_2-distribution in the Ti-mineral fraction observed within group 5 (Fig. 12). The easternmost sample (413123) is from the vertical profile through the sedimentary succession discussed above (*cf.* Fig. 10) and shows the very uniform, almost unimodal TiO_2-distribution dominated by high average TiO_2 contents characteristic for leucoxene and pseudorutile that indicate a very high degree of leaching, and hence maturity. Towards the west, the observed TiO_2-distributions are polymodal and show a higher sample-to-sample variability. The TiO_2-distribution in the sample to the west (413124) shows TiO_2 contents covering the range from unleached Ti-magnetite (~34 wt% TiO_2) to highly leached leucoxene and pseudorutile. However, the most striking feature is the unusually high modal abundance of Ti-magnetite, a mineral phase that is relatively environmentally stable during leaching processes. The two westernmost samples (412773 and 413276) are characterised by polymodal TiO_2-distributions without the presence of a modally dominant cluster. However, in sample 413276 almost the entire range of TiO_2 fractions from 30-98 wt% TiO_2 is present, whereas in sample 412773 the fraction characteristic for primary, unleached ilmenite is absent. The observed polymodal and broad TiO_2-distributions in samples to the west point to a much lower degree of leaching, and hence lower maturity. The lower maturity in these samples is in agreement with the dominance of mudstones in the western part of the Kangerlussuaq Basin, and hence a much lower porosity compared to the sandstone dominated sequences in the eastern part of the basin.

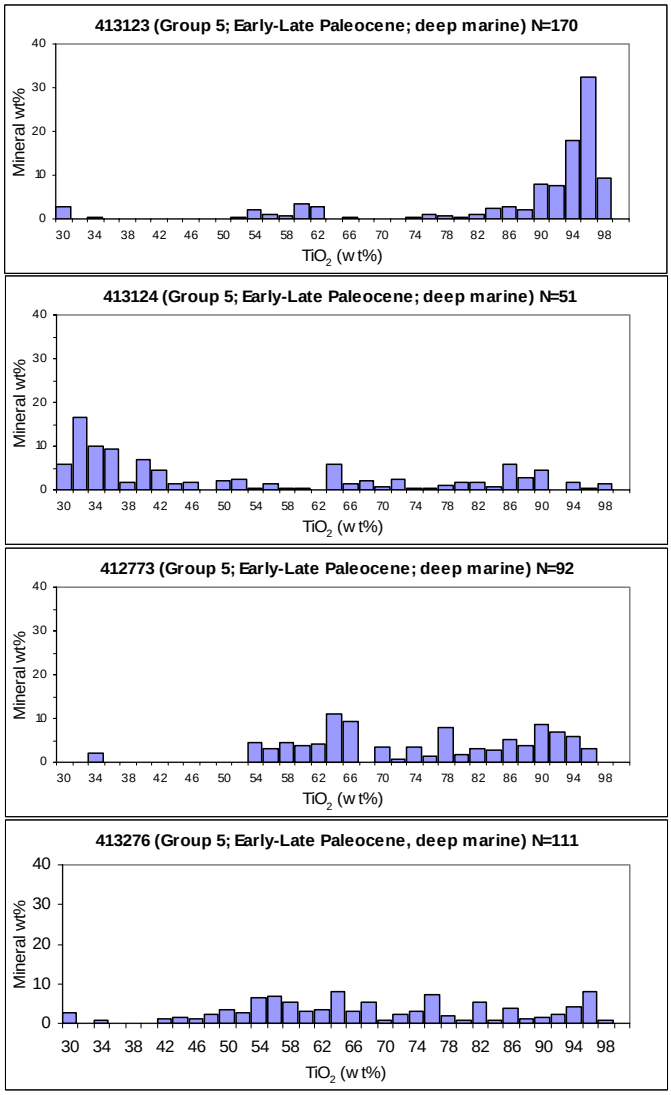

Figure 11. *Lateral variation of TiO_2-distributions in the Ti-mineral fraction of sandstones in Early to Late Paleocene sandstones from group 5. Note the marked gradual change in age distributions from east (sample 413123) to west (samples 412773 and 413276).*

Conclusions

In general, the garnet compositional variations determined by CCSEM are in excellent agreement with the variations of provenance sensitive heavy mineral ratios described by Morton et al. (2005). Furthermore, for those samples were garnet compositional data have been determined by CCSEM (this study) and by EMPA (Morton et al. 2005), the agreement between both methods is generally very good. Minor deviations are subordinate occurrences of high-Mg garnets in samples 413245, 413230, and 406736 reported by Morton et al. (2005) that have not been detected by CCSEM. The only major disagreement is a

population of high-Mg garnets in sample W4671 that has not been detected by CCSEM. The most reasonable explainations for these deviations are (1) systematic bias due to the low numbers of individual garnet grains recovered during hand-picking for CCSEM analysis (some samples contain as low as 20 to 30 garnet grains and are most likely not representative for the entire range of garnet compositions present) and/or (2) systematic bias introduced during hand-picking. However, these minor deviations do not compromise the general conclusions drawn from garnet major element variations determined by CCSEM.

The observed lateral and vertical major element variations of detrital garnets in sandstones from the Kangerlussuaq Basin and in wells from the UK sector of the Faroe-Shetland Basin allow some contraints to be drawn on sediment dispersal patterns on both local and regional scales. The general compositional homogeneity observed within single stratigraphic units or groups in both the Kangerlussuaq Basin and wells from the UK sector of the Faroe-Shetland Basin support the stratigraphic correlations derived from litho- and sequence stratigraphic analysis. In the Kangerlussuaq Basin, prominent changes in the occurrence of high-Mg, Type Ai garnets provides further evidence for the two major changes in sediment sourcing suggested by detrital zircon age distributions (Frei et al 2005d). Furthermore, the observed distributions of garnet major element compositions exclude large-scale reworking of local sediments.

The general lack of primary, unleached ilmenite in the Ti-mineral fractions of most samples points to a high degree of maturity of the sedimentary succession in the Kangerlussuaq Basin. Lateral variations in host-rock lithology (low-porosity mudstones versus high-porosity sandstones) result in lateral variations in TiO_2-distributions, and hence sediment maturity.

A very important result of this study is the observation that the abundance of high-Mg, Type Ai garnets is only subordinate in samples from the Kangerlussuaq Basin. In contrast, these high-Mg garnets occur in significant amounts in allmost all samples from the wells in the UK sector of the Faroe-Shetland Basin. This observation points to a characteristic signature in the major element distribution of detrital garnets in the Kangerlussuaq Basin and in wells from the UK sector of the Faroe-Shetland Basin that allows to distinguish between a western, greenlandic source (dominated by low-Mg, Type Aii garnets) and an eastern source (dominated by high-Mg, Type Ai garnets) and is in agreement with the evidence from conventional petrographic and chemical analysis of heavy minerals (Morton et al. 2005), from detrital zircon age distributions (Frei et al. 2005d), and from detailed chemostratigraphic investigations (Knudsen 2005).

References

Bernstein, S., McLimans, R.K., Knudsen, C., Frei, D., Vasudev, V.N. 2005: Source of titanium-enriched ilmenite in sand deposits, South India. Proceedings of the Heavy Minerals Conference *(in press)*.

Deer W.A, Howie, R.A., Zussman, J. 1992: An introduction to the rock forming minerals. Longman Scientific & Technical, Harlow, Essex, England.

Ellis, D., Bell, B.R., Jolley, D.W., O´Callaghan, M. 2002: The stratigraphy, environment of eruption and age of the Faroes Lava Group, NE Atlantic. *In*: Jolley, D.W. and Bell, B.R. (eds) The North Atlantic Igneous Province. Stratigraphy, Tectonic, Volcanic and Magmatic processes. Geological Society, London, Special Publications **197**, 253-269.

Frei, D., Rasmussen, T., Knudsen, C., Larsen, M., Whitham, A.G., Morton, A. C., 2005a: New methods and techniques for innovative, integrated provenance studies. Annales Societatis Færoensis, Supplementum **43**, 96-108.

Frei, D., Knudsen, C., McLimans, R.K., Bernstein, S., 2005b: Fully automated analysis of chemical and physical properties of individual mineral species in heavy mineral sands by computer controlled scanning electron microscopy (CCSEM). Proceedings of the Heavy Minerals Conference *(in press)*.

Frei, D., Frei, M., Hansen Klünder, M., Rasmussen, T., Knudsen, C., Morton, A.C., Whitham, A.G. 2005c: Evaluation of novel analytical techniques for provenance studies I: CCSEM. Danmarks og Grønlands Geologiske Undersøgelse Rapport **2005/54** *(this volume).*

Frei, D., Rasmussen, T., Frei, M., Knudsen, C., Larsen, M. 2005d: Detrital zircon age constraints on provenance of Paleocene-Eocene sandstones in the Faroe-Shetland Basin. Danmarks og Grønlands Geologiske Undersøgelse Rapport **2005/54** *(this volume).*

Frost, M.T., Grey, I.E., Harrowfield, I.R., Mason, K. 1983: The dependence of alumina and silica contents on the extent of alteration of weathered ilmenites from western Australia. Mineralogical Magazine **47**, 201-208.

Grey, I.E., Reid, A.F. 1975: The structure of pseudorutile and its role in the natural alteration of ilmenite. American Mineralogist **60**, 898-906.

Grey, I.E., Watts, J.A., Bayliss, P. 1994: Mineralogical nomenclature: pseudorutile revalidated and neotype given. Mineralogical Magazine **58**, 597-600.

Henry, D.J., Guidotti, C.V. 1985: Tourmaline as a petrogenetic indicator mineral: an example from the staurolite-grade metapelites of NW Maine. American Mineralogist **70**, 1-15.

Knudsen, C., Frei, D., Rasmussen, T., Rasmussen, E.S., McLimans, R.K. (2005): New methods in provenance studies based on heavy minerals: an example from Miocene sands in Jylland, Denmark. Geological Survey of Denmark and Greenland Bulletin **7**, 29-32.

Larsen, M., Nøhr-Hansen, H., Whitham, A.G., Kelly, S.R.A. 2005: Stratigraphy of the prebasaltic sedimentary succession of the Kangerlussuaq Basin. Volcanic basins of the North Atlantic. Danmarks og Grønlands Geologiske Undersøgelse Rapport **2005/62**.

Morton, A.C. 1985: A new approach to provenance studies: electron microprobe analysis of detrital garnets from Middle Jurassic sandstones of the northern North Sea. Sedimentology **32**, 553-566.

Morton, A.C., Hallsworth, C.R., Chalton, B. 2004: Garnet compositions in Scottish and Norwegian basement terrains: a framework for interpretation of North Sea sandstone provenance. Marine and Petroleum Geology **21**, 393-410.

Morton, A.C., Hallsworth, C.R., Whitham, A. G. 2005: Heavy mineral provenance of Paleocene-Eocene sandstones in the Faroe-Shetland Basin – results from conventional petrographic and mineral-chemical techniques. Danmarks og Grønlands Geologiske Undersøgelse Rapport **2005/54** *(this volume).*

Mücke, A., Bhadra Chaudhuri, J.N. 1991: The continuous alteration of ilmenite through pseudorutile to leucoxene. Ore Geology Reviews **6**, 25-44.

Weibel, H. 2003: Alteration of detrial Fe-Ti oxides in Miocene fluvial deposits, central Jutland, Denmark. Bulletin of the Geological Survey of Denmark and Greenland **4**, 21-24.

Whitham, A.G., Morton, A.C., Fanning, C.M. 2004: Insights into Cretaceous-Paleocene sediment transport paths and basin evolution in the North Atlantic from a heavy mineral study of sandstones from southern East Greenland. Petroleum Geoscience **10**, 61-72.

Detrital zircon age constraints on provenance of Paleocene-Eocene sandstones in the Faroe-Shetland Basin

Dirk Frei[1], Thomas Rasmussen[1], Martina Frei[1], Christian Knudsen[1], Michael Larsen[1], Andrew G. Whitham[2]

[1]Geological Survey of Denmark and Greenland, Øster Voldgade 10, DK-1350 København K, Denmark
[2]CASP, Dept. of Earth Sciences, University of Cambridge, West Building, 181a Huntingdon Road, Cambridge, CB3 ODH, UK

Introduction

One of the most important questions for hydrocarbon exploration in the Faroe region is the understanding of sediment dispersal patterns and depositional systems in the Faroe-Shetland Basin prior to continental break up in the Late Paleocene to Eocene. A powerful tool for tackling these questions is detrital zircon analysis. Detrital zircon analyses uses the interpreted provenance of zircon (usually derived from the age information recorded in zircon) to unravel the geological history of sedimentary basins and their surrounding areas. The age distribution of detrital zircons are especially helpful to indentify the different provenance components present in a sedimentary unit (e.g. Hass et al. 1999) and to correlate between stratigraphic sequences on both a local and regional scale (e.g. Bingen et al. 2001). Thus, the geochronological record of detrital zircons from sediments in the Kangerlussuaq area and the UK sector of the Faroe-Shetland Basin may offer important insights in understanding sedimentary dispersal pattern prior to continantal break-up and can be extremely helpful in establishing wether there is a link between the two regions.

Here, we present the results of a study that investigated the systematics of detrital zircon age distributions in sandstones from East Greenland and the UK sector of the Faroe-Shetland Basin with hiherto unprecedented detail. Furthermore, we present additional data for sandstones from the Orkney Islands (see Plate 5 in Appendix B). In total, we have analysed the ^{207}Pb-^{206}Pb ages of 4347 detrital zircons by means of LA-Q-ICP-MS. Detrital zircons were separated and analysed from 25 samples from East Greenland (2321 zircons), 20 samples from wells in the UK sector of the Faroe-Shetland Basin (1832 zircons) and 2 samples from the Orkney Islands (203 zircons). The results for all 47 investigated samples are presented in binned frequency diagrams in Plates 3, 4 and 5 in Appendix B, and the analytical results are reported in Excel based spreadsheets in the attached data CD-ROM. A map depicting the stratigraphic positions of all analysed samples from the Kangerlussuaq Basin and their respective age distributions (in binned frequency diagrams) is provided in Enclosure 1.

Results and discussion

In the following, the results from representative stratigraphic profiles in the Cretaceous-Eocene succession in Kangerlussuaq, southern East Greenland, and in the Paleocene-Eocene successions drilled in the UK sector of the Faroe-Shetland Basin are discussed. The stratigraphic subdivisions of the sedimentary successions reported by Larsen et al. (2005) are used as a framework.

Kangerlussuaq Basin

The sketch in Fig. 1 depicts the litho- and sequence stratigraphy of the Cretaceous-Paleogen succession of the Kangerlussuaq Basin including the major unconformities and hiatuses according to Larsen et al. (2005).

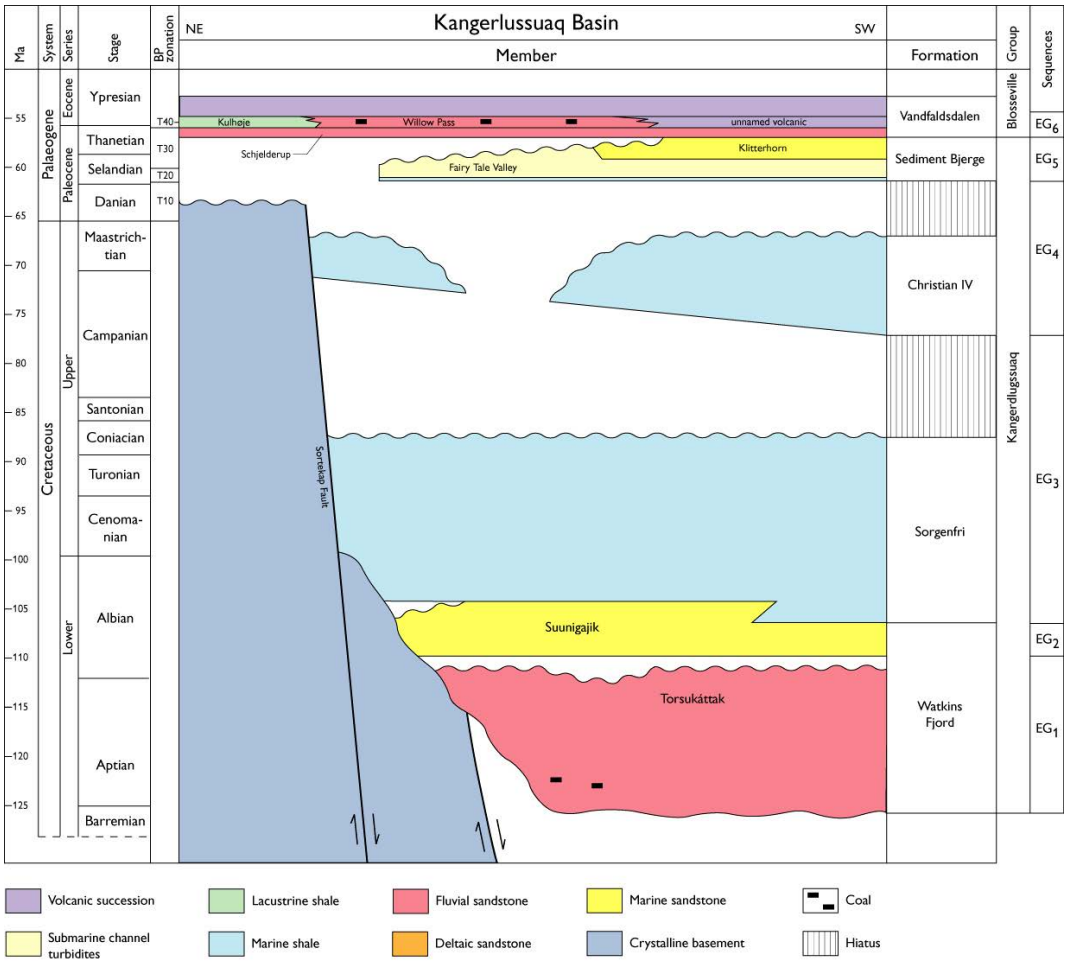

Figure 1. *Litho- and sequence stratigraphy of the Cretaceous-Paleogene succession in Kangerlussuaq, East Greenland (from Larsen et al. 2005).*

The samples from the Kangerlussuaq Basin analysed in this SINDRI project have been assigned to the ten stratigraphic groups identified by Larsen et al. (2005):

Group 1: Early Cretaceous, pre-volcanic, Watkins Fjord Fm., Torsukáttak Mb., fluvial.
Group 2: Early Cretaceous, pre-volcanic, Watkins Fjord Fm., Suunigajik Mb., shallow marine.
Group 3: Early Cretaceous, pre-volcanic, Sorgenfri Fm., shelf.
Group 4: Late Cretaceous, pre-volcanic, Christian IV Fm. ('Lower Ryberg'), shelf.
Group 5: Early Paleocene, pre-volcanic, Sediment Bjerge Fm., Fairy Tale Valley Mb., ('Upper Ryberg'), deep marine.
Group 6: Late Paleocene, pre-volcanic, Sediment Bjerge Fm., Klitterhorn Mb. ('Upper Ryberg'), deltaic.
Group 7: Late Paleocene, pre/syn-volcanic, Vandfaldsdalen Fm., Schjelderup Mb. ('Ryberg Sandstone Bed' *s. s.)*, fluvial.
Group 8: Paleocene-Eocene, syn-volcanic, Vandfaldsdalen Fm., Willow Pass Mb., fluvial.
Group 9: Paleocene-Eocene, syn-volcanic, Vandfaldsdalen Fm., Kulhøje Mb., intra basalt layer.
Group 10: Eocene, post-volcanic, Bopladsdalen Fm., Kap Dalton, Savoia Halvø, post-basalt, (outside the Kangerlussuaq Basin).

In Figs 2, 3 and 4, the results through a representative profile of the succession are displayed in binned frequency diagrams. Based on age distribution patterns, the succession can be divided into three main units.

The first unit (Fig. 2) comprises sandstones from the Early Cretaceous stratigraphic groups 1, 2 and 3. The zircon populations from all three groups almost exclusively comprise Archaean zircons. The age spectrum of group 1 (sample 455107) shows two major clusters with Late Archaean ages (2750-2800 Ma and 2950-3050 Ma), and a minor cluster with Middle Archaean ages (3200 Ma). Only four zircons have post-Archaean, Early Proterozoic ages (~2350 and ~2000 Ma.). The age spectrum of group 2 (sample 455112) is very similar, but the cluster of Late Archaean ages is more prominent, indicating a shift in the sediment proportions supplied from the different sources. Furthermore, three grains with Early Archaean ages occur (3700 and 3850 Ma). The age spectrum of group 3 (sample W4265) is again very similar to those observed for the groups 1 and 2, but Late to Middle Archaean zircon grains (clusters at 3000 Ma and 3150 Ma years) are more frequent.

The almost exclusive Archaean provenance of all Early Cretaceous sandstones points to sourcing from Archaean basement either in the Kangerlussuaq region or the south or southwest (units **[74]** and **[75]** of the Geological Map of Greenland; Escher and Pulvertaft 1995; Henriksen et al. 2000).

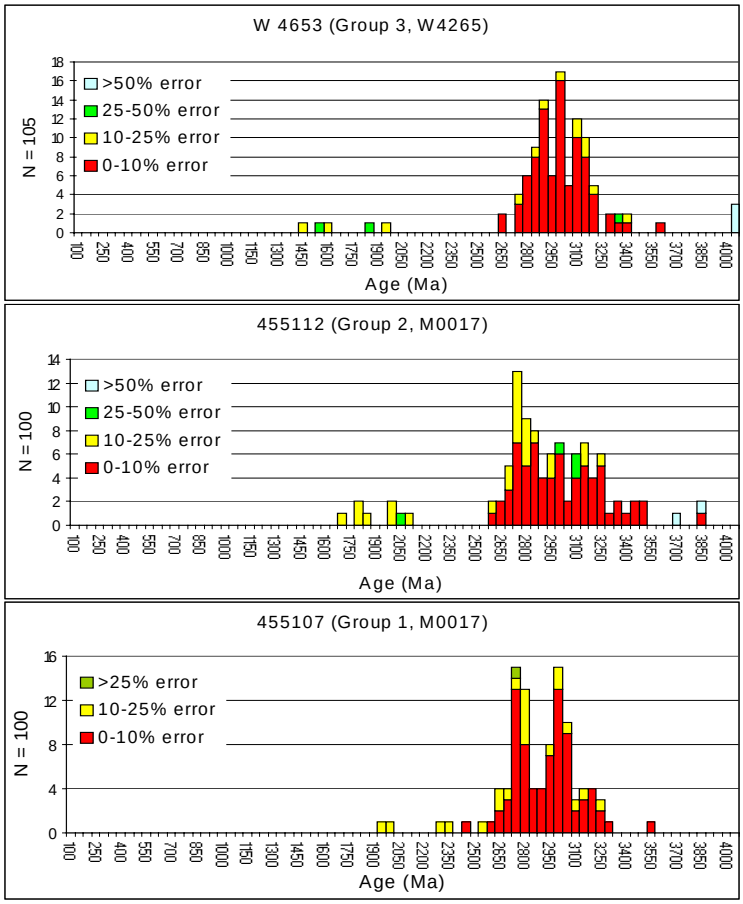

Figure 2. *Binned histograms displaying detrital zircon age distributions in sandstones from the Early Cretaceous groups 1, 2 and 3 of a representative stratigraphic profile through the Kangerlussuaq Basin (with the stratigraphically youngest sample on top). Note the changes in relative frequencies as a function of stratigraphic position.*

The second unit (Fig.3) comprises sandstones from the Late Cretaceous to Late Paleocene groups 4, 5, and 6. In contrast to unit 1, the observed age distributions are strongly polymodal with a high proportion of Proterozoic grains and marked changes in relative frequencies, especially of Proterozoic and Middle Archaean zircons. The age spectrum of group 4 (sample 455636) shows three clusters of Late Archaean ages (peaking at ~2600, ~2750 and 2950 Ma) and a very high proportion of zircon ages that cover almost the entire range of the Proterozoic (with different clusters at ~2500, ~2000, ~1750, ~1400, ~1100 and ~700 Ma). Only three zircons with a Middle Archaean age at 3350 Ma are observed. The age spectrum of group 5 (sample 413124) is reminiscent of the spectra observed in unit 1. The frequency of Archaean ages is much higher than in group 4 and the cluster of Middle Archaean ages (3100-3250 Ma) re-appears. Furthermore, compared to group 4, the presence of Proterozoic zircons has greatly diminished. The age spectrum of group 6 is again characterised by pronounced changes in relative frequencies. The overwhelming majority of older zircons are Late Archaean (with two major clusters at ~2850 and 3000 Ma). Most importantly, only four zircons with Middle Archaean ages are present. Furthermore,

younger, Proterozoic zircons are more frequent compared to group 5 and form three small and relatively wide clusters at 1950, 1750, and 1450 Ma.

The presence of Early Proterozoic, Grenvillian and Caledonian zircons and the much less pronounced occurence of Archaean zircons in the Late Cretaceous to Early-Late Paleocene sandstones requires a source to the north or northeast (units **[43]**, **[44]**, **[46]** and **[52]** of the Geological Map of Greenland; Escher and Pulvertaft 1995; Henriksen et al. 2000) because the area to the south and southwest was unaffected by these orogenic events.

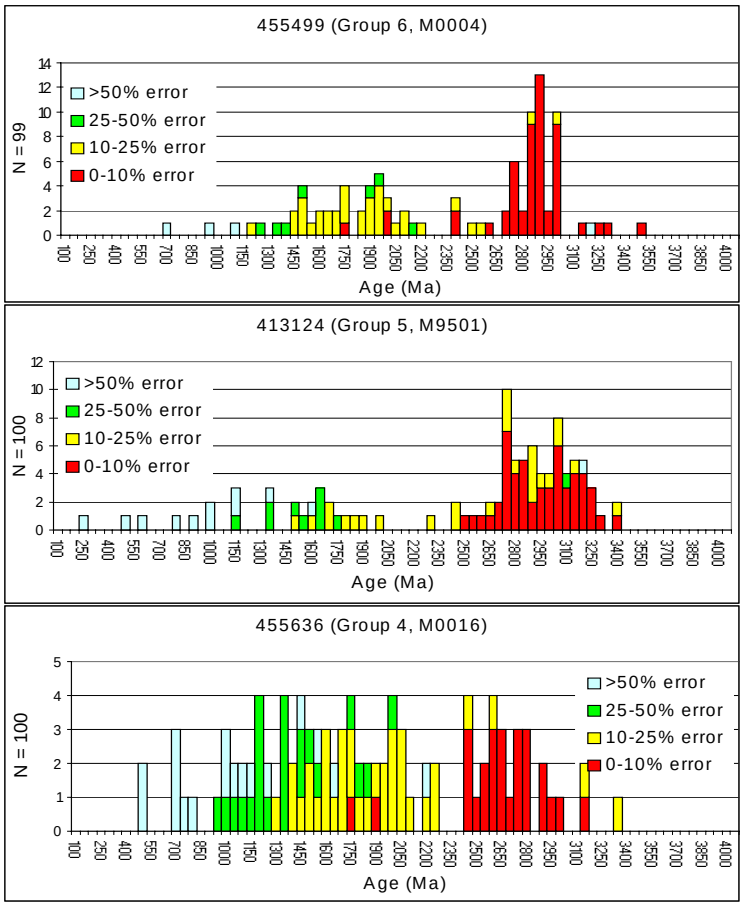

Figure 3. *Binned histograms displaying detrital zircon age distributions in sandstones from the Late Cretaceous to Late Paleocene groups 1, 2 and 3 of a representative stratigraphic profile through the Kangerlussuaq Basin (with the stratigraphically youngest sample on top). Note the marked changes in relative frequencies as a function of stratigraphic position.*

The third unit comprises sandstones from the Late Paleocene to Eocene groups 7, 8 and 9. All age spectra are remarkably similar (Fig. 4) and resemble the age spectra observed in the Early Cretaceous sandstones of groups 1, 2 and 3 (*cf.* Fig. 2). All spectra show almost exclusively Late to Middle Archaean zircon ages and only very few zircons with older or younger ages are present. The age spectrum in group 7 (sample 412784) shows three major age clusters with peaks at 2800, 3000, and 3150 Ma. A few grains fall outside these

groups, most notably some Early Archaean grains. The age spectrum in group 8 (sample 455440) shows a major Late Archaean cluster (2700-3000 Ma with a pronounced peak at 2850 Ma) and a minor Middle Archaean cluster at 3200 Ma. The age spectrum of group 9 (sample 455462) shows two major Late Archaean peaks at 2800 Ma and 2950 Ma and a minor group of Middle Archaean zircons with ages from 3100-3300 Ma. This exclusive Archaean provenance in all Late Paleocene to Eocene sandstones is identical with the provenance infered for Early Cretaceous sandstones (*cf.* Fig. 2) and points to sourcing from the Archaean basement either in the Kangerlussuaq region or to the south or southwest (units **[74]** and **[75]** of the Geological Map of Greenland; Escher and Pulvertaft 1995; Henriksen et al. 2000).

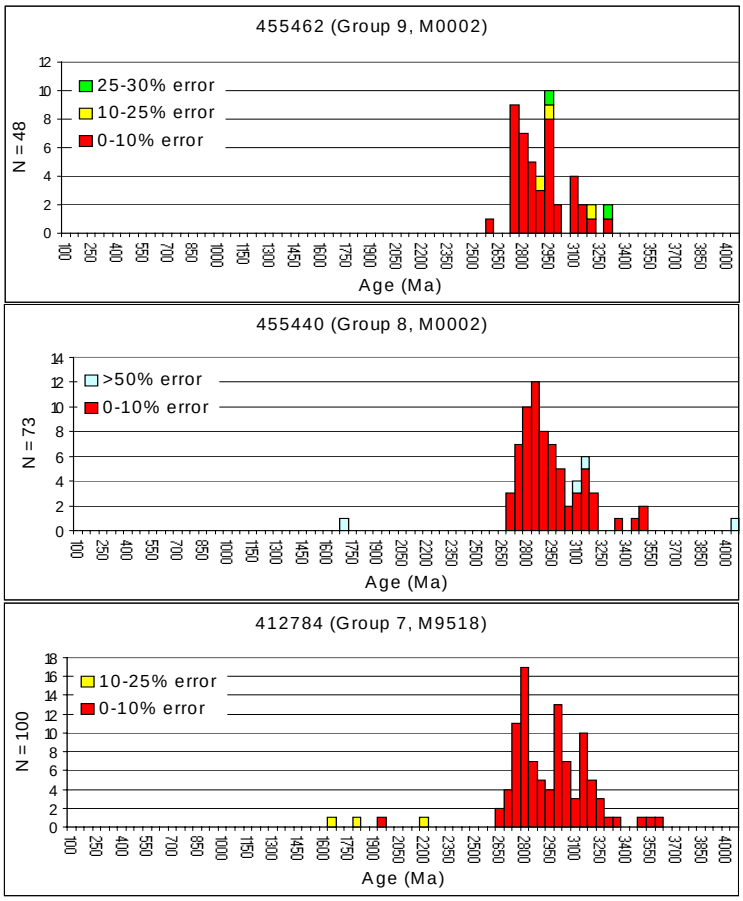

Figure 4. *Binned histograms displaying detrital zircon age distributions in sandstones from Late Paleocene to Late Eocene groups 7, 8 and 9 of a representative stratigraphic profile through the Kangerlussuaq Basin (with the stratigraphically youngest sample on top). Note the remarkable similarity of the age spectra.*

The lateral variation of the age spectra within each group is depicted in the stratigraphic map provided in Enclosure 1. In general, the observed age spectra show only subordinate lateral variation within each group. The only exception is group 5, were a pronounced change in age spectra from east to west can be observed (Fig. 5). The spectra in the easternmost occurrence (sample 413190; Profile 15; Nansen Fjord) shows an almost unimodal,

Late Archaean age distribution with ages ranging from 2700 Ma to 3050 Ma and a pronounced peak at 2750 Ma.

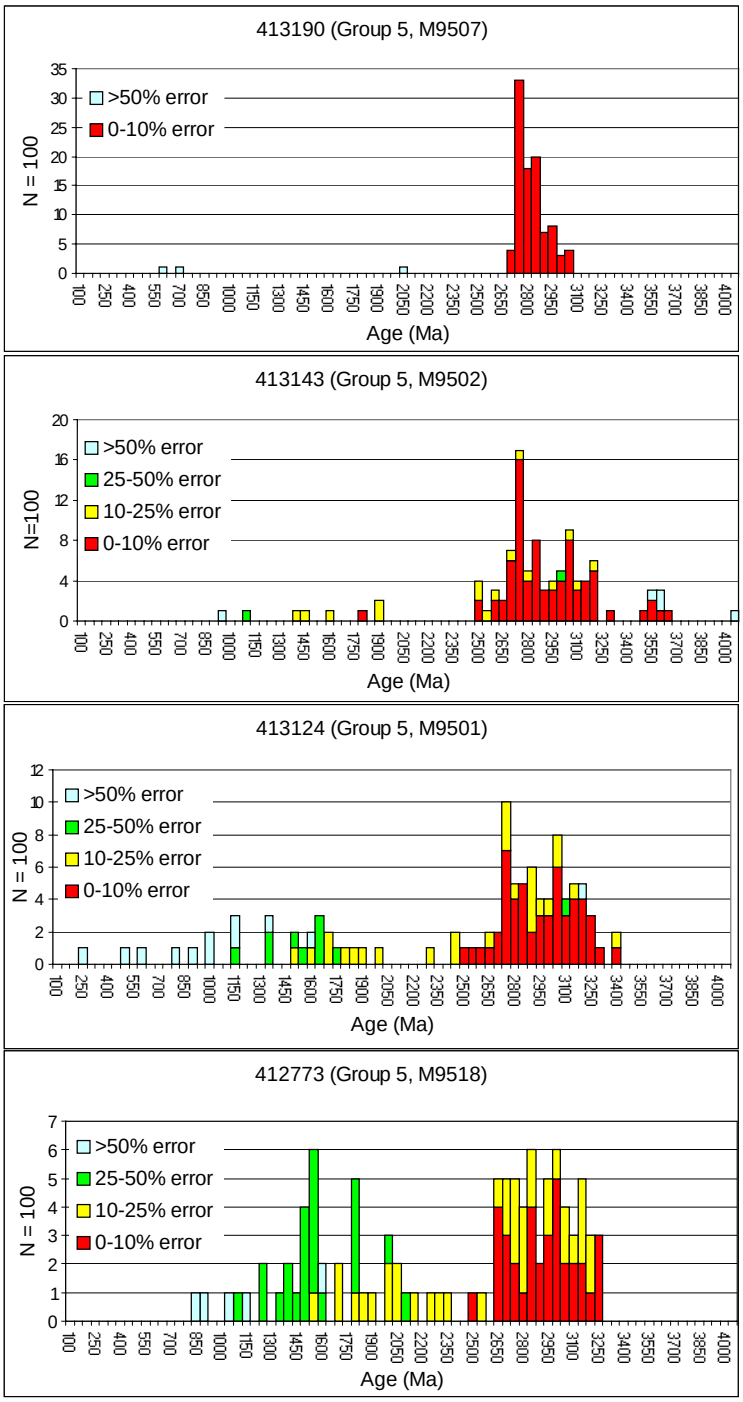

Figure 5. *Binned histograms displaying lateral variation of detrital zircon age distributions in Early to Late Paleocene sandstones from group 5. Note the marked gradual change in age distributions from east (sample 413190) to west (sample 412773).*

Towards the west, this unimodal age spectrum gradually changes via sample 413143 (Profile 6; Fairytale Valley) and sample 413124 (Profile 6; Fairytale Valley) into an entirely polymodal age spectrum in the westernmost occurence (sample 412773; Profile 14; Sor-

genfri Fm.). This polymodal age spectrum is characterised by a broad cluster of Middle and Late Archaean zircons (ranging from 2650-3250 Ma) without the presence of prominent peaks, and a very high occurrence of Early and Middle Proterozoic zircons with three clusters at 2000, 1800, and 1550 Ma. Two additional zircons with Late Proterozoic ages are present. This change in the age spectra indicates either a lateral difference in their source areas or a pronounced local reworking of sandstones from group 4 in the West. Geographical considerations, however, suggest local reworking of sandstones from group 4 as the most likely source.

Paleocene-Eocene, Faroe-Shetland Basin

The stratigraphic correlation of the early Paleogene successions West of Shetland, the Faroes and in Kangerlussuaq (from Larsen et al. 2005) is shown in Fig. 6.

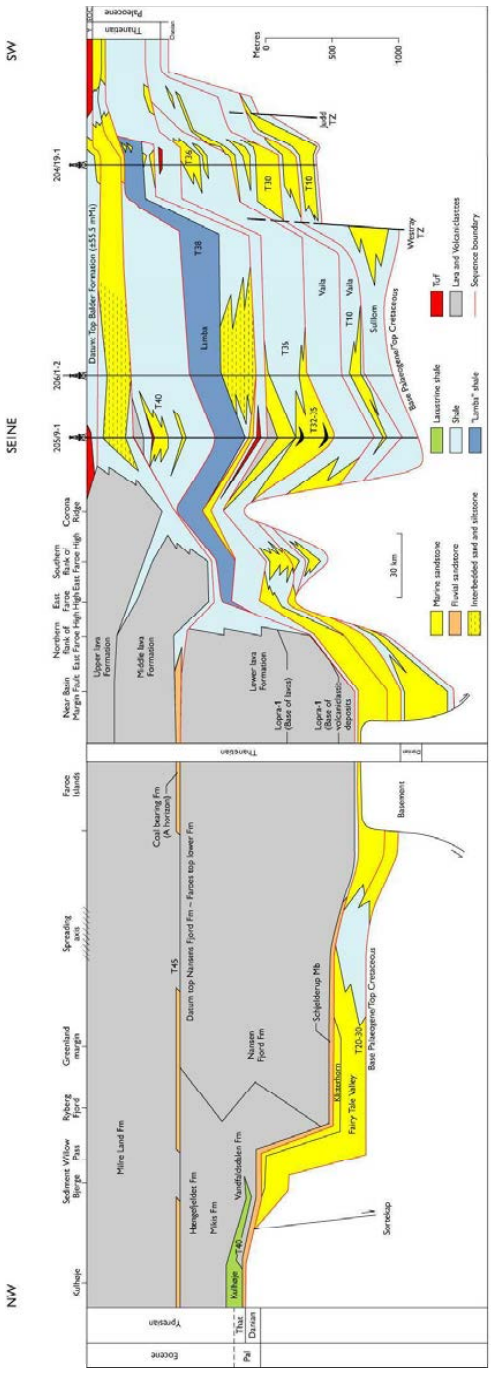

Figure 6. *Correlation of the early Paleogene successions West of Shetland, the Faroes and in Kangerlussuaq (from Larsen et al. 2005; right hand side of the diagramme from Ellis et al., 2002).*

The samples from the Faroe-Shetland Basin analysed during the SINDRI project are from the wells 204/19-3a and 204/24a-7 in the Foinaven sub-basin, and from wells 205/9-1, 206/1-1a and 214/19-1 in the Flett sub-basin. The samples analysed for detrital zircon age distribution cover the sedimentary succession from the Early Paleocene (Vaila Fm. V1) to the Early Eocene (Ypresian; UPD Fm.). Samples have been assigned to the stratigraphic succession using the stratigraphic units outlined by Larsen et al. (2005).

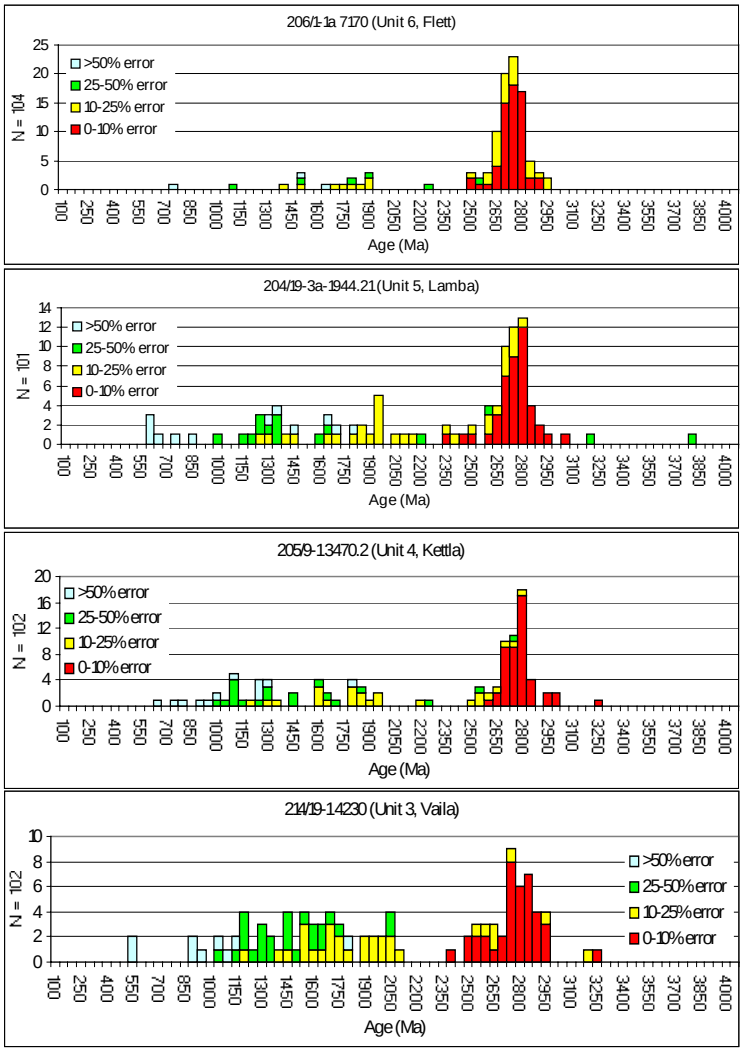

Figure 7. *Binned histograms displaying detrital zircon age distributions in sandstones from Early to Late Paleocene sediments (Vaila, Kettla, Lambda and Flett Fm.) drilled in wells in the UK sector of the Faroe-Shetland Basin. Samples from the different wells are arranged according to their stratigraphic position (with the stratigraphically youngest sample on top). Note the almost complete absence of Middle Archaean zircon ages.*

The most striking observation is the apparent similarity of the age spectra in all units (Figs 7 and 8). All spectra are characterised by a pronounced, relatively narrow cluster in the Late Archaean ranging from ~2550 to 2950 Ma with a peak at 2800 Ma and a wide range of Early to Late Proterozoic ages. Zircons older than 2950 Ma or younger than 600 Ma are extremely rare (only 12 out of 610 measured zircons are > 2950 Ma old and only 6 are of

Caledonian age). The frequency of Proterozoic zircons gradually decreases with increasing stratigraphic level until they are almost completely absent in the Late Paleocene (Flett Fm.), above which their frequency increases again from the Late Paleocene towards the top of the stratigraphic succession in the Early Eocene.

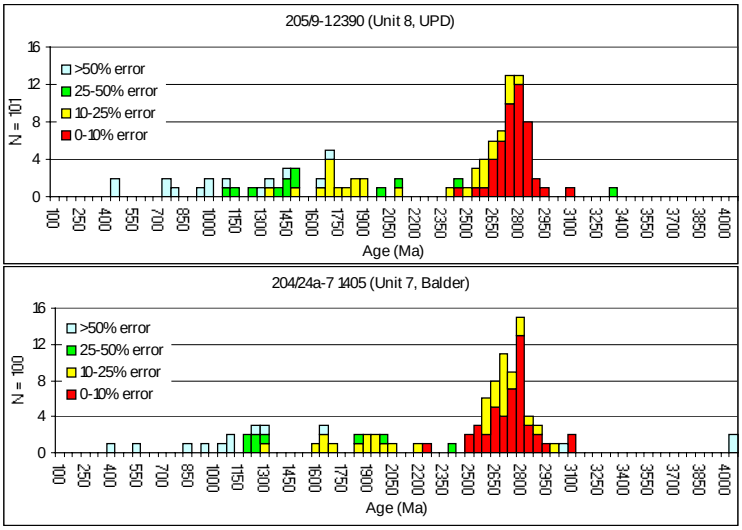

Figure 8. *Binned histograms displaying the detrital zircon age distributions in sandstones from Early Eocene sediments (Balder and UPD Fm.) drilled in wells in the UK sector of the Faroe-Shetland Basin (with the stratigraphically youngest sample on top). Samples from different wells are arranged according to their stratigraphic position. Note the almost complete absence of Middle Archaean zircon ages.*

Conclusions

The observed lateral and vertical variations of detrital zircon age distributions in sandstones from the Kangerlussuaq Basin and wells in the UK sector of the Faroe-Shetland Basin allows some contraints to be drawn on sediment dispersal patterns on both local and regional scales. In the Kangerlussuaq Basin, prominent changes in the age spectra suggest two major changes in sediment sourcing. From the Early to Late Cretaceous, Archaean basement sources in the south or southwest have been replaced by sources in the north and northeast that comprise a high proportion of younger material. During the Late Paleocene, sediment supply has changed back to predominantly Archaean basement sources in the south or southwest. Furthermore, the pronounced changes in the observed age spectra from the Early to Late Cretaceous and during the Late Paleocene excludes large-scale reworking of local sediments as a potential sediment source.

These findings support the conclusions of Whitham et al. (2004) who proposed two major changes in provenance during the deposition of the Cretaceous-Eocene sedimentary succession in Kangerlussuaq. However, the higher vertical and lateral stratigraphic resolution of our study allows us to reconstruct the timing of these changes with much more detail and

allows us to draw some further conclusions. For example, the relative frequency of the main Archaean (i.e. Early, Late and Middle Archaean) and Proterozoic (i.e. Caledonian, Grenvillian, and Early Proterozoic) age groups show clear temporal changes within each of the three main units. These findings suggest that distinctively different age domains in both the Archean and Proterozoic basement have acted as dominant sediment sources at different times during the evolution of each of the main units. The lack of lateral variations in the age spectra in almost all groups strongly supports the validity of the stratigraphic correlations drawn from litho- and sequence stratigraphic observations. Furthermore, they suggest geographically unilateral sediment transport regimes during the deposition of most of the sedimentary succession. The only exception is the lateral variation of the age spectra in the Late Paleocene group 5, which points to small scale local reworking of sediments from group 4 during parts of the Paleocene.

A very important result of this study is the almost complete lack of Middle Archaean zircons in samples from wells in the UK sector, an age component that is characteristic for almost all sandstones exposed in the Kangerlussuaq area. This observation is in agreement with the evidence from conventional petrographic and chemical analysis of heavy minerals (Morton et al. 2005), from geochemistry of detrital garnets (Frei et al. 2005), and from detailed chemostratigraphic investigations (Knudsen 2005). These findings demonstrate that both the Kangerlussuaq area and the eastern margin of the Faroe-Shetland Basin have characteristic signatures that allow distinction between a western, greenlandic source (containing a prominent Middle Archaean age component) and an eastern, predominantly UK margin source (lacking a Middle Archaean age component). Based on these findings it can be concluded that large volumes of the sediments present in the wells in the UK sector of the Faroe-Shetland Basin are not derived from the Kangerlussuaq Basin. However, only relevant stratigraphic intervals in wells from the easternmost parts of the Faroe-Shetland Basin have been examined so far and the structure of the Faroe-Shetland Basin suggests that the western, greenlandic source might be of far more importance for the deeper, central parts of the basin towards the Faroes area. The new techniques available for provenance studies and the distinctive signature of the greenlandic source characterised during this project provide a reliable way to distinguish the eastern and western provenance areas and should therefore be applied to wells in the Faroes area.

References

Bingen, B., Birkeland, A., Nordgulen, Ø., Sigmond, E.M.O. 2001: Correlation of supracrustal terranes in the Sveconorwegian orogen of SW Scandinavia: SIMS data on zircon in clastic metasediments. Precambrian Research **108**, 293-318.

Ellis, D., Bell, B.R., Jolley, D.W., O´Callaghan, M. 2002: The stratigraphy, environment of eruption and age of the Faroes Lava Group, NE Atlantic. *In*: Jolley, D.W. and Bell, B.R. (eds) The North Atlantic Igneous Province. Stratigraphy, Tectonic, Volcanic and Magmatic processes. Geological Society, London, Special Publications **197**, 253-269.

Escher, J.C., Pulvertaft, T.C.R. 1995: Geological Map of Greenland. Scale 1:2.500.000. Geological Survey of Greenland, Copenhagen.

Frei, D., Frei, M., Hansen Klünder, M., Rasmussen, T., Knudsen, C., Morton, A.C., Whitham, A.G. 2005: Heavy mineral characteristics of Cretaceous-Eocene sandstones in the Kangerlussuaq Basin, East Greenland – results from CCSEM. Danmarks og Grønlands Geologiske Undersøgelse Rapport **2005/54** *(this volume).*

Hass, G.J.M.L., de, Andersen, T., Vestin., J. 1999: Detrital zircon geochronology: new evidence for an old model for accretion of the Southwest Baltic Shield. Journal of Geology **107**, 569-586.

Henriksen, N., Higgins, A.K., Kalsbeek, F., Pulvertaft, T.C.R. 2000: Greenland from Archaean to Quaternary. Geology of Greenland Survey Bulletin **185**.

Knudsen, C. 2005: Chemostratigraphy and chemical characteristics of Cretaceous-Paleocene-Eocene sandstones and mudstones in the Kangerlussuaq area, East Greenland, and in the Faroe-Shetland Basin. Danmarks og Grønlands Geologiske Undersøgelse Rapport **2005/54** *(this volume).*

Larsen, M., Nøhr-Hansen, H., Whitham, A.G., Kelly, S.R.A. 2005: Stratigraphy of the prebasaltic sedimentary succession of the Kangerlussuaq Basin. Volcanic basins of the North Atlantic. Danmarks og Grønlands Geologiske Undersøgelse Rapport **2005/62**.

Morton, A.C., Hallsworth, C.R., Whitham, A. G. 2005: Heavy mineral provenance of Paleocene-Eocene sandstones in the Faroe-Shetland Basin – results from conventional petrographic and mineral-chemical techniques. Danmarks og Grønlands Geologiske Undersøgelse Rapport **2005/54** *(this volume).*

Whitham, A.G., Morton, A.C., Fanning, C.M. 2004: Insights into Cretaceous-Paleocene sediment transport paths and basin evolution in the North Atlantic from a heavy mineral study of sandstones from southern East Greenland. Petroleum Geoscience **10**, 61-72.

Trace element geochemistry of detrital garnets – a useful provenance indicator?

Dirk Frei, Martina Frei, Maiken Hansen Klünder, Thomas Rasmussen, Christian Knudsen
Geological Survey of Denmark and Greenland, Øster Voldgade 10, DK-1350 Copenhagen K, Denmark

Introduction

The information extracted from detrital minerals for provenance studies has been thriving in recent years mainly due to improvements in microanalytical techniques, most notably electron microprobe analyses (EMPA) and laser ablation – inductively coupled plasma – mass spectrometry (LA-ICP-MS). The chemical, petrogenetic and radiometric signatures recorded in a wide range of detrital minerals have been used for deciphering characteristics of their source area, e.g., garnet (Morton 1985), chrome spinel (Pober and Faupl 1988; Lenaz 2003), tourmaline (Henry and Guidotti 1985), amphibole (Faupl et al. 2002), white mica (von Eynatten and Wijbrans 2003), epidote (Spiegel et al. 2002), rutile (Zack et al. 2004), and zircon (Belousova et al. 2002; Hoskin and Grapes 2002).

The observed variations in the major element geochemistry of detrital garnet has been proved over the last decade to be a very useful provenance indicator, mainly by the pioneering work of Morton and co-workers. Garnet with a potentially wide compositional range shows significant differences in composition between different types of garnet-bearing lithologies. The compositional variation of the overwhelming majority of garnets from common acidic, intermediate, as well as basic and ultrabasic rocks can be expressed in the ternary composition space almandine (+spessartine) – pyrope – grossular. Morton et al. (2004) subdivide the ternary compositional space into three different detrital garnet assemblages indicative for common source rocks (see Fig. 3 in Frei et al. 2005): pyrope-rich, grossular-poor garnets (= Type A) are believed to be derived from high-grade granulite facies metasedimentary rocks or charnockites; almandine-rich garnets with variable grossular and spessartine contents (= Type B) are predominantly from low- to medium-grade metasediments or from intermediate to acidic gneisses and granites; and grossular- and pyrope-rich garnets (= Type C) are from metabasic rocks. However, there is considerable compositional overlap of garnets occuring in rocks of different character (Deer et al. 1992).

It is a well-known fact that garnet can incorporate a variety of geochemically important trace elements that may be indicative for specific rock types (e.g. Sc, Ti, Cu, Ni, Cr, Y, Zr, REE, and Hf; van Westrenen et al. 1999, and references therein). Therefore, the trace element signature recorded in detrital garnet may yield additional information about the nature of their source rocks. The enormous progress in the development of LA-ICP-MS techniques for the determination of a wide range of trace elements in *in-situ* at low concentration levels in minerals has made it feasible to explore the trace element variation in garnet for fingerprinting their source region. In the course of this project, > 2500 hand-picked garnets have been analysed for their major element chemistry and their content of a wide range of geochemically important trace elements (Li, Sc, Ti, Cr, Co, Ni, Cu, Sr, Y, Zr, Nb, Ba, La, Ce,

Pr, Nd, Sm, Eu, Gd, Tb, Dy, Ho, Er, Tm, Yb, Lu, Hf, Ta, Pb, Th, and U). Here, we briefly evaluate the potential of the trace element signatures recorded in detrital garnet to yield additional constraints on the characteristics of their source rocks. The experimental and analytical details are reported in Appendix B. All garnet major and trace element compositions results are reported in Excel-based spreadsheets in the attached data CD-ROM.

Preliminary results

Here, we briefly describe preliminary results of a on-going reconnaissance study by exploring the variation of trace element signatures recorded in two detrital garnet populations as a funtion of major element chemistry. Both garnet populations (from samples 206-1-1a 7558 and 206-1-1a 7653.8 from the Late Paleocene Flett Fm. In well 206-1-1a) display a particular wide compositional variation in the ternary composition space almandine (+spessartine) – pyrope – grossular (Fig. 1) and are therefore ideally suited for this purpose. Both samples contain a considerable fraction of Type Ai garnets and Type C garnets (for further explanation of garnet types, see Morton et al. 2005; and Frei et al. 2005). An interesting difference between both samples is the distribution of garnet compositions along the pyrope – almandine join: in sample 206-1-1a 7558 are bimodally distributed, whereas in sample 206-1-1a 7653.8 they form a continuous solid solution series.

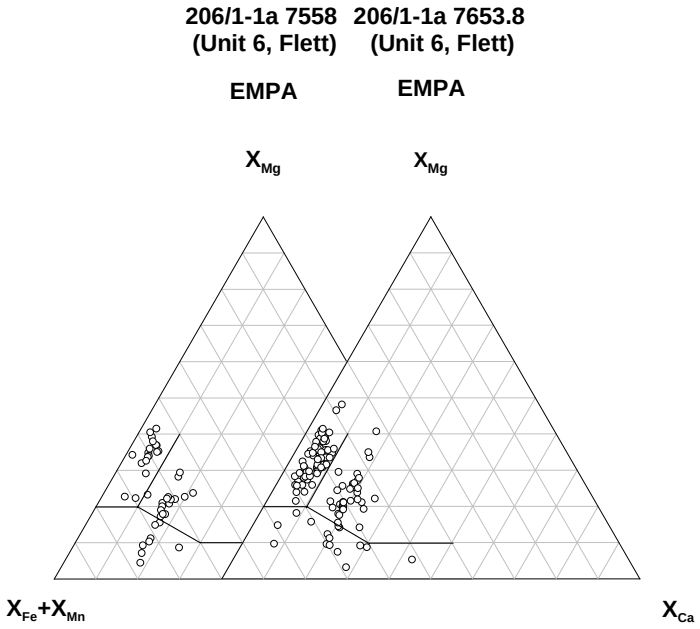

Figure 1. *Garnet major element compositions in samples (**a**) 206-1-1a 7558 and (**b**) 206-1-1a 7653.8 (Late Paleocene, Flett Fm.) as analysed by CCSEM. X_{Fe}, X_{Mn}, X_{Mg} and X_{Ca} are molecular proportions of Fe, Mn, Mg, and Ca, respectively. All Fe was calculated as Fe^{2+}.*

Our approach was (1) to subdivide these garnet populations in three types representative for the different ternary end-member compositions (i.e. Mg-rich, Fe-rich, and Ca-rich); (2) to analyse the elemental covariations by extracting components that describe the chemical variability in multi-dimensional composition space using multivariate statistics (factor analysis using principal component analysis), and (3) to evaluate the variation of these elements using multi-element and element-element cross-plots.

Table 1. *Chemical covariation of major and trace elements in sample 206-1-1a 7558 expressed as elemental scores in principal components in multi-dimensional compositions space. Components extracted are arranged in order of decreasing statistic significance (i.e. component 1 is the most significant component, whereas component 7 is the least significant).*

Component Matrix [a]

	Component						
	1	2	3	4	5	6	7
MGO	-.236	-.382	.831	.211			
AL2O3	-.273	-.412	.753	.315			
SIO2	-.261	-.455	.798				
CAO	.268	.327	-.723	-.230			
TIO2	-.299		-.635				.539
MNO		.492	-.772	.209			
FEO	.254			-.475		-.535	-.349
LI7	.301	.607	.504	.315	-.272		
SC45	.507		.521		.205	.267	
TI47	-.261	.617	.273	-.355	-.444		
CR53	-.346	-.433	.511	.286			.234
CO59		-.364	.801				
NI60	-.346	.652	.479		-.372		
CU63	-.364	.671	.438		-.268		
SR88	-.429	.634			-.326		.207
Y89	.868	.430		.223			
ZR90	-.566	.310		.349	.547		
NB93	-.282	.782	.457				
BA137	-.478	.580	-.454	.265	.227		
LA139	-.373	.848	.211				
CE140	-.302	.846		-.209			
PR141		.756	.343	-.419	.222		
ND146	.524	.309	.387	-.466	.415		
SM147	.712	.273	.295	-.301	.375		
EU153	.439			-.620	.318	.226	-.316
GD157	.749	.423		-.227	.256		.235
TB159	.797	.465					.227
DY163	.849	.458					
HO165	.875	.411		.235			
ER166	.849	.354		.364			
TM169	.805	.307		.440			
YB172	.764	.275		.482			
LU175	.746	.258		.496			-.208
HF178	-.471	.480		.405	.584		
TA181	-.360	.764	.460				
PB208	-.535	.578		.339	.252	-.247	
TH232	-.499	.835					
U238	-.210		.258	.358		-.659	
Ce/Yb	-.629	.579		.235	.245	.224	
Eu/Eu0	-.451		-.754			.224	-.225

Extraction Method: Principal Component Analysis.

a. 7 components extracted.

Table 2. *Chemical covariation of major and trace elements in sample 206-1-1a 7653.8 expressed as elemental scores in principal components in multi-dimensional compositions space. Components extracted are arranged in order of decreasing statistic significance (i.e. component 1 is the most significant component, whereas component 8 is the least significant).*

Component Matrix [a]

	Component							
	1	2	3	4	5	6	7	8
MGO	-.464	.472	-.239	-.544	.231	.304		
AL2O3	-.440	.397	-.271	-.540		.357		
SIO2	-.637	.307		-.324	.448	.232		
CAO	-.250	-.397	.458	.706				
TIO2	-.234	-.453	.307	.401	.312			-.433
MNO	.856		.403					
FEO	.646		-.404	-.242	-.491			
LI7	.907		.341					
SC45	.269			-.568	-.426		-.314	.444
TI47	-.409	.748	.307	.236				
CR53	-.417		.235		.302	.458	.329	.456
CO59	-.610	-.369	.329			.291	.281	
NI60	-.373	-.286	.311	.503			.541	
CU63					-.457	-.384	.721	
SR88		.864		.205	-.224		.286	
Y89	.931		.245					
ZR90				.400	-.524	.704		
NB93	.246	.202	-.793	.341	.305			
BA137	.229		-.809	.315	.303			
LA139	-.242	.946						
CE140	-.243	.946						
PR141	-.243	.948						
ND146	-.221	.954						
SM147	.347	.531	-.640					
EU153			-.567	.600		.260		
GD157	.784	.289	-.481					
TB159	.938	.265						
DY163	.947	.224						
HO165	.930		.245					
ER166	.917		.303					
TM169	.909		.327					
YB172	.903		.342					
LU175	.899		.353					
HF178				.400	-.525	.704		
TA181	.433		-.712	.329	.338			
PB208	-.233	.934						
TH232	-.252	.943						
U238	-.247	.924						
Ce/Yb	-.250	.941						
Eu/Eu0	-.424	-.407	.387	.569	.250			

Extraction Method: Principal Component Analysis.

a. 8 components extracted.

For sample 206-1-1a 7558, seven principal components have been extracted that describe the chemical variability of the garnet population sufficiently and the relative score of the investigated elements for each component are given in Table 1. Only elements with a score > 0.5 are assumed to contribute to the extracted components with statistical significance. The statistically most significant components extracted are (in decreasing order of signifi-

cance): a component indicating a covariation between Sc, and the middle and heavy rare earth elements (MREE and HREE, respectively) (Component 1); a component indicating a covariance between Li, Ni, Cu, the high field strength elements (HFSE) Ti, Nb, and Ta, as well as the large ion lithophile elements (LILE) Sr, Ba, La, Ce, Pb and Th (Component 2); a component indicating a covariance between the major elements Mg, Al, Si, and the trace elements Li, Sc, Cr, and Co (Component 4); and a component with high scores for the HFSE Zr and Hf (Component 5).

For sample 206-1-1a 7653.8, eight principal components have been extracted that describe the chemical variability of the garnet population sufficiently and the relative score of the investigated elements for each component are given in Table 2. Only elements with a score > 0.5 are assumed to contribute to the extracted components with statistical significance. The statistically most significant components extracted are (in decreasing order of significance): a component indicating a covariation between Mn, Fe, Li, and the HREE (Component 1); a component indicating a covariance between Ti and LILE (Sr, Ba, La, Ce, Pr, Nd, Sm, Pb, Th and U) (Component 2); a component indicating a covariance mainly between the major element Ca and Eu (Component 4); and a component with high scores for the HFSE Zr and Hf (Component 6).

Clearly, the most important element group for the observed compositional variability are the REE. However, the relative REE patterns are relatively uniform and the REE contents show no significant covariation with major element compositions. The most striking exception is a distinct variation of the magnitude of the Eu-anomaly with major element composition, especially with Ca (Fig. 2).

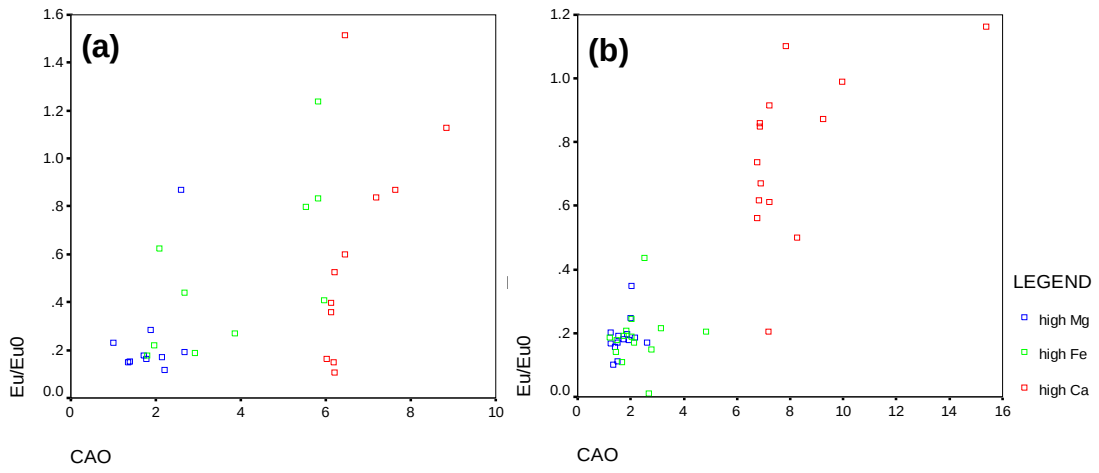

Figure 2. *Magnitude of the Eu-anomaly as a function of the CaO content (wt%) in detrital garnets from samples (**a**) 206-1-1a 7558 and (**b**) 206-1-1a 7653.8.*

In both examined samples, Mg-rich garnets are generally characterised by strong negative Eu-anomalies that show very limited variations in magnitude and cluster at Eu/Eu* values around 0.2. In marked contrast, Ca-rich garnets show a wide range in the magnitude of the Eu-anomalies from strongly positive (Eu/Eu* ~ 1.6) to strongly negative (Eu/Eu* ~ 0.1). Fe-rich, grossular-poor garnets follow the behaviour observed for Mg-rich garnets, whereas

Fe-rich garnets with significant Ca-content are following the trend observed for Ca-rich garnets.

The element group that shows the most pronounced covariations with major elements are the transition metals. The variation of the transition element contents as a function of major element composition in samples 206-1-1a 7558 and 206-1-1a 7653.8 is shown in multi-element crossplots in Fig. 3.

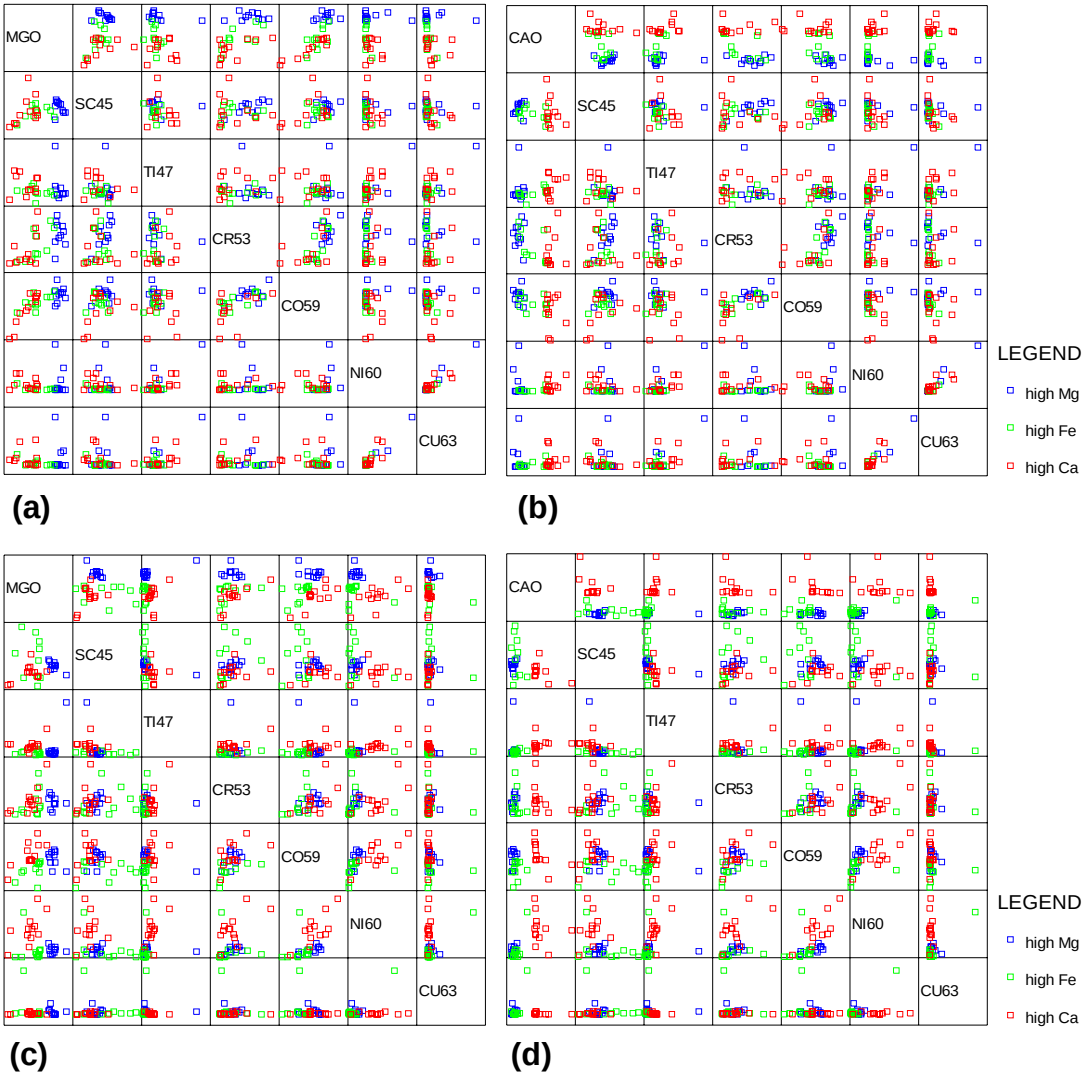

Figure 3. *Multi-element crossplots depicting the variation of transition metals contents (in ppm) with the major elements MgO and CaO (wt%) in samples 206-1-1a 7558 (**a** and **b**, respectively; top) and 206-1-1a 7563.8 (**c** and **d**, respectively; bottom).*

Especially interesting variations are observed for the elements Co and Ni; these elements are displayed in more detail in the Fig. 4.

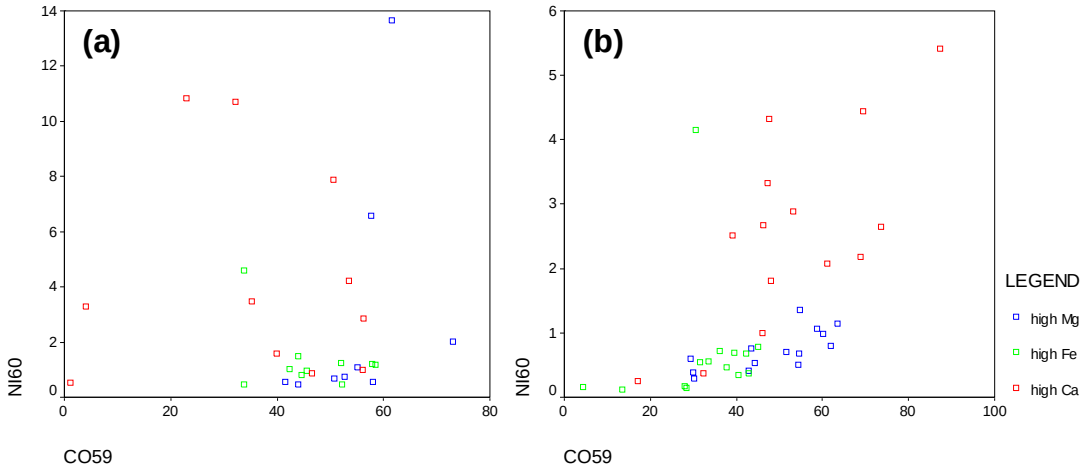

Figure 4. *Variation of Ni (ppm) as a function Co (ppm) in detrital garnets from samples (**a**) 206-1-1a 7558 and (**b**) 206-1-1a 7653.8.*

The content of Ni as a function of Co in garnets from samples 206-1-1a 7558 and 206-1-1-a 7653.8 is displayed in Fig. 4. Although some overlap occurs, all three major garnet types define characteristic fields and the general patterns are similar for both samples. The fields are much better defined in sample 206-1-1a 7653.8: Fe-rich garnets are characterised by low Ni and Co contents, while Mg-rich garnets show higher contents for both elements. Both garnet types define an array along a linear correlation line with a slope of ~ 0.015 indicating a constant Ni/Co-ratio. In contrast, Ca-rich garnets are characterised by much higher and variable Ni and Co contents. This general pattern is also observed for sample 206-1-1a 7558, but there is considerable more overlap between these fields and there are more exceptional datapoints, especially some Mg-rich garnets that show very high Ni contents.

Conclusions

The trace element signatures recorded in detrital garnets clearly hold considerable promise as an important tool for advanced provenance studies. Especially variations of the transition metal and light ion lithophile element signatures have the potential to yield considerable information about their host rocks. The successful application of garnets trace element signatures for provenance purposes has already been demonstrated on a restricted regional scale, were the garnet major and trace element characteristics of the source rocks are well known (Karimzadeh Somarin 2004; Čopjakova et al. 2005). However, in order to take full advantage of the information that the trace element record of detrital garnets may yield for identification of their source rocks, a framework is needed that describes the characteristic trace element signatures of garnets from a wide range of common rock types. This might in turn lead to the identification of elemental abundances, trace element ratios, and/or trace element patterns that are distinctive for specific rock types, similar to those observed for zircon (Belousova et al. 2002) and rutile (Zack et al. 2004). The trace element signatures of the > 2500 detrital garnets from the sedimentary successions exposed in the

Kangerlussuaq basin and drilled in wells in the Faroe-Shetland area obtained in this study form a perfectly suited database that can be used to test such a framework.

In certain garnets (especially in binary pyrope-almandine solid solutions) there is a large overlap for individual trace elements and their use for provenance studies is therefore questionable. A very promising approach, however, is the combination of trace element signatures with radiogenic isotope characteristics, similar to the approach used for epidotes by Spiegel et al. (2002). This approach will be even more promising if performed by individual grain analyses.

References

Belousova, E.A., Griffin, W.L., O´Reilly, S.Y., Fisher, N.I. 2002: Igneous zircon: trace element composition as an indicator of source rock type. Contributions to Mineralogy and Petrology **143**: 602-622.

Čopjakova, R., Sulovský, P., Paterson, B.A. 2005: Major and trace elements in pyrope-almandine garnets as sediment provenance indicators of the Lower Carboniferous Culm sediments, Drahany Uplands, Bohemian Massif. Lithos, 82, 51-70.

Deer W.A, Howie, R.A., Zussman, J. 1992: An introduction to the rock forming minerals. Longman Scientific & Technical, Harlow, Essex, England.

Faupl, P., Petrakakis, K., Migiros, G., Pavlopoulos, A. 2002: Detrital blue amphibole from the western Othrys mountains and their relationship to the blueshist terrains of the Hellenides (Greece). International Journal of Earth Sciences **91**, 433-444.

Frei, D., Frei, M., Hansen Klünder, M., Rasmussen, T., Knudsen, C., Morton, A.C., Whitham, A.G. 2005b: Evaluation of novel analytical techniques for provenance studies I: CCSEM. Danmarks og Grønlands Geologiske Undersøgelse Rapport **2005/54** *(this volume).*

Henry, D.J., Guidotti, C.V. 1985: Tourmaline as a petrogenetic indicator mineral: an example from the staurolite-grade metapelites of NW Maine. American Mineralogist **70**, 1-15.

Hoskin, P.W.O., Grapes, R.H. 2002: Zircon composition of petrogenetic processes and provenance: are we flogging a dead horse? Berichte der Deutschen Mineralogischen Gesellschaft, Beihefte zum European Journal of Mineralogy **14**, 74.

Karimzadeh Somarin, A. 2004: Garnet composition as an indicator of Cu mineralization: evidence from skarn deposits of North-West Iran. Journal of Geochemical Exploration **81**, 47-57

Lenaz, D., Kamenetsky, V.S., Princivalle, F. 2003: Cr-spinel supply in the Brkini, Istrian and Krk Island flysch basins (Slovenia, Italy and Croatia). Geological Magazine **140**: 335-342.

Morton, A.C. 1985: A new approach to provenance studies: electron microprobe analysis of detrital garnets from Middle Jurassic sandstones of the northern North Sea. Sedimentology **32**, 553-566.

Pober, E., Faupl, P. 1988: The chemistry of detrital chromian spinels and its implications for the geodynamic evolution of the Eastern Alps. Geologische Rundschau **77**, 641-670.

Spiegel, C., Siebel, W., Frisch, W., Zsolt, B. 2002. Nd and Sr isotopic ratios and trace element geochemistry of epidote from the Swiss Molasse Basin as provenance indicatos: implications for the reconstruction of the exhumation history of the Central Alps. Chemical Geology **189**, 231-250.

von Eynatten, H., Wijbrans, J.R. 2003: Precise tracing of exhumation and provenance using Ar/Ar-geochronology of detrital white mica: the example of the Central Alps. Geological Society of London, Special Publication **208**, 289-305.

van Westrenen, W., Blundy, J.D., Wood, B.J. 1999: Crystal-chemical controls on trave element partitioning between garnet and anhydrous silicate melt. American Mineralogist **84**, 838-847.

Zack, T., von Eynatten, H., Kronz, A. 2004: Rutile geochemistry and ist potential use in quantitative provenance studies. Sedimentary Geology **171**, 37-58.

Chemostratigraphy and chemical characteristics of Cretaceous-Paleocene-Eocene sandstones and mudstones in the Kangerlussuaq area, East Greenland, and in the Faroe-Shetland Basin

Christian Knudsen

Geological Survey of Denmark and Greenland, Øster Voldgade 10, DK-1350 Copenhagen K, Denmark

Summary

A total of 440 samples representing Cretaceous, Paleocene and Eocene clastic sediments have been analysed for 10 major elements, 33 trace elements and loss on ignition. Of these, 269 samples represent washed and dried cuttings from wells in the Faroe-Shetland Basin., whereas 171 samples represent rocks collected in the Kangerlussuaq area in East Greenland. The approach of analysing a very high number of samples for a very high number of elements with very high sensitivity allows for a novel interpretation of the geology in the potential reservoirs. Conventional provenance analysis is focussed on analysis of heavy minerals which only constitute a small fraction of the sediments, whereas bulk rock geochemical analysis allows evaluation and interpretation of the effects of the complete mineralogical composition of the sediment. Accordingly, the effects of e.g. feldspars and clay minerals, as well as heavy minerals such as zircon, can be evaluated. Further, carbonate cementation and redox conditions in the depositional environment can be investigated.

General findings

In general, it is found that the sedimentary units have distinctive geochemical characteristics. Common sources can be detected for different units as well as internally within units, both vertically and laterally. To achieve this, no single or few parameters can be used but it is necessary to consider the complete dataset. The advantage is that it is possible to generate and interpret such large datasets at fairly low cost due to the new analytical techniques now available.

There is no evidence for a common source shared by the sediments from the Kangerlussuaq and the Faroe-Shetland areas. This is in line with the findings from the studys on provenance sensitive heavy minerals (Morton et al. 2005), detrital garnet major element geochemistry (Frei et al. 2005; Morton et al. 2005) and detrital zircon age distributions (Frei et al. 2005b). If common source areas existed at all, their influence on the geochemistry of the sediments is not distinguishable.

Specific findings

Sediments containing a component of reworked volcanic material can be recognised geochemically by high Ti/Al, Nb/Zr and Eu/Ce ratios. In the Kangerlussuaq area, this effect is seen in the Kulhøje and Willow Pass Members and partly in the Schjelderup Mb. However, it has also been possible to trace the effect of the remote volcanic activity in the basin on the Ti/Al ratio in the mudstones in the Faroe-Shetland Basin: this ratio increases gradually with time during the opening of the North Atlantic Ocean. A similar effect is seen in the Yb/La ratios that increase with time, reflecting an increasing volcanic input and decreasing continental character of the mud component.

Sands containing high proportions of heavy minerals zuch as zircon can be recognised on their high Zr/Al and low Nb/Zr ratios. This is the case for some but not all of the sands in the Fairy Tale Valley Mb. in the Kangerlussuaq area. Further, the relationship beween e.g. U and Zr is characteristic of a sediment with high heavy mineral content. As heavy minerals are concentrated in beach placers this may have implications for the interpretation of the depositional environment.

In the Fairy Tale Valley Mb. of the Kangerlussuaq area, there is a lateral variation in the source of the mudstones, seen as variation in eg. the Ti/Al and the K/Al ratios among the different profiles sampled.

In the Faroe-Shetland Basin, large variations in source among the different units have been found. One example is the Vaila Fm. in well 205/9-1, which due to high Eu/Ce ratios can be separated from the other units. The high Eu/Ce ratios can be explained as caused by a significant component of Na-rich alkali feldspar.

In the Vaila Fm., certain parts contain dolomite cement (3 to 8 wt %), whereas parts of the Sullom Fm. and one sample from the Maastrichtian “Formation E” contain calcite cement. This can be seen by combining information about the Ca, Mg, Al and volatile contents.

Introduction

The present study on chemostratigraphy has been conducted by GEUS in cooperation with CASP for SINDRI in the period May 2002 to September 2005 as part of the study: “Linking the Faroese area and Greenland: An innovative, integrated provenance study”.

Background

A key problem for hydrocarbon exploration in the Faroes region is the understanding of sediment dispersal patterns prior to the Late Paleocene–Eocene continental break-up. Sediment provenance studies on Cretaceous and Tertiary strata in the Greenland–Faroes–Shetland region are just beginning to provide an understanding of sediment transport paths (eg. Whitham & Morton 2001; Morton et al. 2005), and $^{40}Ar/^{39}Ar$ dating of detrital white mi-

cas in Late Cretaceous and some Paleocene mudstones in the UK sector of the Faeroes-Shetland Basin (Pickles & Sherlock 2002) suggests derivation from Greenland. These works showed the benefits of linking the dating of specific heavy mineral suites such as zircons to conventional heavy mineral and mineral-chemical analysis of sandstones The present chapter presents the rock geochemical part of an extended, integrated provenance study, of which the conventional heavy mineral provenance studies and results from application of new heavy mineral provenance methods are reported in the other chapters of this report.

High resolution geochemistry have been applied to sediments from the area before (eg. Hutchison et al. 2001), but the analytical technique used has been restricted to XRF of trace elements like Zr, Cr and Nb, and accordingly the possibilities for interpretation of the signatures have been limited.

Objectives

The main aim of the present geochemical study of rocks from the Kangerlussuaq area and the wells in the Faeroes–Shetland Basin is primarily to characterise the sandy units and then to test if the findings can confirm the provenance studies. Further, it is the aim to test whether it is possible to qualify statements on the provenance of the mud component in the sedimentary sequence.

Samples

From the Kangerlussuaq area, 171 Cretaceous to Paleocene samples available from GEUS and CASP work in East Greenland were analysed. Of these, 90 samples were described as sandstone and 81 samples were described as mudstone. The samples represent the stratigraphy in different parts of the Kangerlussuaq region and were collected in 10 profiles representing the exposed Cretaceous, Paleocene and Eocene sedimentary strata. From the Faroes–Shetland region and the Shetland Platform, 269 samples of cores and cuttings from released wells were analysed. The samples are from the following wells: 204/19-3a, 204/24a-7, 205/9-1, 206/1-1a and 214/19-1, focussing on the Paleocene sediments.

Analytical methods

The samples were analysed using two methods, namely fusion X-Ray Fluorescence (**XRF**) and Inductively Coupled Plasma – Mass Spectrometry (**ICP-MS**) to yield the best chemical basis for the geochemical provenance analysis. Further, the two methods supplement each other. The content of organic material and volatiles was analysed by ignition of the samples. All sample preparation and analytical procedures and details are described in Appendix B. All results are reported in Excel based spreadsheets in the attached data CD-ROM.

Results

The results from the two areas are treated separately in the preliminary presentation given in the following. The primary aim has been to characterise the individual sedimentary units of the lithostratigraphic frame established during the SINDRI project “Stratigraphy of the volcanic basins of the North Atlantic” reported simultaneously with the present study.

Kangerlussuaq area

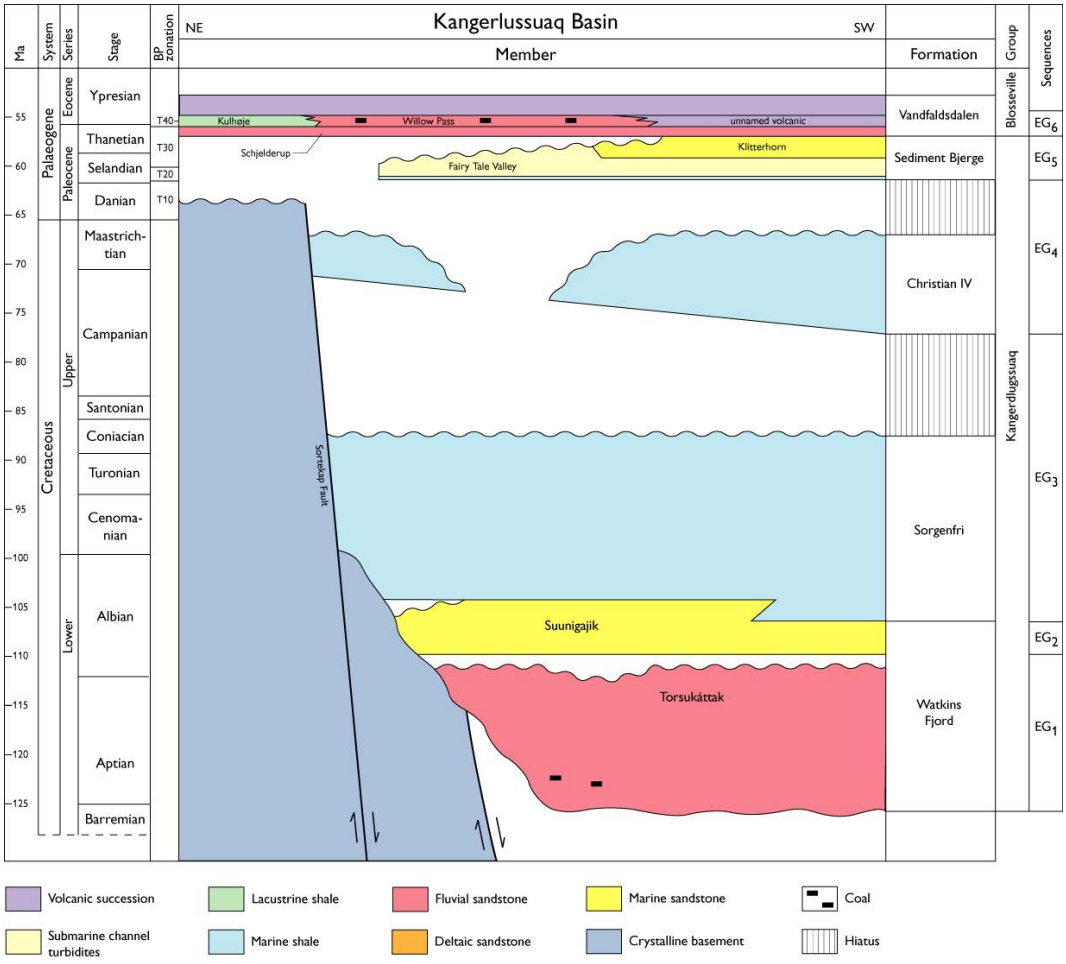

Figure 1. *Stratigraphy in the Kangerlussuaq area. (From Larsen et al. 2004).*

The data represent samples from the following units, listed with the stratigraphically youngest units on the top.

Eocene	Post-volcanic	Kap Dalton Formation	
Paleocene	Syn-volcanic	Kulhøje Member	Vandfaldsdalen For-
mation			
Paleocene	Syn-volcanic	Willow Pass Member	Vandfaldsdalen For-
mation			
Paleocene	Syn-volcanic	Schelderup Member	Vandfaldsdalen For-
mation			
Paleocene	Pre-volcanic	Klitterhorn Member	Sediment Bjerge For-
mation			
Paleocene	Pre-volcanic	Fairy Tale Valley Member	Sediment Bjerge For-
mation			
Late Cretaceous	Pre-volcanic	Christian IV Formation	
Late Cretaceous	Pre-volcanic	Sorgenfri Formation	
Early Cretaceous	Pre-volcanic	Sunnigajak Member	Watkins Fjord Forma-
tion			
Early Cretaceous	Pre-volcanic	Torsukattak Member	Watkins Fjord Forma-
tion			

Sampes from 10 different profiles within the area have been analysed. As the sandstones and the mudstones are very different geochemically, the two rock types are treated separately. To illustrate the geochemistry, a number of simple element cross plots are shown, in which the elemental variation is dependent on the mineralogical composition of the samples.

Sandstone geochemistry

The main chemical components in the sandstones are silica and alumina. As can be observed on Fig. 2, the silica content decreases with increasing alumina. Mineralogically, this reflects decreasing contents of quartz with increasing contents of aluminium-bearing phases – mainly feldspars, mica and clay. Some sampes plot below the main trend, which is mainly caused by elevated contents of carbonates and volatiles. This is the case for samples from eg. Sorgenfri Fm., Kap Dalton Fm. and Kulhøje Mb.

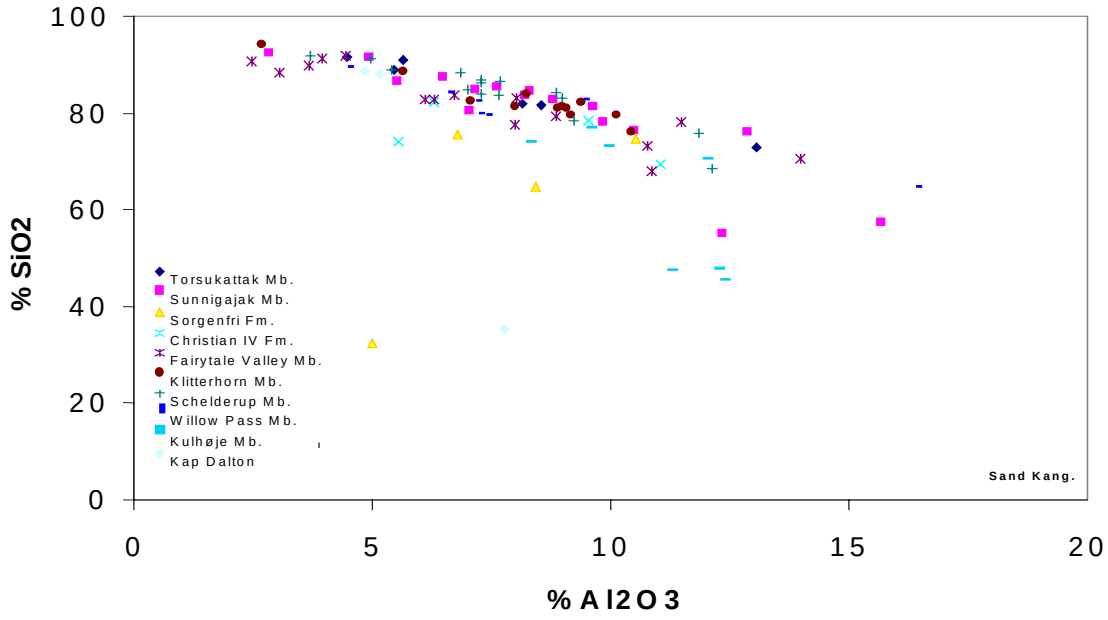

Figure 2. *SiO_2 versus Al_2O_3 in sandstones from the Kangerlussuaq area.*

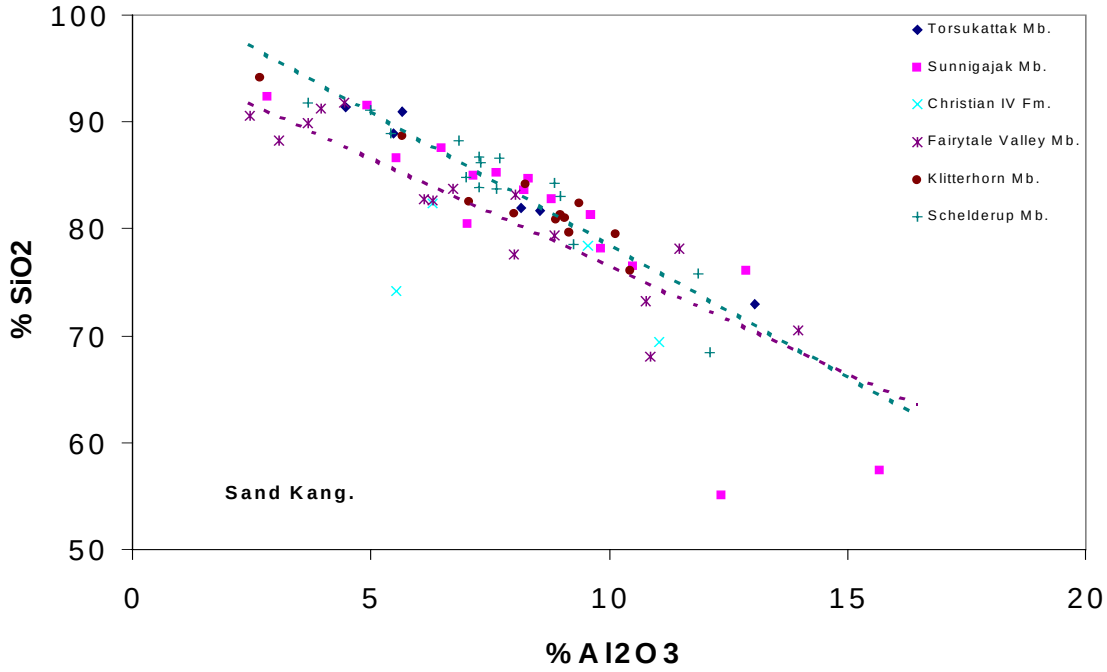

Figure 3. *SiO_2 versus Al_2O_3 in sandstones from the Kangerlussuaq area excluding Sorgenfri Fm., Kap Dalton Fm. and Kulhøje Mb.*

On Fig. 3 it can be seen that the different units roughly follow different trends where eg. samples from Schelderup Mb. define a trend pointing towards ca. 100 % SiO_2, whereas Fairy Tale Valley Mb. (FTVM) defines a trend pointing towards ca. 95 % SiO_2. This indicates that the FTVM contains a fairly high proportion of non-silicates such as iron- and titanium oxides.

As mentioned, increasing Al content in the rock indicates increasing contents of feldspars, mica or clay. A relationship between Al and a given element can be taken to indicate the rough composition of the Al-bearing minerals (mainly clay and mica) with respect to this element. Accordingly, the pattern on Fig. 4 indicates that there is a fairly low Ti content in the Al-bearing minerals in the sandstones belonging to the Torsukattak Mb., the Sunnigajak Mb. and the Schelderup Mb. relative to the other units. The syn- and post-basaltic Kulhøje Mb. and Kap Dalton Fm. on the other hand show high contents of Ti, likely to reflect a significant component of volcanic material.

The fact that eg. the samples from the Sunnigajak Mb. plot on a fairly well-defined trend indicates that the Al-bearing component of the minerals has a uniform composition. This in turn suggests that this component is derived from a specific source. It is further observed that the trend crosses the X-axis at ca. 5 % Al_2O_3 both in Fig. 4 and 5, indicating that the sandstone has a considerable content of feldspar, which is a practically Ti- and Fe-free Al-phase.

Ti in sediments is located mainly in three types of minerals: 1) clay and mica, 2) titanium minerals such as ilmenite and rutile and 3) pyroxenes and amphiboles. Further Ti can be located in rock fragments and volcaniclastics.

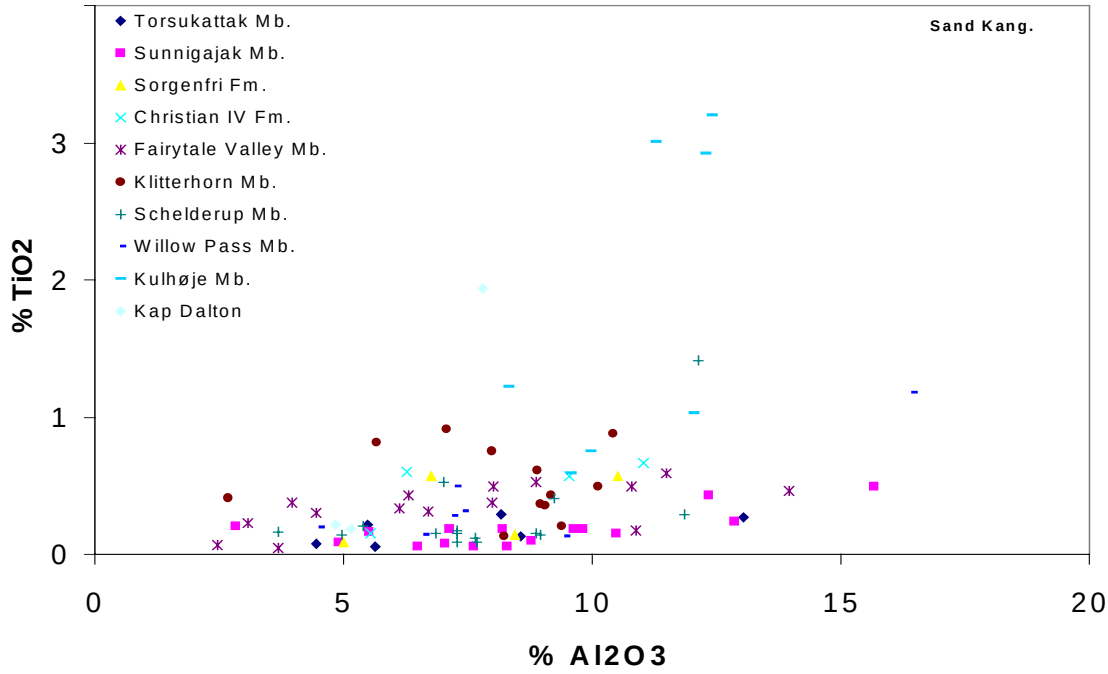

Figure 4. *TiO_2 versus Al_2O_3 in sandstones from the Kangerlussuaq area.*

The distribution of iron (Fe_2O_3) (Fig. 5) reflects a similar evolution from low contents in the Early Cretaceous sandstones, increasing in the Late Cretaceous sandstones, and highest in the Paleocene and Eocene sandstones influenced by the volcanics in the area.

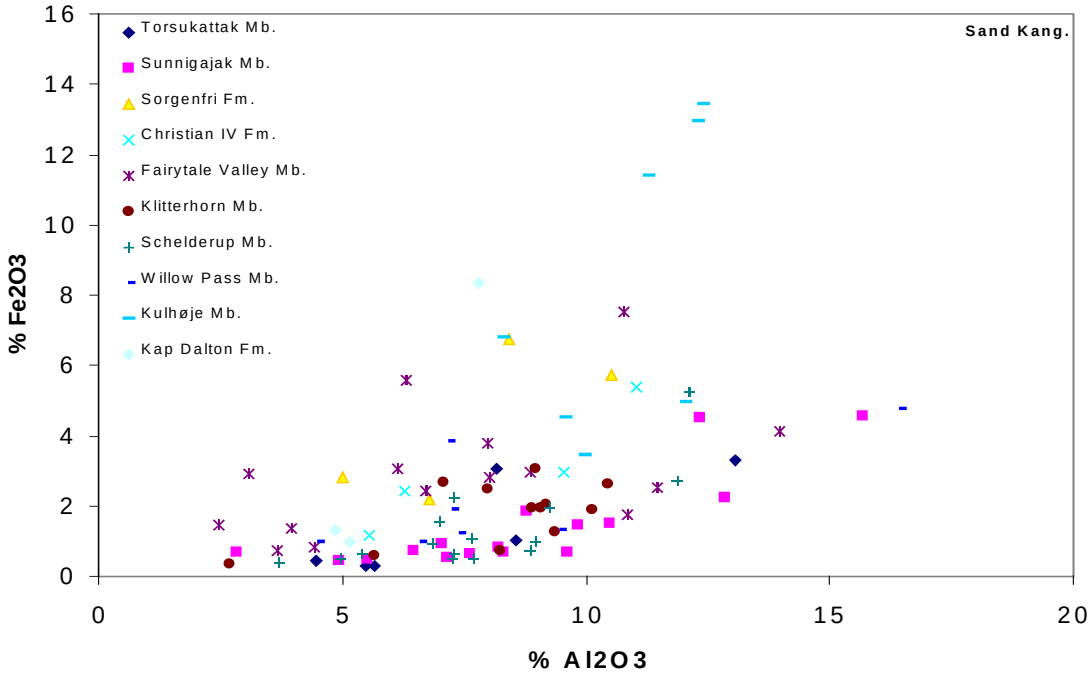

Figure 5. *Fe_2O_3 versus Al_2O_3 in sandstones from the Kangerlussuaq area.*

The Late Cretaceous Christian IV Fm. has distincly higher both Ti/Al and Fe/Al ratios compared to the underlying Early Cretaceous Torsukattaq and Sunnigajak Members, indicating different sources.

The Paleocene Fairy Tale Valley Mb. and Klitterhorn Mb. have variable Ti/Al and Fe/Al ratios, indicating a lateral change of source and sediment composition among the different parts of the unit, whereas samples from individual profiles have similar Ti/Al and Fe/Al ratios.

Zirconium in sediments resides mainly in clays and in the mineral zircon. The variation in the Zr/Al ratio among the samples on Fig. 6 is a function of variable contents of zircon in the sand. Fig. 6 shows that there are high contents of zircon in parts of the Fairy Tale Valley Mb.

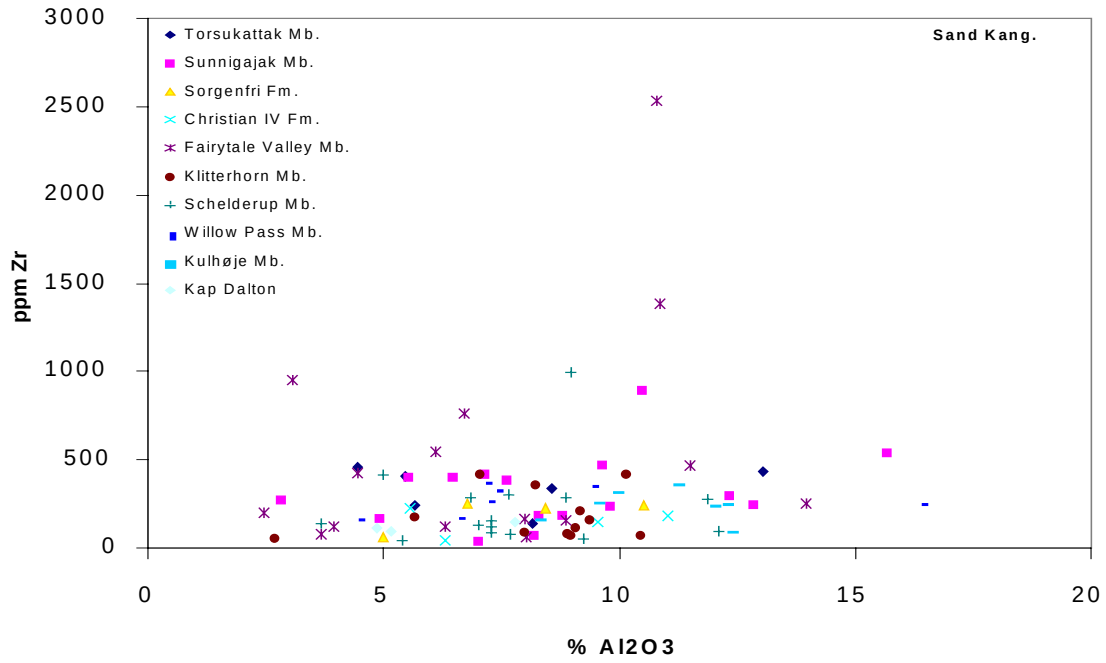

Figure 6. *ppm Zr versus Al_2O_3 in sands from Kangerlussuaq.*

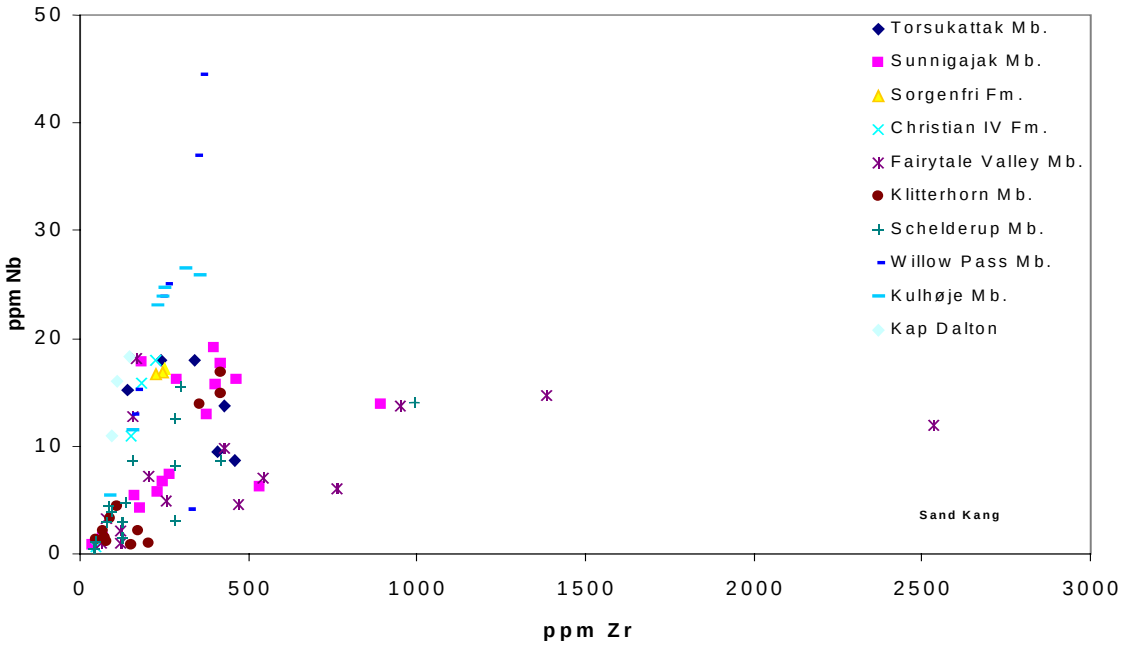

Figure 7. *ppm Nb versus ppm Zr in sands from Kangerlussuaq.*

On Fig. 7, it can be seen that there are high Nb/Zr ratios in the sedimentary units which have an input of reworked volcanic material, i.e. Willow Pass Mb., Kulhøje Mb. and Kap Dalton Fm., and the high Nb/Zr is interpreted as caused by this.

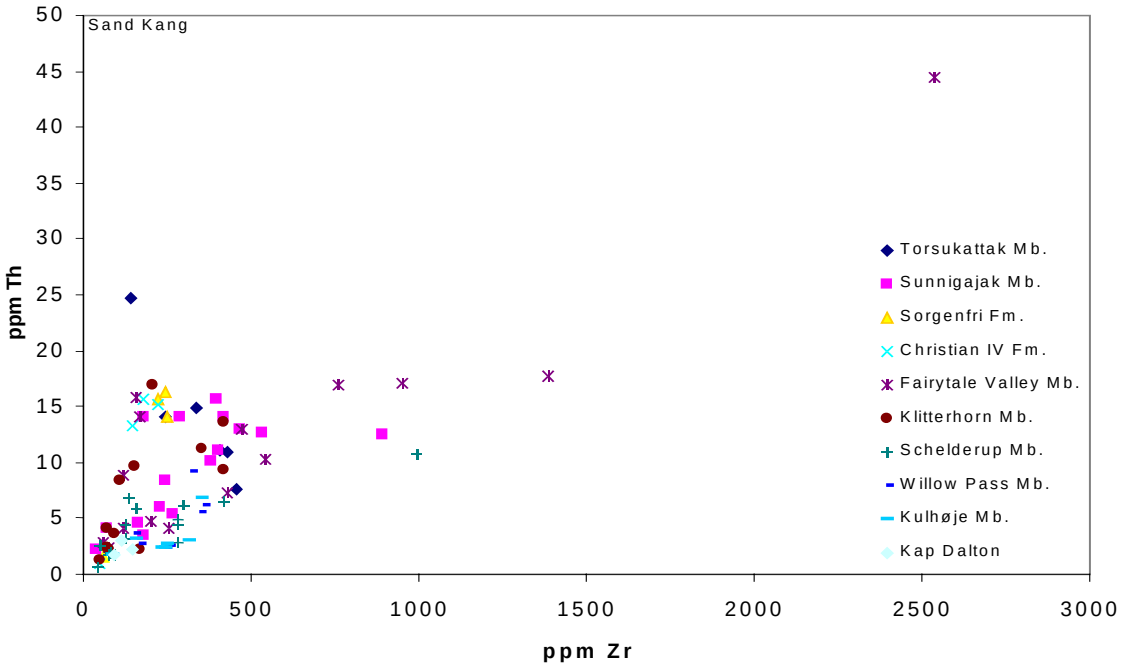

Figure 8. *ppm Th versus ppm Zr in sands from Kangerlussuaq.*

The relationship between Zr and Th in samples from eg. the Fairy Tale Valey Mb. seen on Fig. 8 and 9 confirm that the high Zr in these samples is due to high contents of the mineral zircon, which is a carrier of both Th and U. It can further be seen that the Zr, Th and U contents of units like Sorgenfri Mb. and Christian IV Fm. plot within narrow fields, suggesting high discriminative power of such a diagram. The units containing a volcanic component have relatively low Th/Zr and U/Zr

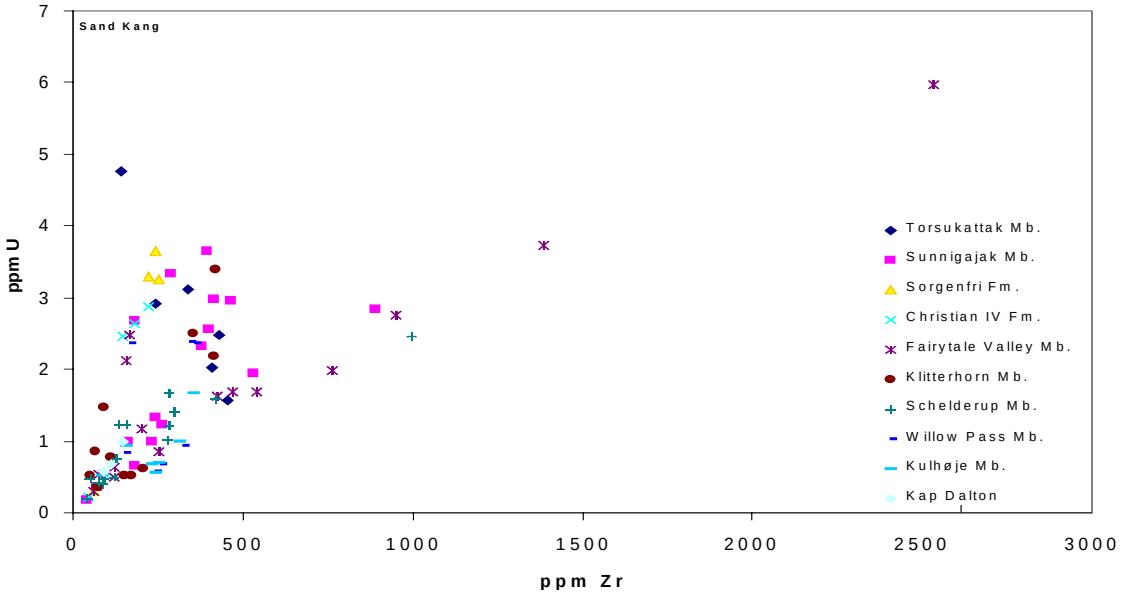

Figure 9. *ppm U versus ppm Zr in sands from Kangerlussuaq.*

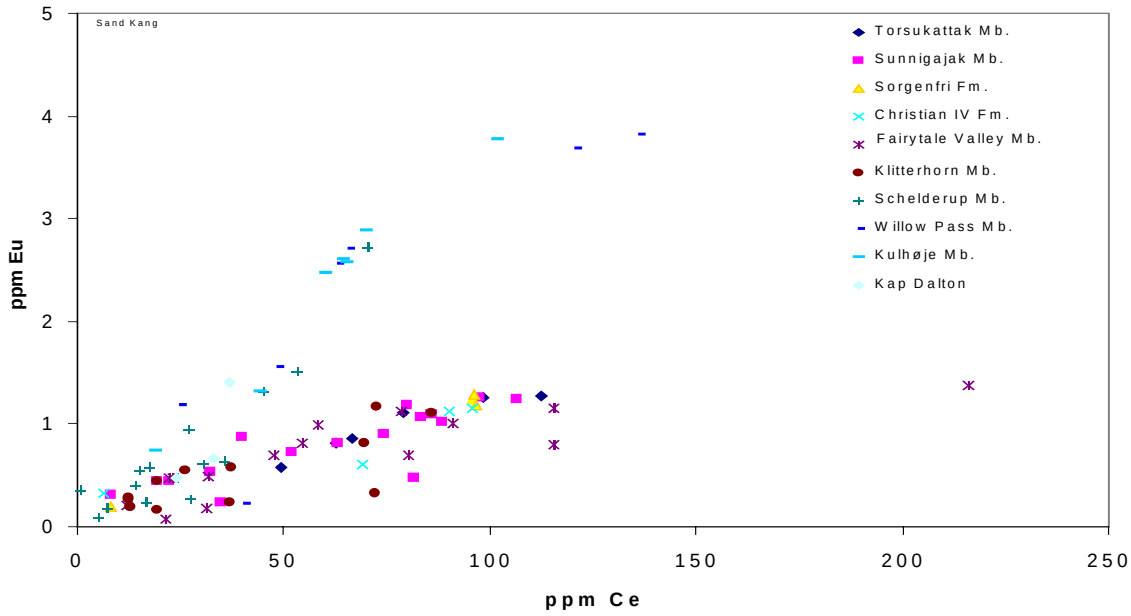

Figure 10. *ppm Eu versus ppm Ce in sands from Kangerlussuaq.*

Fig. 10 shows a clear discrimination between the different sedimentary units based on their Eu/Ce ratios. The three youngest units, which are all considered to contain reworked volcanic material, have distinctly higher Eu/Ce ratios (ca. 1:30) than the other units. In this diagram, the majority of the samples from the Schelderup Mb., the oldest syn-volcanic member, also fall in the group of sediments with a 'volcanic' signature. This was not seen on Fig. 7, which may be because Eu resides in feldspar which does not take up Nb or Zr and therefore does not have any effect on Fig. 7. If this is the case, it suggests that the volcanic imprint will be recorded earlier or farther away from the sediment source by the Eu/Ce distribution than by the Nb/Zr distribution.

The samples with the lowest Eu/Ce ratios are the same samples which above showed high contents of the mineral zircon, which is enriched in LREE. Some of the Ce may also be located in the mineral monazite.

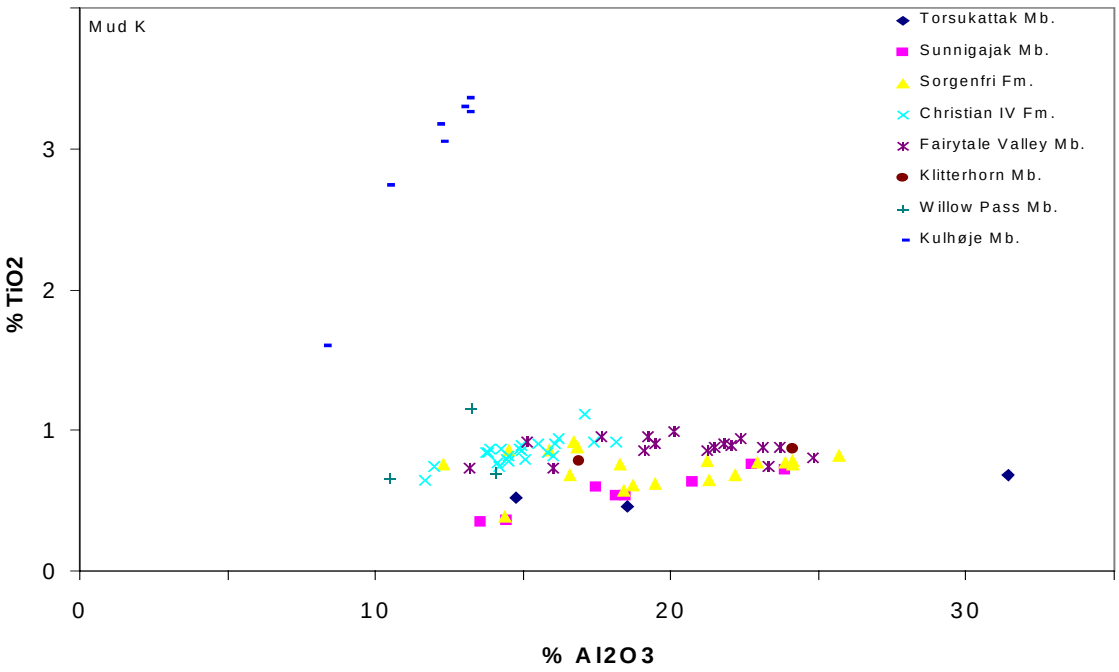

Figure 11. *% TiO_2 versus % Al_2O_3 in mudstones from Kangerlussuaq.*

The distribution of TiO_2 and Al_2O_3 in the mudstones has a strong discriminative power (Fig. 11). Kulhøje Mb. has very high Ti/Al ratios, reflecting the composition of the volcanic units. In Willow Pass Mb. the Ti/Al is elevated reflecting the same but to a minor extent.

Sunnigajak Mb. and Christian IV Fm. have well defined Ti/Al ratios indicating a uniform source, whereas Fairy Tale Valley Mb. and Sorgenfri Fm. have varying Ti/Al ratios indicating that the provenance of the mud varies internally in the units.

In the Sorgenfri Fm., the Ti/Al ratio varies vertically within the individual profiles, indicating changes in the source during deposition of the formation. This is not the case in the the Fairy Tale Valley Mb., where the individual profiles have fairly uniform Ti/Al ratios but show lateral variations in the Ti/Al among the different profiles (Fig. 12), indicating lateral variations in the souce of the mudstones.

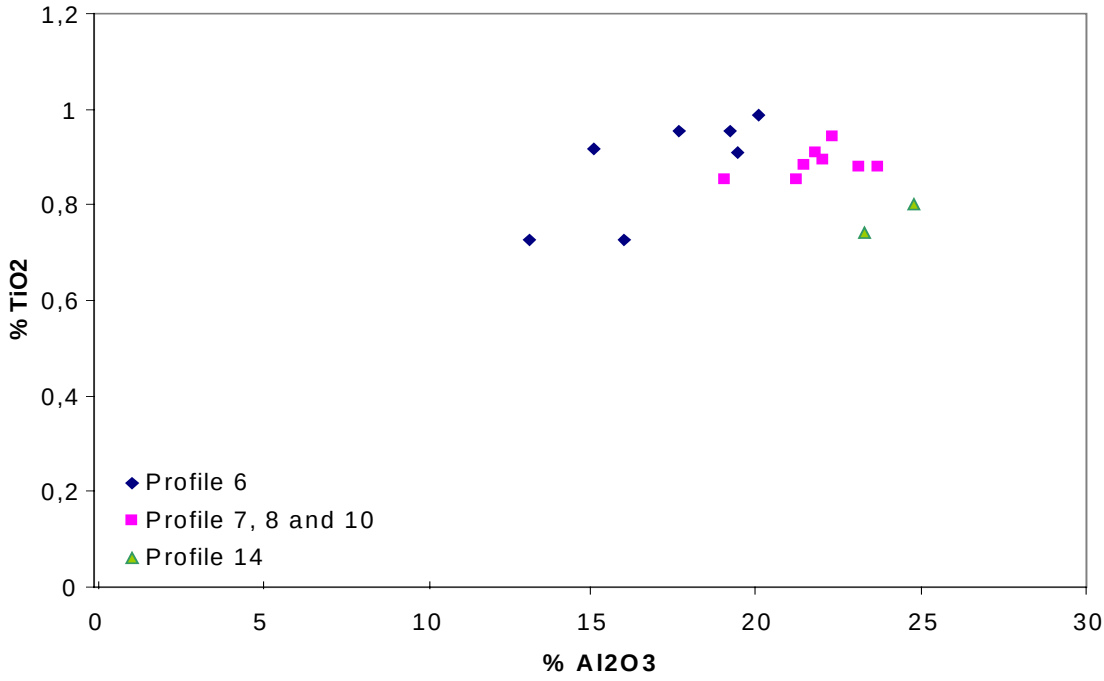

Figure 12. *% TiO_2 versus % Al_2O_3 in mudstones from different profiles in the Fairy Tale Valley Mb., Kangerlussuaq.*

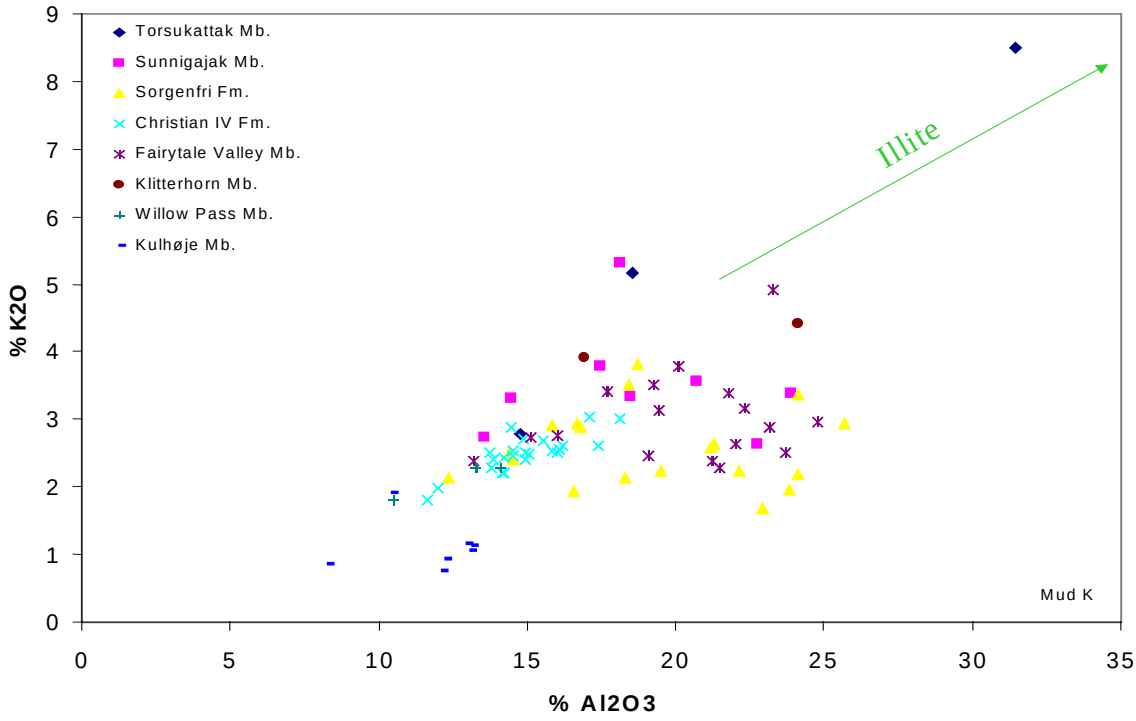

Figure 13. *% K_2O versus % Al_2O_3 in mudstones from Kangerlussuaq.*

The uniform source of the Christian IV Fm. seen on Fig. 11 can also be recognised on Fig. 13, where the K/Al ratio is determined by the mineralogy of the clay mineral fraction. High K/Al ratios are interpreted as high contents of illite, whereas low K/Al ratios indicate eg. high contents of smectite in the Kulhøje Mb. which contains decomposed volcanics.

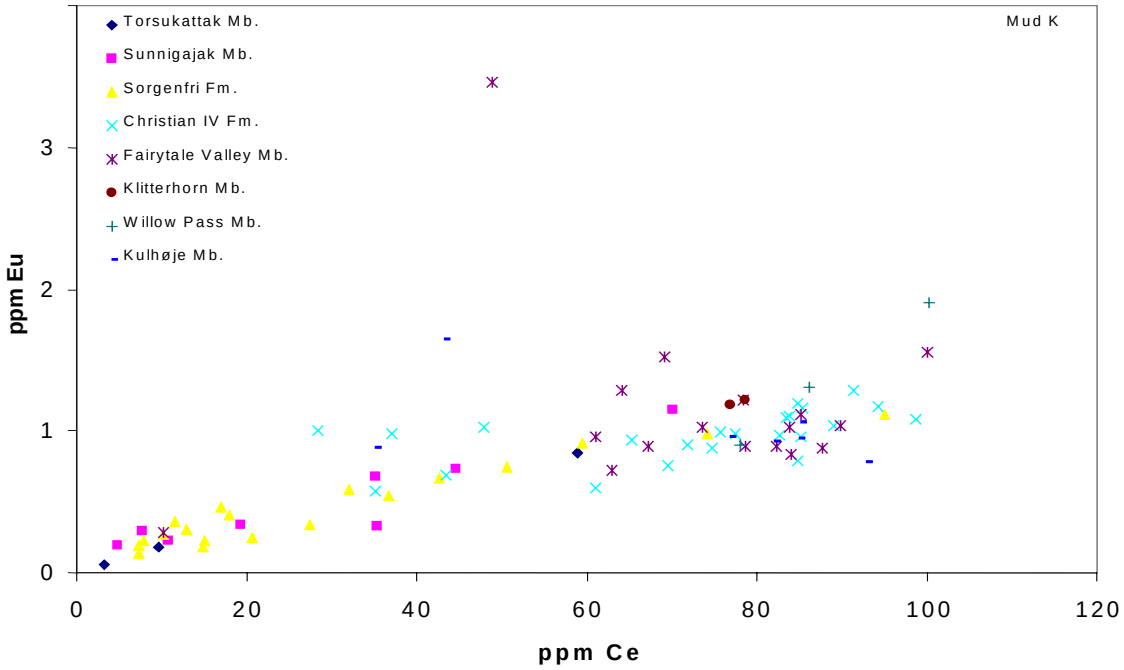

Figure 14. *ppm Eu versus ppm Ce in mudstones from Kangerlussuaq.*

The relationship between Eu and Ce observed among the sandstones in the area (Fig. 14), with high Eu/Ce ratios in the units containing a volcanic component, cannot be identified in the mudstones. This is interpreted as indicating that the Eu signature is carried by the coarser fractions (feldspar), and is not a result of the redox environment, which could be a consideration because Eu is sensitive to changes in oxygen fugacity during deposition.

Geochemical characteristics of the units

Torsukattak Mb., Watkins Fjord Fm., is classified as a fluvial sandstone (Fig. 1). It is characterised by low Ti and Fe in the mud component of the sandstone (Fig. 4 and 5). The mudstones are characterised by low Ti/Al ratios (Fig. 11) and high K/Al ratios (Fig. 13), the latter likely to reflect a high content of illite.

Sunnigajak Mb., Watkins Fjord Fm., is classified as a marine sandstone (Fig. 1). The sandstones in this unit are characterised by a higher Zr/Al ratio (Fig. 6) relative to eg. Torsukattak Mb., compatible with deposition in a marine environment with upgrading of heavy minerals in beach placers in the coastal zone. The mudstones are characterised by low and uniform Ti/Al ratio (Fig. 11), suggesting a source with no volcanic signature. The K/Al ratio (Fig. 13) varies, indicating variable illite content.

Sorgenfri Fm. is classified as dominated by marine shales (Fig. 1). The low Si + Al content in most sandstones from this unit (Fig. 2) indicate carbonate cementation.The low Zr/Al ratio in the sandstones (Fig. 6) indicate low total content of heavy minerals. Further the high Th/Zr and U/Th (Figs 8 and 9 respectively) are not caused by heavy minerals such as zircon, but likely to be tied to organic material. The varying Ti/Al ratios (Fig. 11) indicate that the source of the mud component changed over time – in contrast to eg. the Sunnigajak Mb. High Ti/Al ratios are characteristic for mafic volcanics, and this change may reflect a distal volcanic activity. There is also a large variation in the K/Al ratios (Fig. 13), indicating variations in the illite content in the source of the mud component (matrix).

Christian IV Fm. is also classified as a unit dominated by marine shale (Fig. 1). The sandstones in this unit share many features with the Sorgenfri Fm., eg. low Zr/Al (Fig. 6) and high Th/Zr and U/Th (Figs 8 and 9), probably caused by the high organic content in the unit. The Ti/Al is slightly higher in the sandstone (Fig. 4) as well as in the mudstone (Fig. 11). The Ti/Al and K/Al ratios (Figs 11 and 13) in the mudstone are more uniform than in the Sorgenfri Fm., indicating a more simple source.

Fairy Tale Valley Mb., Sediment Bjerge Fm., is characterised as submarine channel turbidites (Fig. 1). There is a large range in SiO_2 and Al_2O_3 contents indicating a range from fairly pure sandstones to mudstones. The low SiO_2 + Al_2O_3 (Fig. 3) indicate an elevated content of other minerals than silicates. The high Ti/Al and Fe/Al in the relatively pure (low Al, Figs 4 and 5) sandstones suggest that this can be Ti and Fe oxides.The high Zr/Al ratio (Fig. 6) in many samples from this unit indicate the presence of zircon, a suggestion which is supported by the relationship between U and Zr on Fig. 9. This characteristically high content of heavy minerals may stem from enrichment in a beach placer prior to deposition as turbidite. The source of the mudstone is complex (Figs 11 and 13) and changes laterally (Fig. 12).

Klitterhorn Mb., Sediment Bjerge Fm., is classified as a marine sandstone (Larsen et al. 2004). Some of the samples have very high Ti/Al ratios (Fig. 4) suggesting high contents of rutile. Zr contents are low, and it is not likely that this unit was deposited in a beach (placer) environment.

Schelderup Mb., Vandfaldsdalen Fm., is classified as a fluvial sandstone (Larsen et al. 2004). SiO_2 + Al_2O_3 is generally high (Fig. 3), indicating low contents of non-silicates and heavy minerals in most sandstones. This is supported by eg. low Zr/Al ratios indicating low zircon contents in most samples. However, a few samples have high Zr/Al ratios (Fig. 6) indicating elevated contents of zircon. High Eu/Ce ratios (Fig. 10) are interpreted as caused by high influx of feldspar. This feature makes the unit distinct from the underlying units.

Willow Pass Mb., Vandfaldsdalen Fm., is also classified as a fluvial sandstone (Larsen et al. 2004). This unit has a clear volcanic signature seen eg. on the high Nb/Al ratio (Fig. 7). High Eu/Ce ratios (Fig. 10) are interpreted as caused by feldspar in reworked volcanics.

Wells from the Faroe – Shetland area

The samples have been grouped according to the lithostratigraphy of the area West of Shetland (Whitham & Larsen, 2005). Samples from the Paleocene Sullom, Vaila and Lamba Formations and the Eocene Flett and Balder Formations have beed analysed. The Sullom Fm. is subdivided into S1 and S2, but as the main differences are seen between wells the Sullom Fm. is treated as one unit. The Vaila Fm. has been subdivided into V1, V2, V3 and V4. The Lamba Fm. is subdivided into L1, L2 and L3. The Flett Fm. is treated as one unit.

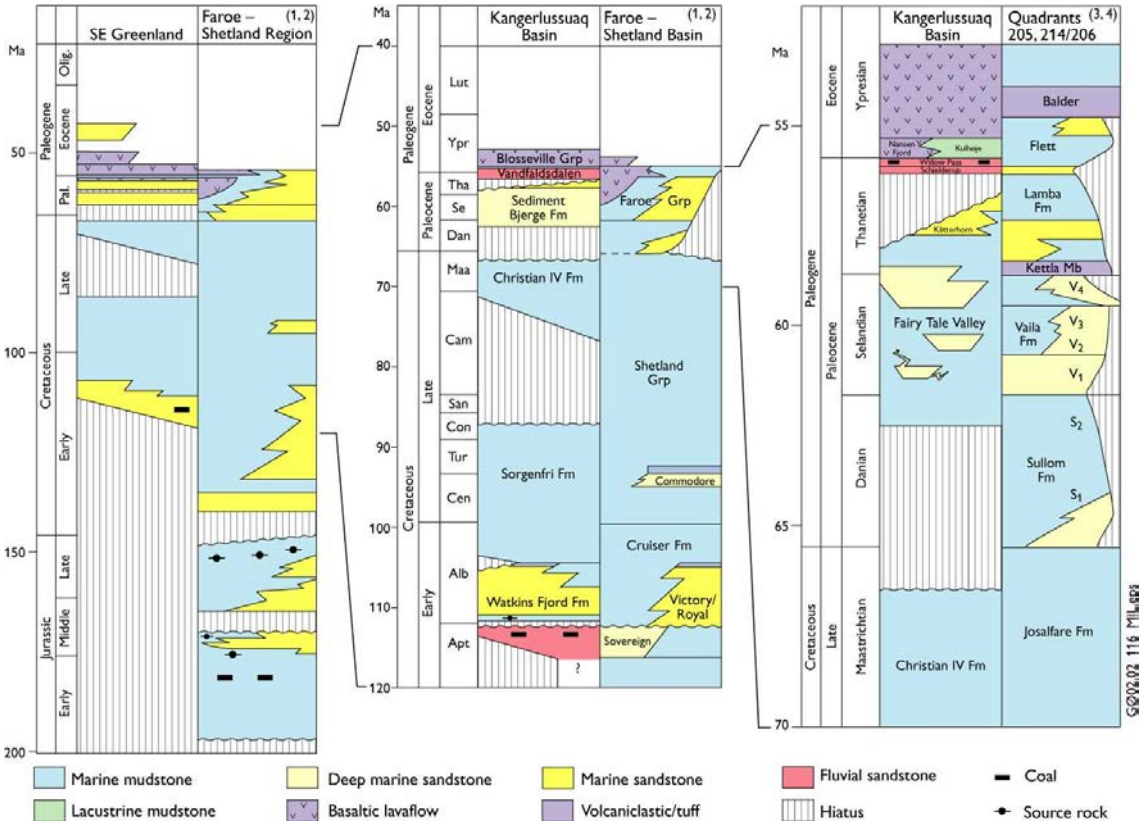

Figure 15. *Sketch of the stratigraphy in the Kangerlussuaq area and the Faroe–Shetland area. From Whitham and Larsen (2004).*

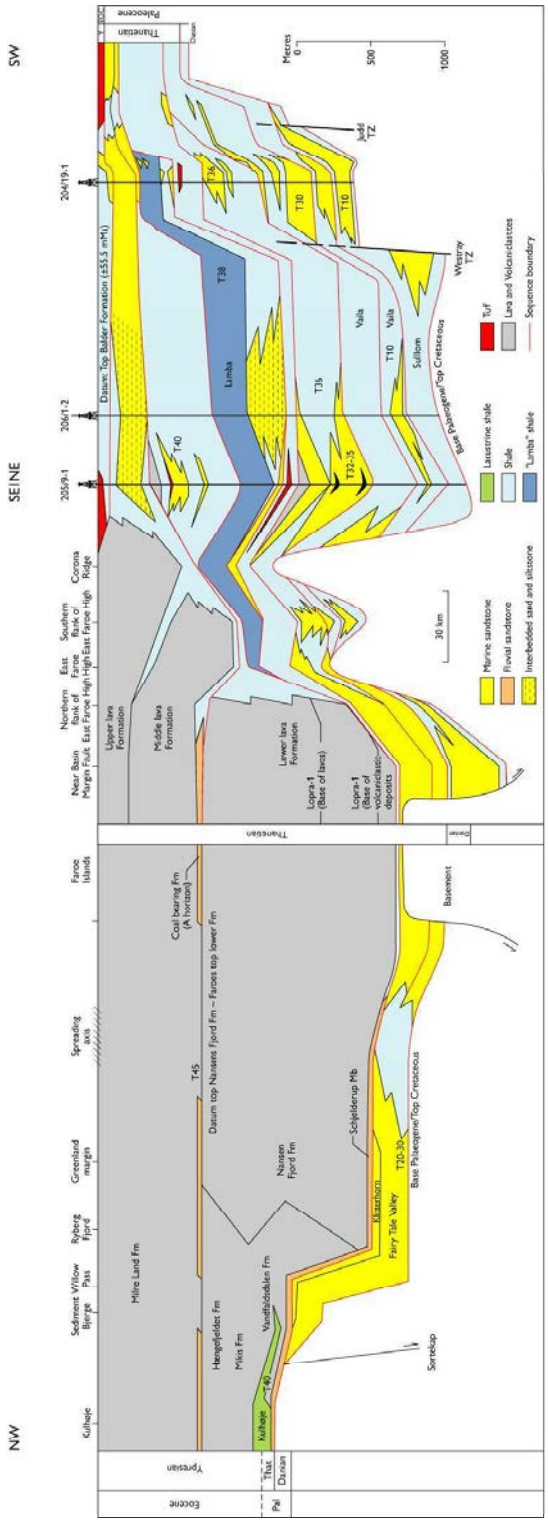

Figure 16. *Sketch section of the Kangerlussuaq and Faroe–Shetland areas, with location of some of the sampled wells. From Whitham and Larsen (2004).*

The samples analysed from the wells consist of washed and dried cuttings, and it has not been possible to differentiate sandstones and mudstones on other basis than the chemical analyses. As the geochemical signatures of the sandstones and mudstones/shales have to be investigated separately, an arbitrary distinction has been chosen. In the following description samples with more than 70% SiO_2 are classified as sandstone and samples with less than 60% SiO_2 are classified as mudstones. Because the samples are cuttings which represent an average composition of rock over an interval, and hence are mixtures, the relatively few samples with a composition between 60% and 70% SiO_2 have been omitted in the plots as they are likely to represent mixtures of sandstone and mudstone, and accordingly would make interpretation of the data difficult.

When analysing cuttings, possible contamination induced during the drilling process has to be considered. The cuttings are washed, but baryte and metal fragments from the tools may remain.

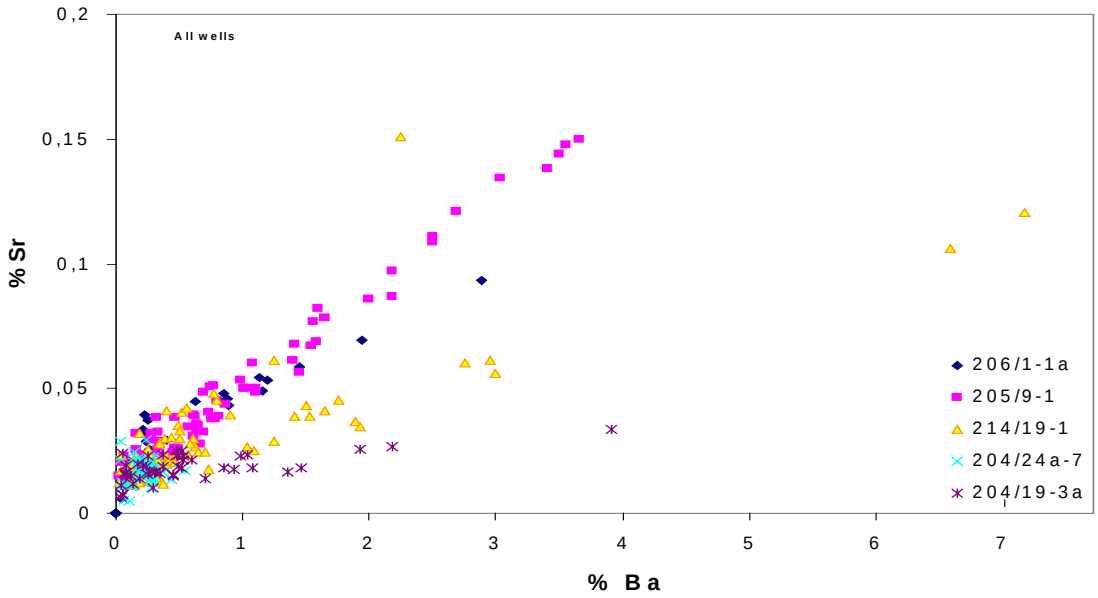

Figure 17. *% Sr versus % Ba in samples from the Faroe–Shetland Basin.*

To investigate the extent of contamination from the drillmud, a plot of Sr versus Ba was generated (Fig. 17). It can be seen that there are considerable amounts of baryte remaining in the cuttings after the washing. The slope of the relationship between these two elements varies among the different wells. This is interpreted as being caused by the use of baryte from different sources (drillmud provenance). It can be observed that only one type of baryte was used in 205/9-1, whereas 214/19-1 was drilled using two types of baryte with different Sr/Ba ratios. In 204/19-3a and 206/1-1a other types of baryte was used, and in 204/24a-7 there is no sign of baryte contamination.

Plots of the varous elements used in the investigation of the sediment geochemistry against Ba indicated no other types of contamination due to the drilling process.

Sandstone geochemistry

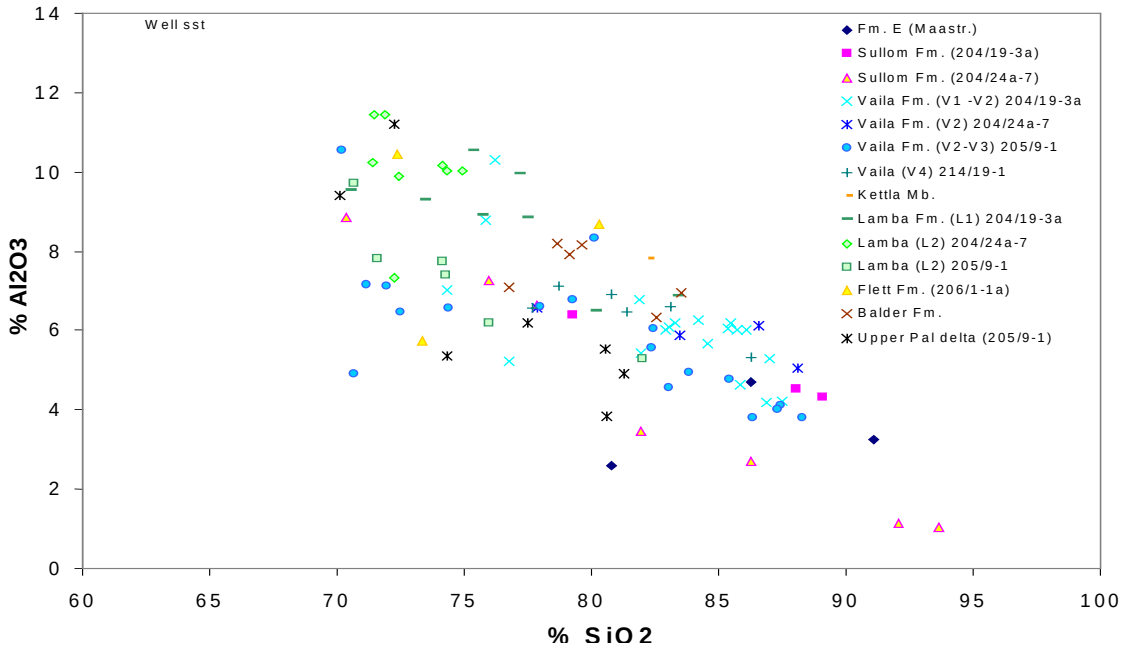

Figure 18. *% Al_2O_3 versus % SiO_2 in sandstone samples from the Faroe–Shetland Basin. Sullom in well 204/19-3a belong to unit S1 whereas 204/24a-7 belongs to unit S2.*

A plot of the main components in the sandstone (Figs 18 and 19) show some main features in the sedimentary units and also variation within the units from well to well. Samples with low Si and low Al (closer to the origo of the diagram Fig. 18) have high contents of other components such as volatiles (carbonate, water in clay and organics), Ca, Mg, Fe and alkalis.

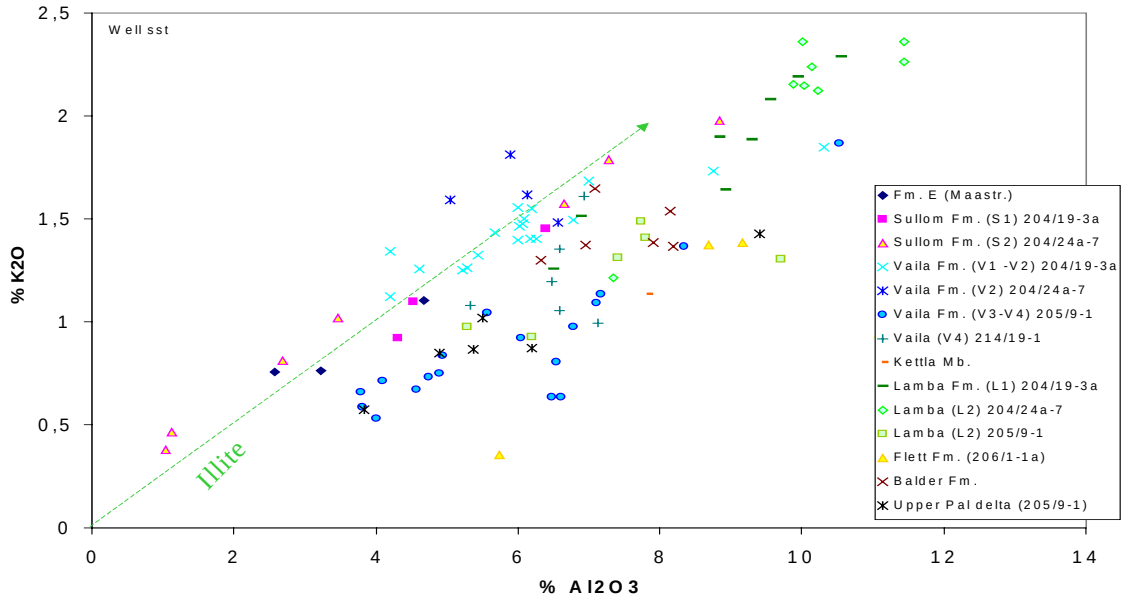

Figure 19. *% K_2O versus % Al_2O_3 in sandstone samples from the Faroe–Shetland Basin.*

The K/Al ratio is fairly high and uniform in the Sullom Fm., indicating a fairly uniform source. The high K may reflect that K-feldspar dominates over plagiclase or, more likely, that illite is the dominating clay mineral in the matrix (Fig. 19).

The Vaila Fm. shows different K/Al ratios among the wells, indicating differences in the sources of the different wells. However, the stratigraphic intervals are also different among the wells according to the description available. In the V1-V2 interval of well 204/19-3a, K dominates over Na (Fig. 20), whereas the opposite is the case in the V-3 - V4 interval in well 205/9-1 (Fig. 20). The high Na content here may be due to the presence of Na-rich feldspar, see also Fig. 27.

The Flett Fm. shows a similar Na -dominated alkali pattern.

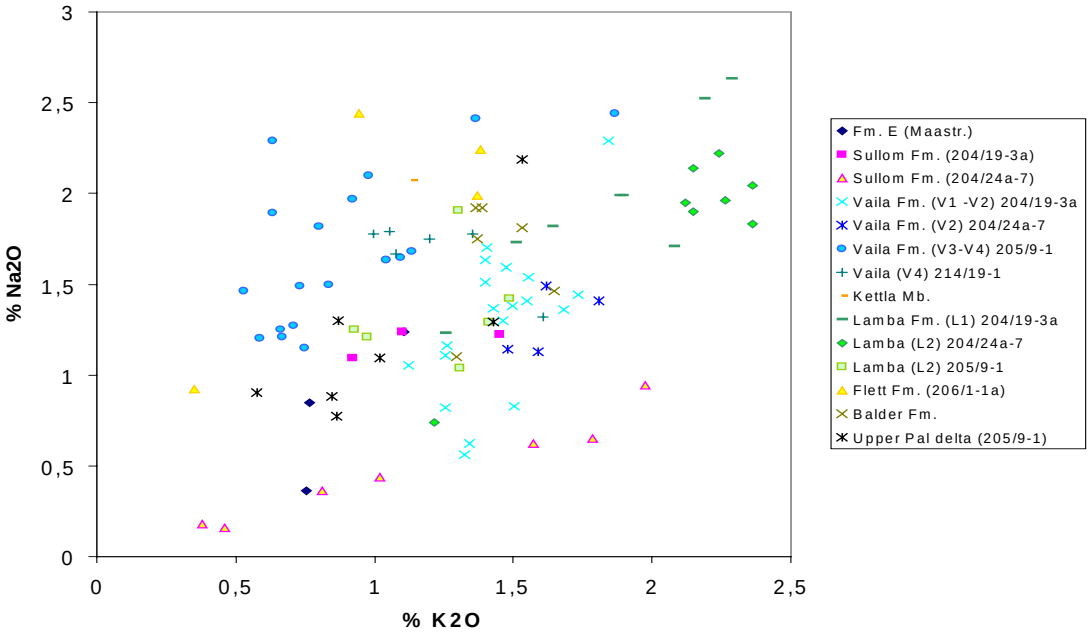

Figure 20. *% Na_2O versus % K_2O in sandstone samples from the Faroe–Shetland Basin.*

The Sullom Fm. (S2) in well 204/24a-7 has low total alkalies, which may indicate that illite is the dominating alkali carrier, ie. a low proportion of feldspar relative to the other units.

In the Lamba Fm. the main differences are based on the total amounts of Al- and alkali-bearing minerals, with relatively low contents of Na in 205/9-1 as compared to 204/24a-7 (Fig. 20). This is likely to reflect the grain-size in the sediments, those in 204/24a-7 being the more fine-grained.

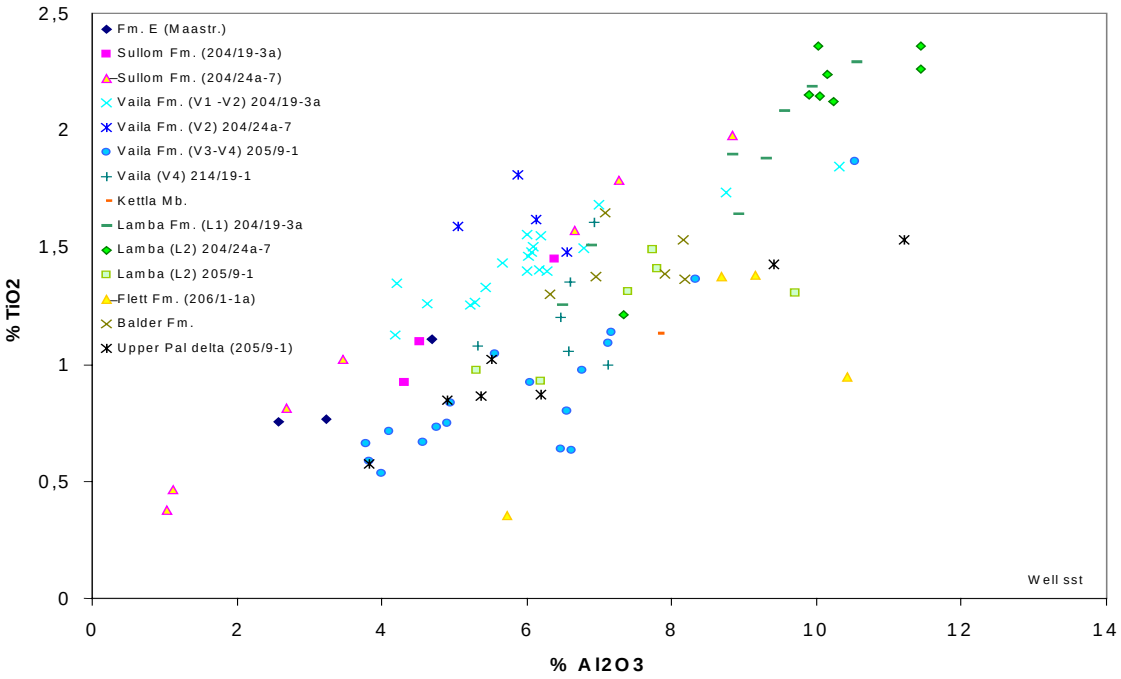

Figure 21. *% TiO_2 versus % Al_2O_3 in sandstone samples from the Faroe–Shetland Basin.*

There is in general a fair relationship between Ti and Al within the individual units (Fig. 21), which suggests that Ti is mainly contained in Al-bearing minerals such as mica and clay in the matrix. The differences in Ti/Al ratios indicate differences in source eg. among Vaila Fm. in V1 and V2 of 204/19-3a and V2 of 204/24a-7.

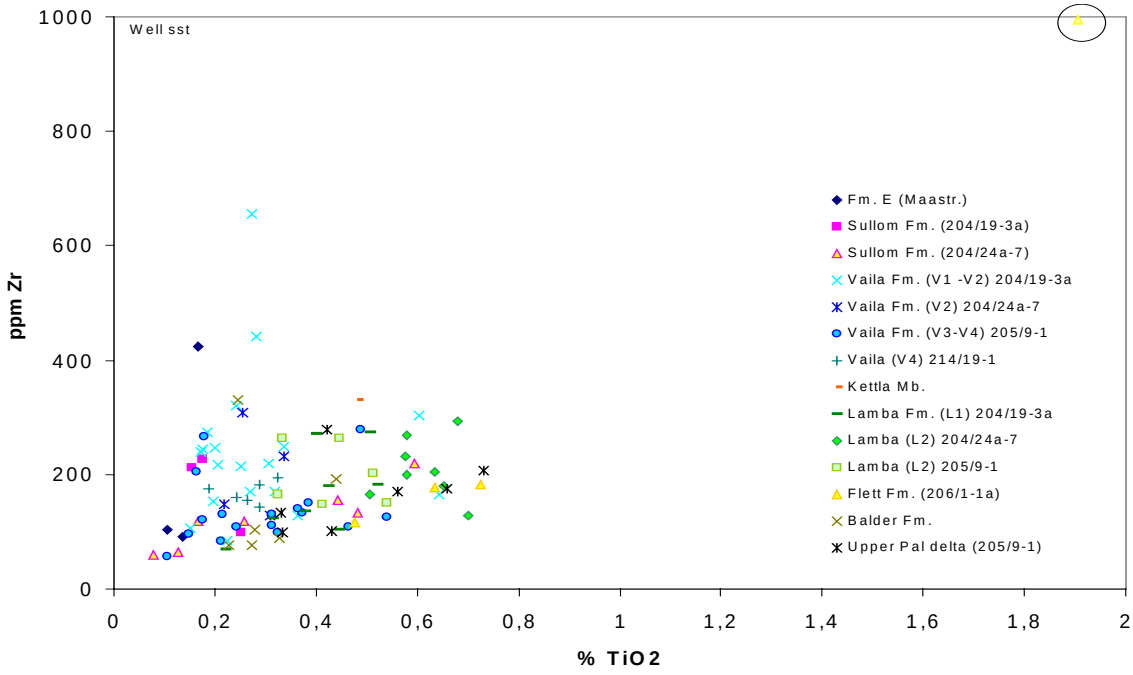

Figure 22. *ppm Zr versus % TiO_2 in sandstone samples from the Faroe–Shetland Basin.*

Zr and Ti both reside in clays as well as in heavy minerals. As can be seen on Fig. 22, a number of samples from the Vaila Fm. in well 204/19-3a have high Zr combined with high Zr/Ti ratio. This is interpreted as due to relatively high contents of zircon as compared to the other samples from the Vaila Fm.

One sample from the Flett Fm. is very high in both Zr and Ti, which is interpreted as high contents of heavy minerals such as zircon and ilmenite-rutile. The Zr/Ti ratio in this sample is distinctly different from that of the Vaila Fm. in well 204/19-3a, indicating differences in the heavy mineral parageneses.

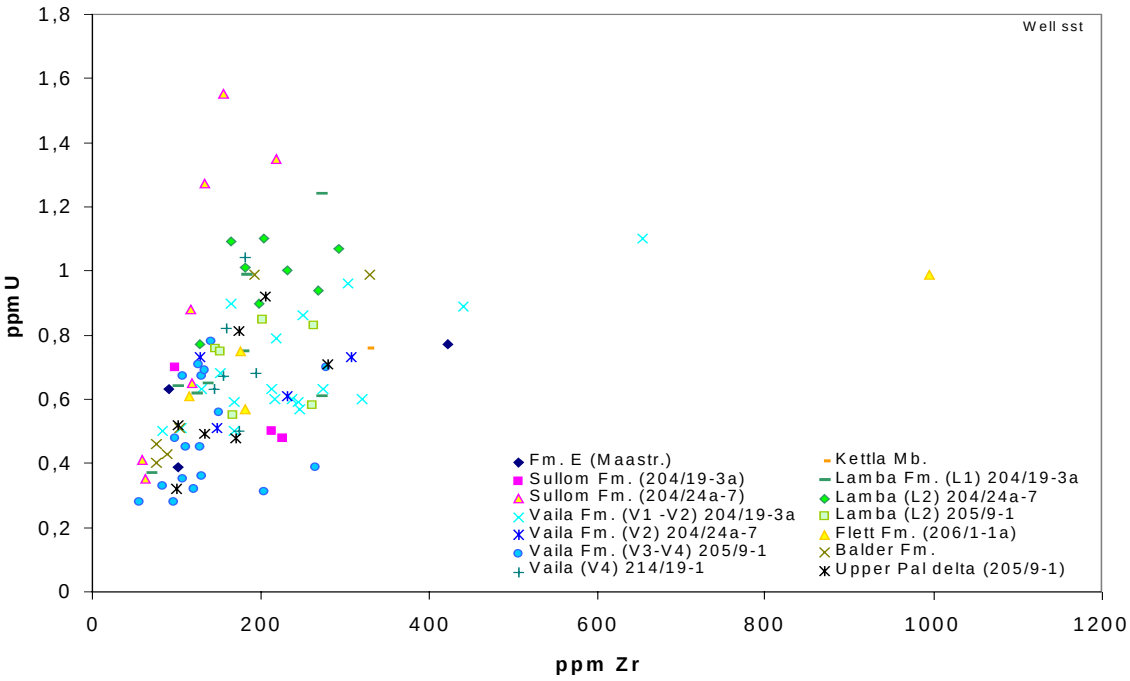

Figure 23. *ppm U versus % ppm Zr in sandstone samples from the Faroe–Shetland Basin.*

The suggestion that the elevated Zr in samples from the Vaila Fm. and the one sample from the Flett Fm. is due to elevated contents of zircon is supported by the information displayed on Fig. 23, where different relationships between U and Zr can be observed. The differences in U/Zr ratio between the Zr-enriched samples from the Vaila and Flett Fms are likely to be caused by differences in the provenance of the zircons.

The high U/Zr ratio in the Sullom Fm. in well 204/24a-7 may indicate a high content of organic material, which is compatible with the fact that these samples plot close to the origo on Fig. 18. In at least three of the samples this is confirmed by the high content of volatiles (Fig. 24).

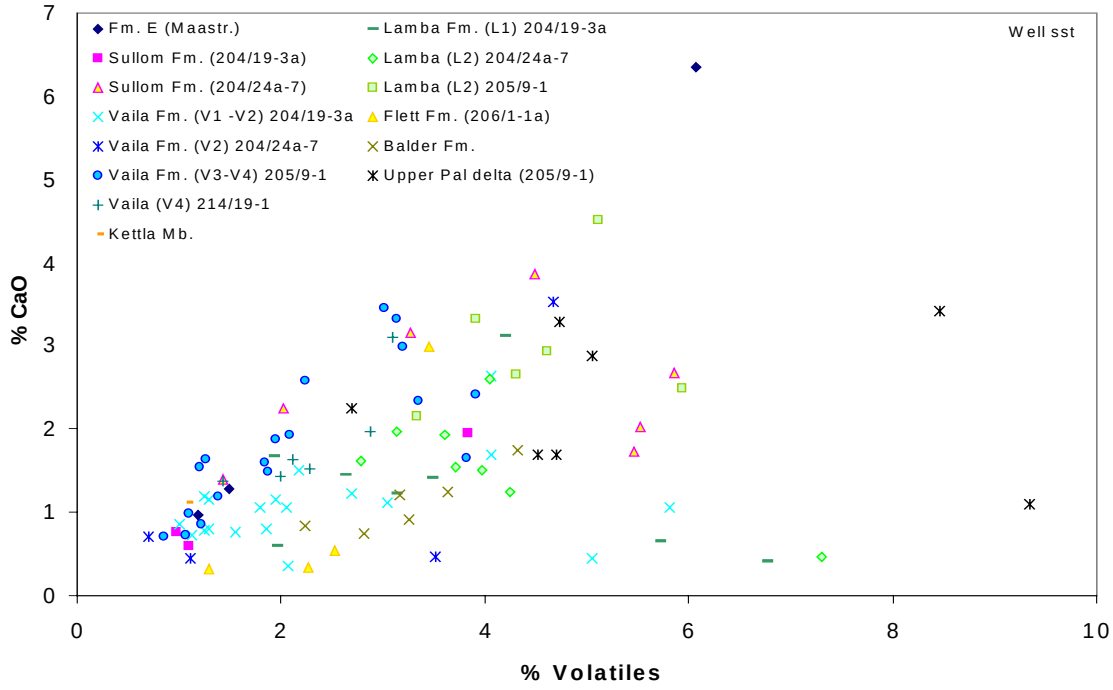

Figure 24. *% CaO versus % volatiles in sandstone samples from the Faroe–Shetland Basin.*

The volatiles are mainly tied to clay minerals and carbonate in the sandstones. In Fig. 24, it can be seen that there is a correlation between CaO and volatiles in samples from the Vaila Fm. (V3-V4), indicating that the sandstones are partly carbonate cemented.

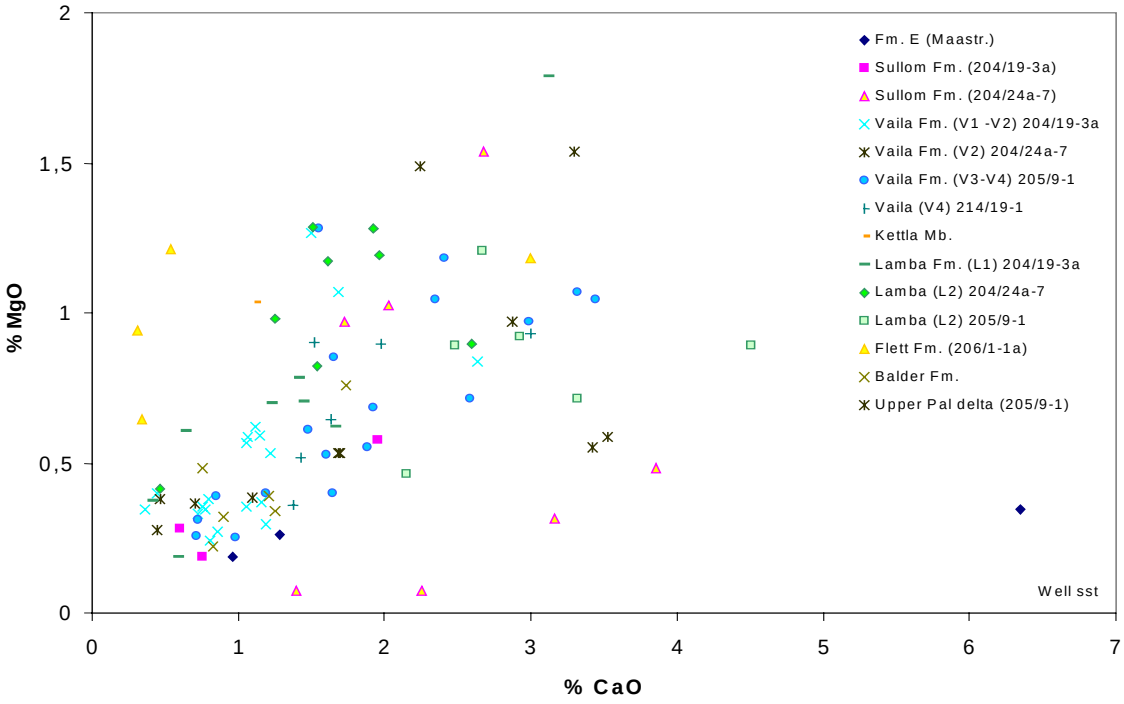

Figure 25. *% MgO versus % CaO in sandstone samples from the Faroe–Shetland Basin.*

The carbonate cement in the above mentioned sands (Vaila Fm. V3-V4) is likely to be dominated by dolomite, judged from the Mg/Ca ratios in Fig. 25.

In the Sullom Fm. (204/24-7a) there are two groups of samples, one with fairly high Mg/Ca ratios (Fig. 25) and high Al (Fig. 26), and one with low Mg/Ca ratio and low Al. The first group also has high Ca/volatile ratios, suggesting that these samples are calcite cemented (ca. 3 to 8 wt % calcite). The Mg and Ca in the second group is likely to be located in clay minerals because these saples have higher Al contents (Fig. 26).

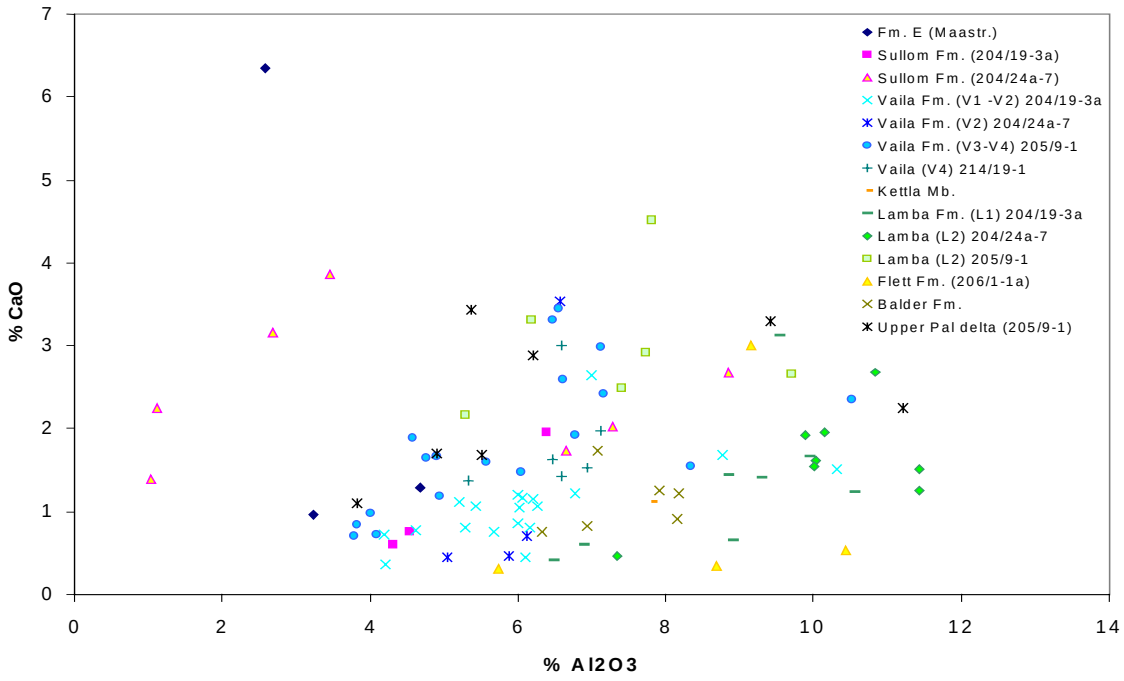

Figure 26. *% CaO versus % Al_2O_3 in sandstone samples from the Faroe–Shetland Basin.*

The sample from the Maastrictian Formation E is also calcite cemented, and to a higher degree than the above mentioned samples from the Sullom Fm.

Most of the samples from the Flett Fm. have very low and distinctive CaO contents coupled with high Mg/Ca ratios (Fig. 25). This together with the observation that they have high Na/K ratios (Na-smectite) may indicate influx of decomposed volcanic material.

On Fig. 27 it can be seen that the Vaila Fm. V3 - V4 interval in well 205/9-1 is characterised by high Eu/Ce ratios relative to all the other samples. The best explanation is that it contains a high proportion of alkali feldspar (Na-rich, Fig. 20) which has a very high Eu/Ce ratio (Larsen 1979).

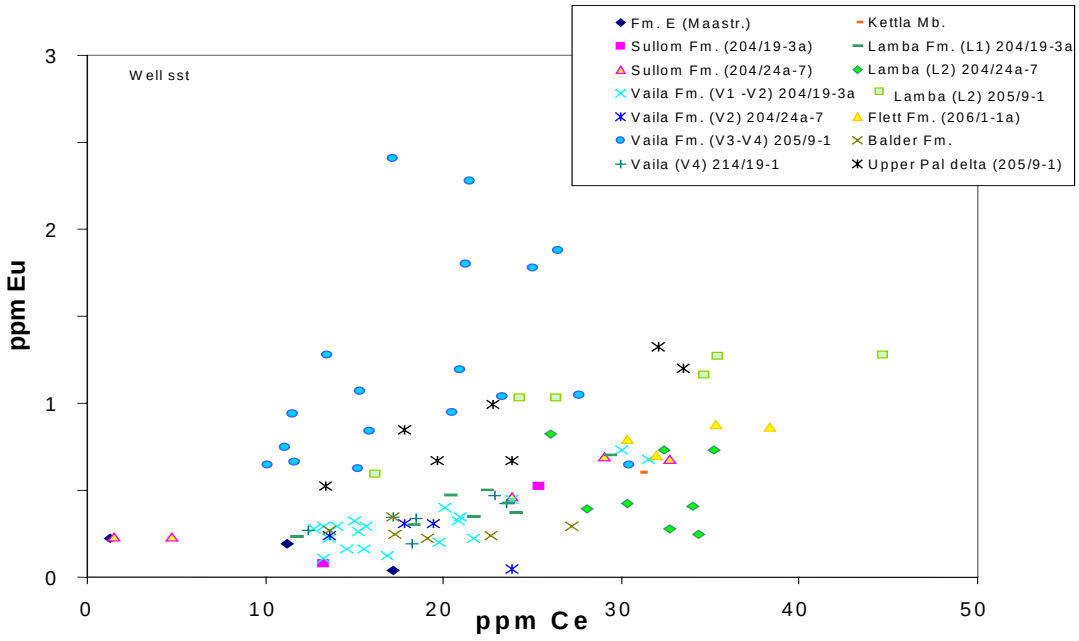

Figure 27. *ppm Eu versus ppm Ce in sandstone samples from the Faroe–Shetland Basin.*

Mudstone/shale geochemistry

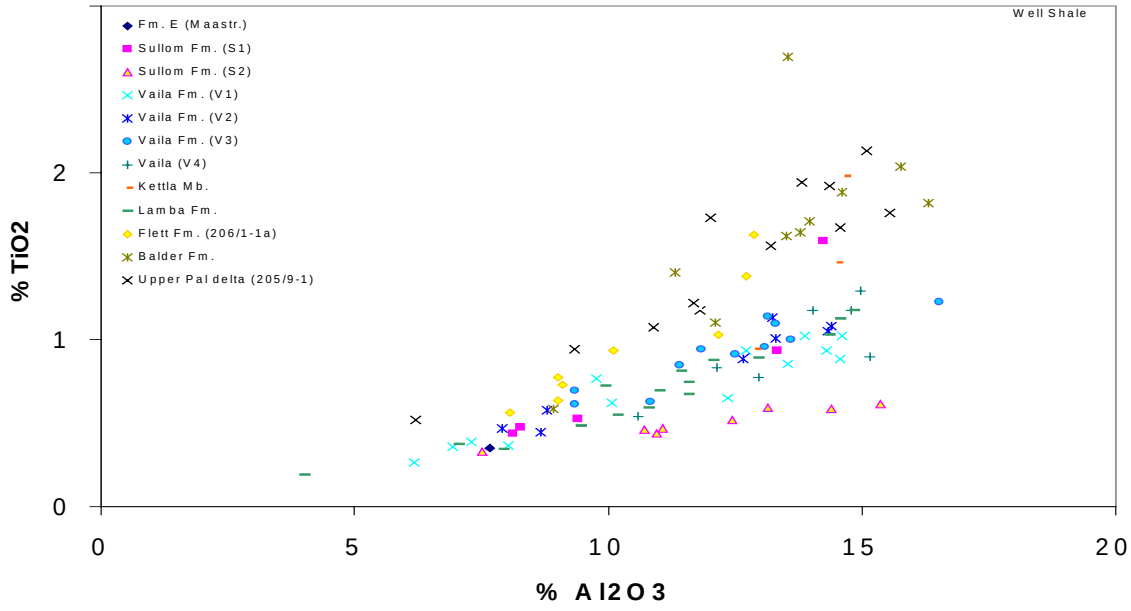

Figure 28. *% TiO_2 versus Al_2O_3 in mudstone samples from the Faroe–Shetland Basin. Note that the units used here as well as the symbols are slightly different from the usage in the previous section.*

On Fig. 28 it is seen that the Ti/Al ratio has strong discriminating power among the different units in the area, indicating that the mudstones of the different units are derived from

grossly different sources. Further, it should be noted that there is a general increase in the Ti/Al ratio with time. This may be caused by a gradual increase of input of material derived from volcanic rocks, which have higher Ti/Al ratios as noted for the Kulhøje Mb. in the Kangerlussuaq area (Fig. 11).

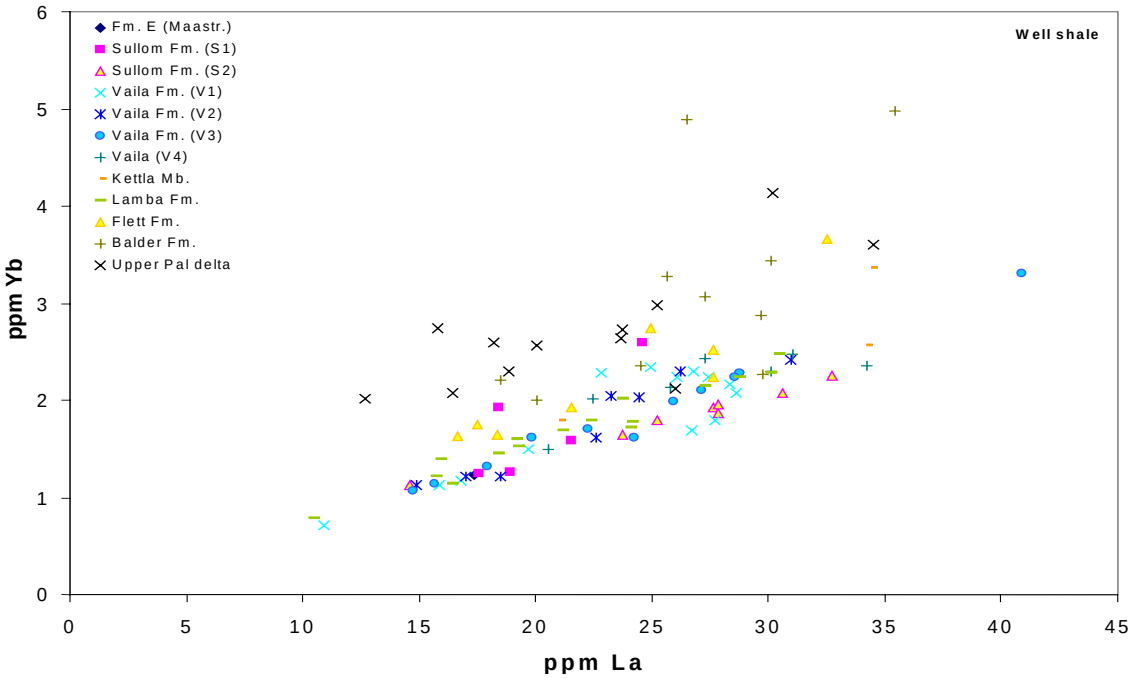

Figure 28. *ppm Yb versus ppm La in mudstone samples from the Faroe–Shetland Basin.*

La and Yb are rare earth elements (REE), and La is light whereas Yb is heavy. Acordingly, the Yb/La ratio is indicative of the slope of the REE spectrum.

On Fig. 28 it can be seen that there is a significant development in the Yb/La ratio from the older to the younger sediments - from low to higher Yb/La ratios. Low ratios indicate a steep REE pattern which is typical for most rocks of the continental crust, whereas high ratios and relatively flat REE patterns are typical for tholeiitic basaltic rocks such as those of the oceanic crust and in the North Atlantic volcanic province. Accordingly, the development from low towards higher Yb/La ratios indicates an increasing “volcanic” character of the mudstones, interpreted as caused by increasing input from basaltic volcanic rocks. The systematic development is less clear than in Fig. 27 but is interpreted as being caused by the same process.

U and Th are sensitive to the redox environment during deposition of the sediment, and Th is the most sesitive, being preferentially deposited in euxinic conditions. The fact that the mudstones belonging to unit S2 of the Sullom Fm. have the highest Th/U ratio is in accordance with the observation that this unit has high contents of organic material as mentioned above.

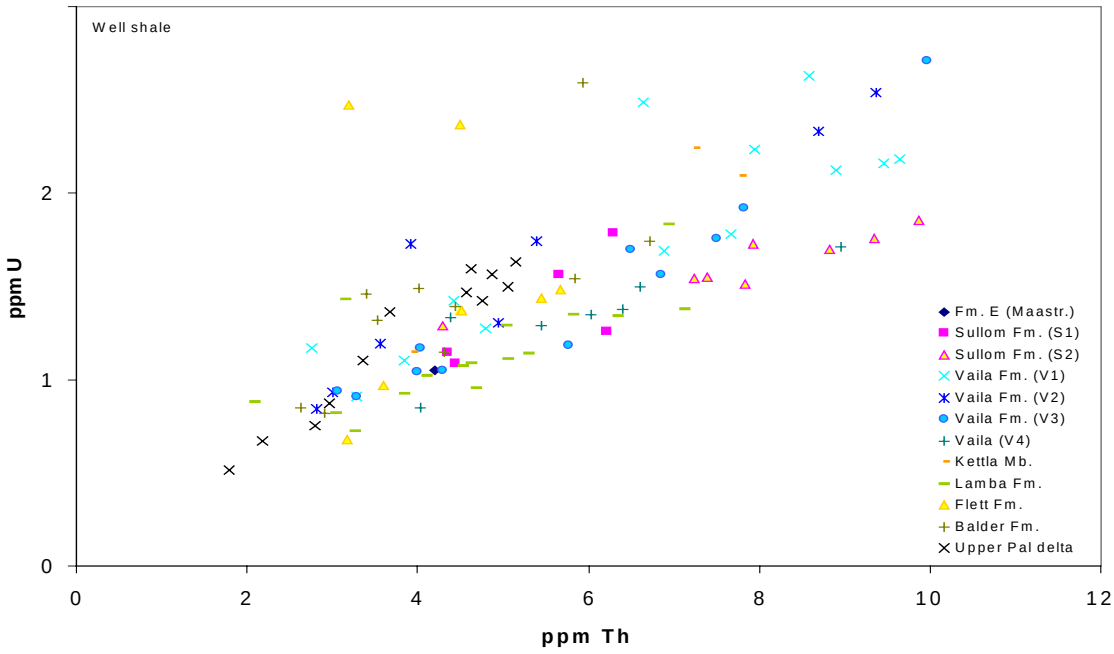

Figure 28. *ppm U versus ppm Th in mudstone samples from the Faroe–Shetland Basin.*

The U/Th ratio can also be measured using wireline logging techniques. K is another element which can be measured using wireline logging. K is often taken as an indicator of the clay content, and the Th/K ratio is an indicator of the redox environment, with high Th/K in the S2 unit on Fig. 29 confirming this.

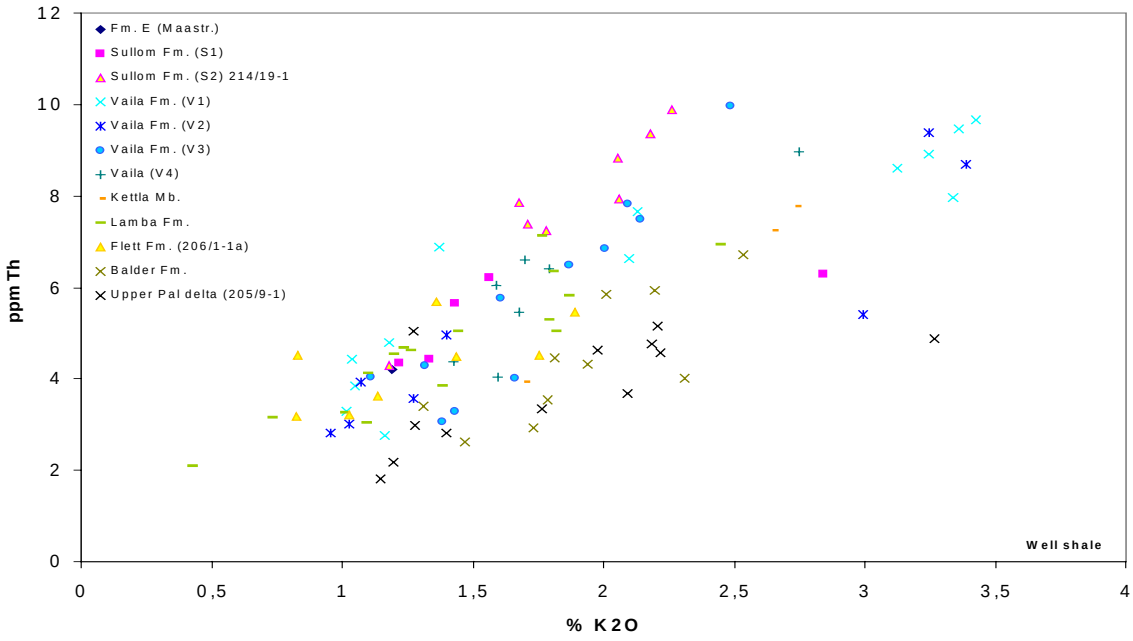

Figure 29. *ppm Th versus % K_2O in mudstone samples from the Faroe–Shetland Basin.*

Geochemical characteristics of the units

The Sullom Fm. is divided into two subunits S1 and S2 (Whitham and Larsen, 2004) dominated by marine mudstones (Fig. 15). The K/Al ratio is fairly high and uniform in the Sullom Fm., indicating a fairly uniform source, and it is likely that illite is the dominating clay mineral in the matrix (Fig. 19). The Ti/Al ratio is very uniform indicating a uniform source of the mud in the matrix. The high U/Zr ratio is interpreted as due to reducing depositional environment. Some sandstone samples are calcite cemented.

The Vaila Fm. (V1 to V4) consists of deep-marine sandstones and marine mudstones (Whitham and Larsen, 2004). The sandstones exhibit different K/Al ratios among the wells and stratigraphic levels, indicating differences in the sources of the different wells and stratigraphic levels (Fig. 19). In the V1-V2 interval of well 204/19-3a, K dominates over Na (Fig. 20), whereas the opposite is the case in the V-3 - V4 interval in well 205/9-1. The high Na content here may be due to the presence of Na-rich feldspar, as indicated by the high Eu/Ce ratio (Fig.. 27). Internal differences in the source in the Vaila Fm. is also indicated by the varying Ti/Al ratio (Fig. 21). A few samples from the V1 - V2 section have hig zircon contents, interpreted as a sign of beach placer enrichment before final emplacement. The V3- V4 sandstones are locally carbonate cemented.

The Lamba Fm. is subdivided into L1 and L2, where L1 is dominated by marine sandstones and L2 is dominated by marine mudstones (Whitham and Larsen, 2004). L2 sandstones have higher Al contents compared to L1, confirming the association with marine mudstones. The L2 in well 205/9-1 is distinctively different from L2 in 204/24a-7 based on Eu/Ce ratios (Fig. 27), indicating a different source, with higher content of alkali feldspar in 205/9-1.

The Flett Fm. sandstones are classified as marine (Whitham and Larsen, 2004). One sample shows high contents of zircon and titanium (Fig. 22), probably due to heavy mineral enricment (beach placer). The Flett sandstones have Na-dominated alkali contents but not high Eu/Ce ratios, indicating that the high Na is not in feldspar, but maybe in smectite from decomposed basaltic material. The signature of volcanic influence is also seen in the elevated Ti/Al ratios (Fig. 28).

The Balder Fm. and “Upper Paleocene delta depostits” are characterised by high Ti/Al ratios characteristic of influx of mafic volcanic material.

The general increase in the Ti/Al ratio of the mudstones from the oldest deposits belonging to the Sullom Fm. through the Vaila and Lamba Fm.’s to Flett and Balder Fm. (Fig. 28) is interpreted as increasing influx of mafic volcanic material into the basin.

Comparison of geochemistry between the two areas

As an example of how the geochemistry compare between the Kangerlussuaq area and the Faroe-Shetland area looks, the Vaila Fm. and the Fairy Tale Valey Mb. is compared in the following. This example is chosen because the units represent similar sedimentary environment, and could be derived from the same source.

It is seen on Fig. 30, that there is somewhat lower K/Al ratio in the sandstones from Fairy Tale Valley Mb as compared to most sandstones from the Vaila Fm. This is likely to reflect composition of the mica and clay minerals and feldspars in the sands. There is an overlap, and this is not conclusive with respect to wether the sandstones are sourced from differnt areas. The Ti/Al ratio (Fig. 31) do not differ between the two areas, and with respect to this feature it is not possible to differentiate between sources among the two areas.

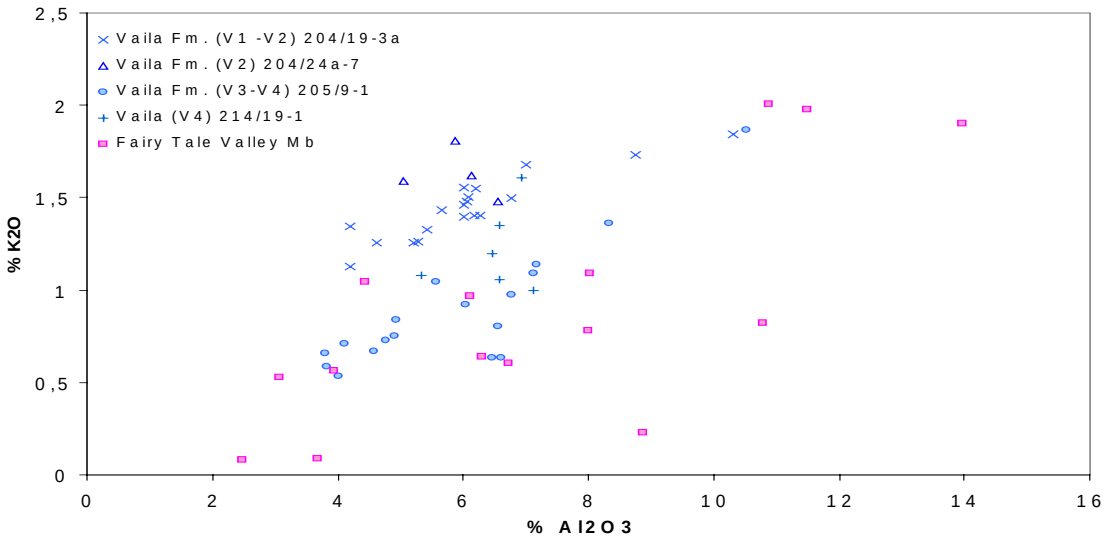

Figure 30. *% K_2O versus % Al2O3 in sandstones from Vaila Fm Faroe-Shetland area and from Fairy Tale Valley Mb., Kangerlussuaq area.*

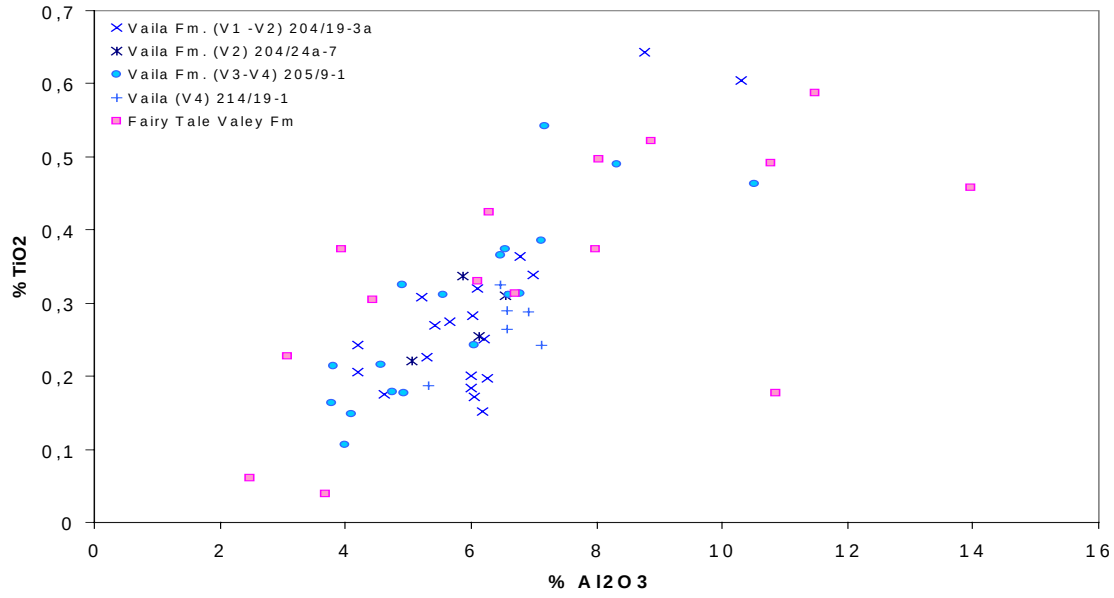

Figure 31. *% TiO_2 versus % Al_2O_3 in sandstones from Vaila Fm. Faroe-Shetland area and from Fairy Tale Valley Mb., Kangerlussuaq area.*

The Zr content and Zr/Al ratios in most of the sandstones from the Fairy Tale Valley Mb. is high compared to the Vaila Fm (Fig. 32). This is probably due to redeposition of beach placer deposits enriched in zircon. This indicate that at least some sandstones in the Fairy Tale Valley Mb originates from a different source compared to the Vaila Fm.

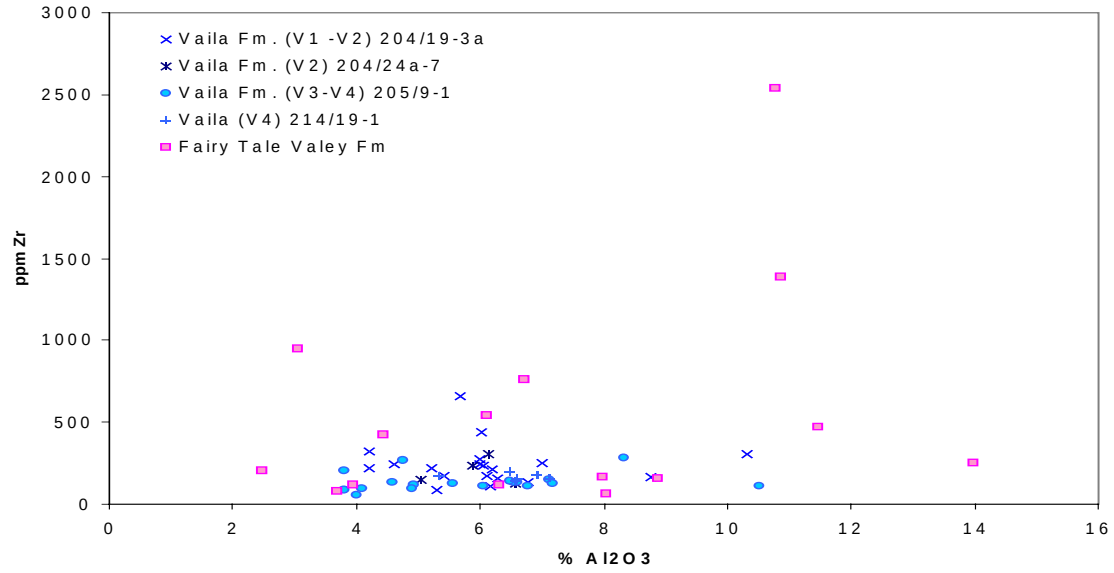

Figure 32. *ppm Zr versus % Al_2O_3 in sandstones from Vaila Fm. Faroe-Shetland area and from Fairy Tale Valley Mb., Kangerlussuaq area.*

The slope of the Rare Earth Element (REE) pattern is reflected by the Yb/La ratio as mentioned above. This is an indication of which mineral that contain most REE, and how the source was composed. As can be seen on Fig. 33, there is a distinct difference in the Yb/La ratio between the two areas, with lower Yb/La ratios in the Fairy Tale Valley Mb. Further there is higher absolute contents of La and to some degree Yb in Fairy Tale Valley Mb. This is likely to reflect that the main mineral containing REE in Fairy Tale Valley Mb is monazite. The different Yb/La ratios indicate different source between the Vaila Fm. and the Fairy Tale Valley Mb.

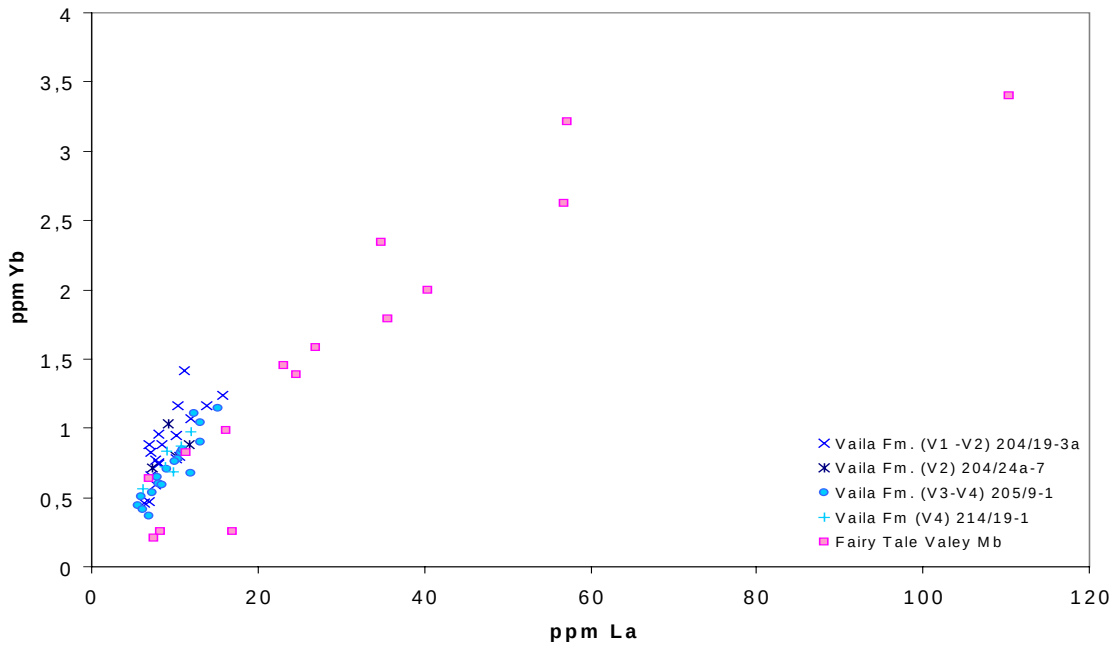

Figure 33. *ppm Yb versus ppm La in sandstones from Vaila Fm. Faroe-Shetland area and from Fairy Tale Valley Mb., Kangerlussuaq area.*

There is also a distinct difference in the Eu/Ce ratios among the different sandstones (Fig. 34). This is likely to be a combination of two effects, namely enrichment in the light REE Ce in monazite in the Fairy Tale Valley Mb. and enrichment in Eu in at least some of the sandstones in the Vaila Fm., probably due to alkali feldspar.

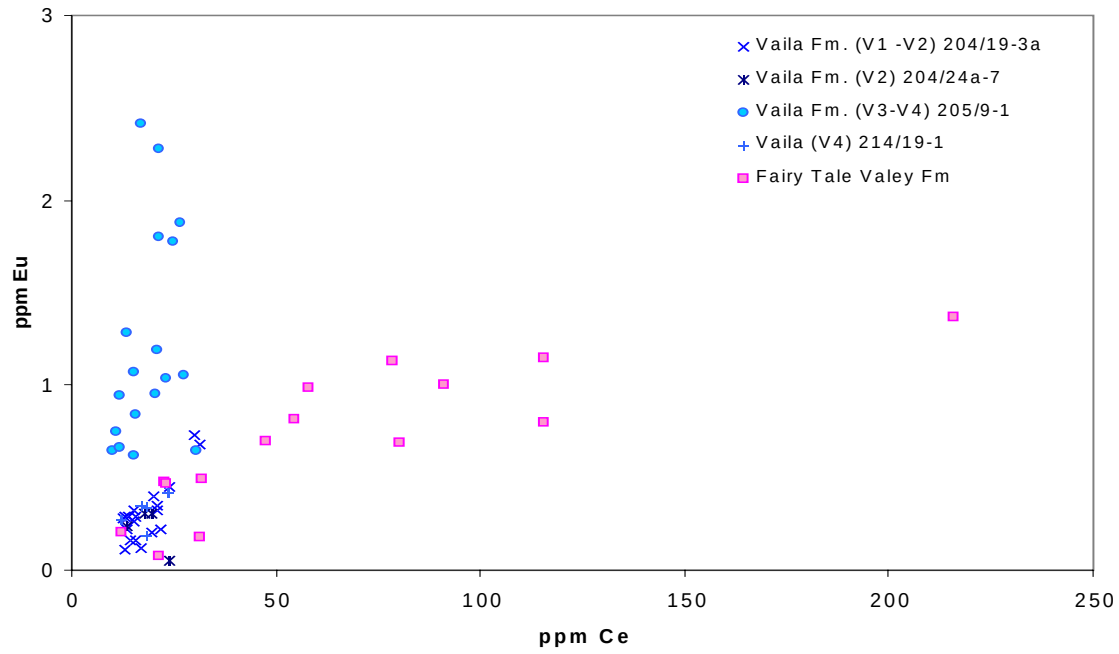

Figure 34. *ppm Eu versus ppm Ce in sandstones from Vaila Fm., Faroe-Shetland area and from Fairy Tale Valley Mb., Kangerlussuaq area.*

Based on the combination of the different crossplots presented, it is concluded that there is no evidence for a common source for the sandstones belonging to the Vaila Fm. and the Fairy Tale Valley Mb. On the contrary, they are likely to have different sources.

Finally it can be concluded, that access to a large number of datapoints from each unit, analysed for a large number of elements at high sensitivity enable provenance analysis based on geochemical evidence. Fortunately, the new analytical techniques now available make such studies possible, both technically and economically.

References

Frei, D., Rasmussen, T., Frei, M., Knudsen, C., Larsen, M. 2005a: Detrital zircon age constraints on provenance of Paleocene-Eocene sandstones in the Faroe-Shetland basin. Danmarks og Grønlands Geologiske Undersøgelse Rapport **2005/54** *(this volume).*

Frei, D., Frei, M., Hansen Klünder, M., Rasmussen, T., Knudsen, C., Morton, A.C., Whitham, A.G. 2005b: Heavy mineral characteristics of Cretaceous-Eocene sandstones in the Kangerlussuaq Basin, East Greenland – results from CCSEM. Danmarks og Grønlands Geologiske Undersøgelse Rapport **2005/54** *(this volume).*

Hutchison, A., Hartley, A., Hole, M., Whear, E., Preston, J. 2001: High resolution geochemical and petrographical correlation of deep marine Palaeocene sandstones from the Foinaven Field, West of Shetland. Petroleum Geoscience **7**, 123-129.

Kystol, J., Larsen, L.M. 1999: Analytical procedures in the Rock Geochemical Laboratory of the Geological Survey of Denmark and Greenland. Geology of Greenland Survey Bulletin **184**, 59-62.

Larsen, L.M., 1979: Distribution of REE and other trace elements between phenocrysts and peralkaline undersaturated magmas, exemplified by rocks from the Gardar igneous province, South Greenland. Lithos **12**, 303–315.

Larsen, M., Nøhr-Hansen, H., Whitham, A.G., Kelly, S.R.A. 2005: Stratigraphy of the prebasaltic sedimentary succession of the Kangerlussuaq Basin. Volcanic basins of the North Atlantic. Danmarks og Grønlands Geologiske Undersøgelse Rapport **2005/62**.

Morton, A.C., Hallsworth, C.R., Whitham, A. G. 2005: Heavy mineral provenance of Paleocene-Eocene sandstones in the Faroe-Shetland Basin – results from conventional petrographic and mineral-chemical techniques. Danmarks og Grønlands Geologiske Undersøgelse Rapport **2005/54** *(this volume).*

Morton, A.C, Whitham, A.G., Fanning, C.M., Claoué-Long, J.C. 2005: The role of East Greenland as a source of sediment to the Vøring Basin during the Late Cretaceous. In B. Wandas et al. (Eds), Onshore-Offshore Relationships on the North Atlantic Margin. NPF Special Publication **12**, 83-110.

Pickles, C.S., Sherlock, S. 2002: Late Cretaceous-Paleocene cross rift sediment transported from Greenland to the Faroes-Shetland region identified by $^{40}Ar/^{39}Ar$ dating of white micas. CASP East Greenland Series, confidential report, 62 pp.

Whitham, A.G., Larsen, M. 2005: Relationship of the Cretaceous-Paleogen succession of Kangerlussuaq to the Faroe-Shetland Region. Danmarks og Grønlands Geologiske Undersøgelse Rapport 2005 *(in press).*

Whitham, A.G., Morton, A.C. 2001: Insights into Paleocene sediment transport paths and basin evolution in the North Atlantic from a heavy mineral study of sandstones from southern East Greenland. Palaeogene Stratigraphy, Tectonics and Petroleum Geology of North West Europe 18-19 September 2001, Programme and Abstracts.

Acknowledgements

All work presented in this volume was perfomed during the project “Linking the Faroese area and Greenland: An innovative, integrated provenance study” funded by the SINDRI group. The SINDRI group was established by the Minister of Petroleum for the Faroe Islands (August 2001). It was formed as a result of the requirement for licensees within the Faroese area to fund and carry out projects of relevance to the future investigation of the Faroese continental shelf.

The current licensees are:

Agip Denmark BV
Amerada Hess (Faroes) Ltd.
Anadarko Faroes Company
P/F Atlantic Petroleum
BP Amoco Exploration Faroes Ltd.
British Gas International BV
DONG Føroyar P/F
Enterprise Oil Exploration Ltd.
Føroya Kolvetni P/F
Petro-Canada Faroes GmbH
Phillips Petroleum Europe Exploration Ltd.
Shell (UK) Ltd.
Statoil Færøyene AS

The following individuals are acknowledged for their support in various aspects of this project: Stefan Bernstein, John Boserup, Peter Czaja, Adam A. Garde, Axel Gerdes, Carsten Guvad, Jette Halskov, Lutz Hecht, Karen Merete Henriksen, Julie Alison Hollis, Jan Košler, Jørgen Kystol, Hanne Lamberts, Lotte Melchior Larsen, Afet Neimi, Karen Løvig Nielsen, Eric A. Nielsen, Ingerliese Nørgard, Henrik Klinge Pedersen, Mikael Pedersen, Mikkel Vognsen and Berit Wenzell.

APPENDIX A: Determination of sandstone provenance and correlation using heavy minerals – Principles and experimental techniques

Andrew Morton

HM Research Associates, 100 Main Street, Woodhouse Eaves, Leicestershire, LE12 8RZ, UK

Heavy mineral assemblages are sensitive indicators of sediment provenance. A large number of species have been found in sandstones, many of which have restricted parageneses that provide a positive indication of the mineralogical composition of the source region. Differences in heavy mineral assemblages facilitate the discrimination of sand bodies derived from different sources via different sediment transport pathways. Stratigraphic changes in heavy mineral assemblages provide a basis for correlation, independent of traditional biostratigraphic or log correlation methods.

The composition of heavy mineral assemblages is not, however, entirely controlled by source rock mineralogy. There are several other processes that overprint the original provenance signal. These processes can introduce a large degree of heterogeneity to assemblages that were derived from the same source and were therefore originally homogeneous. It is crucial for accurate provenance and correlation studies that these factors are fully appreciated and accounted for. The processes are:

1. **Weathering**, which causes modification of source rock mineralogy both at source (prior to incorporation into the transport system) and during periods of exposure on the floodplain during transport (alluvial storage).

2. **Abrasion**, which may reduce proportions of mechanically unstable minerals. Mechanically-induced depletion of minerals may occur through abrasion during transport. Assemblages recovered from ditch cuttings samples may also be affected by abrasion through the aggressive action of the drill bit.

3. **Hydraulic processes** during transport and deposition, which strongly affect relative abundances of minerals with different hydraulic behaviour (controlled by grain size, density and shape).

4. **Diagenesis**, which selectively removes unstable minerals at the site of deposition, both during early diagenesis (through circulation of acidic meteoric pore waters) and during burial diagenesis (through circulation of elevated temperature pore waters).

5. **Sampling and laboratory procedures**, which can also influence the mineralogy, particularly if chemical pretreatment is used.

Source rock mineralogy is undoubtedly altered during weathering process, but the extent to which this affects the detrital mineralogy has not been comprehensively evaluated. How-

ever, qualitative studies of modern river sediments indicate that there is little or no actual reduction in mineral diversity between source rock and transport system. In any case, the extent of source-area weathering can be justifiably viewed as a provenancerelated feature that might have potential value in correlation studies (for example, in sequences deposited during a period of climate change).

It is a common misconception that abrasion during transport is an important factor in controlling heavy mineral assemblages. Although experimental work has shown that some loss of minerals does occur with prolonged simulated transport, case studies have failed to demonstrate that it occurs to any appreciable extent in natural systems (see Morton and Smale, 1990, for example). By contrast, there is evidence that minerals may be depleted through the action of the drill bit, as core and cuttings samples over equivalent sections commonly have slightly different mineralogical compositions. The most severely affected mineral appears to be apatite, presumably because of its relatively low hardness.

The processes of weathering on the floodplain during periods of exposure, and of weathering at the site of deposition, are potentially significant factors, as are variations in hydraulic conditions during deposition and in the extent of burial diagenesis. The effects of both weathering and burial diagenesis are to reduce detrital mineral diversity through dissolution of unstable species. The effects of burial diagenesis are particularly significant and pervasive, being marked by a clear and well-defined progressive reduction in mineral diversity with depth. This is essentially caused by increased dissolution rates resulting from the higher pore fluid temperatures that occur with increasing depth. The relative stability of heavy minerals under both deep burial and weathering are relatively well known, at least for the North Sea (Morton, 1984), the most significant difference between the two processes being that apatite is unstable during weathering but stable in deep burial (Morton, 1986). Thus, absence or reduced contents of apatite suggest that acidic groundwaters may have influenced heavy mineral suites. The effects of variations in hydraulic conditions during deposition are to modify the relative proportions of those minerals that have different hydraulic behaviour. The principal factors influencing hydraulic behaviour are grain size and density. Therefore, the main effect that hydraulic variations have on heavy mineral suites is to vary the ratio of the more dense minerals, such as zircon, garnet or rutile, to the less dense minerals, such as apatite and tourmaline. Grain shape also influences hydraulic behaviour, but this is generally a less important factor, the most obvious exception to this statement being mica, which, although having the density of a heavy mineral, actually behaves as a light mineral. For detailed discussion of the effects of these factors, see Morton and Hallsworth (1999).

The above guidelines serve to indicate how variations in weathering, diagenesis and depositional processes may be detected, but do not indicate how their effects can be minimised, allowing variations in provenance to be detected. There are two approaches to this problem. The first is to utilise the **conventional heavy mineral data**. Identification of variations in sediment source from the conventional data is best made by determining ratios of stable minerals with similar densities, as these are not affected by changes in hydraulic conditions during sedimentation or by diagenetic processes (Morton and Hallsworth, 1994). Ratios that are recommended to best reflect provenance characteristics are apatite:tourmaline, garnet:zircon, rutile:zircon, chrome spinel:zircon and monazite:zircon. Indices are ex-

pressed as index values (ATi, GZi, RZi, RuZi, MZi, CZi) as defined below. In some circumstances, ATi and GZi may not provide a true reflection of the source composition. For example, ATi may be reduced during weathering, and GZi may be lowered during burial diagenesis.

Index Mineral pair Index determination

ATi apatite-tourmaline index 100 x apatite count/total apatite plus tourmaline

GZi garnet-zircon index 100 x garnet count/total garnet plus zircon

RZi TiO_2 mineral-zircon index 100 x TiO_2 mineral count/total TiO_2 minerals plus zircon

RuZi rutile-zircon index 100 x rutile count/total rutile plus zircon

MZi monazite-zircon index 100 x monazite count/total monazite plus zircon

CZi chrome spinel-zircon index 100 x chrome spinel count/total chrome spinel plus zircon

The alternative approach is to undertake **varietal studies**. These are studies that concentrate on variations seen within one mineral group, which strongly diminishes the range of density and stability across the data set. The classical approach to varietal studies is to distinguish types on the basis of their optical properties, such as crystal form or colour, but this approach is commonly subjective and class distinctions tend to be somewhat arbitrary. However, this approach may provide useful information on sedimentary processes (for example, using the extent to which grains are rounded). A more objective approach is to determine the geochemical characteristics of a mineral population using electron microprobe analysis. This also has the advantage of generating data sets that can be readily compared with those generated by other analysts.

Sample preparation

Samples are gently disaggregated by use of a pestle and mortar, avoiding grinding action. This does not apply to cuttings samples, which have already been disaggregated through the action of the bit. No chemical pretreatment is used, thus avoiding the possibility of modifying assemblages in the laboratory. Following disaggregation, the samples are immersed in water and cleaned by ultrasonic probe to removed and disperse any clay might have have been adhering to grain surfaces. The samples are then washed through a 63 µm sieve and resubjected to ultrasonic treatment until no more clay passed into suspension. At this stage, the samples were wet sieved through the 125 and 63 µm sieves, and the resulting >125 µm and 63-125 µm fractions were dried in an oven at 80°C. The 63–125 µm fraction is placed in bromoform with a measured specific gravity of 2.8. Heavy minerals are allowed to separate under gravity, with frequent stirring to ensure complete separation. The heavy mineral residues are mounted under Canada Balsam for optical study using a polarising microscope. Where possible, a split is retained for microprobe study.

Conventional analysis and ratio determination

Heavy mineral proportions were estimated by counting 200 non-opaque detrital grains using the ribbon method described by Galehouse (1971). Identification was made on the basis of optical properties, as described for grain mounts by Mange and Maurer (1992). A qualitative assessment is also made of other components, such as diagenetic minerals, opaques and mica. Provenance-sensitive mineral ratios are also determined using the ribbon counting method, ideally on the basis of a 200 grain count. It is not always possible to achieve the optimum 200 grain count because of the scarcity of some of the mineral phases or because of small sample sizes.

Geochemical analysis

Samples for geochemical analysis using the microprobe are selected on the basis of the results of the conventional optical analysis. The most frequently analysed minerals are garnet and tourmaline, because of their wide variation in composition and their stability. Grains are picked with a needle from the dry residues during optical examination under the polarising microscope, in a manner analogous to the ribbon method of Galehouse (1971). The grains are placed on double sided adhesive tape, coated with carbon, and analysed using a Link Systems AN 10/55S energy-dispersive x-ray analyser attached to a Cambridge Instruments Microscan V electron microprobe. The count time is 30 seconds for each grain.

For garnet, the quality of each result is monitored to ensure that the analytical total does not deviate below 90 % and that the stoichiometrically-determined garnet formula is approximately that of an ideal garnet. Ideally, garnets should give analytical totals of 100 %, but grain surface roughness and poor orientation may cause totals to be lower. Such analyses are accepted providing their stoichiometrically-determined formulae are close to ideal garnet compositions. Studies of North Sea detrital garnets has shown that intragrain variations are usually negligible in grains between 63 and 125 µm diameter (Morton 1985; Morton et al. 1989). Therefore, it is unlikely that compositional zoning has a significant effect on the overall range of garnet compositions in any individual sample. Garnet compositions are expressed in terms of the relative abundance of the Mg, Fe^{2+} , Ca and Mn end members. The compositions of garnet assemblages are shown using ternary diagrams with Fe+Mn, Mg and Ca as poles. The quality of the tourmaline analyses is monitored in a similar fashion to that of garnet. However, the optimum analytical total for tourmaline is around 88 % because of the presence of elements such as boron, lithium and hydrogen which cannot be detected using energy-dispersive analysis. Totals that fall below 80 % because of grain surface roughness or orientation are rejected. Tourmaline compositions are plotted on the source discriminant ternary diagram of Henry and Guidotti (1985).

REFERENCES

Galehouse, J.S. 1971: Point-counting. In: Carver R.E. (ed.) Procedures in Sedimentary Petrology. Wiley- Interscience, New York, 385-407.

Henry, D.J., Guidotti, C.V. 1985: Tourmaline as a petrogenetic indicator mineral: an example from the staurolite-grade metapelites of NW Maine. American Mineralogist **70**, 1-15.

Mange, M.A., Maurer, H.F.W. 1992: Heavy minerals in colour. Chapman and Hall, London.

Morton, A.C. 1984: Stability of detrital heavy minerals in Tertiary sandstones of the North Sea Basin. Clay Minerals **19**, 287-308.

Morton, A.C. 1985: A new approach to provenance studies: electron microprobe analysis of detrital garnets from Middle Jurassic sandstones of the northern North Sea. Sedimentology **32**, 553-566.

Morton, A.C. 1986: Dissolution of apatite in North Sea Jurassic sandstones: implications for the generation of secondary porosity. Clay Minerals **21**, 711-733.

Morton, A.C., Borg, G., Hansley, P.L., Haughton, P.D.W., Krinsley, D.H., Trusty, P. 1989: The origin of faceted garnets in sandstones: dissolution or overgrowth. Sedimentology **36**, 927-942.

Morton, A.C., Hallsworth, C.R. 1994: Identifying provenance-specific features of detrital heavy mineral assemblages in sandstones. Sedimentary Geology **90**, 241-256.

Morton, A.C., Hallsworth, C.R. 1999: Processes controlling the composition of heavy mineral assemblages in sandstones. Sedimentary Geology **124**, 3-29.

Morton, A.C., Smale D. 1990: The effects of transport and weathering on heavy minerals from the Cascade River, New Zealand. Sedimentary Geology **68**, 117-123.

APPENDIX B: Determination of sandstone provenance and correlation using heavy minerals – Experimental techniques used at GEUS

Dirk Frei, Martina Frei, Christian Knudsen

Geological Survey of Denmark and Greenland, Øster Voldgade 10, DK-1350 Copenhagen K, Denmark

Whole rock major and trace element analysis

The degree of sediment maturity is very variable in the sediments in the studied area. Apart from classical optical microscopy, major- and trace element analysis provides a rapid insight into the bulk rock composition and the changes it may have suffered during diagenesis and/or transport. Accordingly, a large number of samples have been analysed for their major and trace element compositions. This data offers the possibility of delineating chemostratigraphical correlations within the basin. Additionally, trace element data provides information about the content of heavy minerals such as zircon, monazite, xenotime and Ti-minerals (i.e. rutile, ilmenite, and leucoxene). This allows comparison between the bulk rock data and data obtained through point-counting of individual heavy mineral grains by e.g. conventional methods and by CCSEM.

All samples were analysed for major-, minor-, and trace elements by XRF and solution ICP-MS to establish a large database for chemostratigraphy. Two grams of each sample were ground to fineness (i.e. particle sizes of 63 µm and below) using a tungsten carbide ball mill and were subsequently dried at 110°C for 2 hours. Aliquots of about 1 to 1.5 grams of the resulting powder were subsequently used for bulk chemical analysis.

Fusion XRF

Dried sample powders are ignited in an electric furnace at 1000ºC for 1 hour. Homogeneous glass discs are produced by fusing 1 gram of ignited powder together with a borate flux in the proportion 1:7. The glass discs are analysed with a Phillips PW1606 multichannel X-ray fluorescence (XRF) spectrometer at GEUS for all major elements excluding Na, which is determined by atomic absorption spectrometry (AAS). Ba and Sr are determined by XRF because of the better precision compared with ICP-MS analyses due to the very high contents of these elements in most of the samples. The combined content of organic material and volatiles are obtained as the loss in ignition of the samples. Analytical details, including precision, accuracy, and detection limits are reported by Kystol and Larsen (1999).

AAS

For the determination of Na by AAS, about 0.25 to 0.5 g of the dried sample is treated with hydrofluoric acid in a PTFE beaker on a hot plate. After evaporation to dryness the residue is dissolved in a hydrochloric acid - potassium chloride solution and Na is determined using a Perkin Elmer PE2280 instrument at GEUS (Kystol and Larsen 1999).

ICP-MS

For solution ICP-MS a piece of the glass disc previously used for XRF (see above) is dissolved in a HF-HNO_3 mixture, evaporated to dryness and subsequently redissolved with HNO_3 and evaporated to dryness twice. The dry residue is then dissolved in HNO_3, and diluted; the resulting solution is analysed for trace elements using a Perkin Elmer 6100 DRC quadrupole ICP-MS at GEUS. This method is a modified version of the method described by Turner et al. (1999). The use of glass discs ensures that refractory minerals such as zircon and chromite are brought completely into solution. Routine analysis of international and in-house geo-standards demonstrated that the precision and accuracy are usually better than 5 % relative for the majority of the elements analysed.

Computer controlled scanning electron microspopy (CCSEM)

Basic principles of CCSEM

The CCSEM method was originally developed for the determination of the size, shape, and semi-quantitative composition of particles in environmentally relevant materials, e.g. minerals in coal and fly ashes (Lee et al. 1978; Huggins et al. 1980; Zygardlicke and Steadman 1990). However, the method can be used to characterise any particulate matter that can be distinguished, by image analysis techniques, from the surrounding material (usually an embedding resin) by its back-scattered electron reflection. In the scanning electron microscope laboratory at GEUS, a dedicated CCSEM technique was initially set up for the rapid, and hence labour- and cost efficient, screening of the mineralogy, titanium grade and grain size distribution of heavy mineral sands (Laursen 1997; Sørensen 1998) during exploration for heavy mineral deposits in Denmark (Knudsen 1998).

Based on this, the CCSEM method was subsequently developed and refined for the fully automated, rapid and simultaneous determination of the average semi-quantitative chemical composition, grain size distribution, grain size parameters (such as aspect ratio and circularity) and modal abundance of a variety of environmentally stable heavy minerals, such as apatite, chrome spinel, garnet, monazite, rutile, and zircon, which show similar hydraulic and diagentic behaviour and hence are provenance-sensitive (e.g. Morton and Hallsworth 1994; 1999).

The basic principle of CCSEM are: First, a back-scattered electron (BSE) image with 512 $\times$ 512 pixels and with magnifications typically ranging from 30 to 100 times is generated. Secondly, grains are segmented from the background by grey-level thresholding and the

binary image is processed by a “holefill” function which fills out minor voids and cracks to simplify the image for subsequent analysis. This processed binary image is finally utilized to control the beam during CCSEM analysis. Clusters of interconnecting pixels are recognized as individual grains and the electron beam is scanned across each grain for 10 seconds in order to aquire data for grain size and shape parameters and energy-dispersive X-ray intensities for specified regions of interest. A guard region filter ensures omission of grains that are cross-cut by the margin of the generated image.

CCSEM sample preparation and operating conditions

For CCSEM analysis of whole rock samples, bulk samples or heavy mineral residues obtained by heavy liquid separation from the bulk sample are embedded in epoxy in 5 mm diameter plastic vials in such a way that no sedimentation occurs during curing of the epoxy and that the majority of the grains do not touch each other. The vials are cut in half longitudinally to obtain a representative section and the section is mounted in epoxy for subsequent grinding and polishing.

For comparison purposes, the garnet populations of 37 samples were retrieved by mineral separation techniques. After crushing, sieving and pre-concentration using a Frantz isodynamic magnetic barrier separator and heavy liquids, indiviual garnet grains were handpicked to optical clearness using a binocular microscope. The obtained garnets were mounted in epoxy for subsequent grinding and polishing.

The data presented in this study were acquired using a Philips XL 40 SEM equipped with a ThermoNoran Voyager 2.7 energy dispersive X-ray analysis (EDX) system with integrated control of sample stage and electron beam. The electron beam was generated using a tungsten filament operated at an accelerating voltage of 17 kV and a sample current of typically 50 to 60 µA. Prior to analysis, all samples were carbon-coated to facilitate conductivity. A CCSEM analysis typically contains data from between 500 to 1500 measured mineral grains. The collected X-ray data are corrected for atomic number, absorption or fluorescence effects by the Proza correction scheme prior to semi-quantitative, standardless calculation of elemental concentrations. Data reduction is performed on in-house developed software-based spreadsheet calculation programs (Laursen 1997; Sørensen 1998).

Electron microprobe analysis (EMPA)

In order to test the reliability and accuracy of the major element variation of garnet populations determined semi-quantitatively by CCSEM using EDX, all sample mounts previously analysed by CCSEM have been re-analysed by fully quantitative, wavelength dispersive X-ray analysis (WDS) using modern, automated electron microprobe analysers at Copenhagen University (KU; electron microprobe used: JEOL JXA 8200 Superprobe) and the Natural History Museum, Humboldt University Berlin (HU; electron microprobe used: JEOL JXA 8800 Superprobe). Prior to analysis, all samples were carbon-coated to facilitate conductivity.

In both Copenhagen and Berlin, analysis were performed using an accelerating voltage and beam current of 15 kV and 15 nA, respectively, and a beam diameter of 1 µm was applied. Smithsonian Institute standards were used as primary standards including albite (Na), diopside (Ca, Si), olivine (Mg), spinel (Al), titanite (Ti), and oxides (Fe, Mn, Cr). All raw data was reduced using a ZAF correction scheme. Typical 1s precision is generally better than 2 % relative for > 5 oxide wt %, 4 % relative for 5 - 3 oxide wt %, and 6 % relative for < 3 oxide wt-%. Analyses of secondary standards (pyrope and almandine) carried out in Berlin were consistently within 2 s of published values.

Laser ablation – inductively coupled plasma – mass spectrometry (LA-ICP-MS)

Basic principles of laser ablation – inductively coupled plasma - mass spectrometry (LA-ICP-MS)

Laser ablation – inductively coupled plasma – mass spectrometry (LA-ICP-MS) was developed as a trace element microprobe for geomaterials in the early nineties (e.g. Arrowsmith 1987; Denoyer et al. 1991; Pearce et al. 1992). In LA-ICP-MS, a laser ablation sampling device is coupled to a mass spectrometer analyser (usually a quadrupole or magnetic sectorfield mass spectrometer). This combination utilizes a relatively simple and inexpensive instrument capable of analysing elemental concentrations *in-situ* in solid samples with a high spatial resolution and low detection limits. In addition, isotopic ratios can be determined simultaneously with moderate to high precision (2 to 0.1 % relative standard deviation, respectively, depending on the operating conditions, the isotopic system investigated and the equipment used). Solid samples are held in a cell at atmospheric pressure and sub-micron particles are ablated from the surface using a laser. The ablated particles are dispersed into a carrier-gas (usually Ar or He) and flushed into the mass spectrometer for analysis. This setup requires only minimum sample preparation and allows quick sample exchange. For an in-depth description and discussion of the capabilities of modern, state-of-the-art LA-ICP-MS systems, the reader is referred to Sylvester (2001).

Pb-Pb and U-Pb zircon geochronology using LA-ICP-MS and SHRIMP

In this study, three different methods and instrumental set-ups were employed for zircon age determinations. For the majority of samples, ^{207}Pb-^{206}Pb model ages were determined using the laser ablation – quadrupole – inductively coupled plasma – mass spectrometry (LA-Q-ICP-MS) facility at GEUS. In order to check the reliability and accuracy of the ^{207}Pb-^{206}Pb model ages derived in this fashion, high precision U-Pb ages were determined for a total of 11 samples employing either sensitive high resolution ion microprobe (SHRIMP) or the newly established laser ablation – high resolution – magnetic sectorfield - inductively coupled plasma– mass spectrometry (LA-SF-ICP-MS) facility at GEUS.

^{207}Pb-^{206}Pb zircon geochronology using LA-Q-ICP-MS

All ^{207}Pb-^{206}Pb zircon age determinations by LA-ICP-MS were performend using a Cetac LSX 200 laser ablation system equipped with a frequency quadrupled Nd-YAG laser emitting at a wavelength of 266 nm, coupled to a PerkinElmer 6100 DRC quadrupole ICP-MS at GEUS. The nominal pulse width of the laser is < 4 ns with a pulse-to-pulse stability of 2 %. The laser was operated at a repetition rate of 20 Hz and a pulse energy of 6 mJ, respectively, for the analyses presented in this study. All data presented here were acquired with a single line scan on each individual zircon grain and with beam diameters of approximately 40 to 50 µm. An example of a single line scan used for analysis is displayed in Figure 8. All measurements were performed in time-resolved analysis (TRA) mode using peak jumping with 1 point per peak. The total acquisition time for each analysis varied between 60 to ~70 s depending on grain size with the first ~20 s used to measure the gas blank. The instrument was tuned to give large, stable signals for the ^{207}Pb and ^{238}U peaks, low background count rates (typically below 10 counts per second for ^{207}Pb) and low oxide production rates (^{232}Th^{16}O/^{232}Th < 0.2 %). The following isotopes were measured: ^{204}Pb, ^{206}Pb, ^{207}Pb, ^{208}Pb, and ^{202}Hg to monitor the ^{204}Hg interference on ^{204}Pb (using a ^{202}Hg/^{204}Hg-ratio of 4.36). It was found that the net intensities for mass 204, corrected for ^{204}Hg, are below the limit of detection (defined as three times the standard deviation of the background intensity) and hence no common Pb-correction was performed. Given the facts that limpid zircons have only a very small amount of common Pb and that the average precision of ^{207}Pb-^{206}Pb age measurements is usually 5 - 10 % relative, the inability to correct for the presence of common Pb in the sample and standard is insignificant for the accuracy of the ^{207}Pb-^{206}Pb ages presented here. The instrumental mass bias during ablation on ^{207}Pb/^{206}Pb-ratios was corrected using the NIST SRM 612 glass reference material. The use of an external standard implies that the mass bias factor remains constant during a reasonable time interval. In order to minimise time-dependent variations in the mass bias factor, the standard was analysed every 20 to 25 minutes. Data reduction and concentration calculations were performed off-line using in-house developed spreadsheets. The computer program IsoplotEx v. 2.60 (Ludwig 1999) was used to carry out the final computation of ^{207}Pb-^{206}Pb ages.

U-Pb zircon geochronology using high resolution LA-SF-ICP-MS

The high resolution LA-SF-ICP-MS used for U-Pb zircon age determinations at GEUS consists of a NewWave Research/Merchantek UP213 laser ablation system equipped with a frequency quintupled Nd-YAG laser emitting at a wavelength of 213 nm coupled to an Element2 (ThermoFinnigan, Bremen) single-collector double focusing magnetic sectorfield ICP-MS equipped with a fast fieldregulator for increased scanning speed.

The nominal pulse width of the laser is 5 ns with a pulse-to-pulse stability of 2 % RSD. The laser was operated at a repetition rate of 10 Hz and a nominal energy output of 44 %, corrsponding to a laser fluency of 8 J cm^{-2}. All data were acquired with a single spot analysis on each individual zircon grain with a beam diameter of 30 µm. For this spot diameter and the ablation time used (55 s) the ablated masses of zircon were approximately 200-500 ng. Samples and standards were held in the standard ablation cell delivered with the UP 213 system. Helium was used to flush the sample cell and was mixed downstream with the Ar sample gas of the mass-spectrometer.The washout time for this configuration is approximately 1 min. All sample mounts were rigorously cleaned before introduction into the sample cell to remove surface Pb contamination.

The total acquisition time for each analysis was 110 s with the first 35 s used to measure the gas blank. The mass spectrometer was tuned to give large, stable signals for the ^{206}Pb and ^{238}U peaks, low background count rates (typically around 300 counts per second for ^{207}Pb) and low oxide production rates ($^{238}U^{16}O/^{238}U$ generally below 2.5 %). All measurements were performed in low resolution mode using electrostatic scanning (E-scan) with the magnetic field resting at mass ^{202}Hg. The following masses were measured: ^{202}Hg, ^{204}(Pb + Hg), ^{206}Pb, ^{207}Pb, ^{208}Pb, ^{232}Th, ^{235}U, and ^{238}U. All Data were acquired on four samples per peak with a sampling and a settling time of 1 ms for each isotope. Mass ^{202}Hg was measured to monitor the ^{204}Hg interference on ^{204}Pb (using a $^{202}Hg/^{204}$Hg-ratio of 4.36). Only if the net intensities for mass ^{204}Pb, corrected for ^{204}Hg, are significantly above the limit of detection a common Pb-correction was performed. The laser induced elemental fractionation and the instrumental mass bias on measured isotopic ratios were corrected by matrix-matched external standardisation using the GJ-1 zircon standard (Jackson et al. 2004). Samples were analysed in sequences where three standards are analysed initially, followed by ten samples, again three standards, and so on. An analytical session typically consists of around one to two hundred pre-set zircon spots analysed automatically. The Plisovice zircon standard (ID-TIMS age 338 ± 1 Ma; Aftalion et al. 1989, provided by Jan Košler, Charles University, Prague) was analysed as an unknown regularly. The results are consistently concordant at 340 ± 2 Ma.

The raw data were exported in ASCII format and processed using in-house data reduction spreadsheets. Final age calculation were also done using in-house age-calculation spreadsheets. The computer program IsoplotEx v. 2.60 (Ludwig 1999) was used to carry out the final computation of ages.

U-Pb zircon geochronology using SHRIMP

Single-grain zircon U-Pb age determinations were performed using the SHRIMP at the Australian National University in Canberra, Australia. The use of SHRIMP for the characterization of detrital zircon age populations is described in detail by Morton et al. (1996) and Witham et al. (2004). The procedures employed for zircon U-Pb age dating with SHRIMP followed those reported by Claoué-Long et al. (1995).

Sample preparation for zircon geochronology

For all age determinations, zircons were separated from the bulk samples using conventional heavy liquid and magnetic separation methods. The final separation step was made by hand-picking individual zircon grains from the heavy and non-magnetic fraction using an binocular microscope.

For ^{207}Pb-^{206}Pb age determinations by LA-Q-ICP-MS, the individual zircon grains are mounted on adhesive tape in a fashion where each grain can be unequivocally related to its LA-ICP-MS age determination for subsequent optical inspection.

For high precision LA-SF-ICP-MS and SHRIMP U-Pb age determinations, the individual zircon grains are mounted on double-sided, transparent adhesive tape and subsequently

embedded in 1-inch diameter circular epoxy mounts for polishing. In order to study their internal structure, back-scattered electron (BSE) images of all analysed zircons were obtained using a Philips XL 40 scanning electron microscope at GEUS.

LA-SF-ICP-MS trace element analytical techniques

All garnets previously analysed for their major element chemistry by CCSEM and EMPA have subsequently been analysed for a range of geochemically important trace elements (Li, Sc, Ti, Cr, Co, Ni, Cu, Sr, Y, Zr, Nb, Ba, La, Ce, Pr, Nd, Sm, Eu, Gd, Tb, Dy, Ho, Er, Tm, Yb, Lu, Hf, Ta, Pb, Th, and U) at GEUS using laser ablation – high resolution – magnetic sectorfield - inductively coupled plasma – mass spectrometry (LA-SF-ICP-MS). The instrumental set-up consists of a NewWave Research/Merchantek UP213 laser ablation system equipped with a frequency quintupled ND-YAG laser emitting at a wavelength of 213 nm coupled to an Element2 (ThermoFinnigan, Bremen) single-collector double focusing magnetic sectorfield ICPMS equipped with a fast fieldregulator for increased scanning speed.

The laser was operated at a repetition rate of 10 Hz and a nominal energy output of 75 %, corresponding to a laser fluency of 30 J cm^{-2}. All data were acquired with a single spot analysis on each individual garnet grain using a beam diameter of 95 µm. Samples and standards were held in the standard ablation cell delivered with the UP 213 system. Helium was used to flush the sample cell and was mixed downstream with the Ar sample gas of the mass-spectrometer.The washout time for this configuration is approximately 90 sec. All sample mounts were rigorously cleaned before introduction into the sample cell to remove surface contaminations.

The total acquisition time for each analysis was 60 s with the first 30 s used to measure the gas blank. The mass spectrometer was tuned to give large, stable signals for the ^{139}La and ^{232}Th peaks, low background count rates (typically around zero counts per second for the REE) and low oxide production rates ($^{232}Th^{16}O/^{232}Th$ generally below 0.1 %). All measurements were performed in low resolution mode using electrostatic scanning (E-scan) with the magnetic field resting at masses ^{7}Li, ^{29}Si, ^{43}Ca, ^{59}Co, ^{88}Sr, ^{137}Ba, ^{181}Ta, and ^{238}U. All Data were acquired in time-resolved analyses (TRA) mode using peak jumping with one sample per peak with a sampling time of 10 ms for each isotope. The following masses were measured and ratioed to ^{29}Si for internal standardization: ^{7}Li, ^{43}Ca, ^{45}Sc, ^{47}Ti, ^{53}Cr, ^{59}Co, ^{60}Ni, ^{63}Cu, ^{88}Sr, ^{89}Y, ^{90}Zr, ^{93}Nb, ^{137}Ba, ^{139}La, ^{140}Ce, ^{141}Pr, ^{146}Nd, ^{147}Sm, ^{153}Eu, ^{157}Gd, ^{159}Tb, ^{163}Dy, ^{165}Ho, ^{166}Er, ^{169}Tm, ^{172}Yb, ^{175}Lu, ^{178}Hf, ^{181}Ta, ^{208}Pb, ^{232}Th, and ^{238}U. For calibration, the NIST SRM 612 glass standard was applied for all analysis. In a typical analyses sequence two standards were analysed initially, followed by ten to fifteen unknown samples, again two standards, and so on. Data reduction and concentration calculation was performed using the GLITTER software package using the calibration values of Pearce et al. (1997). The NIST SRM 614 glass standard was analysed routinely as unknown and the results are consistently within 2 s of published concentrations. Under these conditions, the detection limits are in the lower ppb range for most of the elements analysed.

REFERENCES

Aftalion, M., Bowes, D.R., Vŕana, S. 1989: Early Carboniferous U-Pb zircon ages for garnetiferous perpotassic granulits, Blansky Les Massif, Czechoslovakia. Neues Jahrbuch fűr Mineralogie, Monatshefte **4**, 145-152.

Arrowsmith, P. 1987: Laser ablation of solids for elemental analysis by inductively coupled plasma mass spectrometry. Analytical Chemistry **59**, 1437-1444.

Claoué-Long, J.C., Compston, W., Roberts, J., Fanning, C.M. 1995: Two Carboniferous ages: a comparison of SHRIMP dating with conventional zircon ages and $^{40}Ar/^{39}Ar$ analysis. In: Berggren, W.A, Kent, D.V and Hardenbol, J. (eds) Geochronology, time scales and global stratigraphic correlation. SEPM Special Publications **54**, 3-21.

Denoyer, E.R.; Kenneth, J.F., Hager, J.W. 1991: Laser solid sampling for inductively coupled plasma mass spectrometry. Analytical Chemistry **63**, 445A-457A.

Huggins, F.E.; Kosmack, D.A.; Huffman, G.P., Lee; R.J. 1980: Coal mineralogy by SEM analysis. Scanning Electron Microscopy **1**, 531-540.

Jackson, S.E., Pearson, N.J., Griffin, W.L., Belousova, E.A. 2004: The application of laser ablation – inductively coupled plasma – mass spectrometry to in-situ U-Pb zircon geochronology. Chemical Geology **211**, 47-69.

Knudsen, C. 1998: Heavy mineral exploration in Miocene sediments, Jylland. Danmarks og Grønlands Geologiske Undersøgelse Rapport **1998/45**.

Kystol, J., Larsen, L.M. 1999: Analytical procedures in the rock geochemical laboratory of the Geological Survey of Denmark and Greenland. Geology of Greenland Survey Bulletin **184**, 59-62.

Laursen, K. 1997: Advanced scanning electron microscope analysis at GEUS. Danmarks og Grønlands Geologiske Undersøgelse Rapport **1997/1**.

Lee, R.J., Huggins, F.E., Huffman, G.P. 1978: Correlated Mössbauer-SEM studies of coal mineralogy. Scanning Electron Microscopy **1**, 561-568.

Ludwig, K.R. 1999: IsoplotEx 2.6. Berkeley Geochronological Center Publication **1a**.

Larsen, M., Nøhr-Hansen, H., Whitham, A.G., Kelly, S.R.A. 2005: Stratigraphy of the prebasaltic sedimentary succession of the Kangerlussuaq Basin. Volcanic basins of the North Atlantic. Danmarks og Grønlands Geologiske Undersøgelse Rapport **2005/62**.

Morton, A.C., Hallsworth, C.R. 1994: Identifying provenance-specific features of detrital heavy mineral assemblages in sandstones. Sedimentary Geology **90**, 241-256.

Morton, A.C., Claoué-Long, J.C., Berge, C. 1996: SHRIMP constraints on sediment provenance and transport history in the Mesozoic Statford formation, North Sea. Journal of the Geological Society (London) **153**, 915-929.

Morton, A.C., Hallsworth, C.R. 1999: Processes controlling the composition of detrital heavy mineral assemblages in sandstones. Sedimentary Geology **124**, 3-29.

Pearce, N.J., Perkins W.P., Abell, L., Duller, G.A., Fuge, R. 1992: Mineral microanalysis by laser ablation inductively coupled mass spectrometry. Journal of Analytical Atomic Spectroscopy **7**, 53-57.

Pearce, N.J.G., Perkins, W.T., Westgate, J.A., Gorton, M.P., Jackson, S.E., Neal, C.R., Chenery, S.P. 1997: A compilation of new and published trace element data for NIST SRM 610 and NIST SRM 612 glass reference material. Geostandards Newsletters **21**, 115-144.

Sylvester, P., (ed) 2001: Laser-Ablation-ICPMS in the Earth Sciences - principles and applications. Mineralogical Association of Canada Short Course Series **29**.

Sørensen, H.S. 1998: Computer controlled scanning electron microscopy (CCSEM) of heavy minerals. Danmarks og Grønlands Geologiske Undersøgelse Rapport **1998/74**.

Turner, S.P., Platt, J.P., George, R.M.M., Kelly, S.P., Pearson, D.G., Nowell, G.M. 1999: Magmatism associated with orogenic collapse of the Beltic-Alboran domain, SE Spain. Journal of Petrology **40**, 1011-1036.

Zygardlicke, C.J., Steadman, E.N. 1990: Advanced SEM techniques to characterise coal minerals. Scanning Microscopy **4**, 579-590.

Appendix B: Tables and Plates

Appendix B: Tables and Plates Index

Table 1: Samples from the Kangerlussuaq area used in this study (with stratigraphic position and analytical methods applied)

Table 2: Samples from wells in the UK sector of the Faroe-Shetland Basin used in this study (with stratigraphic position and analytical methods applied).

Plate 1: Compilation of garnet compositions determined by CCSEM and EMPA in samples from wells (204/19-3a, 204/24a-7, 205/9-1, 206/1-1a, 214/19-1) in the Faroe-Shetland area

Plate 2: Compilation of garnet compositions (EMPA, CCSEM, CCSEM WR) in the Kangalusuak region

Plate 3: Compilation of detrital zircon age distributions in samples from the Kangerlussuaq area determined by ^{207}Pb-^{206}Pb age dating (LA-Q-ICP-MS).

Plate 4: Compilation of detrital zircon age distributions in samples from wells (204/19-3a, 204/24a-7, 205/9-1, 206/1-1a, 214/19-1) in the UK sector of the Faroe-Shetland determined by ^{207}Pb-^{206}Pb age dating (LA-Q-ICP-MS)

Plate 5: Compilation of detrital zircon age distributions in samples from the Orkneys determined by ^{207}Pb-^{206}Pb age dating (LA-Q-ICP-MS)

Plate 6: Compilation of detrital zircon age distributions determined by U-Pb age dating (SHRIMP)

Table 1: Samples from the Kangerlussuaq area used in this study (with stratigraphic position and analytical methods applied).

Locality	Sample_ID	Sand/mud	Place	Profile	Number in Profile	Group	CCSEM WR Morton	CCSEM Grt	EMPA Grt	Laser Grt	Zircon age
M.9511	413245	SAND	Watkins S	1	4	1	+	+	+	+	++(Elan)
M.9511	413249	mud	Watkins S	1	1	1					
M.9511	413252	mud	Watkins S	1	2	1					
M.9511	413255	SAND	Watkins S (L3)	1	3	1					
M.9511	413257	SAND	Watkins S	1	5	1					
M.9511	413258	mud	Watkins S	1	6	1					
M.0017	455107	SAND	Sandridge	11	1	1					+(Elan)
W.4293	W 4672	SAND	Round Boulder Valley	3	1	1					
W.4293	W 4673	SAND	Round Boulder Valley	3	2	1					
M.9511	413284	SAND	Watkins S (L3)	1	12	2					
M.9511	413288	SAND	Watkins S (L3)	1	9	2					
M.9511	413292	mud	Watkins S	1	7	2					
M.9511	413293	SAND	Watkins S	1	8	2					
M.0017	455112	SAND	Sandridge	11	2	2					++(Elan)
M.0017	455118	SAND	Sandridge	11	3	2					
M.0008	455592	SAND	Watkins S	1	10	2					
M.0008	455593	SAND	Watkins S	1	11	2					
M.0015	455662	mud	Skiferbjerg Basal	2	1	2					
M.0015	455665	mud	Skiferbjerg Basal	2	2	2					
M.0015	455667	mud	Skiferbjerg Basal	2	3	2					
M.0015	455668	SAND	Skiferbjerg basal	2	4	2					
M.0015	455672	SAND	Skiferbjerg basal	2	5	2					
M.0015	455673	mud	Skiferbjerg basal	2	6	2					
M.0015	455676	SAND	Skiferbjerg basal	2	7	2					
M.0015	455677	SAND	Skiferbjerg basal	2	8	2					
W.4275	K 10942	mud	NW Pyramiden	4	1	2					
W.4275	K 10945	SAND	NW Pyramiden	4	2	2					
W.4275	K 10949	mud	NW Pyramiden	4	3	2					
W.4293	K 11335	mud	Round Boulder Valley	3	3	2					
M0015	W 4629	SAND	Sunnigajak Mb.., Albian	28	1	2		+	+	+	+++(Elan)
W.4293	W 4678	SAND	Round Boulder Valley	3	5	2					
W.4293	W 4683	SAND	Round Boulder Valley	3	4	2					
W.4293	W4683	SAND	Round Boulder Valley	3	57,60 m	2					+(Elan)
M.0402	413270	SAND	Watkins Ridge	1	14	3	+				
M.0009	455585	mud	Watkins N	1	13	3					
M.0015	455678	mud	Skiferbjerg Basal	2	9	3					
M.0015	455684	mud	Skiferbjerg	2	10	3					
M.0015	455686	mud	Skiferbjerg	2	11	3					
M.0015	455689	mud	Skiferbjerg Basal	2	12	3					
M.0015	455690	SAND	Skiferbjerg	2	13	3					
M.0015	455692	mud	Skiferbjerg	2	14	3					
M.0015	455695	mud	Skiferbjerg	2	15	3					
W4271	K 10883	mud	Sill City 3 km NE Larsen 3	10	2	3					
W4271	K 10884	mud	Sill City 3 km NE Larsen 3	10	3	3					
W.4275	K 10950	mud	NW Pyramiden	4	4	3					
W.4275	K 11018	mud	NW Pyramiden	4	5	3					
W.4275	K 11019	SAND	NW Pyramiden	4	6	3					
W.4275	K 11024	mud	NW Pyramiden	4	7	3					
W.4275	K 11026	mud	NW Pyramiden	4	8	3					
W.4293	K 11336	mud	Round Boulder Valley	3	6	3					
W.4293	K 11341	mud	Round Boulder Valley	3	7	3					
W.4293	K 11342	mud	Round Boulder Valley	3	8	3					
W.4282	W 4686	mud	NW Pyramiden	4	10	3					
W.4282	W 4692	mud	NW Pyramiden	4	9	3					

Table 1 continued.

Locality	Sample_ID	Sand/mud	Place	Profile	Number in Profile	Group	CCSEM WR Morton	CCSEM Grt	EMPA Grt	Laser Grt	Zircon age
W.4282	W 4696	mud	NW Pyramiden	4	11	3					
W4265	W4653	SAND	3km NE Larsen 3	10	1	3		+	+	+	+(Elan)
M.0012	406752	SAND	Sequoia W	9	1	4	+				
M.0011	406765	mud	Sequoia	9	2	4					
M.9503	413130	mud	Fairytale Valley	6	1	4					
M.9503	413134	mud	Fairytale Valley	6	2	4					
M.0016	455617	mud	Skiferbjerg	2	18	4					
M.0016	455621	mud	Skiferbjerg	2	19	4					
M.0016	455623	mud	Skiferbjerg	2	20	4					
M.0016	455628	mud	Skiferbjerg	2	21	4					
M.0016	455630	mud	Skiferbjerg	2	22	4					
M.0016	455633	mud	Skiferbjerg	2	23	4					
M.0016	455636	SAND	Skiferbjerg	2	24	4	+				+(Elan)
M.0016	455638	mud	Skiferbjerg	2	25	4					
M.0016	455642	mud	Skiferbjerg	2	26	4					
M.0016	455647	mud	Skiferbjerg	2	27	4					
M.0016	455648	SAND	Skiferbjerg	2	28	4	+				
M.0016	455650	mud	Skiferbjerg	2	29	4					
M.0016	455653	mud	Skiferbjerg	2	30	4					
M.0016	455654	mud	Skiferbjerg	2	31	4					
M.0016	455698	mud	Skiferbjerg	2	16	4					
M.0016	455699	mud	Skiferbjerg	2	17	4					
W.4293	K 11343	mud	Round Boulder Valley	3	9	4					
W.4293	K 11344	mud	Round Boulder Valley	3	10	4					
W.4293	W 11352	mud	Round Boulder Valley	3	11	4					
M0407	W 4627	SAND	Christian IV Fm., Maastricht	27	1	4		+	+	+	+++(Elan)
W.4282	W 4704	mud	NW Pyramiden	4	12	4					
W.4282	W 4709	mud	NW Pyramiden	4	13	4					
W.4282	W 4711	mud	NW Pyramiden	4	14	4					
P.2382	W4685	SAND	N sedimentary Mtns	24	1	4					
M.0003	406721	SAND	Ryberg Glacier	7	1	5					
M.0003	406722	mud	Ryberg Glacier	7	2	5					
M.9518	412773	SAND	Sorgenfri	14	1	5	+				+(Elan)
M.9518	412778	SAND	Sorgenfri	14	2	5					
M.9502	413104	mud	Fairytale Valley	6	7	5					
M.9502	413108	mud	Fairytale Valley	6	8	5					
M.9502	413109	SAND	Fairytale Valley	6	9	5					
M.9502	413111	mud	Fairytale Valley	6	10	5					
M.9501	413123	SAND	Fairytale Valley	6	4	5	+				
M.9501	413124	SAND	Fairytale Valley	6	3	5	+	+	+	+	+(Elan)
M.9501	413127	mud	Fairytale Valley	6	5	5					
M.9501	413129	mud	Fairytale Valley	6	6	5					
M.9502	413139	mud	Fairytale Valley	6	11	5					
M.9502	413140	SAND	Fairytale Valley	6	12	5					
M.9502	413142	mud	Fairytale Valley	6	13	5					
M.9502	413143	SAND	Fairytale Valley	6	14	5	+	+	+	+	+(Elan)
M.9502	413145	SAND	Fairytale Valley	6	15	5					
M.9507	413190	SAND	Nansen Fjord	15	1	5	+	+	+	+	+(Elan)
M.9521	413276	SAND	Canyondal	8	4	5	+				
M.0002	455415	mud	Ryberg Fjord	7	3	5					
M.0005	455536	SAND	Canyondal	8	5	5					
M.0005	455570	SAND	Canyondal	8	3	5					
M.0005	455576	mud	Canyondal	8	1	5					
M.0005	455582	mud	Canyondal	8	2	5					

Table 1 continued.

Locality	Sample_ID	Sand/mud	Place	Profile	Number in Profile	Group	CCSEM WR Morton	CCSEM Grt	EMPA Grt	Laser Grt	Zircon age
W4271	K 10892	mud	Sill City 3 km NE Larsen 3	10	4	5					
W4271	K 10894	mud	Sill City 3 km NE Larsen 3	10	8	5					
W4271	K 10895	SAND	Sill City 3 km NE Larsen 3	10	9	5					
W4271	K 10897	mud	Sill City 3 km NE Larsen 3	10	10	5					
W4271	K 10898	SAND	Sill City 3 km NE Larsen 3	10	11	5					
W4271	K 10901	mud	Sill City 3 km NE Larsen 3	10	12	5					
W4312	K 11046	mud	3km ENE Larsen 3	10	5	5					
W4312	K 11047	mud	3km ENE Larsen 3	10	6	5					
W.4312	W4768	SAND	3km ENE Larsen 3	10	7	5					
M.9514	412725	SAND	Vandfaldsdalen NW	12	1	6					
M.9502	413146	SAND	Fairytale Valley	6	17	6	+				
M.9502	413157	SAND	Fairytale Valley	6	16	6					
M.0006	437813	mud	Sødalen	8	6	6					
M.0002	455419	SAND	Ryberg Fjord	7	4	6					
M.0002	455422	SAND	Ryberg Fjord	7	6	6					
M.0002	455423	SAND	Ryberg Fjord	7	5	6	+				+(Elan)
M.0002	455426	mud	Ryberg Fjord	7	7	6					
M.0002	455429	SAND	Ryberg Fjord	7	8	6					
M.0002	455430	SAND	Ryberg Fjord	7	9	6					
M.0002	455432	SAND	Ryberg Fjord	7	10	6					
M.0004	455499	SAND	Willow Pass	17	1	6					+(Elan)
M.0005	455537	SAND	Canyondal	8	7	6	+				+(Elan)
M.0005	455538	mud	Canyondal	8	8	6					
M.0012	406736	SAND	Sequoia W	9	5	7		+	+	+	++(Elan)
M.0011	406774	SAND	Sequoia	9	3	7					
M.9516	412733	SAND	Vandfaldsdalen S	12	2	7	+				
M.9518	412784	SAND	Sorgenfri	14	3	7					++(Elan)
M.9502	413148	SAND	Fairytale Valley	6	18	7					
M.9507	413166	SAND	Nansen Fjord	15	2	7	+				
M.9508	413211	SAND	Korridoren	21	1	7	+	+	+	+	+(Elan)
M.0006	437815	SAND	Sødalen	8	10	7					
M.0002	455431	SAND	Ryberg Fjord	7	12	7					
M.0002	455433	SAND	Ryberg Fjord	7	11	7					
M.0002	455444	SAND	Ryberg Fjord	7	14	7					
M.0005	455539	SAND	Canyondal	8	9	7					
W4232	K10286	SAND	Sequoia	9	4	7		+	+	+	+(Elan)
W4264	K10793	SAND	Klitterhorn	18	1	7		+	+	+	
P2373	W4671	SAND	N sedimentary Mtns	24	2	7		+	+	+	
M0007	P5219	SAND	Schjelderup Member, Jacobsen inlier	26	1	7					+++(Elan)
M.9507	413192	SAND	Nansen Fjord	15	3	8					
M.9510	413230	SAND	Nansen Fjord Reko 1	22	1	8	+	+	+	+	
M.0002	455438	SAND	Ryberg Fjord	7	17	8		+	+	+	
M.0002	455440	SAND	Ryberg Fjord	7	13	8					+(Elan)
M.0002	455448	mud	Ryberg Fjord	7	15	8					
M.0002	455451	SAND	Ryberg Fjord	7	16	8					
M.0002	455452	mud	Ryberg Fjord	7	18	8					
M.0002	455455	mud	Ryberg Fjord	7	19	8					
M.0002	455457	SAND	Ryberg Fjord	7	20	8					
M.0002	455458	SAND	Ryberg Fjord	7	22	8					
M.0004	455516	SAND	Willow Pass	17	2	8					
M.0011	406775	mud	Sequoia	9	6	9					
M.0011	406778	mud	Sequoia	9	7	9					
M.0011	406779	SAND	Sequoia	9	8	9					
M.0011	406780	mud	Sequoia	9	9	9					
M.0011	406781	SAND	Sequoia	9	10	9					
M.9502	413152	SAND	Fairytale Valley	6	19	9					

Table 1 continued.

Locality	Sample_ID	Sand/mud	Place	Profile	Number in Profile	Group	CCSEM WR Morton	CCSEM Grt	EMPA Grt	Laser Grt	Zircon age
M.0002	455462	SAND	Ryberg Fjord	7	24	9	+				+(Elan)
M.0002	455463	mud	Ryberg Fjord	7	21	9					
M.0006	455550	SAND	Sødalen	8	11	9	+	+	+	+	+(Elan)
M.0010	455606	mud	Sequoia NNP	9	11	9					
M.0010	455610	mud	Sequoia NNP	9	12	9					
M.0011	455612	mud	Sequoia	9	13	9					
M.0010	455613	SAND	Sequoia NNP	9	14	9	+				
X.2001	459679	SAND	Kap Dalton	100	1	10	+	+	+	+	+(Elan)
X.2001	459682	SAND	Kap Dalton	100	2	10	+	+	+	+	+(Elan)
X.2001	459717	SAND	Savoia Halvø	100	3	10	+				

Table 2: Samples from wells in the UK sector of the Faroe-Shetland Basin used in this study (with stratigraphic position and analytical methods applied).

Locality	Sample ID	Group	Fm.		Unit	CCSEM Grt	EMPA Grt	Laser Grt	Zircon age
204/19-3a	2911	Late Maastrichtian,	Formation E		1				
204/19-3a	2938	Late Maastrichtian,			1				
204/24a-7	2904	Late Maastrichtian,			1				
204/24a-7	2934	Late Maastrichtian,			1				
205/9-1	4700	Late Maastrichtian,			1				
204/19-3a	2821	Early Paleocene, Shetland Group, Danian Sands Formation	Sullom	S1	2				
204/19-3a	2851	Early Paleocene, Shetland Group, Danian Sands Formation	Sullom	S1	2				
204/19-3a	2881	Early Paleocene, Shetland Group, Danian Sands Formation	Sullom	S1	2				
204/24a-7	2631	Early Paleocene, Shetland Group, Danian Sands Formation	Sullom	S2	2				
204/24a-7	2661	Early Paleocene, Shetland Group, Danian Sands Formation	Sullom	S2	2				
204/24a-7	2694	Early Paleocene, Shetland Group, Danian Sands Formation	Sullom	S2	2				
204/24a-7	2721	Early Paleocene, Shetland Group, Danian Sands Formation	Sullom	S1	2				
204/24a-7	2753	Early Paleocene, Shetland Group, Danian Sands Formation	Sullom	S1	2				
204/24a-7	2784	Early Paleocene, Shetland Group, Danian Sands Formation	Sullom	S1	2				
204/24a-7	2814	Early Paleocene, Shetland Group, Danian Sands Formation	Sullom	S1	2				
204/24a-7	2844	Early Paleocene, Shetland Group, Danian Sands Formation	Sullom	S1	2				
204/24a-7	2874	Early Paleocene, Shetland Group, Danian Sands Formation	Sullom	S1	2				
205/9-1	4643	Danian, Shetland Group	Sullom	S1	2				
205/9-1	4670	Danian, Shetland Group	Sullom	S1	2				
206/1-1a	9150	Early Paleocene, Shetland Group	Sullom	S1	2				
214/19-1	4521	Middel to Early Paleocene, Montrose Group, 'T10' Palynological marker	Sullom	S2	2				
214/19-1	4551	Middel to Early Paleocene, Montrose Group, 'T10' Palynological marker	Sullom	S2	2				
214/19-1	4581	Middel to Early Paleocene, Montrose Group, 'T10' Palynological marker	Sullom	S2	2				
214/19-1	4614	Middel to Early Paleocene, Montrose Group, 'T10' Palynological marker	Sullom	S2	2				
214/19-1	4644	Middel to Early Paleocene, Montrose Group, 'T10' Palynological marker	Sullom	S2	2				
214/19-1	4674	Middel to Early Paleocene, Montrose Group, 'T10' Palynological marker	Sullom	S2	2				
214/19-1	4707	Middel to Early Paleocene, Montrose Group, 'T10' Palynological marker	Sullom	S2	2				
214/19-1	4737	Middel to Early Paleocene, Montrose Group, 'T10' Palynological marker	Sullom	S2	2				
214/19-1	4767	Middel to Early Paleocene, Montrose Group, 'T10' Palynological marker	Sullom	S2	2				
214/19-1	4797	Early Paleocene, Montrose Group, 'T10' Palynological marker	Sullom	S1	2				
214/19-1	4827	Early Paleocene, Montrose Group, 'T10' Palynological marker	Sullom	S1	2				
214/19-1	4863	Early Paleocene, Montrose Group, 'T10' Palynological marker	Sullom	S1	2				
204/19-3a	2190.8	Late Paleocene, Montrose Group, Lista Formation	Vaila	V4	3				
204/19-3a	2218.8	Late Paleocene, Montrose Group, Lista Formation	Vaila	V4	3				
204/19-3a	2251.3	Late Paleocene, Montrose Group, Lista Formation	Vaila	V4	3	+	+	+	
204/19-3a	2281	Late Paleocene, Montrose Group, Lista Formation	Vaila	V4	3				
204/19-3a	2311	Late Paleocene, Montrose Group, Lista Formation	Vaila	V3	3				
204/19-3a	2341	Late Paleocene, Montrose Group, Lista Formation	Vaila	V3	3				
204/19-3a	2371	Late Paleocene, Montrose Group, Lista Formation	Vaila	V3	3				
204/19-3a	2401	Late Paleocene, Montrose Group, Maureen Formation Equiavalent	Vaila	V2	3	+	+	+	
204/19-3a	2431	Late Paleocene, Montrose Group, Maureen Formation Equiavalent	Vaila	V2	3				

Table 2 contiuned.

Locality	Sample ID	Group	Fm.	Unit	CCSEM Grt	EMPA Grt	Laser Grt	Zircon age
204/19-3a	2461	Late Paleocene, Montrose Group, Maureen Formation Equiavalent	Vaila	V2	3			
204/19-3a	2491	Late Paleocene, Montrose Group,Maureen Formation Equiavalent	Vaila	V2	3			
204/19-3a	2521	Late Paleocene, Montrose Group,Maureen Formation Equiavalent	Vaila	V2	3			
204/19-3a	2551	Late Paleocene, Montrose Group, Maureen Formation Equiavalent	Vaila	V2	3	+	+	+	
204/19-3a	2581	Late Paleocene, Montrose Group, Maureen Formation Equiavalent	Vaila	V2	3				
204/19-3a	2611	Late Paleocene, Montrose Group, Maureen Formation Equiavalent	Vaila	V1	3				
204/19-3a	2641	Late Paleocene, Montrose Group, Maureen Formation Equiavalent	Vaila	V1	3				
204/19-3a	2671	Late Paleocene, Montrose Group, Maureen Formation Equiavalent	Vaila	V1	3	+	+	+	
204/19-3a	2701	Late Paleocene, Montrose Group, Maureen Formation Equiavalent	Vaila	V1	3				
204/19-3a	2731	Late Paleocene, Montrose Group, Maureen Formation Equiavalent	Vaila	V1	3				
204/19-3a	2761	Late Paleocene, Montrose Group, Maureen Formation Equiavalent	Vaila	V1	3	+	+	+	
204/19-3a	2791	Late Paleocene, Montrose Group, Maureen Formation Equiavalent	Vaila	V1	3				
204/24a-7	2090.8	Late Paleocene, Montrose Group, Lista Formation	Vaila	V4	3	+	+	+	
204/24a-7	2121.5	Late Paleocene, Montrose Group, Lista Formation	Vaila	V4	3				
204/24a-7	2182.3	Late Paleocene, Montrose Group, Lista Formation	Vaila	V4	3				
204/24a-7	2210	Late Paleocene, Montrose Group, Lista Formation	Vaila	V3	3				
204/24a-7	2240.5	Late Paleocene, Montrose Group, Lista Formation	Vaila	V3	3	+	+	+	
204/24a-7	2271	Late Paleocene, Montrose Group, Lista Formation	Vaila	V3	3				
204/24a-7	2301	Late Paleocene, Montrose Group, Lista Formation	Vaila	V3	3				
204/24a-7	2331	Late Paleocene, Montrose Group, Maureen Formation Equivalent	Vaila	V2	3				
204/24a-7	2361	Late Paleocene, Montrose Group, Maureen Formation Equivalent	Vaila	V2	3				
204/24a-7	2391	Late Paleocene, Montrose Group, Maureen Formation Equivalent	Vaila	V2	3				
204/24a-7	2421	Late Paleocene, Montrose Group, Maureen Formation Equivalent	Vaila	V2	3				
204/24a-7	2448	Late Paleocene, Montrose Group, Maureen Formation Equivalent	Vaila	V2	3				
204/24a-7	2478	Late Paleocene, Montrose Group, Maureen Formation Equivalent	Vaila	V1	3				
204/24a-7	2505	Late Paleocene, Montrose Group, Maureen Formation Equivalent	Vaila	V1	3				
204/24a-7	2541	Late Paleocene, Montrose Group, Maureen Formation Equivalent	Vaila	V1	3				
204/24a-7	2571	Late Paleocene, Montrose Group, Maureen Formation Equivalent	Vaila	V1	3				
204/24a-7	2607	Late Paleocene, Montrose Group, Maureen Formation Equivalent	Vaila	V1	3				
205/9-1	3680	Thanetian, Montrose Group, Lista Formation, D1 sand unit	Vaila	V4	3				
205/9-1	3712.1	Thanetian, Montrose Group, Lista Formation, D1 sand unit	Vaila	V4	3				+(Elan)
205/9-1	3740	Thanetian, Montrose Group, Lista Formation, D1 sand unit	Vaila	V4	3				
205/9-1	3770	Thanetian, Montrose Group, Lista Formation, D1 sand unit	Vaila	V4	3				
205/9-1	3800	Thanetian, Montrose Group, Lista Formation, D1 sand unit	Vaila	V4	3				
205/9-1	3830	Thanetian, Montrose Group, Lista Formation, D1 sand unit	Vaila	V4	3				
205/9-1	3860	Thanetian, Montrose Group, Lista Formation, D1 sand unit	Vaila	V4	3				
205/9-1	3890	Thanetian, Montrose Group, Lista Formation, D1 sand unit	Vaila	V4	3	+	+	+	
205/9-1	3920	Thanetian, Montrose Group, Lista Formation, D1 sand unit	Vaila	V4	3				
205/9-1	3950	Thanetian, Montrose Group, Lista Formation, D1 sand unit	Vaila	V4	3				
205/9-1	3980	Thanetian, Montrose Group, Lista Formation, D1 sand unit	Vaila	V4	3				
205/9-1	4010	Thanetian, Montrose Group, Lista Formation, D1 sand unit	Vaila	V4	3				
205/9-1	4040	Thanetian, Montrose Group, Lista Formation, D1 sand unit	Vaila	V3	3				
205/9-1	4070	Thanetian, Montrose Group, Lista Formation, D1 sand unit	Vaila	V3	3	+	+	+	+(Elan)
205/9-1	4100	Thanetian, Montrose Group, Lista Formation, D1 sand unit	Vaila	V3	3				
205/9-1	4130	Thanetian, Montrose Group, Lista Formation, D1 sand unit	Vaila	V3	3				
205/9-1	4160	Thanetian, Montrose Group, Lista Formation, D1 sand unit	Vaila	V3	3				
205/9-1	4190	Thanetian, Montrose Group, Lista Formation, D1 sand unit	Vaila	V3	3				
205/9-1	4220	Thanetian, Montrose Group, Lista Formation, D1 sand unit	Vaila	V3	3				
205/9-1	4250	Thanetian, Montrose Group, Lista Formation, D1 sand unit	Vaila	V3	3				
205/9-1	4280	Thanetian, Montrose Group, Lista Formation, D1 sand unit	Vaila	V3	3				
205/9-1	4310	Thanetian, Montrose Group, Lista Formation, D1 sand unit	Vaila	V3	3				
205/9-1	4340	Thanetian, Montrose Group, Lista Formation, D1 sand unit	Vaila	V3	3				

Table 2 contiuned.

Locality	Sample ID	Group	Fm.		Unit	CCSEM Grt	EMPA Grt	Laser Grt	Zircon age
205/9-1	4370	Thanetian, Montrose Group, Lista Formation, D1 sand unit	Vaila	V3	3				
205/9-1	4400	Thanetian, Montrose Group, Maureen Formation	Vaila	V2	3				
205/9-1	4430	Thanetian, Montrose Group, Maureen Formation	Vaila	V2	3				
205/9-1	4460	Thanetian, Montrose Group, Maureen Formation, E sand unit	Vaila	V1	3				
205/9-1	4490	Thanetian, Montrose Group, Maureen Formation, E sand unit	Vaila	V1	3				
205/9-1	4520	Thanetian, Montrose Group, Maureen Formation, E sand unit	Vaila	V1	3				
205/9-1	4550	Danian, Montrose Group, Maureen Formation, E sand unit	Vaila	V1	3				
205/9-1	4580	Danian, Montrose Group, Maureen Formation, E sand unit	Vaila	V1	3				
205/9-1	4610	Danian, Montrose Group, Maureen Formation, E sand unit	Vaila	V1	3				
206/1-1a	8090	Late Paleocene, Montrose Group, Andrew Formation	Vaila	V4	3				
206/1-1a	8180	Late Paleocene, Montrose Group, Andrew Formation	Vaila	V4	3				
206/1-1a	8310	Late Paleocene, Montrose Group, Andrew Formation	Vaila	V4	3				
206/1-1a	8390	Late Paleocene, Montrose Group, Andrew Formation	Vaila	V4	3				
206/1-1a	8490	Late Paleocene, Montrose Group, Andrew Formation	Vaila	V3	3				
206/1-1a	8600	Late Paleocene, Montrose Group, Andrew Formation	Vaila	V3	3				
206/1-1a	8690	Late Paleocene, Montrose Group, Maureen Formation	Vaila	V2	3				
206/1-1a	8810	Late Paleocene, Montrose Group, Maureen Formation	Vaila	V2	3				
206/1-1a	8910	Early Paleocene, Montrose Group, Maureen Formation	Vaila	V1	3				
206/1-1a	9020	Early Paleocene, Montrose Group, Maureen Formation	Vaila	V1	3				
214/19-1	3702	Middel Paleocene, Montrose Group, 'T35' Palynological marker	Vaila	V4	3				
214/19-1	3732	Middel Paleocene, Montrose Group, 'T35' Palynological marker	Vaila	V4	3				
214/19-1	3762	Middel Paleocene, Montrose Group, 'T35' Palynological marker	Vaila	V4	3				
214/19-1	3798	Middel Paleocene, Montrose Group, 'T34' Palynological marker	Vaila	V4	3				
214/19-1	3828	Middel Paleocene, Montrose Group, 'T34' Palynological marker	Vaila	V4	3				
214/19-1	3852	Middel Paleocene, Montrose Group, 'T34' Palynological marker	Vaila	V4	3				
214/19-2	3876	Middel to Early Paleocene, Montrose Group, 'T32' Palynological marker	Vaila	V3	3				+(Elan)
214/19-1	3900	Middel to Early Paleocene, Montrose Group, 'T32' Palynological marker	Vaila	V3	3				
214/19-1	3930	Middel to Early Paleocene, Montrose Group, 'T31' Palynological marker	Vaila	V3	3				
214/19-1	3960	Middel to Early Paleocene, Montrose Group, 'T31' Palynological marker	Vaila	V3	3				
214/19-1	3990	Middel to Early Paleocene, Montrose Group, 'T28' Palynological marker	Vaila	V2	3				
214/19-1	4020	Middel to Early Paleocene, Montrose Group, 'T28' Palynological marker	Vaila	V2	3				
214/19-1	4050	Middel to Early Paleocene, Montrose Group, 'T22' Palynological marker	Vaila	V1	3				
214/19-1	4080	Middel to Early Paleocene, Montrose Group, 'T22' Palynological marker	Vaila	V1	3				
214/19-1	4140	Middel to Early Paleocene, Montrose Group, 'T22' Palynological marker	Vaila	V1	3				
214/19-1	4170	Middel to Early Paleocene, Montrose Group, 'T22' Palynological marker	Vaila	V1	3				
214/19-1	4200	Middel to Early Paleocene, Montrose Group, 'T22' Palynological marker	Vaila	V1	3				
214/19-1	4230	Middel to Early Paleocene, Montrose Group, 'T22' Palynological marker	Vaila	V1	3				+(Elan)
214/19-1	4260	Middel to Early Paleocene, Montrose Group, 'T22' Palynological marker	Vaila	V1	3				
214/19-1	4290	Middel to Early Paleocene, Montrose Group, 'T22' Palynological marker	Vaila	V1	3				
214/19-1	4320	Middel to Early Paleocene, Montrose Group, 'T22' Palynological marker	Vaila	V1	3				
214/19-1	4350	Middel to Early Paleocene, Montrose Group, 'T22' Palynological marker	Vaila	V1	3				

Table 2 contiuned.

Locality	Sample ID	Group	Fm.		Unit	CCSEM Grt	EMPA Grt	Laser Grt	Zircon age
214/19-1	4380	Middel to Early Paleocene, Montrose Group, 'T22' Palynological marker	Vaila	V1	3				
214/19-1	4404	Middel to Early Paleocene, Montrose Group, 'T22' Palynological marker	Vaila	V1	3				
214/19-1	4431	Middel to Early Paleocene, Montrose Group, 'T22' Palynological marker	Vaila	V1	3				+(Elan)
214/19-1	4461	Middel to Early Paleocene, Montrose Group, 'T22' Palynological marker	Vaila	V1	3				
214/19-1	4491	Middel to Early Paleocene, Montrose Group, 'T22' Palynological marker	Vaila	V1	3				
204/19-3a	2070	Late Paleocene, Montrose Group, Lista Formation	Kettla		4				
204/19-3a	2101	Late Paleocene, Montrose Group, Lista Formation	Kettla		4				
204/19-3a	2161	Late Paleocene, Montrose Group, Lista Formation	Kettla		4				
204/24a-7	2034	Late Paleocene, Montrose Group, Lista Formation	Kettla		4				
204/24a-7	2061	Late Paleocene, Montrose Group, Lista Formation	Kettla		4				
205/9-1	3470.2	Thanetian, Montrose Group, Lista Formation, Andrew Tuff member	Ketla		4				++Elan
205/9-1	3500	Thanetian, Montrose Group, Lista Formation, Andrew Tuff member	Ketla		4				
205/9-1	3530	Thanetian, Montrose Group, Lista Formation, Andrew Tuff member	Ketla		4				
205/9-1	3560	Thanetian, Montrose Group, Lista Formation, Andrew Tuff member	Ketla		4				
205/9-1	3590	Thanetian, Montrose Group, Lista Formation, Andrew Tuff member	Ketla		4				
205/9-1	3609	Thanetian, Montrose Group, Lista Formation, Andrew Tuff member	Ketla		4	+	+	+	
205/9-1	3650	Thanetian, Montrose Group, Lista Formation, Andrew Tuff member	Ketla		4				
204/19-3a	1770	Late Paleocene, Montrose Group, Lista Formation	Lamba	L2	5				
204/19-3a	1798	Late Paleocene, Montrose Group, Lista Formation	Lamba	L2	5				
204/19-3a	1831	Late Paleocene, Montrose Group, Lista Formation	Lamba	L2	5				
204/19-3a	1864	Late Paleocene, Montrose Group, Lista Formation	Lamba	L2	5				
204/19-3a	1894	Late Paleocene, Montrose Group, Lista Formation	Lamba	L2	5				
204/19-3a	1921	Late Paleocene, Montrose Group, Lista Formation	Lamba	L2	5				
204/19-3a	1944.2	Late Paleocene, Montrose Group, Lista Formation	Lamba	L1	5				++(Elan)
204/19-3a	1981	Late Paleocene, Montrose Group, Lista Formation	Lamba	L1	5				
204/19-3a	2012	Late Paleocene, Montrose Group, Lista Formation	Lamba	L1	5				
204/19-3a	2038.9	Late Paleocene, Montrose Group, Lista Formation	Lamba	L1	5	+	+	+	+(Elan)
204/24a-7	1525	Late Paleocene, Montrose Group, Lista Formation	Lamba	L2	5				
204/24a-7	1555	Late Paleocene, Montrose Group, Lista Formation	Lamba	L2	5				
204/24a-7	1585	Late Paleocene, Montrose Group, Lista Formation	Lamba	L2	5				
204/24a-7	1615	Late Paleocene, Montrose Group, Lista Formation	Lamba	L2	5				
204/24a-7	1645	Late Paleocene, Montrose Group, Lista Formation	Lamba	L2	5				
204/24a-7	1675	Late Paleocene, Montrose Group, Lista Formation	Lamba	L2	5				
204/24a-7	1705	Late Paleocene, Montrose Group, Lista Formation	Lamba	L2	5				
204/24a-7	1735	Late Paleocene, Montrose Group, Lista Formation	Lamba	L2	5				
204/24a-7	1765	Late Paleocene, Montrose Group, Lista Formation	Lamba	L2	5				
204/24a-7	1795	Late Paleocene, Montrose Group, Lista Formation	Lamba	L2	5				
204/24a-7	1825	Late Paleocene, Montrose Group, Lista Formation	Lamba	L1	5				
204/24a-7	1855	Late Paleocene, Montrose Group, Lista Formation	Lamba	L1	5				
204/24a-7	1880	Late Paleocene, Montrose Group, Lista Formation	Lamba	L1	5				
204/24a-7	1910	Late Paleocene, Montrose Group, Lista Formation	Lamba	L1	5				
204/24a-7	1940	Late Paleocene, Montrose Group, Lista Formation	Lamba	L1	5				
204/24a-7	1970	Late Paleocene, Montrose Group, Lista Formation	Lamba	L1	5				
204/24a-7	2001	Late Paleocene, Montrose Group, Lista Formation	Lamba	L1	5				

Table 2 contiuned.

Locality	Sample ID	Group	Fm.		Unit	CCSEM Grt	EMPA Grt	Laser Grt	Zircon age
205/9-1	3080	Thanetian, Montrose Group, Lista Formation	Lamba	L2	5				
205/9-1	3110	Thanetian, Montrose Group, Lista Formation	Lamba	L2	5				
205/9-1	3140	Thanetian, Montrose Group, Lista Formation, C1 sand unit	Lamba	L2	5				
205/9-1	3170	Thanetian, Montrose Group, Lista Formation, C1 sand unit	Lamba	L2	5				
205/9-1	3200	Thanetian, Montrose Group, Lista Formation, C1 sand unit	Lamba	L2	5				
205/9-1	3230	Thanetian, Montrose Group, Lista Formation, C1 sand unit	Lamba	L2	5				
205/9-1	3260	Thanetian, Montrose Group, Lista Formation, C1 sand unit	Lamba	L1	5				
205/9-1	3290	Thanetian, Montrose Group, Lista Formation, C1 sand unit	Lamba	L1	5				
205/9-1	3320	Thanetian, Montrose Group, Lista Formation, C1 sand unit	Lamba	L1	5				
205/9-1	3350	Thanetian, Montrose Group, Lista Formation, C1 sand unit	Lamba	L1	5				
205/9-1	3380	Thanetian, Montrose Group, Lista Formation, C1 sand unit	Lamba	L1	5				
205/9-1	3410	Thanetian, Montrose Group, Lista Formation, C1 sand unit	Lamba	L1	5				
205/9-1	3440	Thanetian, Montrose Group, Lista Formation, C1 sand unit	Lamba	L1	5				
214/19-1	3252	Upper Paleocene, Montrose Group, 'T38' Palynological marker	Lamba	L2	5				
214/19-1	3282	Upper Paleocene, Montrose Group, 'T38' Palynological marker	Lamba	L2	5				
214/19-1	3312	Upper Paleocene, Montrose Group, 'T38' Palynological marker	Lamba	L2	5				
214/19-1	3342	Upper Paleocene, Montrose Group, 'T38' Palynological marker	Lamba	L2	5				
214/19-1	3375	Middel Paleocene, Montrose Group, 'T38' Palynological marker	Lamba	L2	5				
214/19-1	3402	Middel Paleocene, Montrose Group, 'T38' Palynological marker	Lamba	L1	5				
214/19-1	3432	Middel Paleocene, Montrose Group, 'T38' Palynological marker	Lamba	L1	5				
214/19-1	3462	Middel Paleocene, Montrose Group, 'T36' Palynological marker	Lamba	L1	5				
214/19-1	3492	Middel Paleocene, Montrose Group, 'T36' Palynological marker	Lamba	L1	5				
214/19-1	3522	Middel Paleocene, Montrose Group, 'T36' Palynological marker	Lamba	L1	5				
214/19-1	3552	Middel Paleocene, Montrose Group, 'T36' Palynological marker	Lamba	L1	5				
214/19-1	3582	Middel Paleocene, Montrose Group, 'T36' Palynological marker	Lamba	L1	5				
214/19-1	3615	Middel Paleocene, Montrose Group, 'T36' Palynological marker	Lamba	L1	5				
214/19-1	3645	Middel Paleocene, Montrose Group, 'T36' Palynological marker	Lamba	L1	5				
214/19-1	3672	Middel Paleocene, Montrose Group, 'T36' Palynological marker	Lamba	L1	5				
205/9-1	2330	Ypresian, Moray Group, Sele Formation	Flett		6				
206/1-1a	6930	Late Paleocene, Moray Group, Sele Formation	Flett	F2	6				
206/1-1a	7020	Late Paleocene, Moray Group, Sele Formation	Flett	F2	6				
206/1-1a	7170	Late Paleocene, Moray Group, Sele Formation	Flett	F2	6				+(Elan)
206/1-1a	7230	Late Paleocene, Moray Group, Sele Formation	Flett	F2	6				
206/1-1a	7320	Late Paleocene, Moray Group, Sele Formation	Flett	F2	6				
206/1-1a	7450	Late Paleocene, Moray Group, Sele Formation	Flett	F1	6				
206/1-1a	7558	Late Paleocene, Moray Group, Sele Formation	Flett	F1	6	+	+	+	+(Elan)
206/1-1a	7653.8	Late Paleocene, Moray Group, Sele Formation	Flett	F1	6	+	+	+	+(Elan)
206/1-1a	7740	Late Paleocene, Moray Group, Sele Formation	Flett	F1	6	+	+	+	+(Elan)
206/1-1a	7789	Late Paleocene, Moray Group, Sele Formation	Flett	F1	6	+	+	+	+(Elan)
206/1-1a	7910	Late Paleocene, Montrose Group, Forties Formation	Flett	F1	6				
206/1-1a	7990	Late Paleocene, Montrose Group, Forties Formation	Flett	F1	6				
214/19-1	3009	Lower Eocene, Rogaland Group, Sele (? 'T45')	Flett	F3	6				
214/19-1	3039	Upper Paleocene, Montrose Group, 'T40' Palynological marker	Flett	F2	6				
214/19-1	3069	Upper Paleocene, Montrose Group, 'T40' Palynological marker	Flett	F2	6				
214/19-1	3102	Upper Paleocene, Montrose Group, 'T40' Palynological marker	Flett	F1	6				
214/19-1	3132	Upper Paleocene, Montrose Group, 'T40' Palynological marker	Flett	F1	6				
214/19-1	3162	Upper Paleocene, Montrose Group, 'T40' Palynological marker	Flett	F1	6				
214/19-1	3192	Upper Paleocene, Montrose Group, 'T40' Palynological marker	Flett	F1	6				
214/19-1	3222	Upper Paleocene, Montrose Group, 'T40' Palynological marker	Flett	F1	6				
204/19-3a	1470	Early Eocene, Balder formation	Balder		7				
204/19-3a	1500	Early Eocene, Balder formation	Balder		7	+	+	+	+(Elan)

Table 2 contiuned.

Locality	Sample ID	Group	Fm.	Unit	CCSEM Grt	EMPA Grt	Laser Grt	Zircon age
204/19-3a	1530	Early Eocene, Balder formation	Balder	7				
204/19-3a	1560	Early Eocene, Balder formation	Balder	7				
204/19-3a	1590	Early Eocene, Balder formation	Balder	7				
204/19-3a	1620	Early Eocene, Balder formation	Balder	7				
204/19-3a	1650	Early Eocene, Balder formation	Balder	7				
204/19-3a	1680	Early Eocene, Balder formation	Balder	7				
204/19-3a	1710	Early Eocene, Balder formation	Balder	7	+	+	+	+(Elan)
204/24a-7	1405	Early Eocene, Balder formation	Balder	7	+	+	+	+(Elan)
204/24a-7	1435	Early Eocene, Balder formation	Balder	7				
204/24a-7	1465	Early Eocene, Balder formation	Balder	7				
204/24a-7	1495	Early Eocene, Balder formation	Balder	7				
205/9-1	2300	Ypresian, Moray Group, Balder Formation	Balder	7				
206/1-1a	6750	Late Paleocene, Moray Group, Balder Formation	Balder	7				
206/1-1a	6830	Late Paleocene, Moray Group, Balder Formation	Balder	7				
214/19-1	2965	Lower Eocene, Rogaland Group, Balder ('T 50' marker)	Balder	7				
214/19-1	2980	Lower Eocene, Rogaland Group, Balder ('T 50' marker)	Balder	7				
205/9-1	2360	Ypresian, Moray Group, Upper Paleocene deltas	UPD	8				
205/9-1	2390	Ypresian, Moray Group, Upper Paleocene deltas	UPD	8	+	+	+	+(Elan)
205/9-1	2420	Ypresian, Moray Group, Upper Paleocene deltas	UPD	8				
205/9-1	2450	Ypresian, Moray Group, Upper Paleocene deltas	UPD	8				
205/9-1	2480	Ypresian, Moray Group, Upper Paleocene deltas	UPD	8				
205/9-1	2507	Ypresian, Moray Group, Upper Paleocene deltas	UPD	8				
205/9-1	2540	Ypresian, Moray Group, Upper Paleocene deltas	UPD	8				
205/9-1	2570	Thanetian, Moray Group, Upper Paleocene deltas		8				
205/9-1	2600	Thanetian, Moray Group, Upper Paleocene deltas		8				
205/9-1	2633	Thanetian, Moray Group, Upper Paleocene deltas		8				
205/9-1	2660	Thanetian, Moray Group, Upper Paleocene deltas		8				
205/9-1	2690	Thanetian, Moray Group, Upper Paleocene deltas		8				
205/9-1	2720	Thanetian, Moray Group, Upper Paleocene deltas		8				
205/9-1	2750	Thanetian, Moray Group, Upper Paleocene deltas		8				
205/9-1	2780	Thanetian, Moray Group, Upper Paleocene deltas		8				
205/9-1	2810	Thanetian, Moray Group, Upper Paleocene deltas		8				
205/9-1	2840	Thanetian, Moray Group, Upper Paleocene deltas		8				
205/9-1	2870	Thanetian, Moray Group, Upper Paleocene deltas		8				
205/9-1	2900	Thanetian, Moray Group, Upper Paleocene deltas		8				
205/9-1	2930	Thanetian, Moray Group, Upper Paleocene deltas		8				
205/9-1	2960	Thanetian, Moray Group, Upper Paleocene deltas		8				
205/9-1	2990	Thanetian, Moray Group, Upper Paleocene deltas		8				
205/9-1	3020	Thanetian, Moray Group, Upper Paleocene deltas		8				
205/9-1	3050	Thanetian, Moray Group, Upper Paleocene deltas		8				

Plate 1: Compilation of garnet compositions determined by CCSEM and EMPA in samples from wells (204/19-3a, 204/24a-7, 205/9-1, 206/1-1a, 214/19-1) in the Faroe-Shetland area.

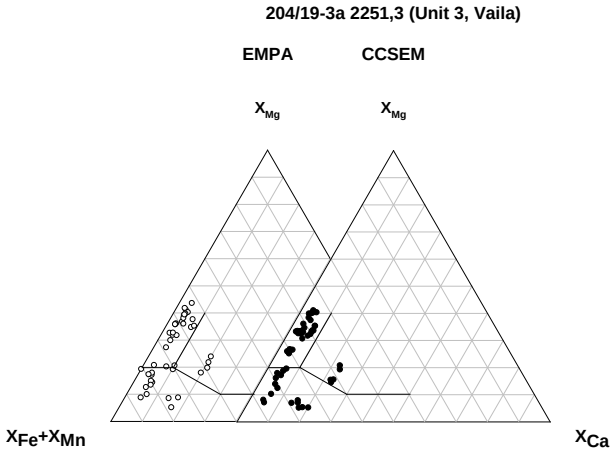

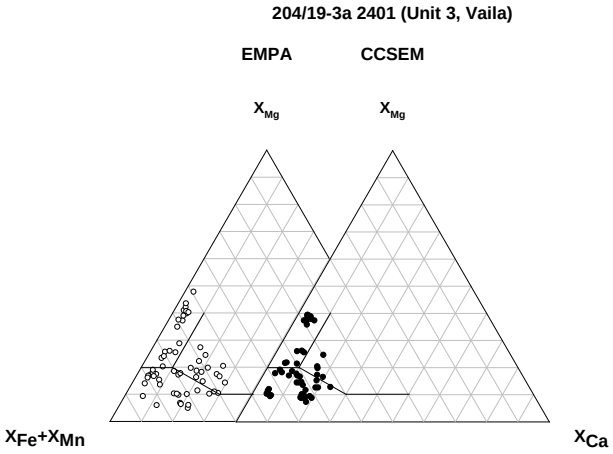

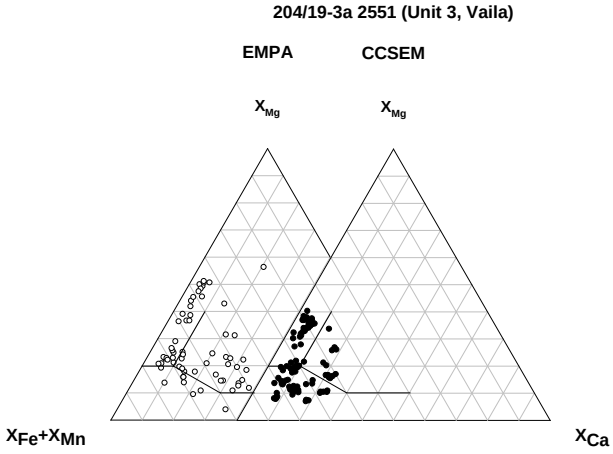

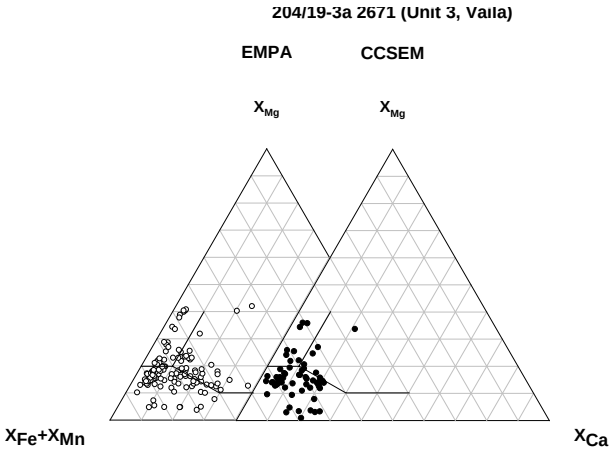

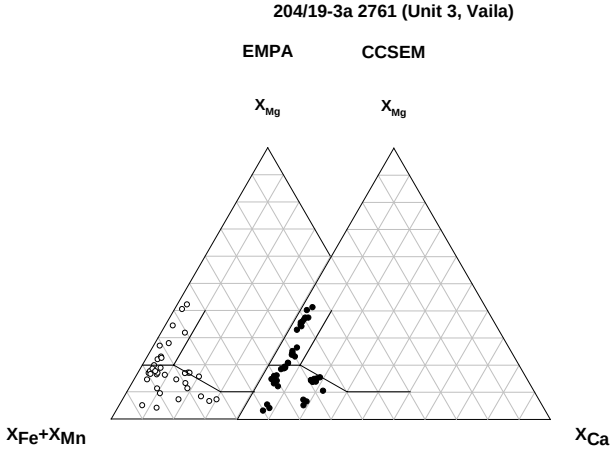

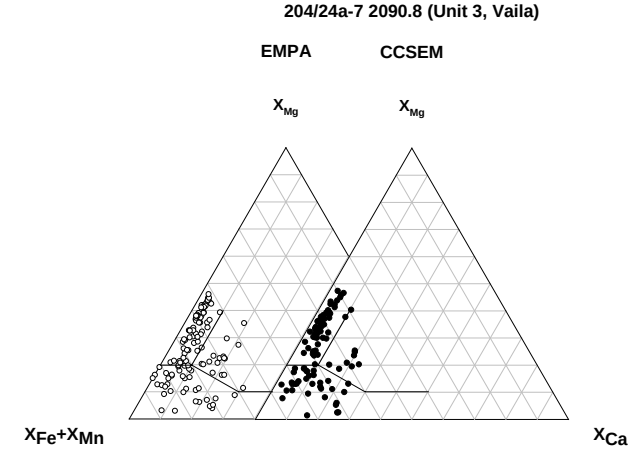

Plate 1 continued

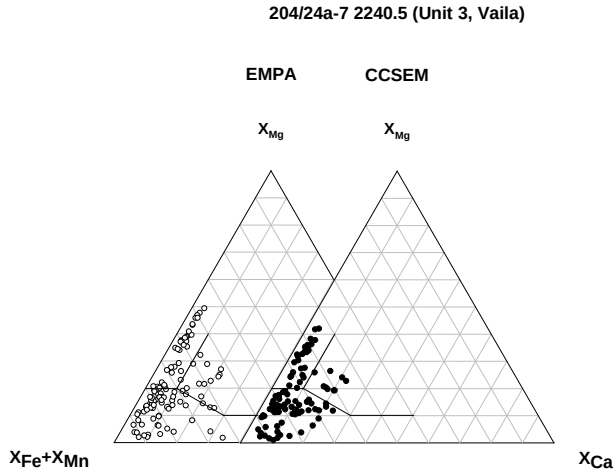

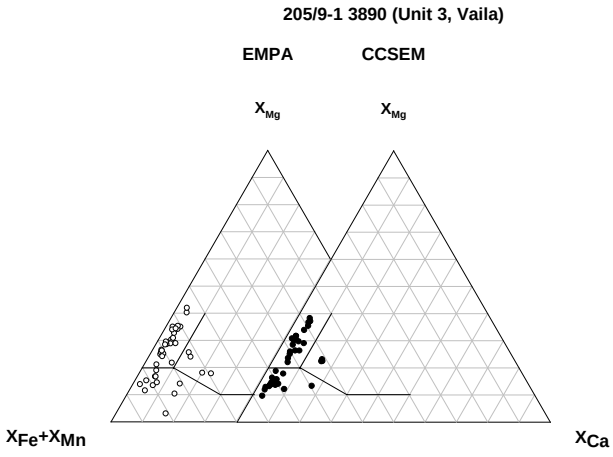

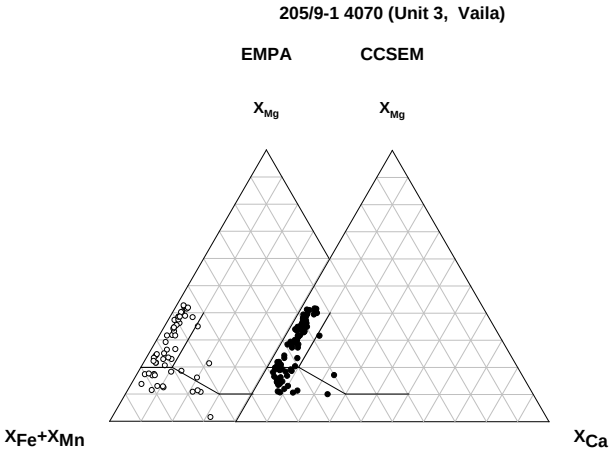

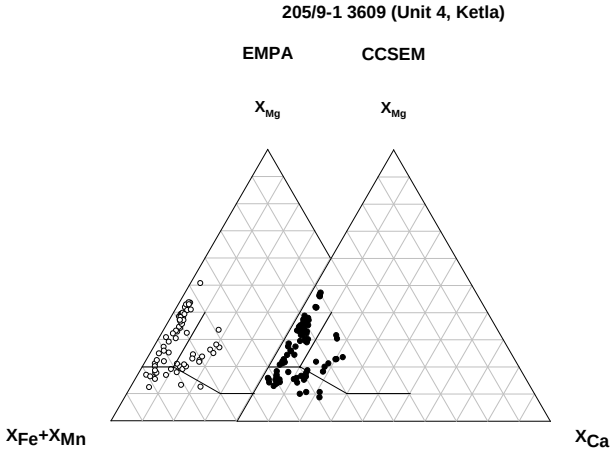

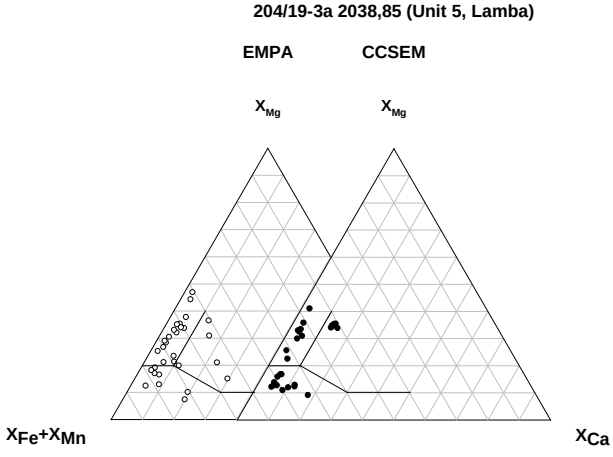

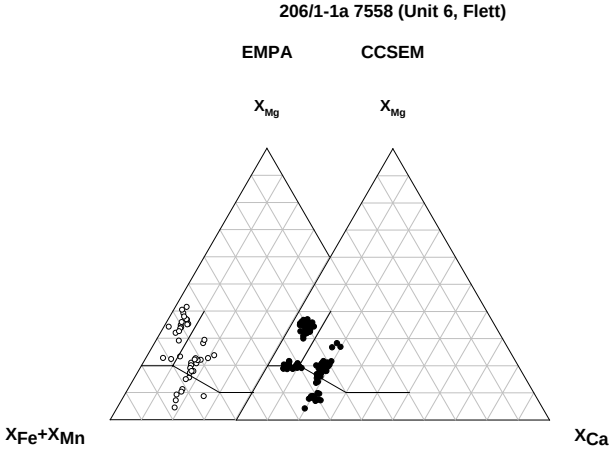

Plate 1 continued.

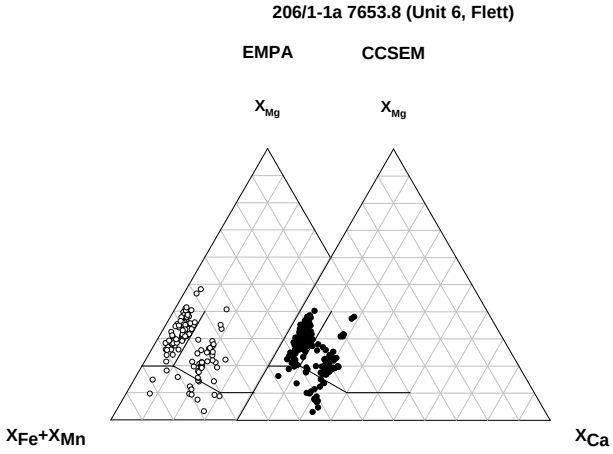

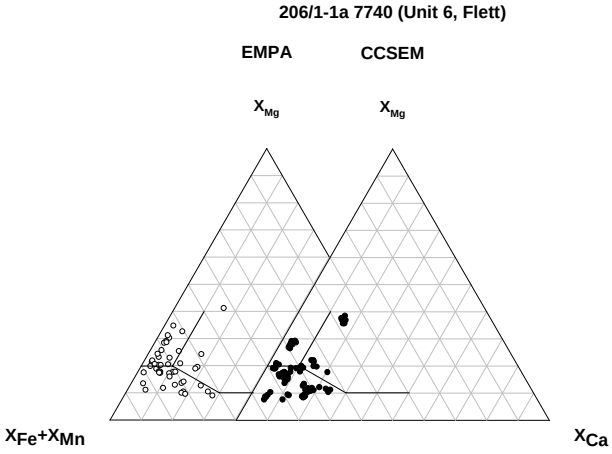

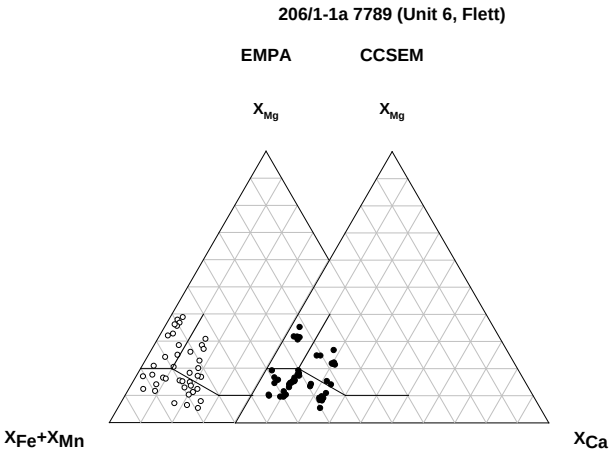

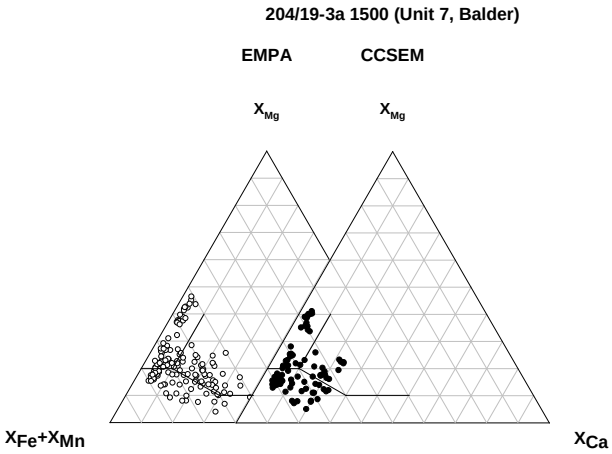

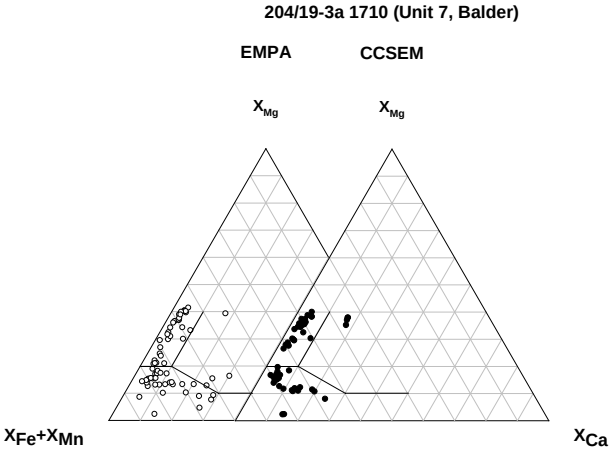

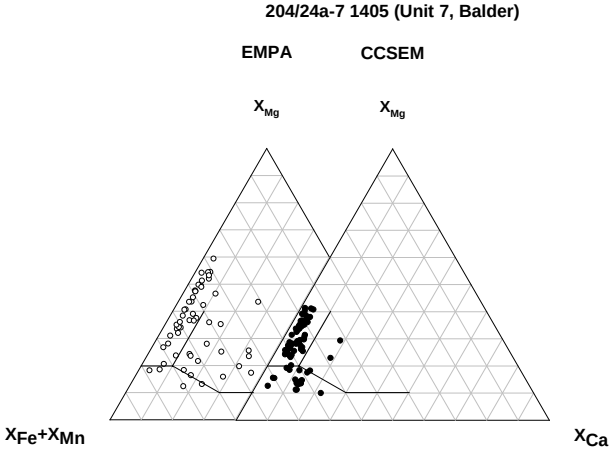

Plate 1 continued.

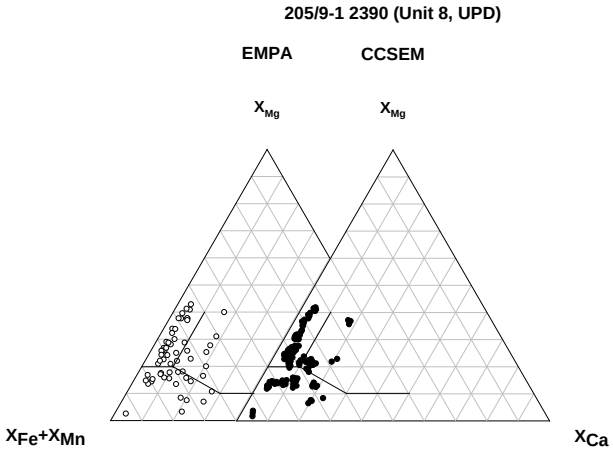

Plate 2: Compilation of garnet compositions determined by CCSEM and EMPA in samples from the Kangerlussuaq area.

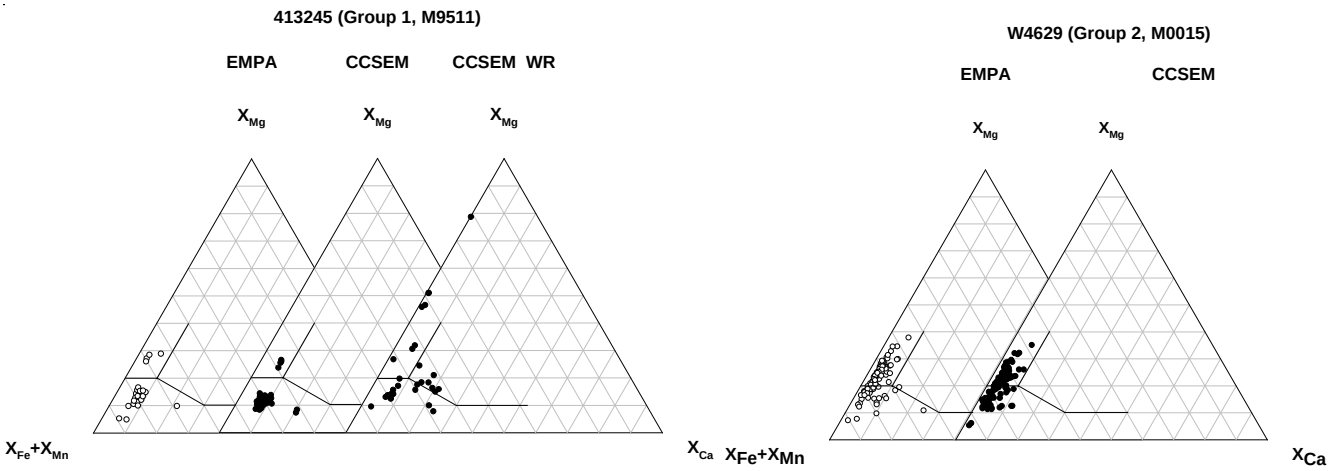

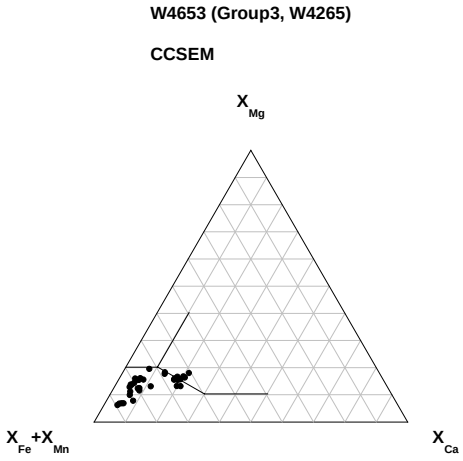

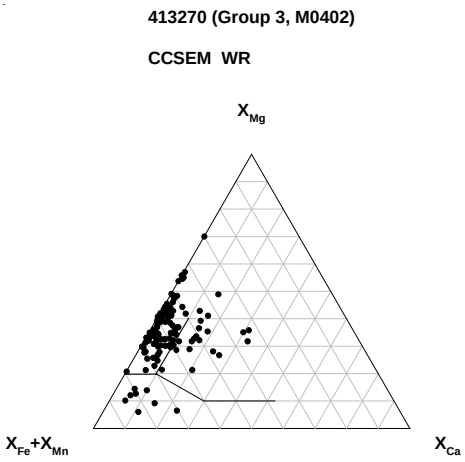

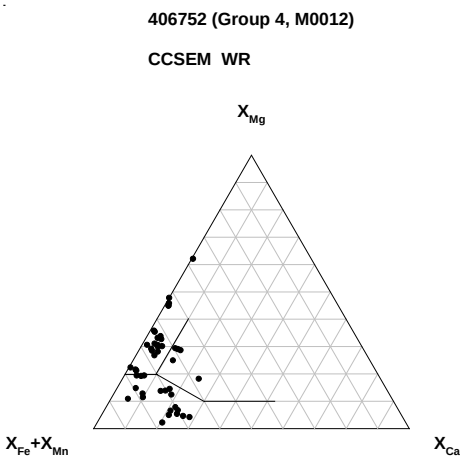

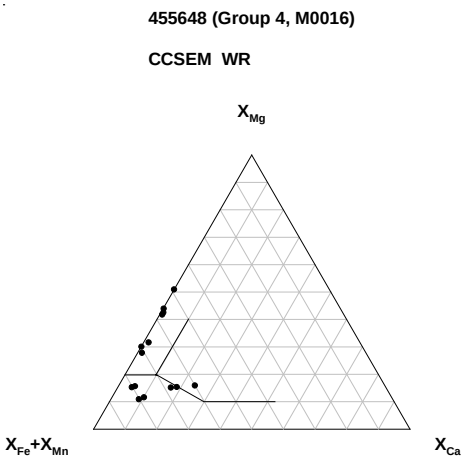

413123 (Group 5, M9501)

CCSEM WR

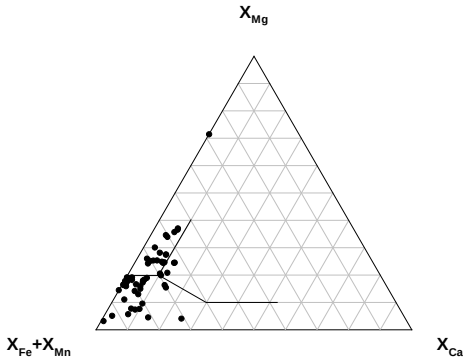

413124 (Group 5, M9501)

CCSEM

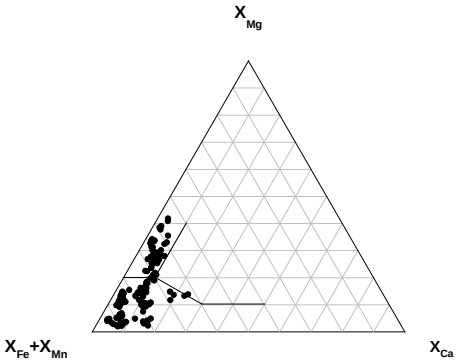

413143 (Group 5, M9502)

CCSEM **CCSEM WR**

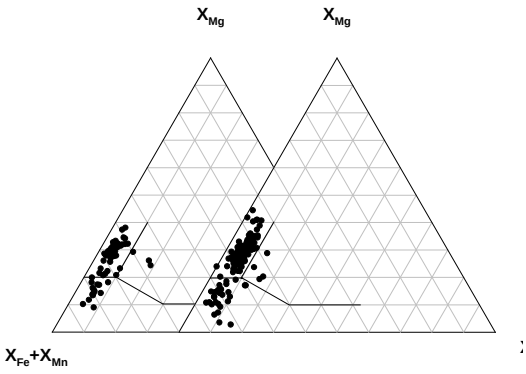

413190 (Group 5, M9507)

CCSEM **CCSEM WR**

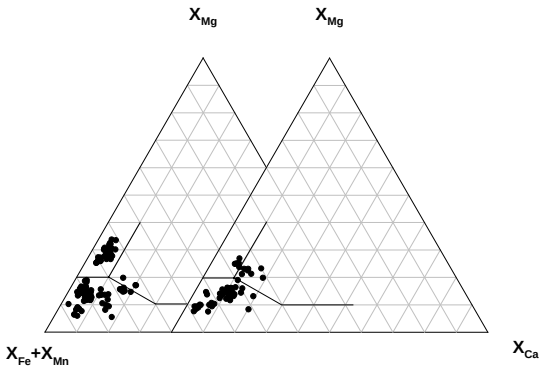

413276 (Group 5, M9521)

CCSEM WR

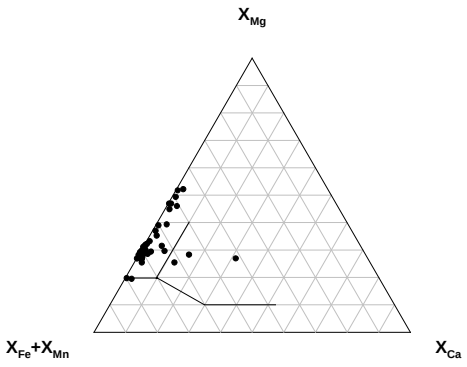

455423 (Group 6, M0002)

CCSEM WR

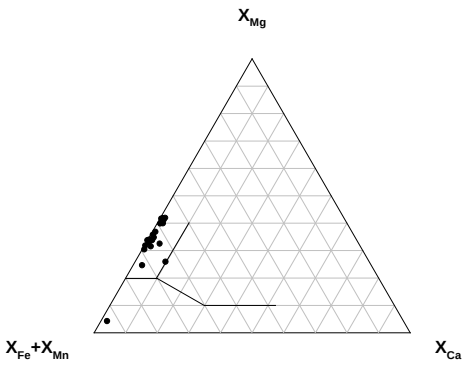

Plate 2 continued.

406736 (Group 7, M0012)

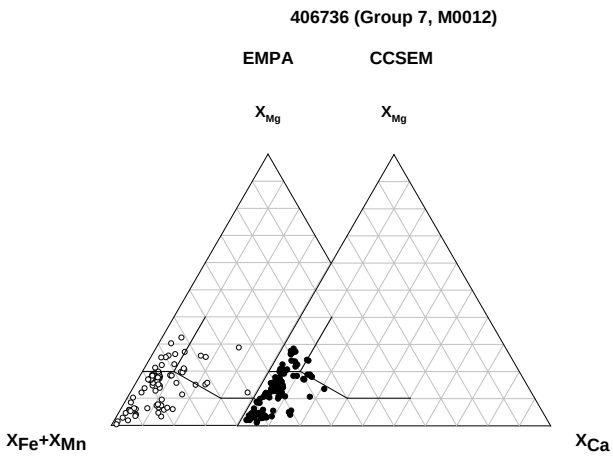

413166 (Group 7, M9507)

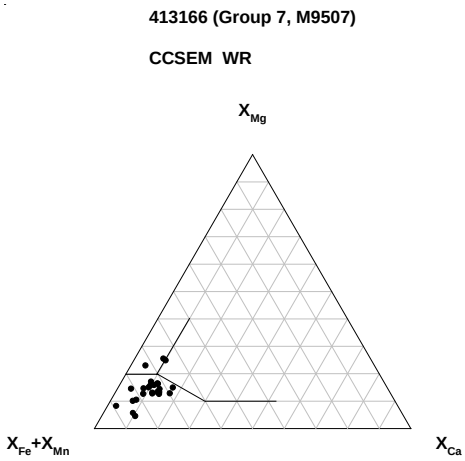

413211 (Group 7, M9508)

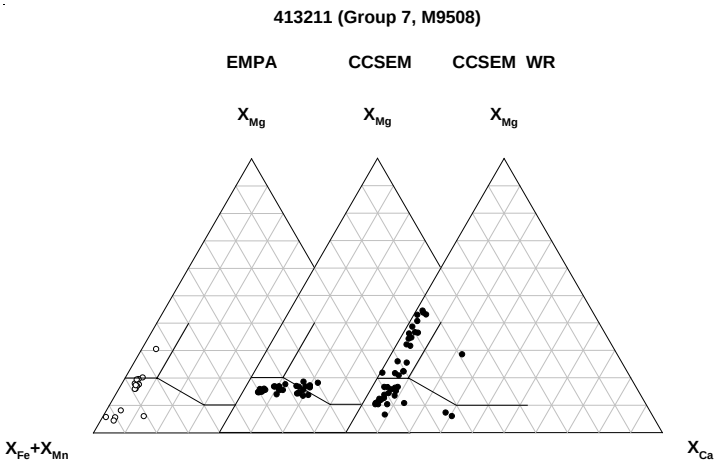

K10286 (Group 7, W4232)

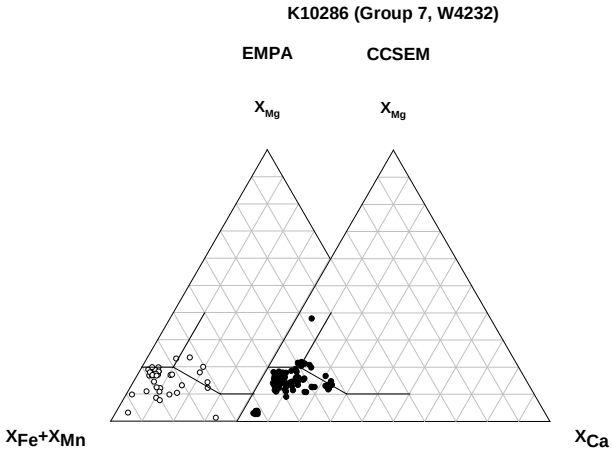

K10793 (Group 7, W4264)

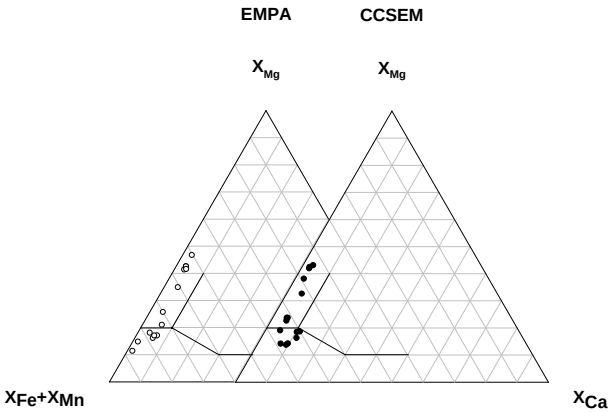

W4671 (Group 7, P2373)

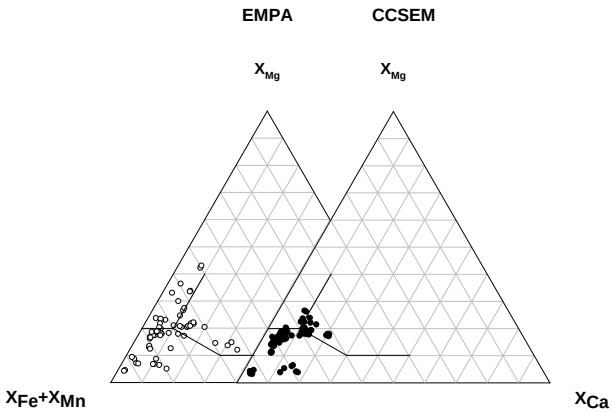

Plate 2 continued.

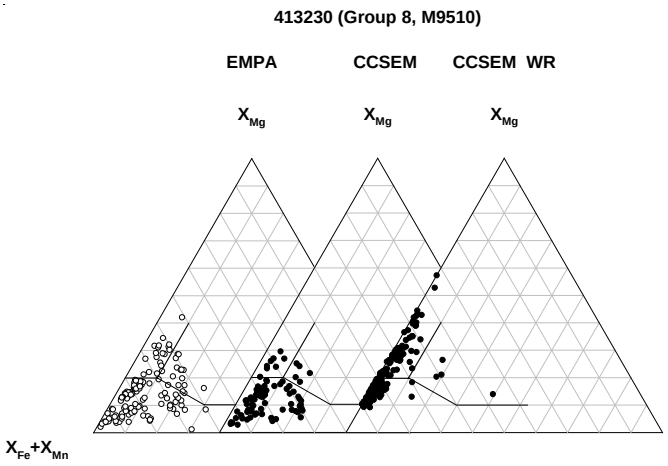

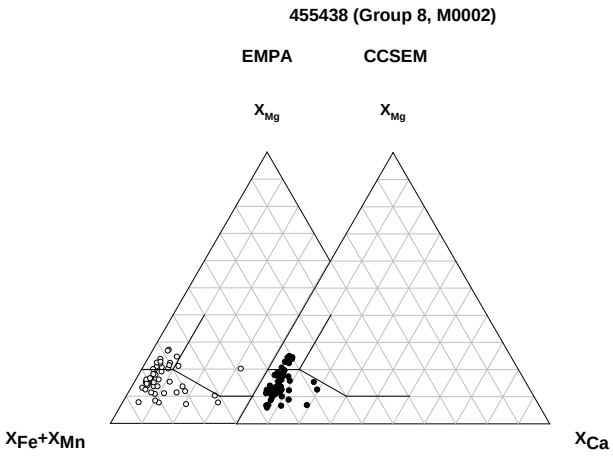

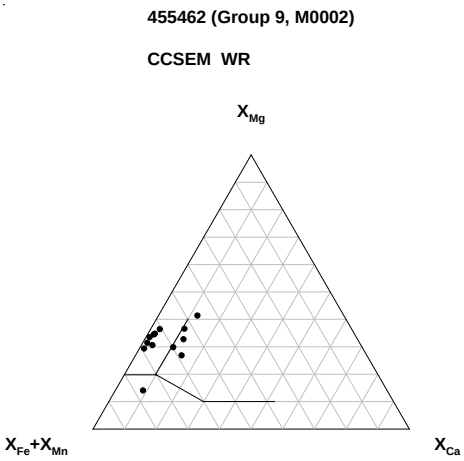

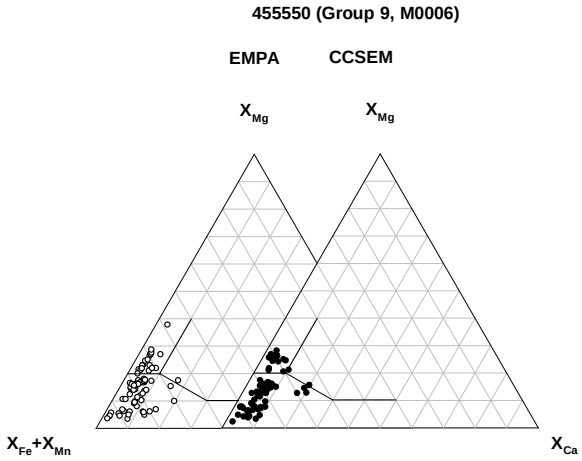

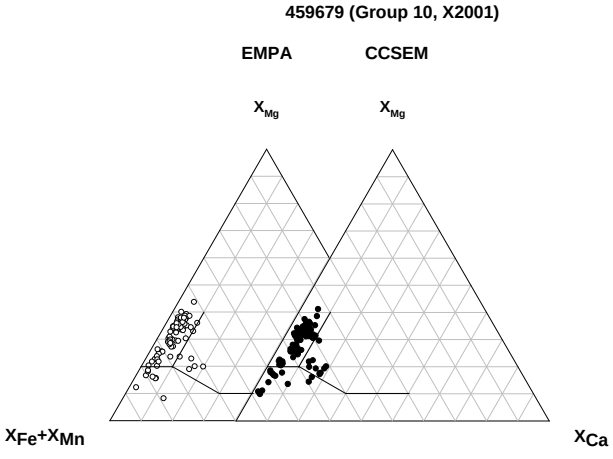

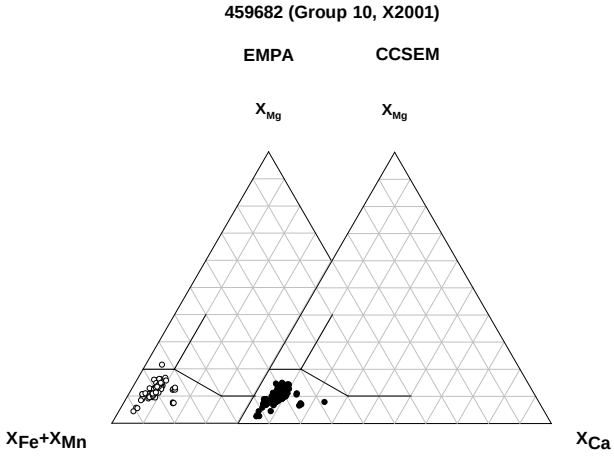

Plate 3: Compilation of detrital zircon age distributions in samples from the Kangerlussuaq area determined by ^{207}Pb-^{206}Pb age dating (LA-Q-ICP-MS).

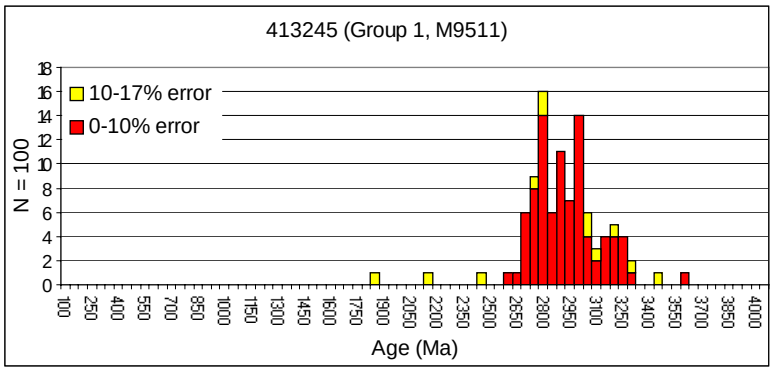

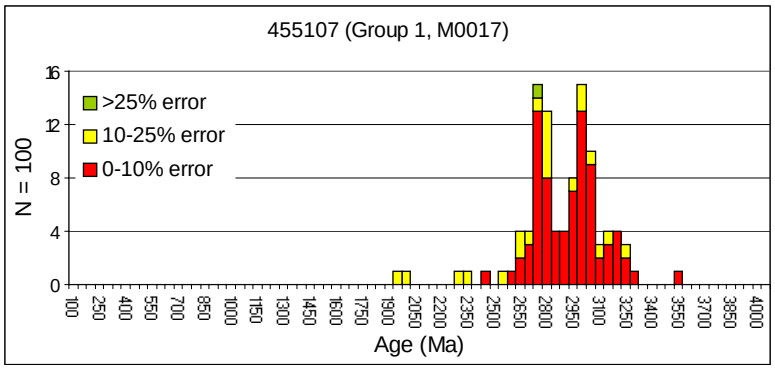

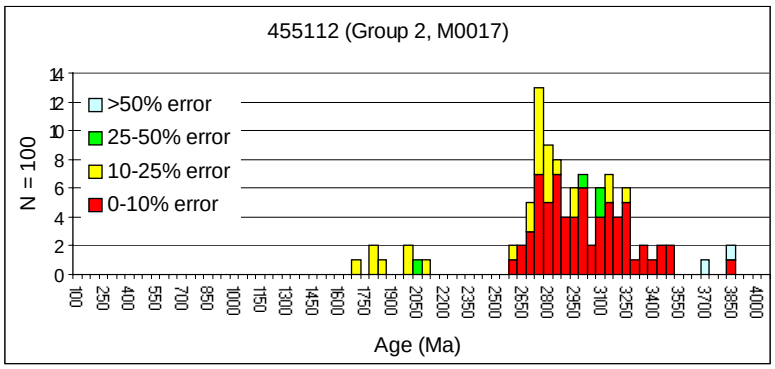

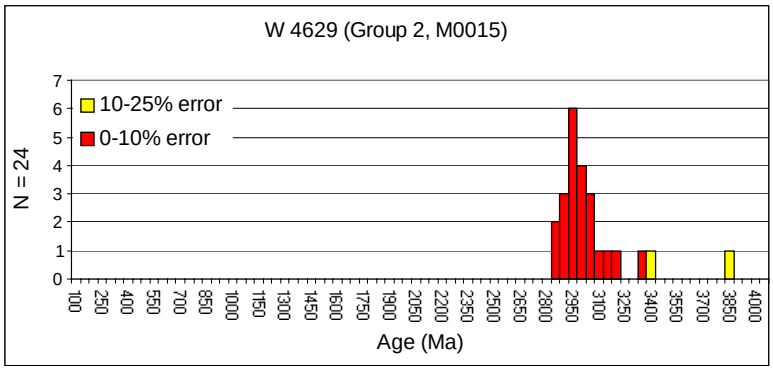

Plate 3 continued.

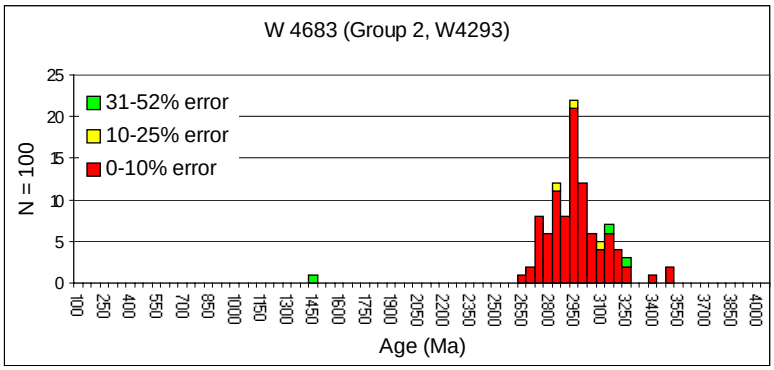

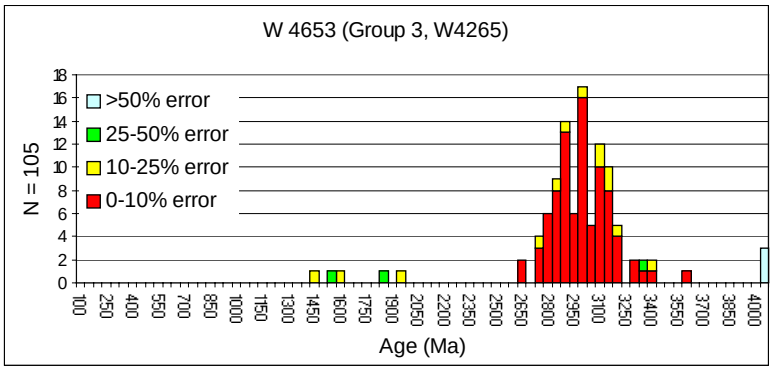

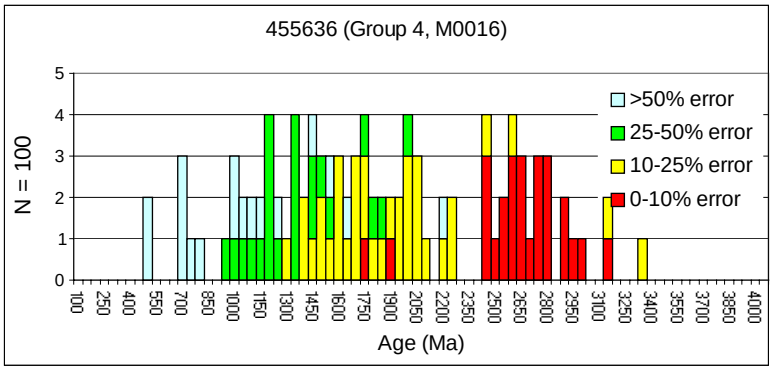

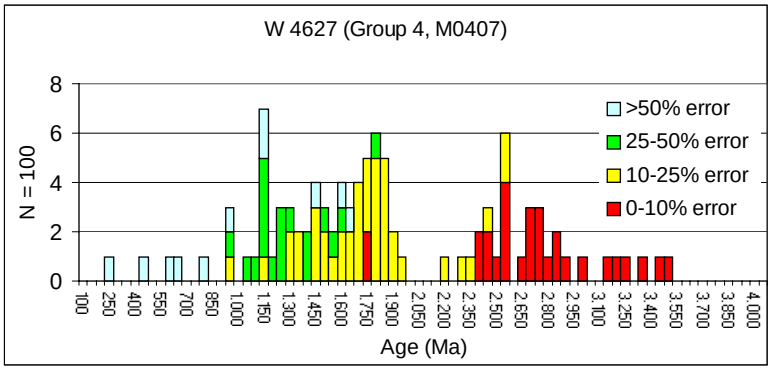

Plate 3 continued.

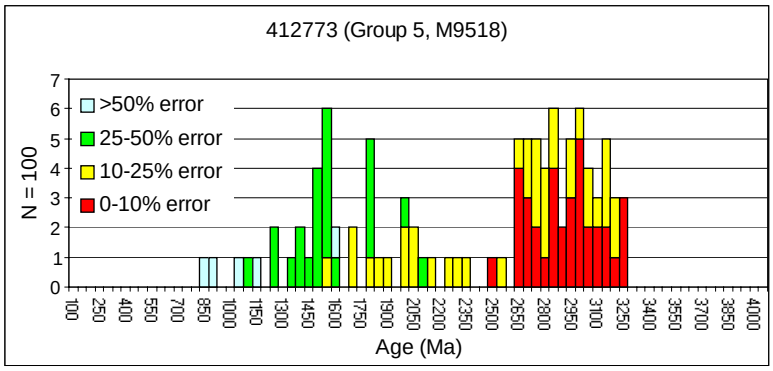

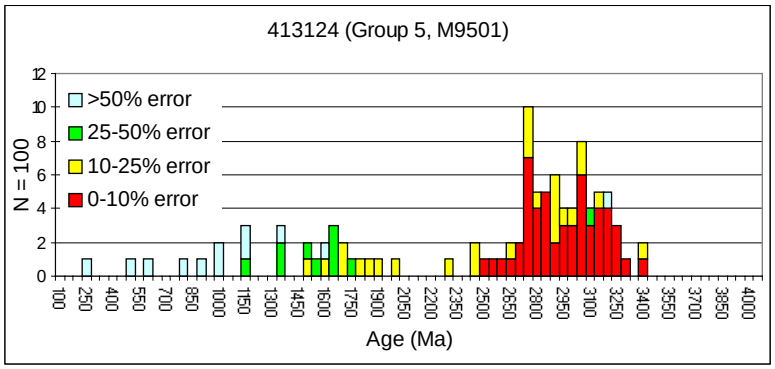

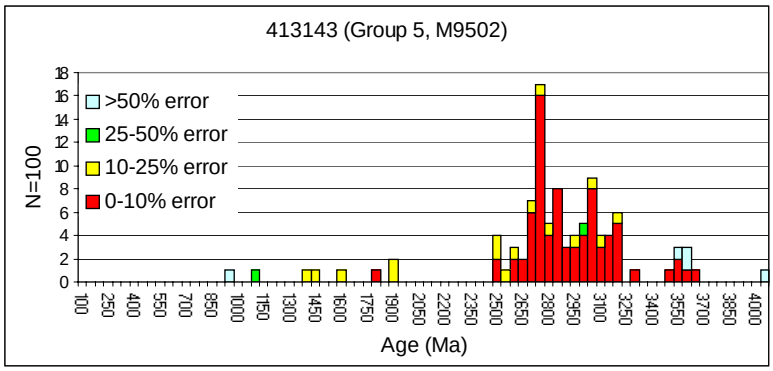

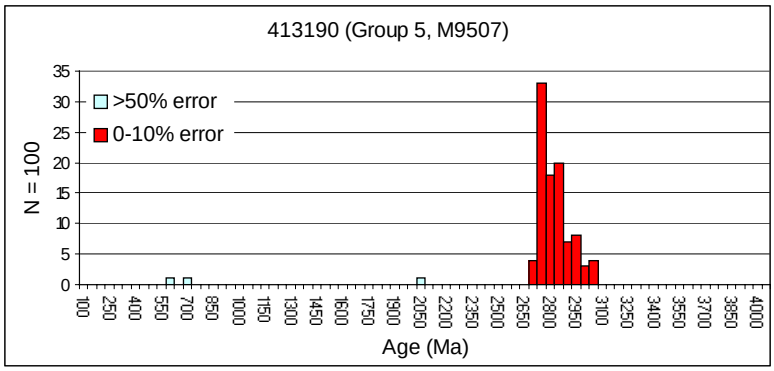

Plate 3 continued.

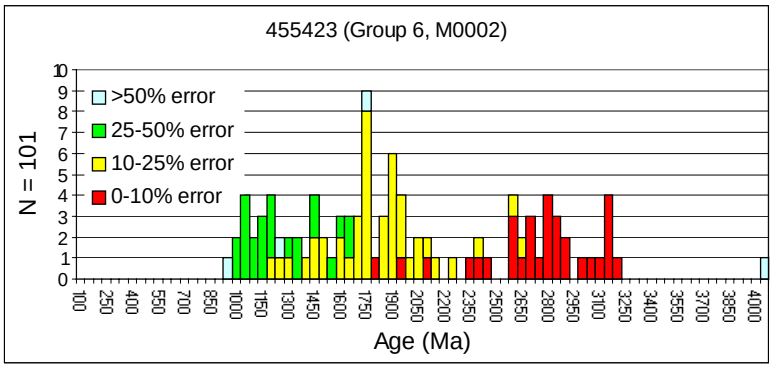

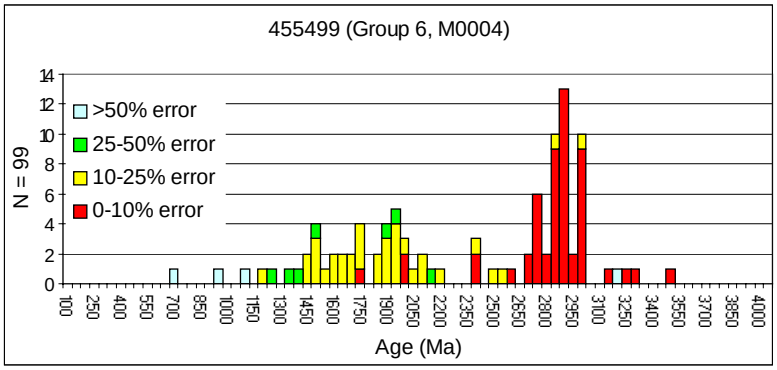

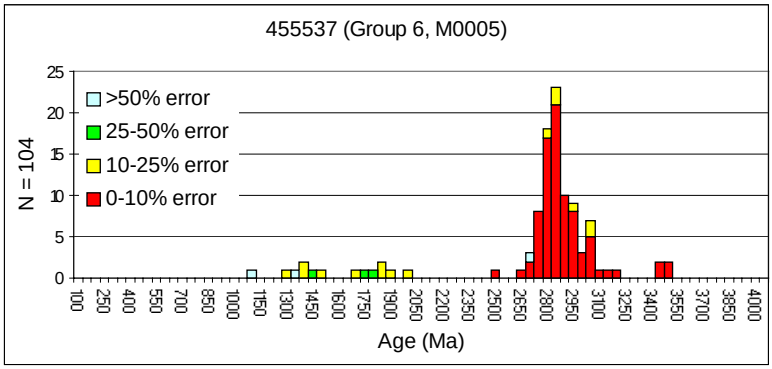

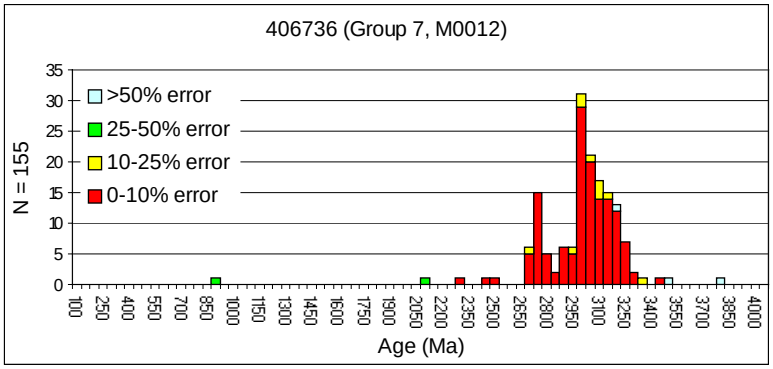

Plate 3 continued.

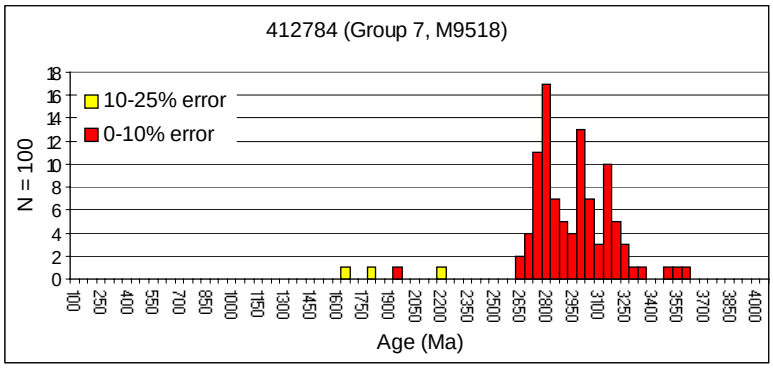

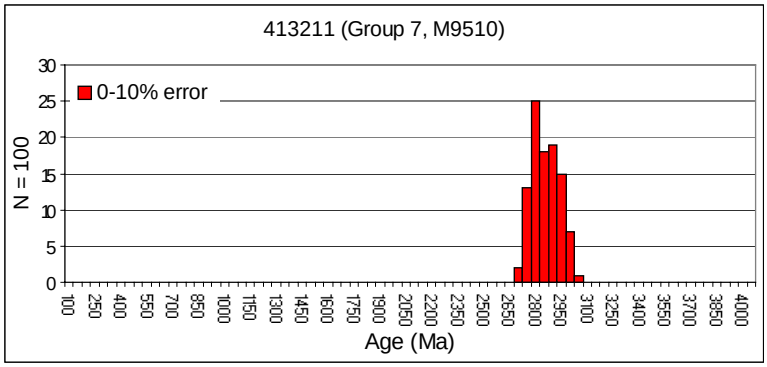

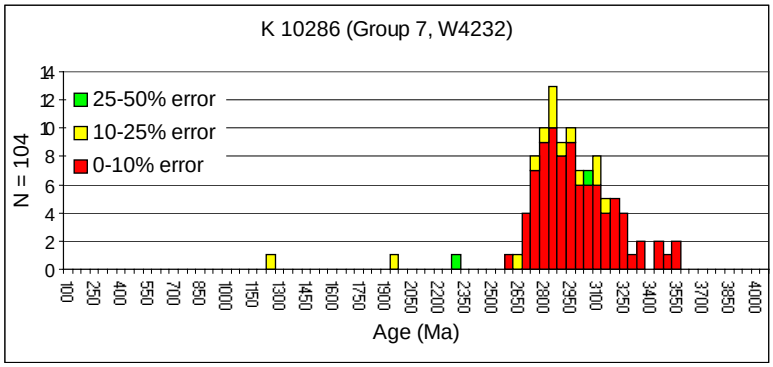

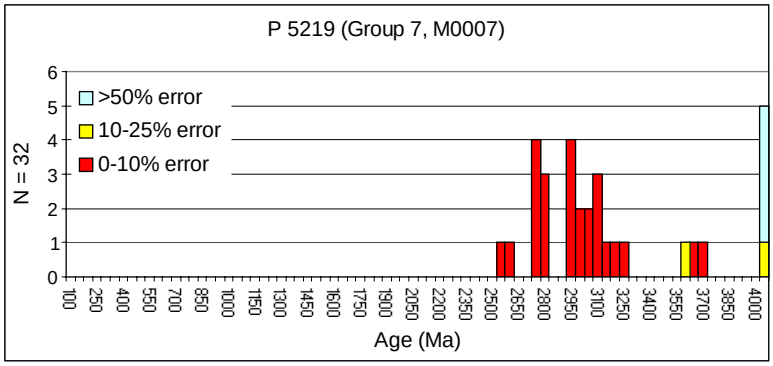

Plate 3 continued.

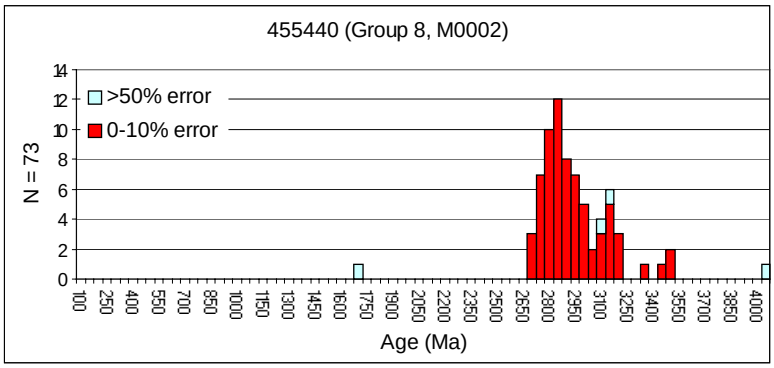

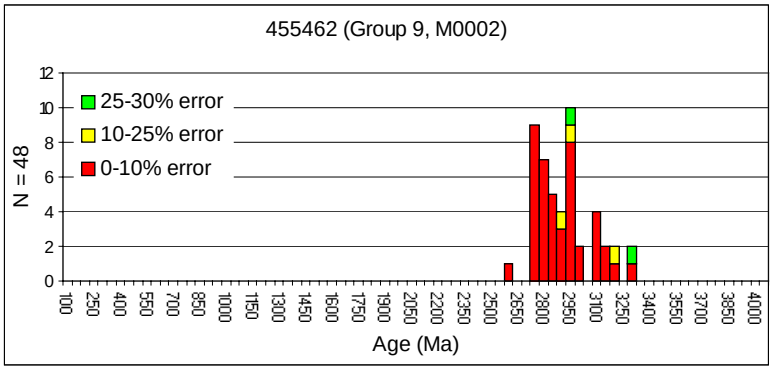

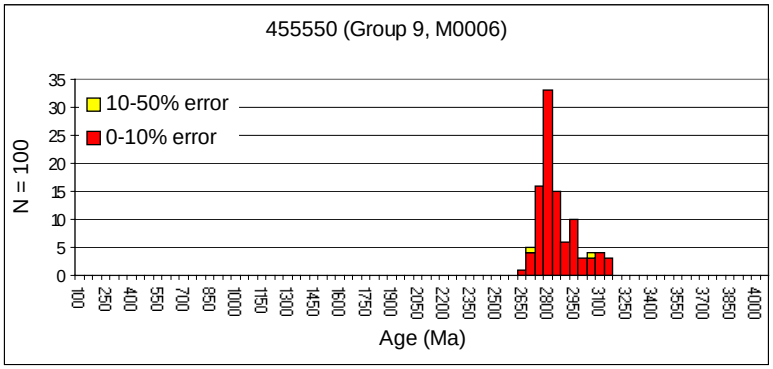

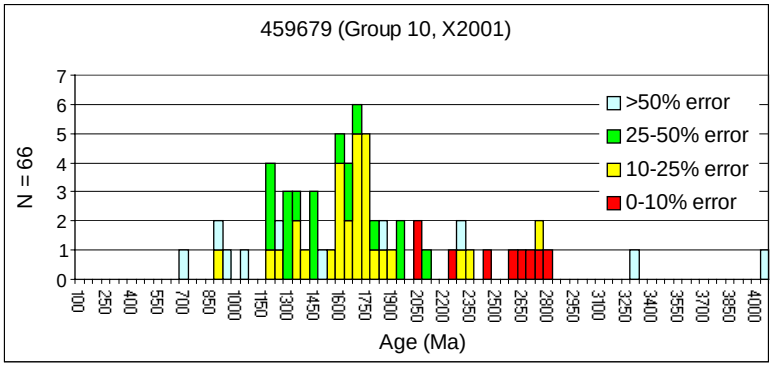

Plate 3 continued.

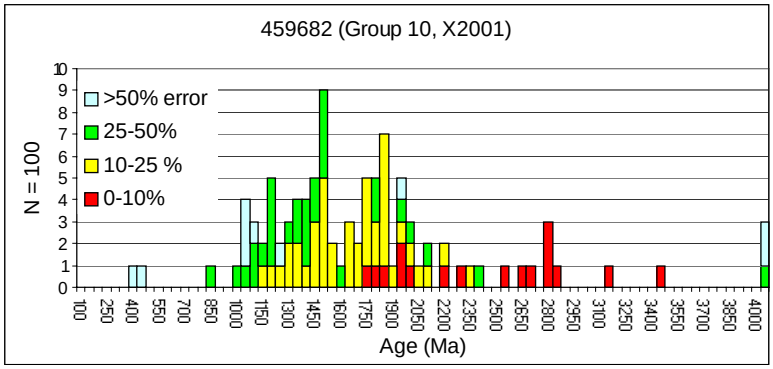

Plate 4: Compilation of detrital zircon age distributions in samples from wells (204/19-3a, 204/24a-7, 205/9-1, 206/1-1a, 214/19-1) in the UK sector of the Faroe-Shetland determined by ^{207}Pb-^{206}Pb age dating (LA-Q-ICP-MS).

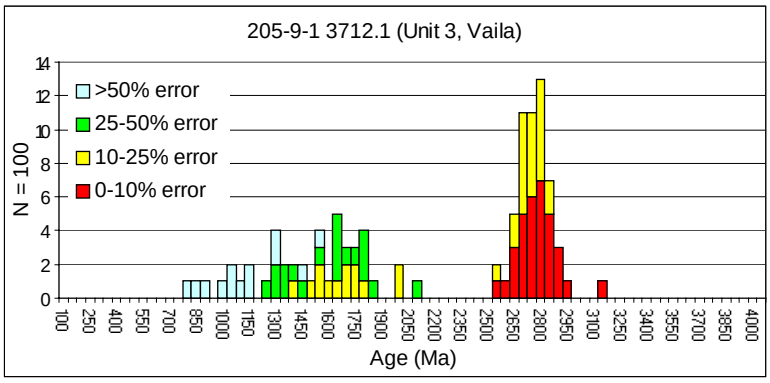

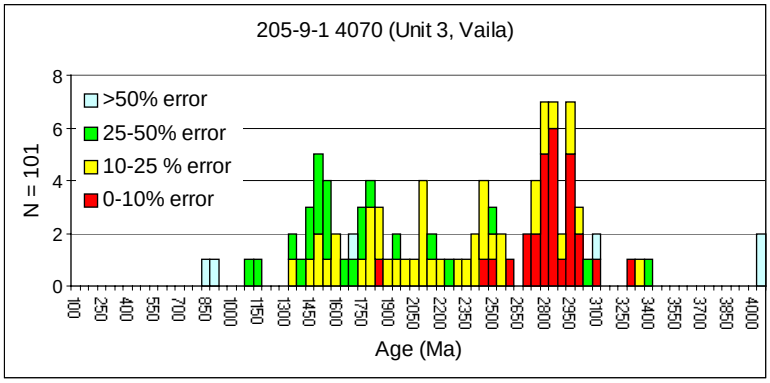

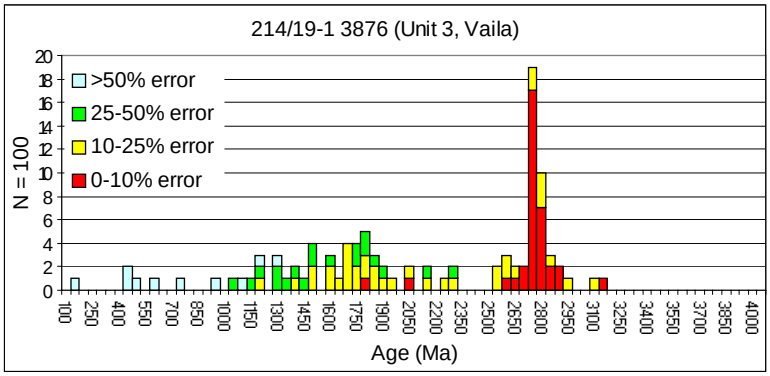

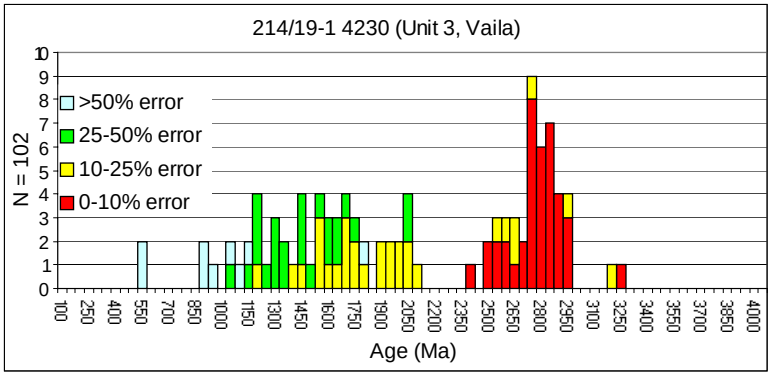

Plate 4 continued.

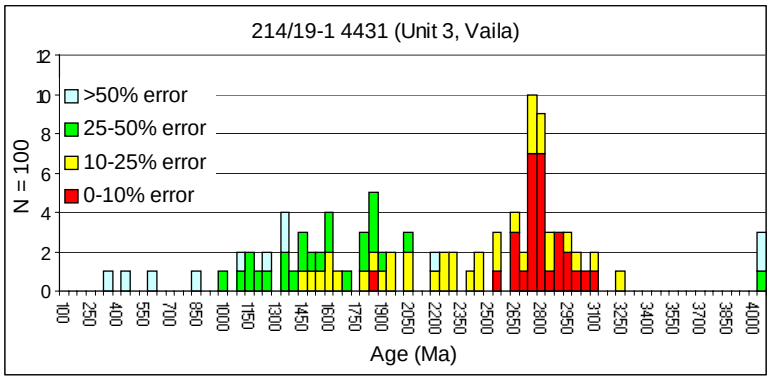

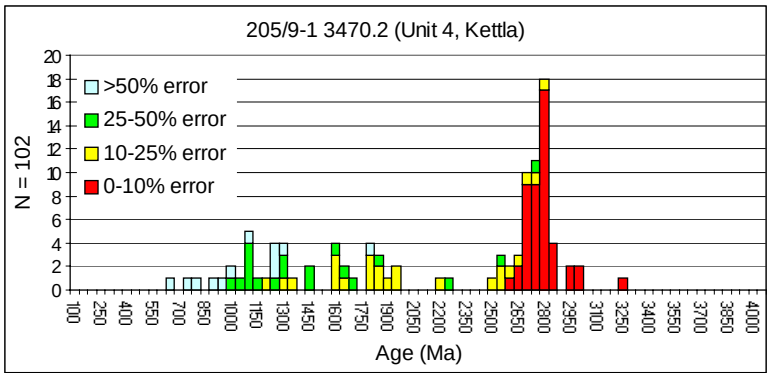

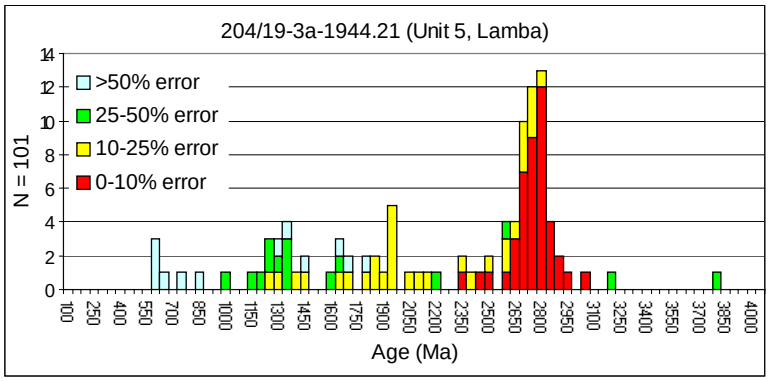

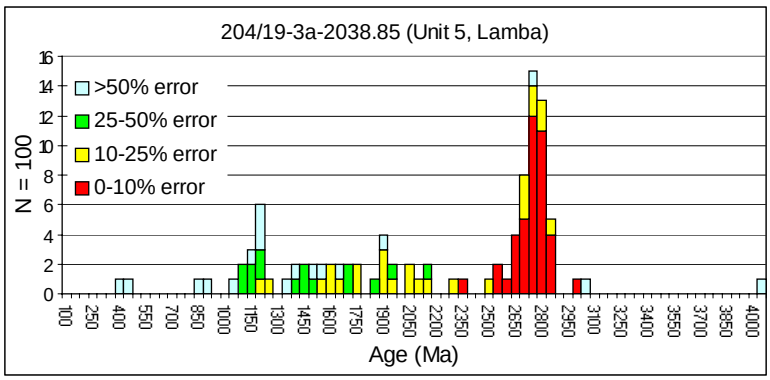

Plate 4 continued.

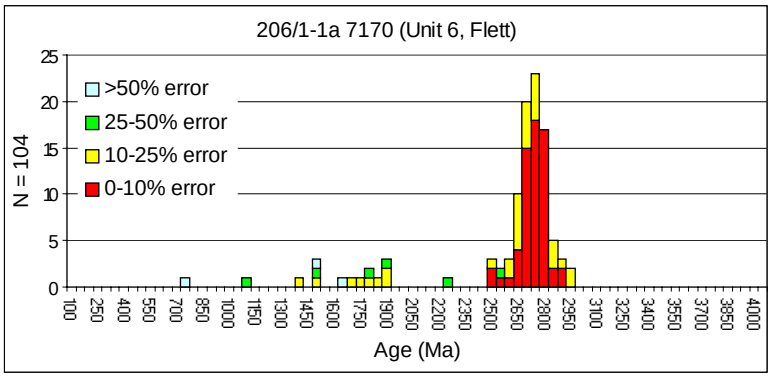

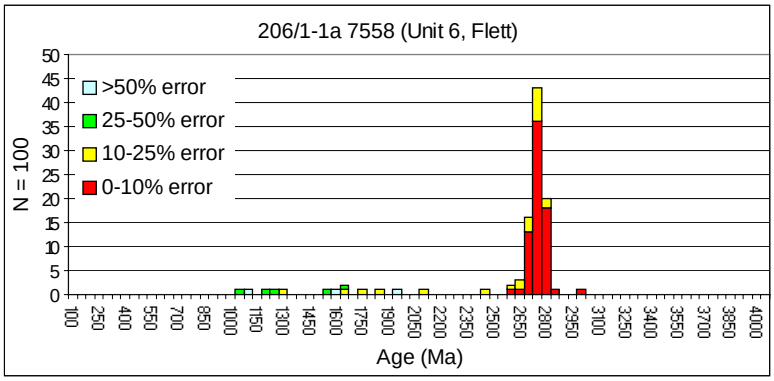

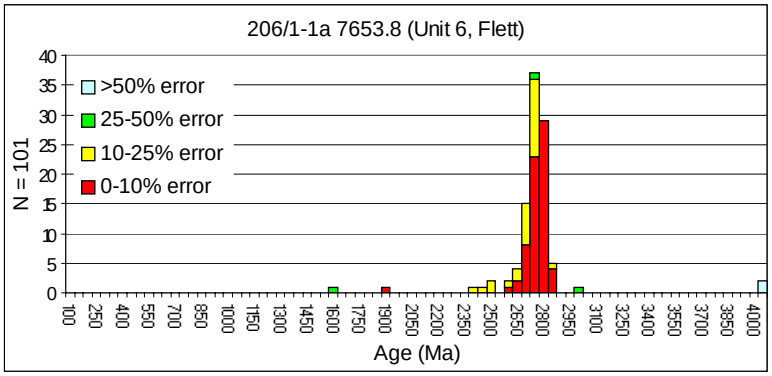

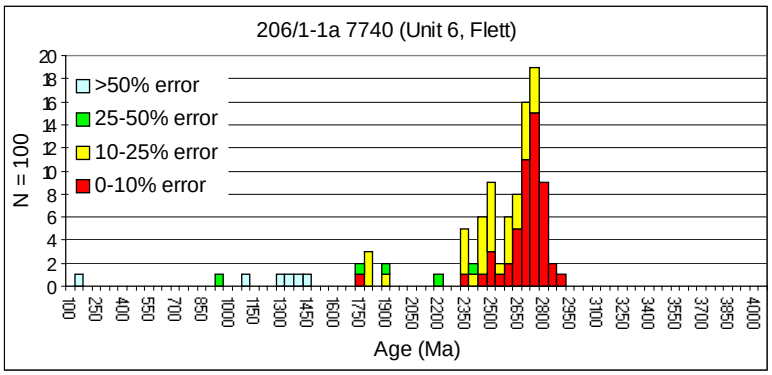

Plate 4 continued.

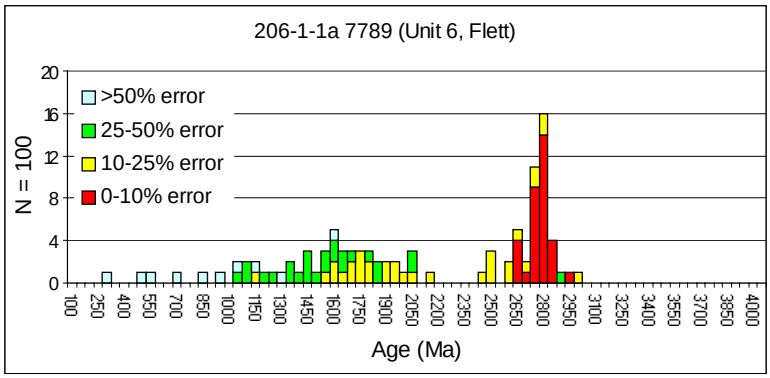

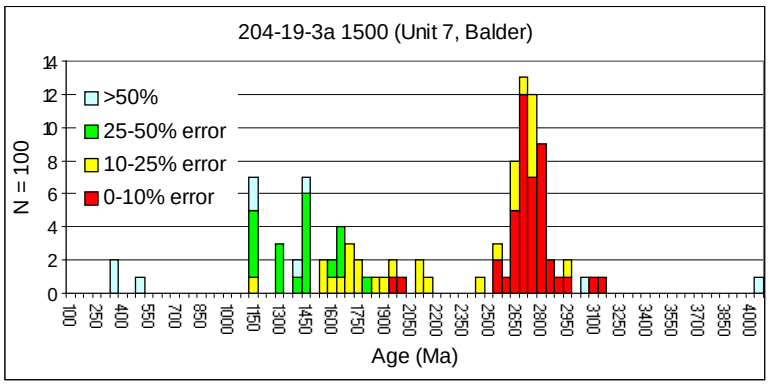

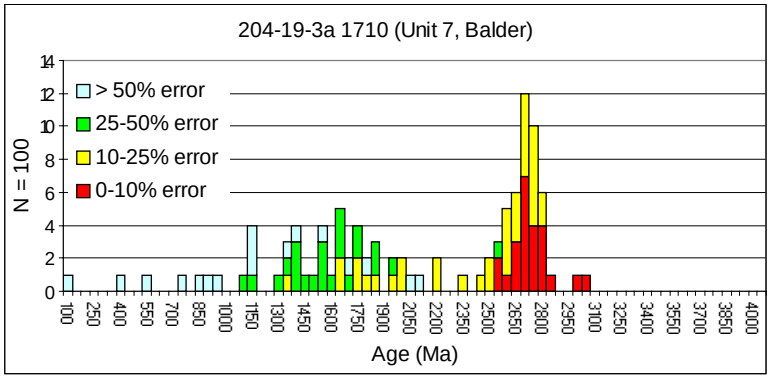

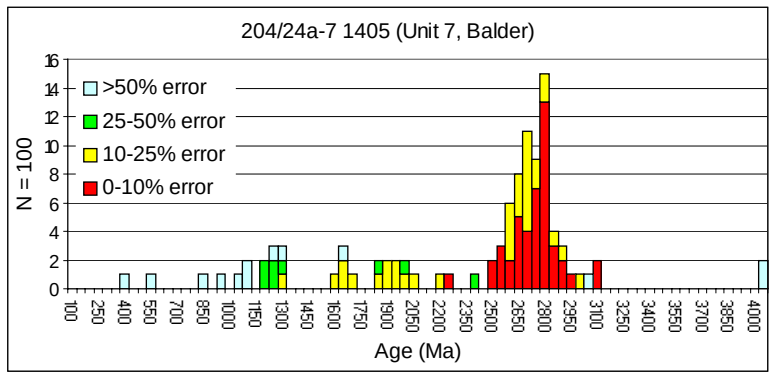

Plate 4 continued.

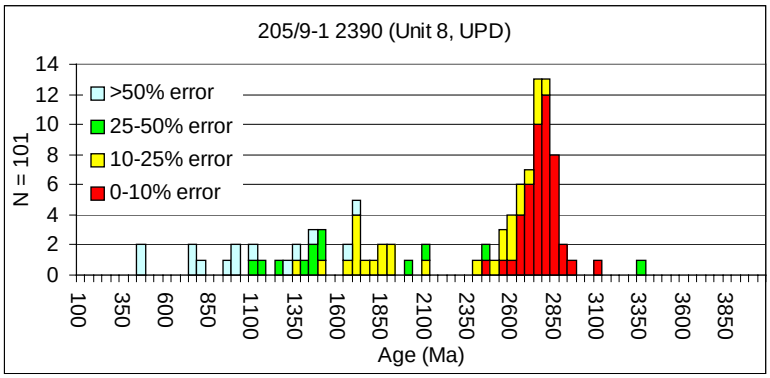

Plate 5: Compilation of detrital zircon age distributions in samples from the Orkneys determined by ^{207}Pb-^{206}Pb age dating (LA-Q-ICP-MS).

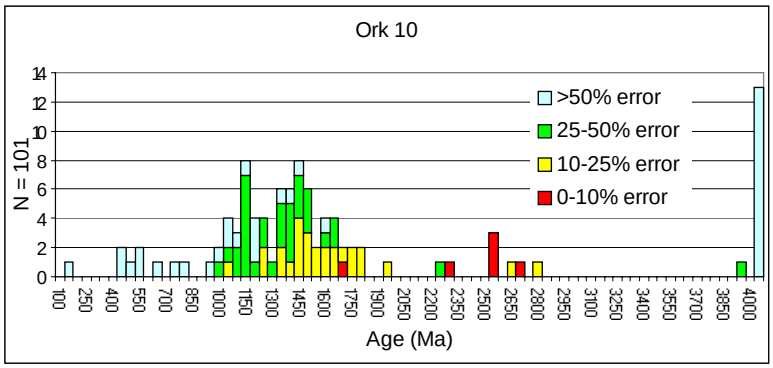

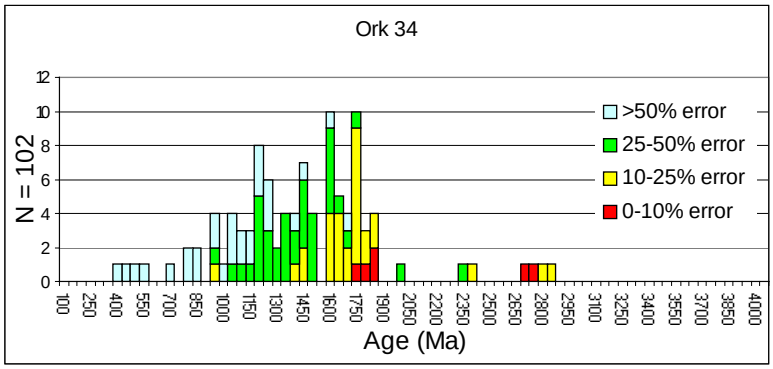

Plate 6: Compilation of detrital zircon age distributions determined by U-Pb age dating (SHRIMP).

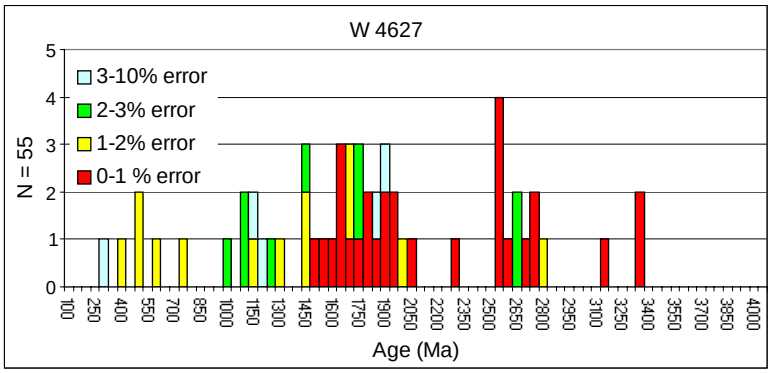

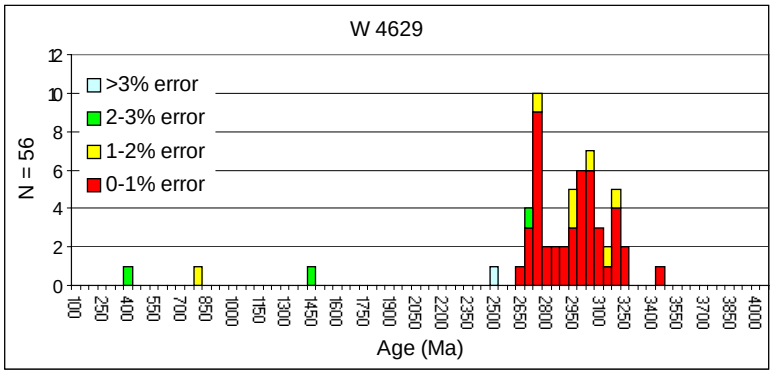

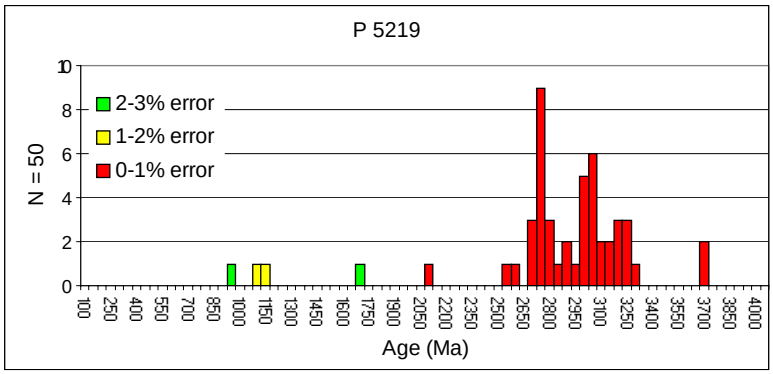

Plate 7: Compilation of detrital zircon age distributions determined by U-Pb age dating (LA-SF-ICP-MS) and ^{207}Pb-^{206}Pb age dating (LA-Q-ICP-MS).

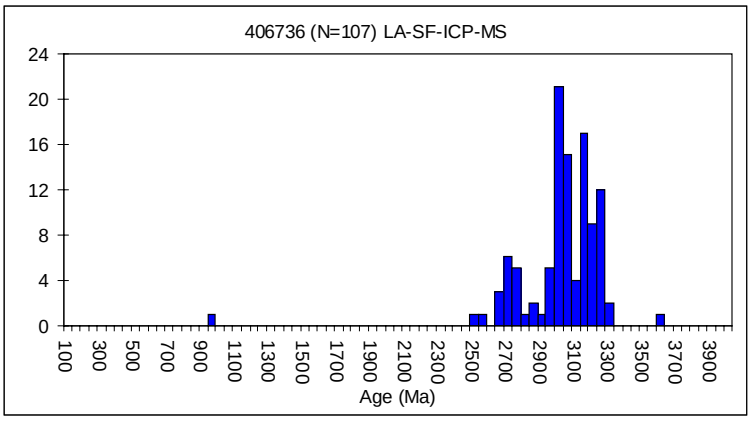

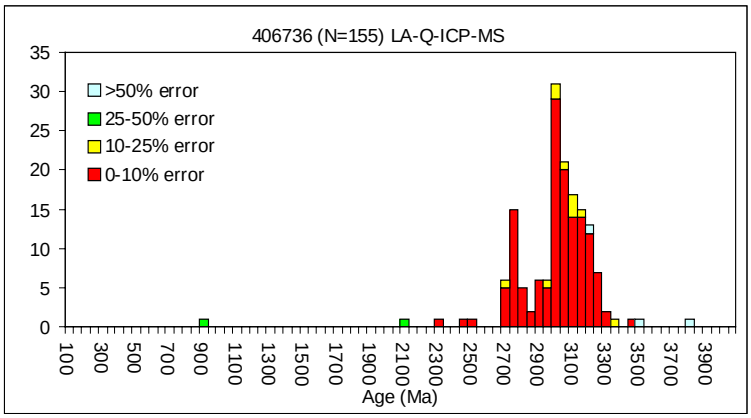

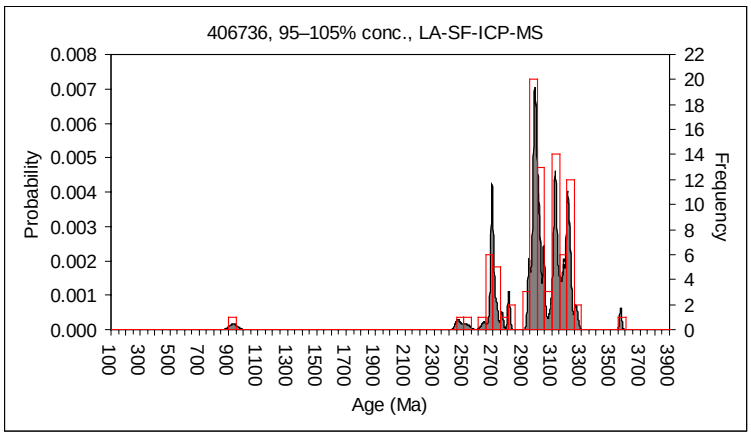

Plate 7 continued.

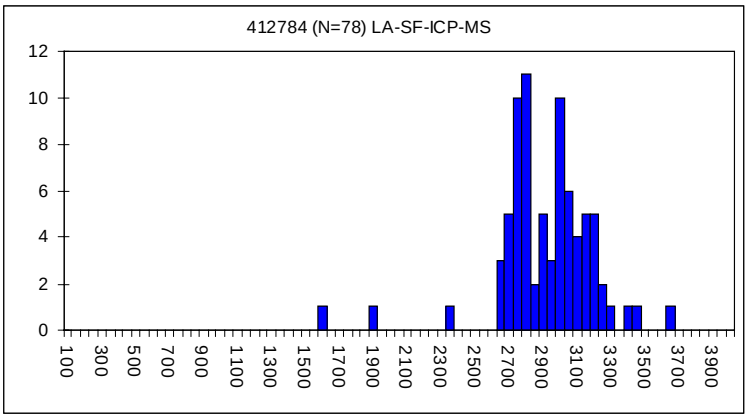

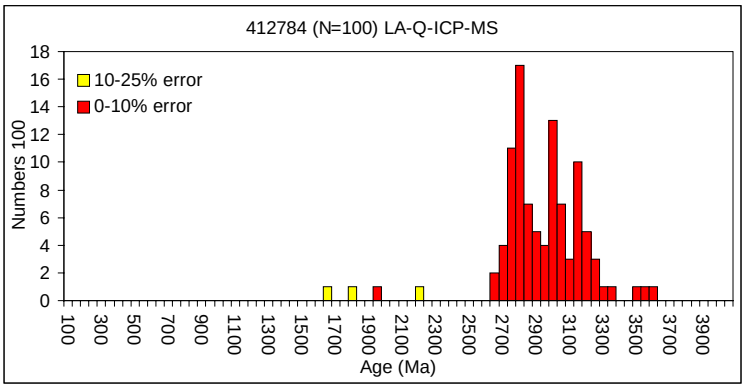

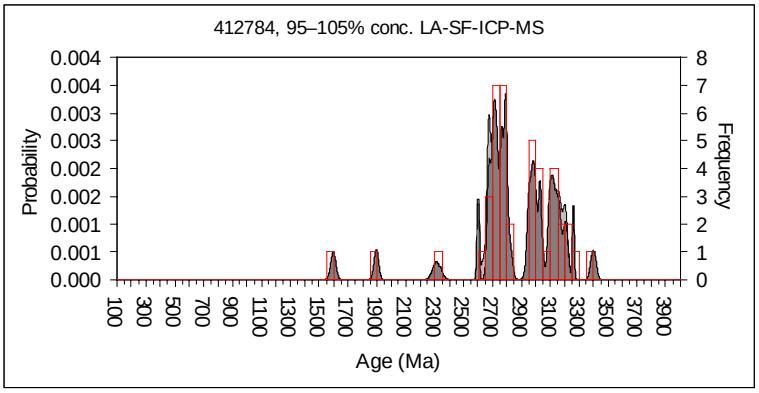

Plate 7 continued.

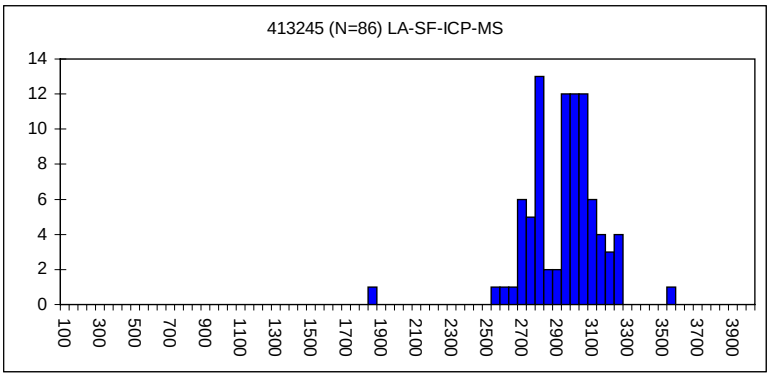

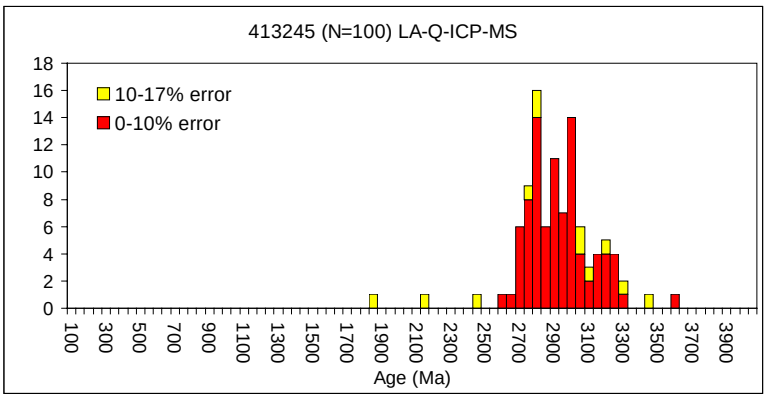

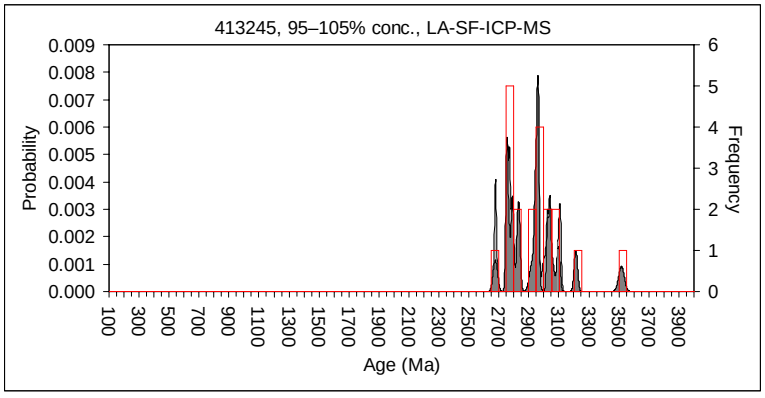

Plate 7 contiuned.

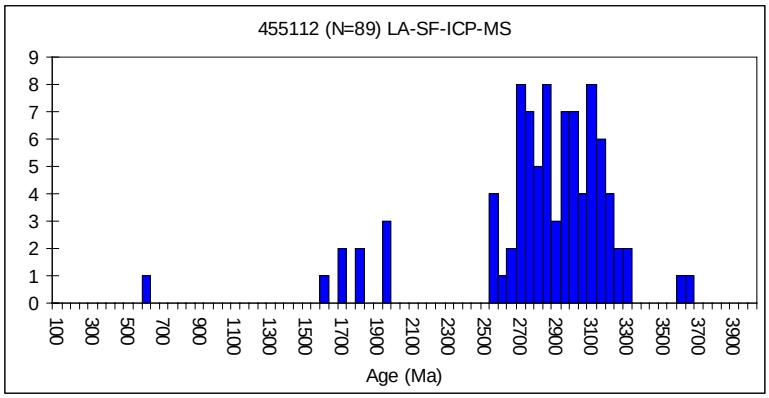

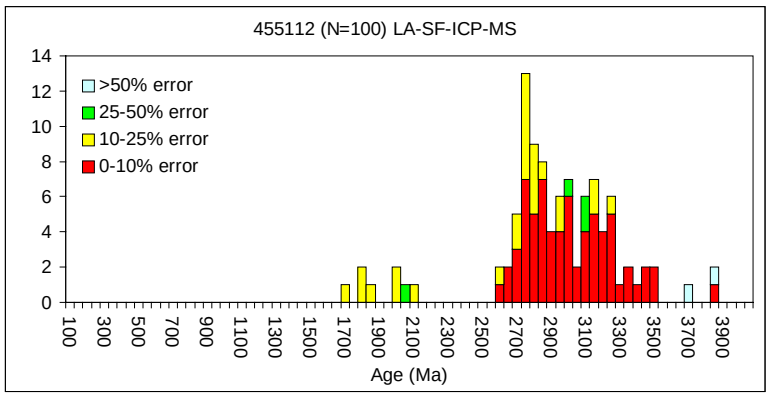

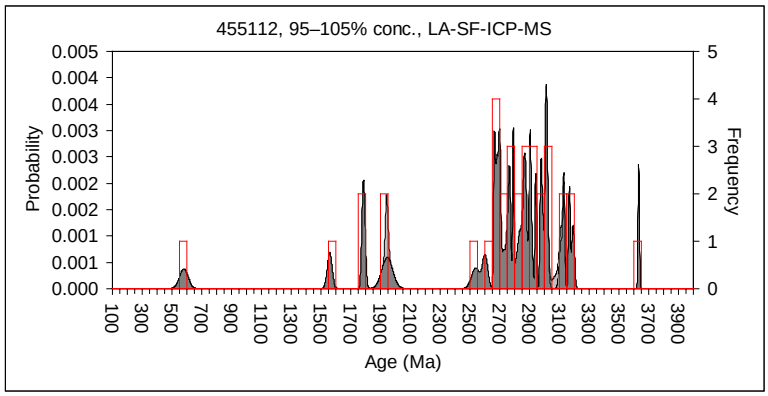

Plate 7 contiuned.